UNIVERSITÉ FRANÇOIS-RABELAIS DE TOURS

Année Universitaire : 2017/2018

HABILITATION A DIRIGER DES RECHERCHES

Discipline : Sciences de la vie et de la santé

MICROBULLES ET CELLULES ACOUSTIQUES

présentée et soutenue publiquement

par :

Michiel Arjen Benjamin POSTEMA

le 11 décembre 2017

JURY :

M. Ayache BOUAKAZ	Directeur de Recherche	INSERM – Université de Tours
M. Christian CACHARD	Professeur des Universités	Université Lyon 1
Mme Liesbet GERIS	Professeur	Université de Liège, KU Leuven
Mme Marie-Pierre KRAFFT	Directrice de Recherche	CNRS – Université de Strasbourg
Mme Dominique LANGEVIN	Directrice de Recherche	CNRS – Université Paris-Sud
Mme Nathalie LASSAU	PU – PH	Université Paris-Sud
M. Frédéric PATAT	PU – PH	Université de Tours

Avant-propos

Je remercie les membres du jury d'avoir accepté de juger ce travail.

Je remercie les rapporteurs, M. Christian Cachard, Mme Liesbet Geris et Mme Marie-Pierre Krafft, pour les suggestions qu'ils ont formulées pour la correction de ce manuscrit.

Je remercie mon référent, M. Ayache Bouakaz, pour son soutien et son support de ma recherche.

Je remercie les co-auteurs des articles présentés dans ce mémoire.

Je remercie les membres de l'équipe 5 : Imagerie et Ultrasons de l'Unité Inserm UMR 930 de m'avoir offert un environnement de travail professionnel et pour leurs discussions animées.

Je remercie M. Charles Sennoga pour l'aide avec les observations expérimentales des antibulles.

Je remercie M. Jean-Michel Escoffre, Mme Stéphanie Lepaire et Mme Aurélie Pétereau pour l'aide avec les préparations du mémoire et de la soutenance.

Je remercie M. Jean-René Jacquet, M. Léopold Kritly, M. Jules Moualeu et M. Anthony Novell d'avoir corrigé mon français.

Je remercie LE STUDIUM Loire Valley Institute for Advanced Studies de m'avoir donné l'opportunité de m'impliquer dans la recherche en région Centre.

Je remercie la Commission Recherche de l'Université François-Rabelais de Tours de m'avoir donné la confiance de contribuer au rayonnement international de l'Université.

« La science a des bons jours et des mauvaises années »

attribué à E. Hagen

Table des matières

Partie I

Notice individuelle

La notice individuelle est composée de trois chapitres.

Le premier chapitre contient un curriculum vitae qui décrit mes parcours académiques, mes activités d'encadrement et mes activités d'administration.

Le deuxième chapitre contient une liste détaillée de mes publications.

Le troisième chapitre contient une liste détaillée de mes contrats de recherche obtenus en tant que responsable ou co-responsable.

I.1 Curriculum vitae

Pr. Dr. Michiel Arjen Benjamin POSTEMA

Né le 19 août 1973 à Brederwiede aux Pays-Bas.

Citoyen et résident des Pays-Bas.

Adresses professionnelles

UMR Inserm U930

Université François-Rabelais de Tours

10, boulevard Tonnellé

37000 Tours

France

School of Electrical and Information Engineering

Chamber of Mines Building

University of the Witwatersrand

1 Jan Smuts Avenue

Braamfontein

Johannesburg 2050

Afrique du Sud

Adresse personnelle

[redacted]

I.1.1 Cursus

Cursus universitaire

1992 : *Propaedeuse* en Géophysique, Université d'Utrecht, Pays-Bas.

1996 : Master en Géophysique, Université d'Utrecht, Pays-Bas.

2004 : Doctorat en Physique des Fluides, Université de Twente, Pays-Bas.

Formations complémentaires

1993 : Conseil municipal. Fondation de Haya van Someren, Pays-Bas.

1996 : Techniques des réunions efficientes et effectives. GTIP, Pays-Bas.

1997 : Gestion et conseil. Boertien, Pays-Bas.

1998 : Présentations anglaises professionnelles. Moc inter-lingua, Pays-Bas.

1999 : Analyse d'information. Cap Gemini Opleidingen, Pays-Bas.

2000 : Percevoir, interpréter, communiquer. Schouten & Nelissen, Pays-Bas.

2000 : Sécurité de l'information et gestion des risques. VGM, Pays-Bas.

2000 : Examen de l'Etat en politique de sécurité de l'information. EXIN, Pays-Bas.

2003 : Pathophysiologie de la cardiopathie ischémique. CŒUR Ecole de Recherche, Pays-Bas.

2004 : Tendances en technologie médicale. Nicolaes Tulp Instituut, Pays-Bas.

2004 : Ablation par fréquences radio des anomalies du foie sous le couvert d'échographie. LUMC, Pays-Bas.

2005 : Fondements de l'action communicative. RUB Weiterbildungszentrum, Allemagne.

2005 : Rhétorique des conférences et comportement de la parole. RUB WBZ, Allemagne.

2005 : Visualisation et présentation. RUB Weiterbildungszentrum, Allemagne.

2008 : Élargir les horizons de l'acoustique. Université de Reading, Angleterre.

2008 : Rencontre des trois pays d'ultrasons. Société Suisse d'Ultrasons en Médecine, Suisse.

2010 : Ecole d'été EUROSON, Echographie abdominale, EFSUMB, Norvège.

2017 : La prévention, le risque incendie, le risque biologique, le risque chimique. Institut national de la santé et de la recherche médicale, France.

I.1.2 Expériences de recherche

Académie Royale Néerlandaise des Sciences, Pays-Bas.

2000–2004 : Chercheur Junior en Génie Médical.
Projet de recherche : Fondation de Technologie STW projet RKG.5104.
Compétences acquises : Photographie à grande vitesse, microscopie, expérimentation acoustique, préparation et manipulation des agents de contraste ultrasonores.

Ruhr-Université de Bochum, Allemagne.

2005–2007 : Chercheur en Génie Médical.
Projet de recherche : RUB 603151, RUB 603042.
Compétences acquises : Analyse des microbulles coalescantes.

2009–2010 : Maître de Conférence en Génie Médical.
Projet de recherche : Communauté de Recherche Allemande DFG 38355133.
Compétences acquises : Sonoporation à pressions basses.

Université de Hull, Angleterre.

2007–2009 : Maître de Conférence en Génie Mécanique.
Projet de recherche : Leverhulme F/00181/N, EPSRC EP/F037023/1.
Compétences acquises : Eradication des cyanobactéries, manufacture des transducteurs à ultrasons.

2009–2011 : Chercheur invité.
Projet de recherche : EPSRC EP/F037023/1.
Compétences acquises : Sonoporation à pressions basses.

Université de Bergen, Norvège.

2010–2016 : Professeur en Acoustique Expérimentale.
Projet de recherche : MIMT.
Compétences acquises : Manufacture des transducteurs translucides, sonoporation des tissus vivants.

I.1.3 Postes d'invités

Université d'Orléans, France.

05/2010–10/2010 : Enseignant Invité en Biophysique.
Projet de recherche : ANR Programme Blanc SVSE 5.
Compétences acquises : Transfert des gènes in vivo.

Université de Dundee, Écosse.

01/2012–03/2012 : Erasmus Professeur Visiteur en Astrophysique.
Projet de recherche : Erasmus GfNA-II-C-ERA.
Compétences acquises : Géophysique planétaire, mesure des distances galactiques.

Institut Israélien de Technologie Technion, Israël.

04/2012–06/2012 : Maître de Conférence en Génie Médicale.
Compétences acquises : Manipulation des globules avec des transducteurs cylindriques.

Université du Cap, Afrique du Sud.

16–22/03/2015 : Professeur Visiteur en Génie Médicale.
Compétences acquises : Traitement d'image.

Université du Witwatersrand, Afrique du Sud.

12/2014–04/2015 : Professeur Visiteur en Physique.

06/2015–05/2018 : Professeur Visiteur en Ingénierie Electronique.
Compétences acquises : Électroporation.

Académie Polonaise des Sciences, Pologne.

04/2016–09/2016 : Professeur en Ultrasons, Chef de département intérimaire.
Compétences acquises : Conception de transducteurs pour le traitement du cancer du sein.

Inserm – Université François-Rabelais de Tours, France.

02/2017–01/2018 : Le Studium Fellow.
Projet de recherche : Marie Skłodowska-Curie 665790.
Compétences acquises : Analyse des antibulles et des globules.

I.1.4 Expériences d'enseignements universitaires

1994–1996 : **Université d'Utrecht, Pays-Bas.**

Module F1002 : TD en Algèbre linéaire.

Master en Géologie. 16 HETD ;

Module M1008 : TD en Biostatistique.

Licence en Médecine. 24 HETD ;

Module F3016 : TD en Gravimétrie et magnétométrie.

Master en Géophysique. 6 HETD.

2005–2007 : **Ruhr-Université de Bochum, Allemagne.**

Module STS I : TD en Signaux stochastiques I.

Master en Ingénierie Electrique. 16 HETD ;

Module STS II : TD en Signaux stochastiques II.

Master en Ingénierie Electrique. 16 HETD ;

Module TAV : TD en Imagerie tomographique.

Master en Ingénierie Electrique. 16 HETD ;

Module UIM : TP en Échographie médicale.

Master en Ingénierie Electrique. 3 HETD.

2007–2009 : **Université de Hull, Angleterre.**

Module 57020 : Dynamique.

Licence en Génie Mécanique. 10 crédits ;

Module 57034 : Tension mécanique.

Licence en Génie Mécanique. 5 crédits ;

Module 57041 : Analyse de tension.

Licence en Génie Mécanique. 5 crédits ;

Module 57042 : Acoustique.

Licence en Génie Mécanique. 5 crédits ;

Module 57064 : L'imagerie médicale.

Master en Génie Médicale. 5 crédits.

2010 : **Université d'Orléans – UPR 4301, France.**

Module : Bioimagerie.

Master en Biochimie, Biologie Moléculaire et Biotechnologie. 8 HETD.

2012 : **Institut Israélien de Technologie Technion, Israël.**

Module 336325 : Ultrasons médicaux : principe et application.

Master en Génie Médicale. 10 crédits.

2010–2014 : **Université de Bergen, Norvège.**

Module PHYS212 : Physique et technologie médicales.

Master en Physique Médicale. 5 crédits ;

Module PHYS371 : Acoustique sous-marine.

Master en Physique Acoustique. 10 crédits ;

Module PHYS372 : Acoustique non-linéaire.

Master en Physique Acoustique. 10 crédits.

2012 : **Université de Dundee, Écosse.**

Module PH12001 : Phénomènes astronomiques.

Licence en Physique. 10 crédits.

2014 : **Université de Hokkaidō, Japon.**

Module IST_BIO 5130 : Ingénierie des systèmes médicaux.

Master en Génie Médicale. 4 HETD.

2015 : **UMI Georgia Tech – CNRS 2958, France.**

Module ECE 8002 – ME 8002 : Séminaire de master.

Master en Ingénierie Electrique et Génie Mécanique. 4 HETD.

2015 : **Université du Cap, Afrique du Sud.**

Module HUB4045F : Introduction à l'imagerie médicale et au traitement d'images.

Master en Génie Médicale. 6 HETD.

2015 : **Université du Witwatersrand, Afrique du Sud.**

Module ELEN3008 : Mesure biomédicale, instrumentation et imagerie.

Master en Ingénierie Electrique. 12 HETD.

Séminaires externes

2003 : **University College de Londres, Angleterre.**

Master en Génie Mécanique. 2 HETD.

2007 : **Université catholique néerlandophone de Louvain, Belgique.**

Master en Physique. 2 HETD.

2010–2013 : **Institut Israélien de Technologie Technion, Israël.**

Master en Génie Médicale. 12 HETD.

2010 : **Université de Bergen, Norvège.**

Master en Physique. 4 HETD.

2011 : **Université de Southampton, Angleterre.**

Master en Ingénierie Acoustique. 2 HETD.

2011 : **Université de Caroline du Nord à Chapel Hill, États-Unis.**

Master en Génie Médicale. 2 HETD.

2011 : **Université norvégienne de sciences et de technologie, Norvège.**

Master en Physique. 2 HETD.

2013 : **Université de l'Est de la Finlande, Finlande.**

Master en Sciences Naturelles et Sylviculture. 2 HETD.

2014 : **Université d'État de Moscou, Russe.**

Master en Physique. 2 HETD.

2015 : **Université catholique néerlandophone de Louvain, Belgique.**

Master en Biotechnologie. 2 HETD.

2015 : **Université du Witwatersrand, Afrique du Sud.**

Master en Physique. 2 HETD.

I.1.5 Encadrement d'étudiants

Doctorat

2007–2010 : Winder PN	PhD Elec Eng	Université de Hull ($2^{\text{ième}}$ co-encadrant)
2008–2011 : Kotopoulis S	PhD Mech Eng	Université de Hull
2009–2012 : Siepmann AM	PhD Elec Eng	Ruhr-Université de Bochum ($2^{\text{ième}}$ co-encadrant)

Master

2006 : Mleczko M	MSc Elec Eng	Ruhr-Université de Bochum ($2^{\text{ième}}$ co-encadrant)
2006 : Schultz S	MSc Elec Eng	Ruhr-Université de Bochum *(Studienarbeit)*
2008 : Schommartz A	MSc Elec Eng	Ruhr-Université de Bochum / Université de Hull *(Studienarbeit)*
2009 : Katsamatsa MI	MEng Mech Eng	Université de Hull
2015 : Johansen K	MSc Phys	Université de Bergen
2015 : Yddal T	MSc Phys	Université de Bergen
2017 : Abraham H	MSc Med Eng	Université d'Addis Ababa ($2^{\text{ième}}$ co-encadrant)
2017 : Malan K	MSc Elec Eng	Université du Witwatersrand ($2^{\text{ième}}$ co-encadrant)

Licence

2009 : Bonner AP	BEng Mech Eng	Université de Hull
2009 : Holland SJR	BSc Design Tech	Université de Hull
2009 : Keir DG	BEng Mech Eng	Université de Hull
2009 : McKeegan MJ	BEng Mech Med Eng	Université de Hull
2009 : Murray N	BEng Mech Eng	Université de Hull

Examinateur externe

2008 : Burns J	PhD Phys	Université de Dundee
2011 : Delalande A	Dr Cell Mol Biol	Université d'Orléans
2012 : Dixon TL	MSc Biomed Eng	Université du Cap
2012 : Tezoo T	MSc Biomed Eng	Université du Cap
2013 : Leskinen JTT	PhD Forestry Nat Sci	Université de l'Est de la Finlande
2013 : Mazzawi N	MSc Biomed Eng	Institut Israélien de Technologie
2013 : Stipdonk HL	Dr Tech Pol Man	Université de Technologie de Delft
2013 : Zantow M	MSc Biomed Eng	Université du Cap
2014 : Perks TD	MSc Biomed Eng	Université du Cap
2015 : Assa M	PhD Biomed Eng	Institut Israélien de Technologie
2015 : Rovers T	Dr Food Phys	Université de Wageningen
2016 : Dung LT	PhD Phys	Nanyang Université de Technologie

I.1.6 Activités administratives

Organisation de congres internationaux

2011–2023 : Membre du conseil d'administration du congrès international d'ultrasons ICU.

2011 : Organisateur de la conférence « Workshop on Micro-acoustics in Marine and Medical Research », Bergen, Norvège.

2014 : Co-organisateur de la conférence « 2nd Workshop on Micro-acoustics in Marine and Medical Research », Druskinkai, Litovie.

2015–2017 : Membre du conseil d'administration de la conférence internationale pour les scientifiques jeunes « Wave Electronics and its Applications in Information and Telecommunication Systems ».

2015 : Co-organisateur de la conférence « 3rd Workshop on Micro-acoustics in Marine and Medical Research », Valaam, Russe.

Sociétés savantes

2008 : Membre senior de l'IEEE.

2008 : Compagnon (Fellow) de l'Institut d'Acoustique IOA.

Editeur associé

2009–2014 : Bubble Science, Engineering and Technology. Maney.

2010–2018 : Applied Acoustics. Elsevier.

2012–2018 : Ultrasonics. Elsevier.

2013–2018 : IEEE Transactions on Ultrasonics, Ferroelectrics, and Frequency Control. IEEE.

I.2 Liste de publications

I.2.1 Publications dans des revues à comité de lecture, articles de synthèse et actes de colloque

Publications dans des revues à comité de lecture

1. Johansen K, Kimmel E, Postema M. Theory of red blood cell oscillations in an ultrasound field. Archives of Acoustics 2017 ; 42(1) : 121–126.
2. Kujawska T, Secomski W, Byra M, Postema M, Nowicki A. Annular phased array transducer for preclinical testing of anti-cancer drug efficacy on small animals. Ultrasonics 2017 ; 76 : 92–98.
3. Stapelmann K, Fiebrandt M, Lackmann JW, Raguse M, Postema M, Moeller R, Awakowicz P. A combined low-pressure hydrogen peroxide evaporation plus hydrogen plasma treatment method for sterilization. Part 1 : characterization of the condensation process and proof-of-concept. Plasma Processes and Polymers 2017 ; e1600198 : 1–10.
4. van Leusden P, den Hartog GJM, Bast A, Postema M, van der Linden E, Sagis LMC. Permeation of probe molecules into alginate microbeads : effect of salt and processing. Food Hydrocolloids 2017 ; 73 : 255–261.
5. Dimcevski G, Kotopoulis S, Bjånes T, Hoem D, Schjøtt J, Gjertsen BT, Biermann M, Molven A, Sorbye H, Mc Cormack E, Postema M, Gilja OH. A human clinical trial using ultrasound and microbubbles to enhance gemcitabine treatment of inoperable pancreatic cancer. Journal of Controlled Release 2016 ; 243 : 172–181.
6. Johansen K, Postema M. Lagrangian formalism for computing oscillations of spherically symmetric encapsulated acoustic antibubbles. Hydroacoustics 2016 ; 19 : 197–208.
7. Klimonda Z, Postema M, Nowicki A, Litniewski J. Tissue attenuation estimation by mean frequency downshift and bandwidth limitation. IEEE Transactions on Ultrasonics, Ferroelectrics, and Frequency Control 2016 ; 63(8) : 1107–1115.
8. van Leusden P, den Hartog GJM, Bast A, Postema M, van der Linden E, Sagis LMC. Strength of microbeads for the encapsulation of heat sensitive, hydrophobic components. Food Hydrocolloids 2016 ; 56(1) : 318–324.
9. van Leusden P, den Hartog GJM, Bast A, Postema M, van der Linden E, Sagis LMC. Structure engineering of filled protein microbeads to tailor release of oil droplets in gastric digestion. Food and Function 2016 ; 7 : 3539–3547.

10. Yddal T, Gilja OH, Cochran S, Postema M, Kotopoulis S. Glass-windowed ultrasound transducers. Ultrasonics 2016 ; 68 : 108–119.

11. Delalande A, Leduc C, Midoux P, Postema M, Pichon C. Efficient gene delivery by sonoporation is associated with microbubble entry into cells and the Clathrin-dependent endocytosis pathway. Ultrasound in Medicine and Biology 2015 ; 41(7) : 1913–1926.

12. Kotopoulis S, Johansen K, Gilja OH, Poortinga AT, Postema M. Acoustically active antibubbles. Acta Physica Polonica A 2015 ; 127(1) : 99–102.

13. Mazzawi N, Postema M, Kimmel E. Bubble-like response of living blood cells and microparticles in an ultrasound field. Acta Physica Polonica A 2015 ; 127(1) : 103–105.

14. Yddal T, Cochran S, Gilja OH, Postema M, Kotopoulis S. Open-source, high-throughput, ultrasound treatment chamber. Biomedizinische Technik 2015 ; 60(1) : 77–87.

15. Johston K, Tapia-Siles C, Gerold B, Postema M, Cochran S, Cuschieri A, Prentice P. Periodic shock-emission from acoustically driven cavitation clouds : a source of the subharmonic signal. Ultrasonics 2014 ; 54(8) : 2151–2158.

16. Kotopoulis S, Delalande A, Popa M, Mamaeva V, Dimcevski G, Gilja OH, Postema M, Gjertsen BT, Mc Cormack E. Sonoporation-enhanced chemotherapy significantly reduces primary tumour burden in an orthotopic pancreatic cancer xenograft. Molecular Imaging and Biology 2014 ; 16(1) : 53–62.

17. Kotopoulis S, Dimcevski G, Gilja OH, Hoem D, Postema M. Treatment of human pancreatic cancer using combined ultrasound, microbubbles, and gemcitabine : a clinical case study. Medical Physics 2013 ; 40(7) : 072902(1–9).

18. Delalande A, Bouakaz A, Renault G, Tabareau F, Kotopoulis S, Midoux P, Arbelle B, Uzbekov R, Chakravarti S, Postema M, Pichon C. Ultrasound and microbubble-assisted gene delivery in Achilles tendons : long lasting gene expression and restoration of fibromodulin KO phenotype. Journal of Controlled Release 2011 ; 156(2) : 223–230.

19. Delalande A, Kotopoulis S, Rovers T, Pichon C, Postema M. Sonoporation at a low mechanical index. Bubble Science, Engineering and Technology 2011 ; 3(1) : 3–11.

20. Gerold B, Kotopoulis S, McDougall C, McGloin D, Postema M, Prentice P. Laser-nucleated acoustic cavitation in focused ultrasound. Review of Scientific Instruments 2011 ; 82(4) : 044908.

21. Kotopoulis S, Wang H, Cochran S, Postema M. Lithium niobate transducers for MRI-guided ultrasonic microsurgery. IEEE Transactions on Ultrasonics, Ferroelectrics and Frequency Control 2011 ; 58(8) : 1570–1576.

22. Kotopoulis S, Postema M. Microfoam formation in a capillary. Ultrasonics 2010 ; 50(2) : 260–268.

23. Aygün H, Attenborough K, Postema M, Lauriks W, Langton CM. Predicted angle dependent tortuosity and elasticity effects on sound propagation in cancellous bone. Journal of the Acoustical Society of America 2009 ; 126(6) : 3286–3290.

24. Kotopoulis S, Schommartz A, Postema M. Sonic cracking of blue-green algae. Applied Acoustics 2009 ; 70(10) : 1306–1312.

25. Mleczko M, Postema M, Schmitz G. Discussion of the application of finite Volterra series for the modeling of the oscillation behavior of ultrasound contrast agents. Applied Acoustics 2009 ; 70(10) : 1363–1369.

26. Postema M, Schmitz G. Ultrasonic bubbles in medicine : influence of the shell. Ultrasonics Sonochemistry 2007 ; 14(4) : 438–444.

27. Postema M, ten Cate FJ, Schmitz G, de Jong N, van Wamel A. Generation of a droplet inside a microbubble with the aid of an ultrasound contrast agent : first result. Letters in Drug Design & Discovery 2007 ; 4(1) : 74–77.

28. Postema M, Bouakaz A, ten Cate FJ, Schmitz G, de Jong N, van Wamel A. Nitric oxide delivery by ultrasonic cracking : some limitations. Ultrasonics 2006 ; 44(S1) : e109–e113.

29. Postema M, Bouakaz A, Versluis M, de Jong N. Ultrasound-induced gas release from contrast agent microbubbles. IEEE Transactions on Ultrasonics, Ferroelectrics and Frequency Control 2005 ; 52(6) : 1035–1041.

30. Postema M, van Wamel A, ten Cate FJ, de Jong N. High-speed photography during ultrasound illustrates potential therapeutic applications of microbubbles. Medical Physics 2005 ; 32(12) : 3707–3711.

31. Postema M, Bouakaz A, de Jong N. Noninvasive microbubble-based pressure measurements : a simulation study. Ultrasonics 2004 ; 42(1-9) : 759–762.

32. Postema M, Marmottant P, Lancée CT, Hilgenfeldt S, de Jong N. Ultrasound-induced microbubble coalescence. Ultrasound in Medicine and Biology 2004 ; 30(10) : 1337–1344.

33. Postema M, van Wamel A, Lancée CT, de Jong N. Ultrasound-induced encapsulated microbubble phenomena. Ultrasound in Medicine and Biology 2004 ; 30(6) : 827–840.

34. Postema M, Bouakaz A, Chin CT, de Jong N. Simulations and measurements of optical images of insonified ultrasound contrast microbubbles. IEEE Transactions on Ultrasonics, Ferroelectrics and Frequency Control 2003 ; 50(5) : 523–536.

Articles de synthèse

35. Aygün H, Attenborough K, Postema M. A review of the state of art in applying Biot theory to acoustic propagation through the bone. Open Access Library Journal 2014 ; 1 : e994-1–e994-12.

36. Delalande A, Kotopoulis S, Postema M, Midoux P, Pichon C. Sonoporation : mechanistic insights and ongoing challenges for gene transfer. Gene 2013 ; 525(2) : 191–199.

37. Delalande A, Postema M, Mignet N, Midoux P, Pichon C. Ultrasound and microbubble-assisted gene delivery : recent advances and ongoing challenges. Therapeutic Delivery 2012 ; 3(10) : 1199–1215.

38. Postema M, Gilja OH. Contrast-enhanced and targeted ultrasound. World Journal of Gastroenterology 2011 ; 17(1) : 28–41.

39. Postema M, Gilja OH. Ultrasound-directed drug delivery. Current Pharmaceutical Biotechnology 2007 ; 8(6) : 355–361.

40. Postema M, Schmitz G. Bubble dynamics involved in ultrasonic imaging. Expert Review of Molecular Diagnostics 2006 ; 6(3) : 493–502.

Actes de colloque

41. Johansen K, Kotopoulis S, Poortinga AT, Postema M. Nonlinear echoes from encapsulated antibubbles. Physics Procedia 2015 ; 70 : 1079–1082.

42. Johansen K, Kotopoulis S, Postema M. Introduction to antibubbles. In : Proceedings of the 38th Scandinavian Symposium on Physical Acoustics. Bergen : Norwegian Physical Society 2015 (ISBN 978-82-8123-013-2) 1–6.

43. Johansen K, Kotopoulis S, Postema M. Ultrasonically driven antibubbles encapsulated by Newtonian fluids for active leakage detection. Lecture Notes in Engineering and Computer Science 2015 ; 2216 : 750–754.

44. Johansen K, Yddal T, Kotopoulis S, Postema M. Acoustic filtering of particles in a flow regime. IEEE International Ultrasonics Symposium Proceedings 2014 : 1436–1439.

45. Kotopoulis S, Dimcevski G, Gjertsen BT, Gilja OH, Mc Cormack E, Postema M. Sonoporation : from the lab to human clinical trials. IEEE International Ultrasonics Symposium Proceedings 2014 : 846–849.

46. Kotopoulis S, Haugse R, Mujić M, Sulen A, Gullaksen SE, Mc Cormack E, Gilja OH, Postema M, Gjertsen BT. Evaluation of the effects of clinical diagnostic ultrasound

in combination with ultrasound contrast agents on cell stress : single cell analysis of intracellular phospho-signaling pathways in blood cancer cells and normal blood leukocytes. IEEE International Ultrasonics Symposium Proceedings 2014 : 1186–1190.

47. Yddal T, Kotopoulis S, Gilja OH, Cochran S, Postema M. Transparent glass-windowed ultrasound transducers. IEEE International Ultrasonics Symposium Proceedings 2014 : 2079–2082.

48. Kotopoulis S, Eder SD, Greve MM, Holst B, Postema M. Lab-on-a-chip device for fabrication of therapeutic microbubbles on demand. Biomedizinische Technik 2013 ; 58(S1) : #4037.

49. Kotopoulis S, Delalande A, Pichon C, Postema M. Real-time sonoporation through HeLa cells. AIP Conference Proceedings 2012 ; 1474 : 271-274.

50. Kotopoulis S, Wang H, Cochran S, Postema M. High-frequency transducer for MR-guided FUS. Biomedizinische Technik 2012 ; 57(S1) : #972.

51. Kotopoulis S, Postema M. Therapeutic ultrasound and sonoporation. Biomedizinische Technik 2011 ; 56(S1) : #525.

52. Stapelmann K, Lackmann J, Bibinov N, Bandow JE, Postema M, Awakowicz P. Characterization of a novel VHF-CCP for sterilization and decontamination of medical instruments. Proceedings of the 20th International Symposium on Plasma Chemistry 2011 : #368.

53. Delalande A, Bouakaz A, Midoux P, Postema M, Pichon C. Ultrasound-activated microbubbles for tendon gene transfer : in vivo efficiency and confocal microscopy real time intracellular investigations. Proceedings of the International Congress on Acoustics 2010 : #524.

54. Kotopoulis S, Postema M. Forming morphing microfoam. Proceedings of the International Congress on Acoustics 2010 : #25.

55. Kotopoulis S, Wang H, Cochran S, Postema M. Lithium niobate ultrasound transducers for high-resolution focused ultrasound surgery. IEEE International Ultrasonics Symposium Proceedings 2010 : 72–75.

56. Postema M, Gilja OH. Jetting does not cause sonoporation. Biomedizinische Technik 2010 ; 55(S1) : 19–20.

57. Winder P, Postema M, Paulson K. Noise reduction in acoustic disdrometry. Acta Acustica united with Acustica 2009 ; 95(S1) : S123.

58. Kotopoulis S, Schommartz A, Postema M. Safety radius for algae eradication at 200 kHz – 2.5 MHz. IEEE International Ultrasonics Symposium Proceedings 2008 1706–1709.

59. Stipdonk H, van Toorenburg J, Postema M. Phase diagram distortion from traffic parameter averaging. European Transport Conference (ETC) Proceedings 2008 : #3534.

60. Mleczko M, Wilkening WG, Postema M, Schmitz G. Optimisation of pulse sequences for ultrasound contrast agent imaging. Biomedizinische Technik 2007 ; 52(S1) : #G2.

61. Mleczko M, Postema M, Schmitz G. Identifying nonlinear characteristics for the bulk response of ultrasound contrast agent. IEEE International Ultrasonics Symposium Proceedings 2006 : 1369–1372.

62. Mleczko M, Postema M, Schmitz G. Nonlinear modeling of ultrasound contrast agents with Wiener series. Gemeinsame Jahrestagung der Deutschen, Österreichischen und Schweizerischen Gesellschaft für Biomedizinische Technik 2006 : #V77.

63. Postema M, Mleczko M, Schmitz G. Contrast microbubble clustering at high MI. IEEE International Ultrasonics Symposium Proceedings 2006 : 1564–1567.

64. Postema M, Mleczko M, Schmitz G. Experimental setup for synchronous optical and acoustical observation of contrast microbubbles. Gemeinsame Jahrestagung der Deutschen, Österreichischen und Schweizerischen Gesellschaft für Biomedizinische Technik 2006 : #V75.

65. Chaudhry SK, Khaled W, Postema M, Ermert H, Schmitz G. Accelerated block-based 2D motion estimation for pre-processing in elastography. Biomedizinische Technik 2005 ; 50(S1) : S637–S638.

66. Mienkina MP, Postema M, Hansen C, Schmitz G. Modelling ultrasonic backscattering of an SPIO-MRI contrast agent. Biomedizinische Technik 2005 ; 50(S1) : 750–751.

67. Postema M, de Jong N, Schmitz G. Shell rupture threshold, fragmentation threshold, Blake threshold. IEEE International Ultrasonics Symposium Proceedings 2005 ; 3 : 1708–1711.

68. Postema M, de Jong N, Schmitz G. The physics of nanoshelled microbubbles. Biomedizinische Technik 2005 ; 50(S1) : 748–749.

69. Postema M, de Jong N, Schmitz G, van Wamel A. Creating antibubbles with ultrasound. IEEE International Ultrasonics Symposium Proceedings 2005 ; 2 : 977–980.

70. Postema M, Schmitz G. Ultrasonic fragmentation of microbubbles : a theoretical approach of the flash in flash-echo. IEEE Engineering in Medicine and Biology Society. Conference

Proceedings 2005 : 4023–4026.

71. Postema M, Marmottant P, Lancée CT, Versluis M, Hilgenfeldt S, de Jong N. Ultrasound-induced coalescence of free gas microbubbles. IEEE International Ultrasonics Symposium Proceedings 2004 ; 1 : 1–4.

72. Postema M, Bouakaz A, Chin CT, de Jong N. Optically observed microbubble coalescence and collapse. IEEE International Ultrasonics Symposium Proceedings 2002 ; 2 : 1900–1903.

73. Postema M, Bouakaz A, Chin CT, de Jong N. Real-time optical imaging of individual microbubbles in an ultrasound field. IEEE International Ultrasonics Symposium Proceedings 2001 ; 2 : 1679–1682.

Editoriaux

74. Kulakov SV, Postema M, Voloshinov VB, Yakimov AN, Bugaev A. Wave electronics and applications thereof in information and telecommunication systems. Applied Acoustics 2016 ; 112 : 116.

75. Postema M, Kotopoulis S, Delalande A, Gilja OH. Sonoporation : why microbubbles create pores. Ultraschall in der Medizin 2012 ; 33(1) : 97–98.

76. Postema M. Bubbles and ultrasound. Applied Acoustics 2009 ; 70(10) : 1035.

I.2.2 Ouvrages et chapitres d'ouvrage

Ouvrages

77. Kotopoulis S, Delalande A, Godø OR, Postema M, Eds. Micro-acoustics in marine and medical research. Bergen : UiB 2012 (ISBN 978-82-303-1945-1).
78. Postema M. Fundamentals of Medical Ultrasonics. London : Spon Press 2011 (ISBN 978-0-415-56353-6).
79. Attenborough K, Postema M. A pocket-sized introduction to acoustics. Kingston upon Hull : University of Hull 2008 (ISBN 978-9081258821).
80. Attenborough K, Postema M. A pocket-sized introduction to dynamics. Kingston upon Hull : University of Hull 2008 (ISBN 978-9081258838).
81. Fagan MJ, Postema M. Introduction to stress and strain analysis. Kingston upon Hull : University of Hull 2007 (ISBN 978-9081258814).
82. Postema M. Medical Bubbles. Veenendaal : Universal Press 2004 (ISBN 90-365-2037-1).

Chapitres d'ouvrage

83. Postema M, Kotopoulis S, Jenderka KV. Basic principles : basic physical principles of medical ultrasound. In : Dietrich CF, Ed. EFSUMB — European Course Book. London : EFSUMB 2012 9-26.
84. Postema M. Bubble physics. In : Postema M. Fundamentals of Medical Ultrasonics. London : Spon press 2011 (ISBN 978-0-415-56353-6) 177–204.
85. Postema M. Introduction. In : Postema M. Fundamentals of Medical Ultrasonics. London : Spon press 2011 (ISBN 978-0-415-56353-6) 17–24.
86. Postema M, Attenborough K. Vibrations. In : Postema M. Fundamentals of Medical Ultrasonics. London : Spon press 2011 (ISBN 978-0-415-56353-6) 51–61.
87. Postema M, Attenborough K. Waves and sound. In : Postema M. Fundamentals of Medical Ultrasonics. London : Spon press 2011 (ISBN 978-0-415-56353-6) 63–87.
88. Postema M, Fagan MJ. Stress, strain and elasticity. In : Postema M. Fundamentals of Medical Ultrasonics. London : Spon press 2011 (ISBN 978-0-415-56353-6) 25–49.
89. Postema M, Gilja OH, van Wamel A. CEUS and sonoporation. In : Postema M. Fundamentals of Medical Ultrasonics. London : Spon press 2011 (ISBN 978-0-415-56353-6) 205–217.

90. Hiltawsky KM, Haisch C, Mienkina MP, Postema M, Schmitz G. Optoakustik in der medizinischen Bildgebung. In : Niederlag W, Lemke HU, Semmler W, Bremer C, Eds. Molecular imaging : Innovationen und Visionen in der medizinischen Bildgebung. Dresden : Health Academy 2006 (ISBN 3-00-017900-3) 177–192.

91. Postema M, Hiltawsky KM, Schmitz G. Ultraschallkontrastmittel — Grundlegende Überlegungen. In : Niederlag W, Lemke HU, Semmler W, Bremer C, Eds. Molecular imaging : Innovationen und Visionen in der medizinischen Bildgebung. Dresden : Health Academy 2006 (ISBN 3-00-017900-3) 221–236.

I.2.3 Communications et conférences

92. Dimcevski GG, Kotopoulis S, Bjånes T, Hoem D, Schjøtt J, Gjertsen BT, Biermann M, Molven A, Sorbye H, Mc Cormack E, Postema M, Gilja OH. Ultrasound and microbubble enhanced treatment of inoperable pancreatic adeonocarcinoma. Journal of Clinical Oncology 2016 ; 34(15) : e15703.
93. Johansen K, Kotopoulis S, Poortinga AT, Postema M. Harmonic antibubbles. Archives of Acoustics 2016 ; 41(2) : 364.
94. Kotopoulis S, Dimcevski G, Mc Cormack E, Postema M, Gjertsen BT, Gilja OH. Ultrasound- and microbubble-enhanced chemotherapy for treating pancreatic cancer : a phase I clinical trial. Journal of the Acoustical Society of America 2016 ; 139 : 2092.
95. Johansen K, Kotopoulis S, Poortinga AT, Postema M. Antibubbles. In : Bestugin A, Kulakov S, Yakimov A, Eds. XVIII International Conference for Young Researchers. Wave Electronics and its Applications in the Information and Telecommunication Systems. St. Petersburg : St. Petersburg State University of Aerospace Instrumentation 2015 (ISBN 978-5-8088-1000-6) 15.
96. Johansen K, Kotopoulis S, Postema M. Active leakage detection by searching for antibubbles. In : Bestugin A, Kulakov S, Yakimov A, Eds. XVIII International Conference for Young Researchers. Wave Electronics and its Applications in the Information and Telecommunication Systems. St. Petersburg : St. Petersburg State University of Aerospace Instrumentation 2015 (ISBN 978-5-8088-1000-6) 16–17.
97. Kotopoulis S, Dimcevski G, Hoem D, Postema M, Gilja OH. Ultrasound sonoporation in pancreatic adenocarcinoma. Ultrasound in Medicine and Biology 2015 ; 41(4) : S94.
98. Kotopoulis S, Wang H, Yddal T, Cochran S, Gilja OH, Postema M. Novel multipurpose, low cost, modular, ultrasound transducers. In : Bestugin A, Kulakov S, Yakimov A, Eds. XVIII International Conference for Young Researchers. Wave Electronics and its Applications in the Information and Telecommunication Systems. St. Petersburg : St. Petersburg State University of Aerospace Instrumentation 2015 (ISBN 978-5-8088-1000-6) 17–18.
99. Kotopoulis S, Johansen K, Poortinga A, Gilja OH, Postema M. Acoustically active antibubbles for ultrasound imaging and targeted drug delivery. In : Gilja OH, Haraldseth O, Nortvedt R, Eds. The 2014 Joint National PhD Conference in Medical Imaging and MedViz Conference. Bergen : Medim, MedViz, Haukeland University Hospital, University of Bergen, Christian Michelsen Research Bergen 2014 (ISBN 978-82-998920-3-2) 115.

100. Yddal T, Kotopoulis S, Gilja OH, Postema M. Ultrasound transducers with an optical window. In : Gilja OH, Haraldseth O, Nortvedt R, Eds. The 2014 Joint National PhD Conference in Medical Imaging and MedViz Conference. Bergen : Medim, MedViz, Haukeland University Hospital, University of Bergen, Christian Michelsen Research Bergen 2014 (ISBN 978-82-998920-3-2) 36.

101. Dimcevski G, Kotopoulis S, Hoem D, Postema M, Gjertsen BT, Bjånes TK, Biermann M, Mc Cormack E, Sorbye H, Molven A, Gilja OH. Ultrasound-assisted treatment of an inoperable pancreatic cancer. In : Nortvedt R, Gilja OH, Eds. MedViz Conference 2013. Bergen : MedViz, Haukeland University Hospital, University of Bergen, Christian Michelsen Research Bergen 2013 (ISBN 978-82-998920-1-8) 49–52.

102. Kotopoulis S, Delalande A, Popa M, Dimcevski G, Gilja OH, Postema M, Gjertsen BT, Mc Cormack E. Ultrasound and microbubble enhanced therapy of orthotopic human pancreatic cancer in mice. In : Nortvedt R, Gilja OH, Eds. MedViz Conference 2013. Bergen : MedViz, Haukeland University Hospital, University of Bergen, Christian Michelsen Research Bergen 2013 (ISBN 978-82-998920-1-8) 45–47.

103. Kotopoulis S, Haugse R, Postema M. Sonoporation : the hurdles that need to be surpassed. In : Nortvedt R, Gilja OH, Eds. MedViz Conference 2013. Bergen : MedViz, Haukeland University Hospital, University of Bergen, Christian Michelsen Research Bergen 2013 (ISBN 978-82-998920-1-8) 41–42.

104. Kotopoulis S, Postema M. High-speed photography of encapsulated microbubbles. Abstracts of Papers of the American Chemical Society 2013 ; 245 : 198-COLL.

105. Kotopoulis S, Postema M. Using ultrasound to separate oil, gas, and water. In : Crocker MJ, Pawelczyk M, Paosawatyanyong B, Eds. Proceedings of the 20th International Congress on Sound and Vibration : Recent Developments in Acoustics, Noise and Vibration, 2013. Bangkok : International Institute of Acoustics and Vibration 2013 (ISBN 978-616-551-682-2) #512.

106. Mujić M, Haugse R, Kotopoulis S, Sulen A, Gilja OH, Postema M, Gjertsen BT. Ultrasound combined with microbubbles modulates signal transduction pathways in blood cells. In : Nortvedt R, Gilja OH, Eds. MedViz Conference 2013. Bergen : MedViz, Haukeland University Hospital, University of Bergen, Christian Michelsen Research Bergen 2013 (ISBN 978-82-998920-1-8) 119–120.

107. Delalande A, Kotopoulis S, Pichon C, Gjertsen BT, Postema M. Microbubbles and cell interactions. In : Dimcevski GG, Gilja OH, Eds. MedViz Conference 2012. Bergen :

MedViz, Haukeland University Hospital, University of Bergen, Christian Michelsen Research 2012 (ISBN 978-82-998920-0-1) 53–54.

108. Kotopoulis S, Delalande A, Pichon C, Postema M. Nonlinear microbubble behaviour for enhanced drug uptake. In : Čiplys D, Ed. Recent Developments in Acoustics, Noise and Vibration. Vinius : International Institute of Acoustics and Vibration, Vilnius University 2012 (ISBN 978-609-459-079-5) #685.

109. Kotopoulis S, Delalande A, Pichon C, Postema M. Sonoporation : using ultrasound for targeted drug delivery. In : Dimcevski GG, Gilja OH, Eds. MedViz Conference 2012. Bergen : MedViz, Haukeland University Hospital, University of Bergen, Christian Michelsen Research 2012 (ISBN 978-82-998920-0-1) 49–51.

110. Postema M. Nonlinear microbubble behaviour for enhanced drug uptake. In : Čiplys D, Ed. The 19th International Congress on Sound and Vibration. Vilnius : International Institute of Acoustics and Vibration, Vilnius University 2012 (ISBN 978-609-459-080-1) 129.

111. Delalande A, Kotopoulis S, Midoux P, Postema M, Pichon C. Ultrasound and microbubble-assisted gene delivery : insights for intracellular mechanism. In : Kotopoulis S, Delalande A, Godø OR, Postema M, Eds. Micro-acoustics in marine and medical research. Bergen : UiB 2012 (ISBN 978-82-303-1945-1) 119–130.

112. Gerold B, Kotopoulis S, Cochran S, Postema M, Prentice P. Hybrid laser-ultrasound cavitation for cloud evolution studies. In : Kotopoulis S, Delalande A, Godø OR, Postema M, Eds. Micro-acoustics in marine and medical research. Bergen : UiB 2012 (ISBN 978-82-303-1945-1) 51–60.

113. Kotopoulis S, Delalande A, Godø OR, Postema M. Preface. In : Kotopoulis S, Delalande A, Godø OR, Postema M, Eds. Micro-acoustics in marine and medical research. Bergen : UiB 2012 (ISBN 978-82-303-1945-1) 5.

114. Kotopoulis S, Delalande A, Pichon C, Postema M. Biological and medical applications of low-intensity ultrasound. In : Kotopoulis S, Delalande A, Godø OR, Postema M, Eds. Micro-acoustics in marine and medical research. Bergen : UiB 2012 (ISBN 978-82-303-1945-1) 67–105.

115. Mujić M, Kotopoulis S, Delalande A, Enger M, Gilja OH, Mc Cormack E, Postema M, Gjertsen BT. Flow cytometic characterization and sorting of ultrasound contrast agents. In : Kotopoulis S, Delalande A, Godø OR, Postema M, Eds. Micro-acoustics in marine and medical research. Bergen : UiB 2012 (ISBN 978-82-303-1945-1) 171–183.

116. Delalande A, Kotopoulis S, Midoux P, Postema M, Pichon C. Cell-microbubble interaction and intracellular fate of plasmid DNA and microbubbles during the sonoporation process. In : Linde BBJ, Markiewicz A, Ponikwicki N, Eds. International Congress on Ultrasonics : ICU 2011. Gdańsk : University of Gdańsk Publishing 2011 (ISBN 978-83-7531-215-7) 323–324.

117. Delalande A, Kotopoulis S, Pichon C, Postema M. Cancer cell sonoporation at low acoustic amplitudes. In : 18th International Congress on Sound & Vibration. Auburn : International Institute of Acoustics and Vibration 2011 (ISBN 978-85-63243-01-0) S34-1645.

118. Delalande A, Kotopoulis S, Pichon C, Postema M. Sonoporation at a low MI. Ultrasound in Medicine and Biology 2011 ; 37(8S) : S61.

119. Delalande A, Midoux P, Pichon C, Kotopoulis S, Postema M. Investigations of microbubble-cell interactions during the sonoporation process. In : 18th International Congress on Sound & Vibration. Auburn : International Institute of Acoustics and Vibration 2011 (ISBN 978-85-63243-01-0) S34-1644.

120. Kotopoulis S, Delalande A, Pichon C, Postema M. On cells and sound. In : Korneliussen RJ, Ed. Proceedings of the 34th Scandinavian Symposium on Physical Acoustics, Geilo, Norway, 30 January - 2 February 2011. Trondheim : Norwegian Physical Society 2011 (ISBN 978-82-8123-004-0).

121. Kotopoulis S, Postema M. Biomedical ultrasonics, cavitation, and sonoporation. In : Linde BBJ, Markiewicz A, Ponikwicki N, Eds. International Congress on Ultrasonics : ICU 2011. Gdańsk : University of Gdańsk Publishing 2011 (ISBN 978-83-7531-215-7) 317–318.

122. Kotopoulis S, Postema M, Cochran S. Ultrasound transducers made with lithium niobate for HF HIFU. In : Linde BBJ, Markiewicz A, Ponikwicki N, Eds. International Congress on Ultrasonics : ICU 2011. Gdańsk : University of Gdańsk Publishing 2011 (ISBN 978-83-7531-215-7) 318–319.

123. Postema M. CEUS and sonoporation. In : Haslene-Hox H, Silden E, Mujić M, Matre K, Mc Cormack EM, Eds. 2011 Joint National Ph.D. Conference in Medical Imaging and MedViz Conference. Bergen : Norwegian Research School in Medical Imaging, MedViz, University of Bergen 2011 (ISBN 978-82-993786-6-6) 49.

124. Postema M, Kotopoulis S, Delalande A, Gilja OH. Ultrasound-guided delivery and sonoporation. In : Ultrasound in Gastroenterology : 10-years Anniversary of National

Centre for Ultrasound in Gastroenterology. A Symposium in Honour of Professor Svein Ødegaard. Bergen : National Centre for Ultrasound in Gastroenterology 2011 (ISBN 978-82-303-1950-5) 57-59. 124. Postema M. Physical principles of CEUS and sonoporation. In : Nylund K, Gilja OH, Ødegaard S, Eds. Abdominal ultrasound – focus on CEUS and EUS. Bergen : National Centre for Ultrasound in Gastroenterology 2010 (ISBN 9788299263429) 23–26.

125. Winder P, Postema M, Paulson K. Noise reduction in acoustic disdrometry. In : Institute of Acoustics (IOA). 8th European Conference on Noise Control 2009 (EURONOISE 2009). Red Hook : Curran Associates, Inc. 2009 (ISBN 978-1615676804) #3.

126. Postema M, Schommartz A. Bubbles, ultrasound, and swimmer safety. In : Institute of Acoustics (IOA). Spring Conference of the Institute of Acoustics 2008 : Widening Horizons in Acoustics. Red Hook : Curran Associates, Inc. 2008 (ISBN 978-1605601427) 384–386.

127. Postema M, Schommartz A. Ultrasound and swimmer safety. In : Jekosch U, Hoffmann R, Eds. Fortschritte der Akustik : Plenarvorträge und Fachbeiträge der 34. Deutschen Jahrestagung für Akustik DAGA 2008, Dresden. Berlin : DEGA 2008 (ISBN 978-3-9808659-4-4) 467–468.

128. Mleczko M, Postema M, Schmitz G. Nonlinear modeling of ultrasound contrast agents with Wiener series. In : Mehra S-R, Leistner P, Eds. Fortschritte der Akustik : Plenarvorträge und Fachbeiträge der 33. Deutschen Jahrestagung für Akustik DAGA 2007, Stuttgart. Berlin : DEGA 2007 (ISBN 978-3-9808659-3-7) 333–334.

129. Postema M. Sound, shells, and sonoporation. In : Calvo-Monzano A, Péréz-López A, Santiago S, Eds. Official Publication of the 19th International Congress on Acoustics : Acoustics of the 21st Century. Madrid : Sociedad Española de Acústica 2007 (ISBN 84-87985-12-2) #NLA-01-015.

130. Postema M, Mleczko M, Schmitz G. Mutual attraction of oscillating microbubbles. In : Buzug TM, Holz D, Weber S, Bongartz J, Kohl-Bareis M, Hartmann U, Eds. Advances in Medical Engineering. Berlin : Springer 2007 (ISBN 978-3-540-68763-4) 75–80.

131. Postema M, de Jong N, Schmitz G. Nonlinear behavior of ultrasound-insonified encapsulated microbubbles. In : Atchley AA, Sparrow VW, Keolian RM, Eds. Innovation in Nonlinear Accoustics : ISNA 17 : 17th International Symposium on Nonlinear Acoustics Including the International Sonic Boom Forum. Melville : American Institute of Physics (AIP) 2006 (ISBN 0-7354-0330-9) 275–278.

132. Postema M, Schmitz G. Messung und Modellierung physikalischer Eigenschaften von Kontrastmitteln. In : Langer S, Scholl W, Wittstock V, Eds. Fortschritte der Akustik : Plenarvorträge und Fachbeiträge der 32. Deutschen Jahrestagung für Akustik DAGA '06, Braunschweig. Berlin : DEGA 2006 (ISBN 3-9808659-2-4) 37–38.

133. Postema M. Medical bubbles. Medical Physics 2005 ; 32(5) : 1450.

134. Postema M. Medical bubbles. Virtual Journal of Biological Phyisics Research 2005 ; 9(9).

135. Postema M, ten Cate FJ, Lancée CT, Schmitz G, de Jong N, van Wamel A. Ultrasonic destruction of medical microbubbles : an overview. Ultraschall in der Medizin 2005 ; 26 : S32–S33.

136. Schmitz G, Postema M. Properties of ultrasound contrast agents for diagnosis and therapy. Abstracts of Papers of the American Chemical Society 2005 ; 230 : U1220–U1221.

137. de Jong N, Bouakaz A, van Wamel A, Postema M, Versluis M. Microbubbles for ultrasound imaging and therapy. Proceedings of the Workshop on Ultrasound in Biomeasurements, Diagnostics and Therapy 2004 ; 2 : 123–126.

138. Postema M, Bouakaz A, Chin CT, de Jong N. Optical observations of ultrasound contrast agent destruction. Acta Acustica united with Acustica 2003 ; 89 : 728.

139. Postema M, Marmottant P, Lancée C ; Hilgenfeldt S, de Jong N. Ultrasound-induced microbubble coalescence by parametric instability. In : Pontenagel WMGF, Feijen J, Eds. Proceedings of the 10th Dutch Annual Conference on BioMedical Engineering. Enschede : Institute of Biomedical Technology, University of Twente 2003 (ISBN 90-365-1973-X) 177.

I.2.4 Publications à visée de vulgarisation

140. Kotopoulis S, Postema M, Mc Cormack E, Gjertsen BT, Gilja OH, Dimcevski G. Ultrasound fights cancer with microbubbles. Health Management 2016 ; 16(2) : 1–3.

141. Hagen E, Postema M. Herzsprung auf Malle. Sine Loco : Sine Nomine Verlag 2016.

142. Постема М. Как выступают с докладами по физике в Западной Европе и странах бывшего Советского Союза. Советский Физик 2016 ; 117(1) : 44–49.

143. Postema M. Medische bellen. Nederlands Tijdschrift voor Natuurkunde 2005 ; 71(5) : 136–138.

144. Postema M, van Wamel A, Schmitz G, de Jong N. Slingerende belletjes, gerichte medicijnbezorging en microïnjectienaalden. Klinische Fysica 2004 ; (3-4) : 6–9.

145. Postema M, Bouakaz A, de Jong N. March 2002. IEEE Transactions on Ultrasonics, Ferroelectrics and Frequency Control 2002 ; 49(3) : c1–c2.

I.2.5 Demandes de brevet

146. Walther T, Postema M. Device for the identification, separation and/or cell type-specific manipulation of at least one cell of a cellular system. United States Patent Application US 2016/0060615 A1.

147. Walther T, Postema M. Vorrichtung und Verfahren zur Identifikation, Separation und/ oder zelltypspezifischen Manipulation wenigstens einer Zelle eines Zellsystems sowie von Mikroorganismen. European Patent Application EP 2 634 246 A1 2013.

148. Postema M, Smith AJ. Tablet Processing Unit. International Patent Application WO/ 2010/055337 2010.

149. Postema M, Smith AJ. Tablet Processing Unit. UK Patent Application GB0820586.6 2008.

I.3 Liste des contrats de recherche obtenus en tant que responsable (PI) ou co-responsable

2016 :	Postema M (PI), Bouakaz A. Sonic antibubbles in harmonic imaging and therapy. Le Studium Fellowship grant (2017-2018).	€ 110 000.
2015 :	Postema M. UiB Oppholdsmidler (2015).	NOK 160 000 ;
:	Postema M. Statoil Akademieavtalet (2015).	NOK 19 500 ;
:	Postema M. UiB Porsjektetableringsmidler 102347 (2015).	NOK 30 000 ;
2014 :	Douglas TS, Postema M. UCT VLF 2014-2 (2015).	ZAR 7 714 ;
:	Postema M. The Michelsen Centre for Industrial Measurement Science and Technology (MIMT) research grant (2014).	NOK 1 530 000 ;
:	Postema M. Strategic Programme for International Research and Education (SPIRE) Workshop and/or Contact Grant 710022 (2014–2015).	NOK 75 000 ;
:	Postema M. Statoil Travel Fund SH2014 (2014).	NOK 25 000 ;
:	Postema M. UiB Porsjektetableringsmidler 102347 (2014).	NOK 80 000 ;
2013 :	Postema M. L. Melzers Høyskolefond — Oppstartmidler (2013).	NOK 166 000 ;
:	Postema M. Strategic Programme for International Research and Education (SPIRE) Workshop and/or Contact Grant (2013–2014).	NOK 75 000 ;
:	Postema M. Små driftsmidler 12/13626 (2013).	NOK 8 400 ;
2012 :	Postema M. Erasmus Programme GfNA-II-C-ERA HEI mobility grant (2012).	€ 1 600 ;
:	Postema M. The Michelsen Centre for Industrial Measurement Science and Technology (MIMT) research grant (2012–2014).	NOK 1 800 000 ;
:	Postema M. The Michelsen Centre for Industrial Measurement Science and Technology (MIMT) travel grants (2012).	NOK 110 000 ;
:	Postema M. Statoil Travel Fund SH2012 (2012).	NOK 25 000 ;
:	Postema M. UiB Porsjektetableringsmidler 102347 (2012).	NOK 100 000 ;
:	Postema M. UiB Oppstartsmidler 222133 (2012–2013).	NOK 100 000 ;
:	Postema M. L. Meltzers Høyskolefond — Reisestipend (2012–2013).	NOK 26 500 ;
2011 :	Prentice P (PI), Postema M. Cavitation in dual-frequency focussed ultrasound surgery for enhanced drug delivery. The Research Council of Norway (NFR) Yggdrasil scholarship 210949/F11 (2011–2012).	NOK 104 000 ;

	: Pichon C (PI), Bessodes M, Postema M, Renault G. Formulations originales de liposomes acoustiques pour une deliverance assistée par des ultrasons. Agence Nationale de Recherche (ANR) Programme Blanc SVSE 5 (2012–2014).	€ 1 361 153 ;
	: den Hartog GJM (PI), Bast A, Sagis LMC, van der Linden E, Postema MAB. Ultrasound-guided shielding : a sound way to improve safety and efficacy of chemotherapeutics. Graduate School VLAG (2011–2014).	€ 160 000 ;
	: Dimcevski G (PI), Gilja OH, Gjertsen BT, Hoem D, Postema M. Treatment of pancreatic adenocarcinoma by combining contrast agent and Gemcitabine under sonication. Kreftforeningen (2011–2013).	NOK 17 000 000 ;
	: Biermann M (PI), Brauckhoff M, Varhaug JE, Al-Khafaji E, Gilja OH, Postema M, Akslen L, Mellgren G, Radulovic A. Kontrast-ultralyd for ikke-invasiv diagnostikk av biskjoldbruskkjerteladenomer. Helse Vest (2011–2012).	NOK 230 000 ;
	: Postema M. Bergen universitetsfond (2011–2012).	NOK 121 400 ;
	: Postema M. L. Meltzers Høyskolefond — Reisestipend (2011–2012).	NOK 25 000 ;
	: Postema M. UiB Porsjektetableringsmidler 102345 (2011).	NOK 120 000 ;
	: Postema M. Statoil Travel Fund SH2011 (2011).	NOK 23 500 ;
2010	: Postema M. The Michelsen Centre for Industrial Measurement Science and Technology grant 801656 (2010–2011).	NOK 200 000 ;
2009	: Postema M. Algenzerstörung mit Ultraschall. RUB Programm zur Anschubfinanzierung von Forschungsprojekten des wissenschaftlichen Nachwuchses (2009–2010).	€ 9 996 ;
2008	: Postema MAB. Observing and predicting encapsulated microbubble disruption with an optical and acoustical setup. Engineering and Physical Sciences Research Council (EPSRC) First Grant Scheme EP/F037023/1 (2008–2011).	£ 133 913 ;
	: Langton CM (PI), Attenborough K, Lauriks W, Postema M. Ultrasound propagation through cancellous bone, a complex porous composite. Leverhulme Trust Research Project Grant F/00181/N (2008–2010).	£ 82 027 ;

	: Postema M, Douglas TS. Signal and image processing for tissue perfusion assessment using ultrasound. The Royal Society / National Research Foundation (NRF) South Africa–UK Science Networks (2008).	£ 817 ; ZAR 14 000 ;
	: Postema M. The Royal Academy of Engineering (RAEng) International Travel Grant L7-1062 (2008).	£ 800 ;
	: Postema M. HERI Research Pump Priming Fund (2008–2009).	£ 5 000 ;
2007	: Postema M. Modellierung von schwingendem, zusammenschmelzendem und zerstörtendem Verhalten von Ultraschallkontrastmitteln anhand akustischer und optischer Abbildung. Deutsche Forschungsgemeinschaft (DFG) Emmy-Noether-Programm 38355133 (2009–2013).	€ 468 000.
	Montant des contrats en euro :	€ 5 242 012.

Partie II

Contexte scientifique

Le contexte scientifique expose une synthèse de mes travaux de recherche sur les microbulles et cellules acoustiques, organisée en trois chapitres.

Le premier chapitre contient trois articles sur la physique fondamentale des microbulles constituant agents de contraste ultrasonore.

Le deuxième chapitre contient trois articles sur la manipulation des cellules avec des ultrasons.

Le troisième chapitre contient deux articles sur la sonoporation des cellules cancéreuses avec l'aide d'un agent de contraste ultrasonore.

II.1 Agents de contraste ultrasonore

Les bulles sont des cavités gazeuses ou vaporeuses, entourées par un liquide. Grâce à la pression de surface de Laplace, les bulles sont typiquement sphériques. Lorsque la taille des bulles est inférieure à 10 μm, on les appelle des microbulles.

Dans un champ ultrasonore, les microbulles oscillent ; elles se contractent et se dilatent répétitivement. L'oscillation d'une microbulle génère son propre son. Les agents de contraste ultrasonore sont des microbulles, encapsulées par des membranes élastiques. Les membranes empêchent la dissolution rapide du gaz.

Les agents de contraste ultrasonore sont utilisés dans l'imagerie médicale. Les microbulles sont injectées en intraveineux. Pendant la perfusion, elles se comportent comme des indicateurs de présence du sang, détectables avec un échographe.

La physique basique des microbulles encapsulées est donnée dans l'article de synthèse « Contrast-enhanced and targeted ultrasound ». [1] Des examples de l'utilisation des agents de contrast ultrasonore en gastroentérologie sont données dans cet article (p. 45).

Le comportement dynamique des microbulles est dépendant de leurs propriétés élastiques ainsi que des conditions acoustiques auxquelles elles sont exposées. Les bulles n'oscillent pas seulement, elles peuvent aussi migrer, se fragmenter, se coaliser, se propulser, se regrouper et se craquer. Chacun de ces phénomènes dynamiques a ses applications médicales, dont le contrôle de la taille des tumeurs et la délivrance des agents thérapeutiques assistée par ultrasons.

L'influence de l'encapsulation sur l'oscillation et le rupture d'une microbulle est analysée dans ll'article « Ultrasonic bubbles in medicine : influence of the shell » (p. 60). [2]

La présence d'une coque élastique augmente la fréquence de résonance d'une microbulle et change sa phase d'oscillation par rapport au champ ultrasonore incident. Si l'énergie cinétique d'une microbulle oscillante surpasse un seuil de l'énergie de surface, la microbulle se fragmente en un nombre de bulles equivalent au cube d'un nombre entier.

En régimes acoustiques avec des pressions basses, les microbulles d'un agent de contraste ultrasonore peuvent créer une mousse qui se comporte comme une grosse bulle. Ce phénomène est analysé dans « Microfoam formation in a capillary » (p. 68). [3]

Grâce à des forces de radiation primaire, les microbulles oscillantes ont été forcées de former des mousses sphériques composées de milliers de microbulles. Les forces de radiation secondaire

1. Postema M, Gilja OH. Contrast-enhanced and targeted ultrasound. World Journal of Gastroenterology 2011 ; 17(1) : 28–41.
2. Postema M, Schmitz G. Ultrasonic bubbles in medicine : influence of the shell. Ultrasonics Sonochemistry 2007 ; 14(4) : 438–444.
3. Kotopoulis S, Postema M. Microfoam formation in a capillary. Ultrasonics 2010 ; 50(2) : 260–268.

ont amené ces mousses à se coalescer. Les mousses résultantes ont été forcées de migrer en direction du champ ultrasonore.

World Journal of Gastroenterology

Online Submissions: http://www.wjgnet.com/1007-9327office
wjg@wjgnet.com
doi:10.3748/wjg.v17.i1.28

World J Gastroenterol 2011 January 7; 17(1): 28-41
ISSN 1007-9327 (print) ISSN 2219-2840 (online)

TOPIC HIGHLIGHT

Adrian Săftoiu, MD, PhD, Professor, and Peter Vilmann, MD, PhD, Professor, *Series Editors*

Contrast-enhanced and targeted ultrasound

Michiel Postema, Odd Helge Gilja

Michiel Postema, Emmy Noether Research Group, Institute of Medical Engineering, Department of Electrical Engineering and Information Sciences, Ruhr-Universität Bochum, 44780 Bochum, Germany
Michiel Postema, Department of Physics and Technology, University of Bergen, 5007 Bergen, Norway
Michiel Postema, Department of Engineering, The University of Hull, Kingston upon Hull HU6 7RX, United Kingdom
Michiel Postema, Centre de Biophysique Moléculaire, UPR 4301 CNRS affiliated to the University of Orléans, 45071 Orléans, France
Odd Helge Gilja, National Center for Ultrasound in Gastroenterology, Department of Medicine, Haukeland University Hospital, Bergen, Norway
Odd Helge Gilja, Institute of Medicine, University of Bergen, 5007 Bergen, Norway
Author contributions: Postema M and Gilja OH wrote the paper.
Correspondence to: Dr. Michiel Postema, Professor, Department of Physics and Technology, University of Bergen, Allégaten 55, 5007 Bergen, Norway. michiel.postema@rub.de
Telephone: +47-555-82880 Fax: +47-555-89440
Received: July 2, 2010 Revised: September 3, 2010
Accepted: September 10, 2010
Published online: January 7, 2011

Abstract

Ultrasonic imaging is becoming the most popular medical imaging modality, owing to the low price per examination and its safety. However, blood is a poor scatterer of ultrasound waves at clinical diagnostic transmit frequencies. For perfusion imaging, markers have been designed to enhance the contrast in B-mode imaging. These so-called ultrasound contrast agents consist of microscopically small gas bubbles encapsulated in biodegradable shells. In this review, the physical principles of ultrasound contrast agent microbubble behavior and their adjustment for drug delivery including sonoporation are described. Furthermore, an outline of clinical imaging applications of contrast-enhanced ultrasound is given. It is a challenging task to quantify and predict which bubble phenomenon occurs under which acoustic condition, and how these phenomena may be utilized in ultrasonic imaging. Aided by high-speed photography, our improved understanding of encapsulated microbubble behavior will lead to more sophisticated detection and delivery techniques. More sophisticated methods use quantitative approaches to measure the amount and the time course of bolus or reperfusion curves, and have shown great promise in revealing effective tumor responses to anti-angiogenic drugs in humans before tumor shrinkage occurs. These are beginning to be accepted into clinical practice. In the long term, targeted microbubbles for molecular imaging and eventually for directed anti-tumor therapy are expected to be tested.

Key words: Ultrasound; Drug delivery systems; Drug targeting; Sonoporation; Contrast media; Liver; Pancreas; Gastrointestinal tract

Peer reviewer: Dr. Mirella Fraquelli, Postgraduate School of Gastroenterology, IRCCS Ospedale Maggiore, Milano, 20122, Italy

Postema M, Gilja OH. Contrast-enhanced and targeted ultrasound. *World J Gastroenterol* 2011; 17(1): 28-41 Available from: URL: http://www.wjgnet.com/1007-9327/full/v17/i1/28.htm DOI: http://dx.doi.org/10.3748/wjg.v17.i1.28

INTRODUCTION

Advanced medical imaging has a strong impact on research and clinical decision-making in real-time assessment of angiogenesis in digestive cancers. Ultrasonic imaging is becoming the most popular medical imaging modality, owing to the low price per examination[1] and its safety[2]. A B-mode ultrasound scan shows contrasted regions from transitions in acoustic impedance, i.e. transitions in tissue type, in the form of brighter pixels. However, blood is a poor scatterer of ultrasound waves at clinical diagnostic transmit frequencies, which lie between 1 and 40 MHz. For perfusion imaging, markers have been designed to en-

hance the contrast in B-mode imaging. These so-called ultrasound contrast agents consist of microscopically small gas bubbles encapsulated in biodegradable shells.

Contrast-enhanced ultrasound (CEUS) represents a significant advancement in the evaluation of angiogenesis in digestive cancers. In particular, in the study of focal liver lesions, CEUS has been widely used for detection and characterization of malignancy. The unique feature of CEUS of non-invasive assessment in real-time liver perfusion throughout the vascular phases has led to a great improvement in diagnostic accuracy of ultrasound, but also in guidance and evaluation of responses to therapy. Currently, CEUS is part of the state-of-the-art diagnostic work-up of focal liver lesions, resulting in safe and cost-effective patient management.

In this review, the physical principles of ultrasound contrast agent microbubble behavior and adjustments for drug delivery, including sonoporation, are described. Furthermore, an outline of clinical imaging applications of CEUS is given.

Ultrasound

The sound that humans can perceive lies within the frequency range 20 Hz-20 kHz. Ultrasound is by definition all sound higher than 20 kHz. The ultrasound frequencies utilized in medical imaging are mainly in the range 1-40 MHz. Such high frequencies cannot be transmitted through air but can be transmitted satisfactorily through solid or fluid materials. An ultrasonic transducer serves a dual function as both transmitter and receiver of ultrasound. A signal generated by an ultrasonic transducer typically consists of a pulse of a few μs with a certain center frequency. Part of this signal propagates through target tissue, part is reflected by macroscopic tissue structures, part is absorbed by tissue, and part is scattered by structures in the tissue smaller than the acoustic wavelength. Only a small portion of the transmitted acoustic energy is received by the transducer, but this portion is used to build an ultrasonic image. The received signal is the superposition of specular reflections at tissue boundaries and echoes from tissue backscattering[3]. Current real-time 2-dimensional imaging capabilities are in excess of 30 frames per second[4]. Contemporary imaging techniques have been summarized by Wells[5].

The quality of a B-mode scan is expressed by the contrast-to-noise ratio, which is defined as the absolute difference of the signal-to-noise ratio in the target tissue and the signal-to-noise ratio in the surrounding tissue[4].

On clinical ultrasound devices, the intensity of the ultrasonic field is generally adjusted with a switch for the mechanical index (MI) instead of the acoustic amplitude. The MI depends on the maximum value of peak negative pressure and the centre frequency of the ultrasound field[6]. For MI < 0.3, the acoustic amplitude is considered low. For 0.3 < MI < 0.7, there is a possibility of minor damage to neonatal lung or intestine[6]. These are considered moderate acoustic amplitudes. For MI > 0.7, there is a risk of cavitation if an ultrasound contrast agent containing gas microspheres is being used, and there is a theoretical risk of cavitation without the presence of ultrasound contrast agents[6]. The risk increases with MI values above this threshold[6]. These are considered high acoustic amplitudes[7]. In commercial scanners, the MI has been limited to 1.9 for medical imaging[8]. Figure 1 shows examples of B-mode scans recorded at different MI. At higher MI, the contrast-to-noise ratio increases.

Microbubble physics

The density and compressibility parameters of blood cells hardly differ from those of plasma. Therefore, blood cells are poor scatterers in the clinical diagnostic frequency range[9]. Since imaging blood flow and measuring organ perfusion are desirable for diagnostic purposes, markers should be added to the blood to differentiate between blood and other tissue types. Such markers must have resonance frequencies in the medical ultrasonic range. Figure 2 shows the resonance frequencies of free and encapsulated gas microbubbles as a function of their equilibrium radius. The resonance frequencies of encapsulated microbubbles lie slightly higher than those of free gas bubbles[10,11], but clearly well within the clinical diagnostic range, too. Based on their acoustic properties, microbubbles are well suited as an ultrasound contrast agent.

The pressure inside a bubble must be higher than the ambient pressure[12]. This difference is generally referred to as the surface pressure. The smaller the bubble, the higher is the surface pressure. Since fluids are forced to flow from a location with a higher pressure to a location with a lower pressure, a bubble cannot exist in true equilibrium. For example, a free air bubble with a 6 μm diameter dissolves within 100 ms[13]. To prevent quick dissolution, ultrasound contrast agent microbubbles contain low-solubility gas, such as SF_6 or C_3F_8[14]. The encapsulating shells are made of biodegradable materials, such as phospholipids or albumin[15]. With mean diameters below 6 μm, these microbubbles are small enough to pass through the lung capillaries. Detailed overviews of the compositions of the ultrasound contrast agents used most in imaging research have been given by Postema *et al*[3], Sboros[16] and Tinkov *et al*[17]. In this section, we classify ultrasound contrast agents into only 4 categories, based on the presence of an encapsulating shell and its thickness, similar to Tinkov *et al*[17].

A bubble in a low-amplitude sound field can be considered a forced damped harmonic oscillator[18,19] and its oscillating behavior can, as a result, be modeled as a mass-spring-dashpot system[20]. The spherically symmetric oscillating behavior of ultrasound contrast agent microbubbles has been described with models based on the Rayleigh-Plesset equation[21], modified for the presence of an encapsulating shell[22-32]. Generally, the presence of blood has a relatively small effect on bubble dynamics[33]. To give an indication of the vast amount of existing models: Qin *et al*[34] defined 16 separate dynamic bubble model classes. The reason for the high number of existing models is the fact that most physical properties of en-

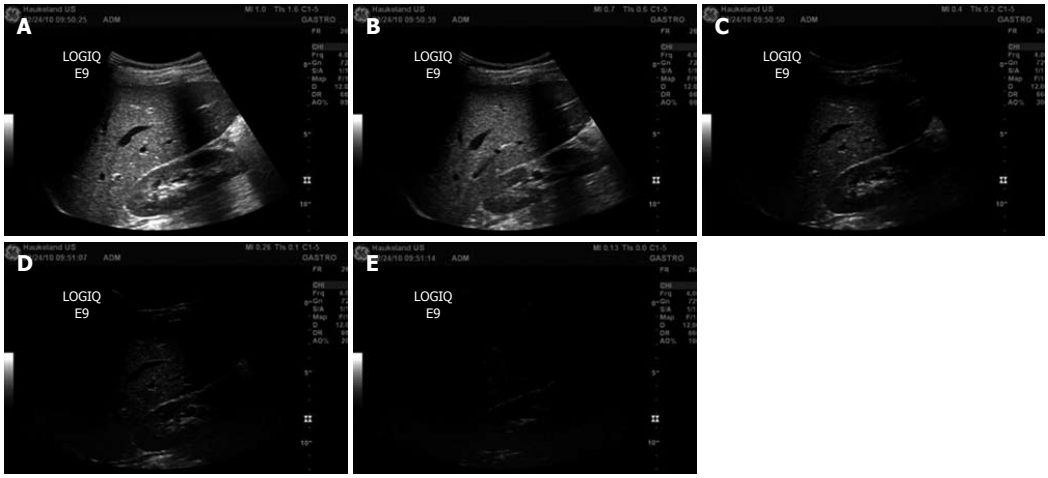

Figure 1 B-mode images of the liver recorded at decreasing mechanical index values (A-E). A: Mechanical index (MI) = 1.0; B: MI = 0.7; C: MI = 0.4; D: MI = 0.26; E: MI = 0.13.

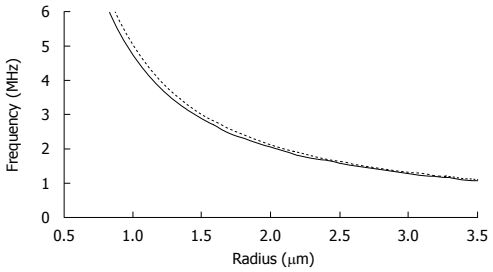

Figure 2 Resonance frequencies of free (solid line) and lipid-encapsulated (dotted line) microbubbles as a function of equilibrium radius.

capsulated microbubbles cannot actually be measured, so that pseudo-material properties have to be chosen when predicting ultrasound contrast agent microbubble behavior. Examples of such pseudo-material properties are shell elasticity parameters and shell friction parameters. At low-amplitude driving pressures, an ultrasound contrast agent microbubble oscillates linearly, i.e. the bubble excursion if proportional to the instantaneous pressure. However, at high-amplitude driving pressures, it oscillates nonlinearly. Figure 3 demonstrates the oscillation behavior of 2 contrast microbubbles subjected to continuous sine pressure waves with low, moderate, and high amplitudes. Both bubbles oscillate linearly at MI = 0.01. With increasing driving amplitude, asymmetries in radial excursion and expansion time rise, especially for the bigger bubble, which is closer to the resonance size. At MI = 0.8, both bubbles expand to a factor of the initial size, followed by a rapid collapse of the smaller bubble. The bigger bubble demonstrates collapse at MI = 0.18 and higher.

A dynamic bubble generates an acoustic signal that depends on the fluid displacement by the bubble as a function of time. Detection strategies have been developed to discriminate acoustic signal-generated by ultrasound contrast agent microbubbles from other acoustic signals such as specular reflections and tissue scattering. These strategies are the reason that CEUS is suitable for the detection of blood. The 10 most common detection strategies include coded excitation, harmonic power Doppler, phase inversion and power modulation[34,35]. All single-pulse and multi-pulse imaging detection strategies make use of the nonlinear behavior of microbubbles[34,35].

Other types of nonlinear behavior than asymmetric oscillations are discussed below.

If a bubble with a negligible shell collapses near a free or a solid boundary, the retardation of the liquid near the boundary may cause bubble asymmetry. This asymmetry causes differences in acceleration on the bubble surface. During further collapse, a funnel-shaped jet may protrude through the bubble, shooting liquid to the boundary[36]. Such jets have been observed in high-speed observations of ultrasound contrast agent microbubbles[37-40]. Empirical relations exist between the collapsing bubble radius, the jet length, and the pressure at the tip of jets[41-43]. It has been speculated whether microbubble jetting can be applied for ultrasound-guided drug delivery[38,39,42].

During the collapse phase, a bubble may fragment into a number of smaller bubbles[44]. Fragmentation has been observed with contrast agents with thin elastic shells. The number of fragments into which a contrast microbubble breaks up has been associated with asymmetric oscillations[40,45]. Fragmentation can be predicted from the moment when the kinetic energy of the bubble surpasses its surface energy[27]. Bubble fragmentation costs energy, but the subsequent coalescence of bubble fragments generates enough acoustic energy to be detected[27].

Thick-shelled microbubbles have demonstrated sonic cracking during a high-amplitude ultrasonic cycle[46,47]. The increased pressure difference between inside and outside of

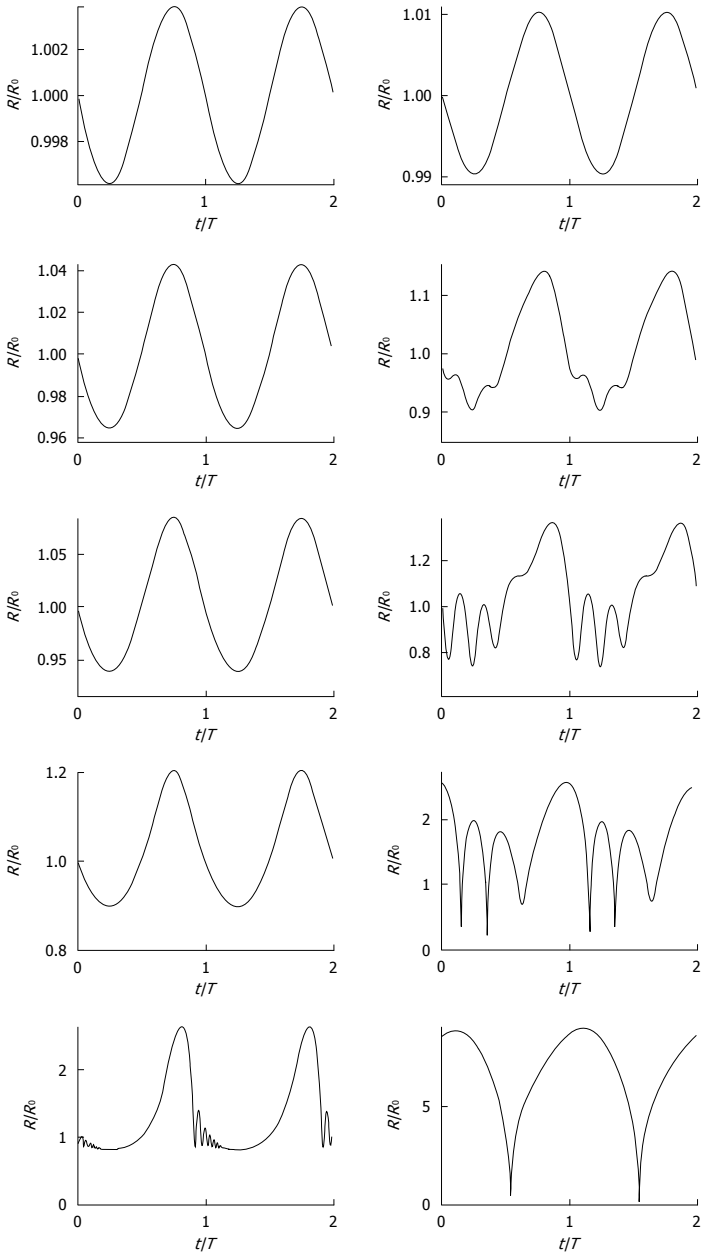

Figure 3 Simulated radius-time curves (radius *R* normalized with equilibrium radius R_0, time *t* normalized with period T_0) of ultrasound contrast microbubbles with 0.55 μm (left column) and 2.3 μm (right column) equilibrium radii, respectively, modeled with a conservative Rayleigh-Plesset equation[3], using a conservative shell stiffness parameter[148]. The modeled ultrasound field was a continuous sine wave with a frequency of 0.5 MHz and acoustic amplitudes corresponding to (top-bottom). Mechanical index = 0.01, 0.10, 0.18, 0.35, and 0.80, similar to the experiments by Karshafian *et al*[92].

the microbubble during the expansion phase of the wave[48] causes the shell to be stretched until it surpasses a critical deformation[49], resulting in its mechanical cracking. The released bubble has an expansion amplitude much higher than an encapsulated bubble of identical size. Therefore, the acoustic signal from an ultrasound contrast agent after gas release differs from that of the same contrast agent before gas release, until the released gas has dissolved[50].

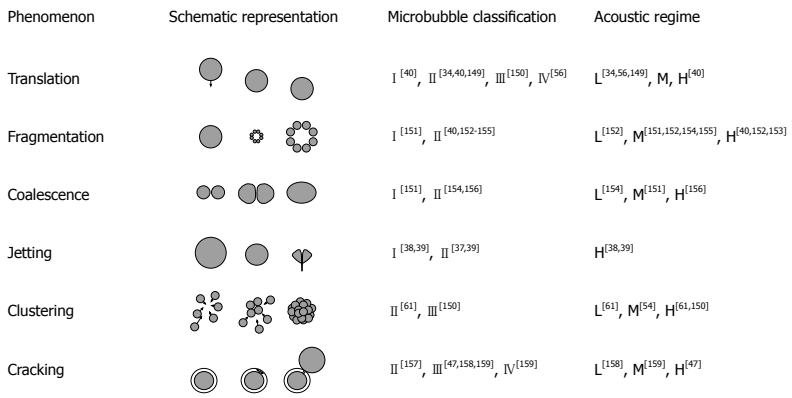

Figure 4 Nonlinear phenomena and the regimes for their occurrence. Microbubble shell classes: (Ⅰ) free or released gas; (Ⅱ) thin shells < 10 nm; (Ⅲ) thick shells < 500 nm; (Ⅳ) very thick shells > 500 nm. Acoustic regimes: low (L) for mechanical index (MI) < 0.3; medium (M) for 0.3 < MI < 0.7; high (H) for MI > 0.7. The figure has been based on Postema[12].

After a disruptive ultrasonic burst, the disappearance of microbubble fragments or released gas can be traced with low-amplitude ultrasound, as well as the wash-in rate of fresh contrast agent[51]. Hence, the efficiency of the disruptive burst can be measured.

Bubble translation in the direction of the sound field is caused by a primary radiation force resulting from a pressure gradient across the bubble surface[52]. The translation is maximal in the contraction phase of the oscillating microbubble. Making use of this phenomenon, ultrasound contrast agent microbubbles can be forced to move farther away from the transducer, towards vessel walls[53-61], increasing the success rate of targeting to a boundary.

In a standing sound wave field[62], bubbles can aggregate to clusters ultimately a quarter of the acoustic wavelength apart[61]. The formation of ultrasound contrast agent microbubble clusters and the ultrasonic pushing of these clusters towards a vessel wall have been recently observed using high-speed photography[61].

The occurrence of the above-mentioned phenomena is influenced by (1) the ultrasonic parameters: transmit frequency, acoustic amplitude, pulse length, pulse repetition rate and transmit phase; (2) the ultrasound contrast agent composition: the composition of the shell, the bubble sizes, the size distribution and the gas; and (3) the physical properties of the medium: viscosity, surface tension, saturation.

Figure 4 gives an overview of the nonlinear phenomena that have been observed with ultrasound contrast agents, the type of ultrasound contrast agent in which they have occurred, and the minimum acoustic regime required.

Molecular imaging

Dayton *et al*[35] defined molecular imaging as the non-invasive application of an imaging modality to discern changes in physiology on a molecular level[12]. Although ultrasound contrast agents were intended for perfusion imaging, they have proven useful in molecular imaging as well, after modification of the microbubble shell. Dayton *et al*[35] discerned 2 targeting strategies: active targeting, in which a ligand specific for the molecular target, and passive targeting, in which the physiochemical properties of the agent are used to achieve retention at the target site[12]. Molecular imaging and targeting have been reviewed elsewhere in depth[35,63]. In summary, the main applications include the detection of angiogenesis, inflammation, plaques and thrombi[8,12,17].

Drug delivery

It has been proven by numerous groups, that the cellular uptake of drugs and genes is increased, when the region of interest is under sonication, and even more so when a contrast agent is present[12,64-91]. This increased uptake has been attributed to the formation of transient porosities in the cell membrane, which are big enough for the transport of drugs into the cell. The transient permeabilization and resealing of a cell membrane is called sonoporation[64]. The sonoporation-induced cellular uptake of markers with molecular weights between 10 kDa and 3 MDa has been reported in several studies[17,74,92]. Schlicher *et al*[93] showed that ultrasound-induced cavitation facilitated cellular uptake of macromolecules with diameters up to 56 nm. Even solid spheres with a 100 nm diameter have been successfully delivered with the aid of sonoporation[82]. This implies that drug size is not a limiting factor for intracellular delivery[92]. However, the pore opening times can be so short that, if the drug is to be effectively internalized, it should be released close to the cell membrane when poration occurs[94].

There are 2 hypotheses for explaining the sonoporation phenomenon, the first being microbubble oscillations near a cell membrane, the second being microbubble jetting through the cell membrane. Based on modeling, high-speed photography, and recent cellular uptake measurements, we concluded that microbubble jetting behavior can be excluded as the dominant sonoporation

mechanism[7]. The influence of microbubble disruption, i.e. fragmentation or sonic cracking, on sonoporation will have to be further investigated[7]. Without the presence of an agent, it has been assumed that sonoporation is caused by bubbles, which have been generated in the transducer focus as a result of inertial cavitation[95,96].

Instead of just facilitating the transient opening up of cell membranes, a microbubble might also act as the vehicle itself to carry a drug or gene load to a perfused region of interest, in which case the load has to be released with the assistance of ultrasound. Apart from mixing ultrasound contrast agent with a therapeutic agent, several schemes have been proposed to combine microbubbles with a therapeutic load[97]. Tinkov *et al*[17] discriminated the following 7 microbubble structure classes for drug delivery: (1) attachment to the outer shell surface; (2) intercalation between monolayer phospholipids; (3) incorporation in a layer of oil; (4) formation of complexes with smaller particles (secondary carriers); (5) physical encapsulation in a polymer layer and coating with biocompatible material; (6) surface loading of protein-shelled microbubbles; and (7) entire volume loading of protein-shelled microbubbles. The drugs are to be released at the site of interest during insonication[98], presumably by disrupting the microbubble shell. It has been demonstrated *in vitro*, that higher doses of DNA were delivered during ultrasound insonication when the DNA was loaded on albumin-encapsulated microbubbles than when unloaded microbubbles were mixed with plasmid DNA[67]. Amounts of DNA loading on microbubbles have been between 0.002 (pg/μm^2)[99] and 2.4 (pg/μm^2)[17,67].

Instead of attaching a drug to the capsule, therapeutic compounds in the gas phase might be encapsulated with thick shells, to keep them from dissolving. At the region of interest, the shell should be cracked with ultrasound, releasing the gaseous content[46,47,100,101]. However, only a few therapeutic compounds exist in the gaseous phase, e.g. nitric oxide[48] and several gaseous anesthetics.

A therapeutic agent inside the microbubble shell may react with the shell and dampen the bubble oscillations. Therefore, it might be more suitable to have the therapeutic agent in the core of the microbubble, separated from the shell by a gaseous layer. Incorporating a liquid drop containing drugs or genes inside an ultrasound contrast agent microbubble, however, is technically challenging[102]. As opposed to bubbles, antibubbles consist of a liquid core encapsulated by gas[103]. Such a droplet inside a bubble may be generated with the jetting phenomenon: the collapse of a bubble near a free surface produces a liquid jet[104], which may break up into one or several droplets[105]. Another option would be to stabilize the liquid core by means of a biodegradable skeleton attached to the microbubble shell.

It has been noted, that, if microbubbles can create pores, it is also possible to create severe cell and tissue damage[106]. There is an inverse correlation between cell permeability and cell viability[92,107-109], i.e. not all cell membrane pores are temporary. This indicates that sonoporation is just a transitory membrane damage in the surviving cell[92]. Cell lysis results from irreversible mechanical cell membrane damage[110], which allows the intracellular content to leak out[64]. Only recently, ultrasound-induced apoptosis has been observed with cancer cells *in vitro*[110,111], and also in the presence of an ultrasound contrast agent[112]. Apart from situations where lysis is desired (sonolysis)[113], ultrasonic settings should be chosen such that cell lysis is minimal. Side effects observed are capillary rupture, hemorrhage, and dye extravasation[106]. These side effects, however, have been associated with relatively high microbubble concentrations, long ultrasonic pulse lengths, and high acoustic intensities[106].

CLINICAL IMAGING APPLICATIONS

Liver

Ultrasonography is the most commonly used imaging modality worldwide for diseases of the liver. However, it has limited sensitivity in the detection of small tumor nodules. In addition, ultrasonographic findings are often nonspecific, as images of benign and malignant liver lesions overlap considerably. The introduction of microbubble contrast agents and the development of contrast-specific techniques have opened new prospects in liver ultrasonography. The advent of second-generation agents that enable continuous real-time contrast-enhanced imaging has been instrumental in improving the acceptance and reproducibility of the examination. With the publication of guidelines for the use of contrast agents in liver ultrasonography by the European Federation of Societies for Ultrasound in Medicine and Biology (EFSUMB)[114,115], CEUS is now routinely used in clinical practice.

As opposed to contrast media used with computed tomography (CT) and magnetic resonance (MR) imaging, ultrasound contrast agents can visualize the capillary net of the examined tissue, because CEUS is considerably more sensitive to very small amounts of contrast agent, even to single bubbles. Furthermore, because sonography is a dynamic method that is performed in real time, additional information about tissue perfusion can be deduced from the influx and washout of the contrast media, thus facilitating the differential diagnosis of tumors. In addition, signals from the microbubbles enable the visualization of slow flow in microscopic vessels without Doppler-related artifacts. Various software packages have been developed to enable quantification of changes in contrast intensity and to provide additional objective information over the entire course of the contrast examination.

Microbubbles enable dynamic imaging of tumor angiogenesis. This approach is now routinely used for diagnosis, particularly for the detection and characterization of various liver tumors.

The most common malignancy of the liver is metastases. Hepatic metastasis is a sign of advanced tumor stage, and curative treatment is only possible in a very small number of patients. When the objective is cure, liver resection is the most effective therapy, but several ablation

Figure 5 B-mode image of a metastasis from a colon cancer to the liver appearing hyperechoic with a dark halo.

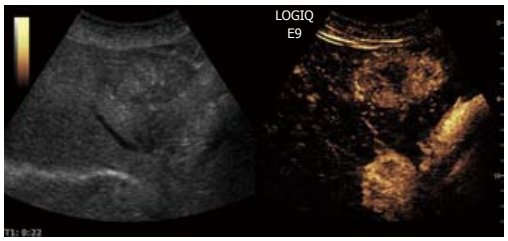

Figure 6 Contrast-enhanced ultrasound B-mode image of a colon cancer metastasis (same as in Figure 5) in the arterial phase showing marked hyperenhancement in the right panel. Note also the dark centre of the tumor, indicating a necrotic portion of the metastasis.

techniques have evolved. For directed tumor therapy, accurate imaging of the number and distribution of the metastases is required. On grey-scale ultrasound images, metastases may appear as hypo-, iso- or hyperechoic lesions, and some of them have a halo (Figure 5). Unenhanced ultrasonography achieves a sensitivity between 45% and 80% in detecting liver metastases[116,117]. Not surprisingly, this compares unfavorably with the results of studies with contrast-enhanced CT and MR. However, the application of an intravascular ultrasound contrast agent during transcutaneous ultrasonography of the liver improves detection of metastases significantly[118-120].

After injection, 3 phases of contrast enhancement can be differentiated: the arterial phase, in which the contrast agent reaches the liver first *via* the hepatic artery; the portal phase, where the contrast agent has passed circulation and spreads through the liver in the portal branches; and the late or parenchymal phase, in which the agent slowly distributes within the entire liver parenchyma. Metastases show characteristic features in all 3 phases after contrast agent injection. Differentiation of hypervascular from hypovascular metastases is achieved perfectly by real-time imaging during the arterial phase: hypervascular metastases, e.g. from malignant melanoma, thyroid carcinoma, or neuroendocrine carcinoma, appear as hyperenhancing, usually with a typical rim enhancement of varying size (Figure 6). In contrast, hypovascular metastases le-

Figure 7 Contrast-enhanced ultrasound B-mode image of a colon cancer metastasis (same as in Figure 5) in the sinusoidal (late) phase, showing marked hypoenhancement in the right panel.

sions, e.g. from colorectal carcinoma (great variability) or bronchogenic carcinoma, may appear as hypoenhancing lesions in the arterial phase. Large metastases may have inhomogeneous enhancement because of necrosis, as shown in Figure 6. At the beginning of the portal phase, the enhancement fades and the entire lesion becomes increasingly hypoechoic. In the late phase, both hypovascular and hypervascular metastases invariably appear as dark defects, whereas the enhancement persists in the normal liver parenchyma (Figure 7). During this phase, the lesions are usually particularly well defined, often with sharp punched-out borders. Both portal venous and late-phase imaging markedly increase the contrast between the enhancing normal liver and the nonenhancing metastases and thus improve detection, particularly of small lesions, i.e. < 1 cm in diameter. The improved detection obtained by the use of ultrasound contrast agents allows for the implementation of CEUS for the follow-up of patients undergoing surgery and chemotherapy, to assess the efficacy of antineoplastic treatment[121-124]. To determine the utility of CEUS as a prognostic tool for metastatic renal cell carcinoma patients receiving sunitinib, Lassau and co-workers studied 38 patients receiving 50 mg/d sunitinib[125]. They found that time to peak intensity and slope of the wash-in curve were significantly associated with disease-free survival; time to peak intensity was also significantly associated with overall survival[125]. Furthermore, they concluded that CEUS is a useful tool for predicting early efficacy of sunitinib in metastatic renal cell carcinoma patients[125].

Hepatocellular carcinoma

Hepatocellular carcinoma (HCC) is the second common malignant liver tumor and the most common primary liver cancer, usually occurring as a complication of chronic liver disease and most often arising in a cirrhotic liver. The accurate and early diagnosis of HCC is essential for treatment of the affected patients. Surgical resection, liver transplantation, percutaneous alcohol ablation and radiofrequency ablation are potentially curative therapies. On grey-scale sonography, HCCs may be hypoechoic (26%), hyperechoic (13%) or have mixed (61%) echogenicity depending on the size of the tumor, the fat content, the degree of differentiation and the scarring of necrosis[126].

Figure 8 B-mode image of hepatocellular carcinoma with well-demarcated margins and a perilesional halo.

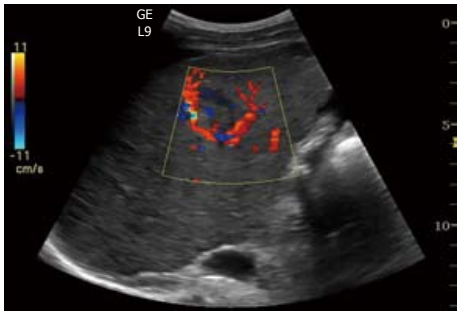

Figure 9 Color Doppler in hepatocellular carcinoma reveals a basket pattern around the tumor, illustrating the anatomy of the arterial tumor supply.

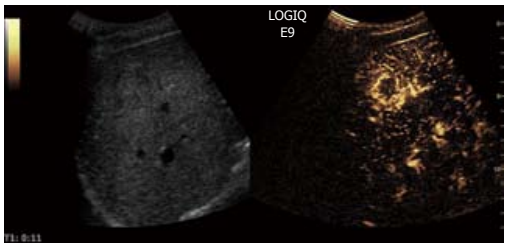

Figure 10 Contrast-enhanced ultrasound allows for visualization of the arteriogram of hepatocellular carcinoma in the early arterial phase. The feeding vessel is visible on the tumor right side. Typically there is initial peripheral enhancement before the centripetal influx to the center of the tumor.

HCCs with well-demarcated margins, perilesional halos or a hypoechoic pattern have a greater rate of detection by ultrasonography (Figure 8). Controversially, infiltrative or iso-hyperechoic HCCs without peripheral halos, as well as HCCs with internal septa or posterior echo enhancement, are harder to detect, with lower reported sensitivities. The use of Doppler in HCC can sometimes reveal a basket pattern around the tumor, depicting the anatomy of the arterial tumor supply (Figure 9).

When CEUS is applied, HCCs are typically characterized by hypervascularity in the arterial phase. Using real-time evaluation with low MI, early and usually intense arterial enhancement is identified and in most cases a feeding artery is clearly visible. Tumor vessels, often appearing with a basket-like pattern, tend to enhance in a centripetal fashion extending from the periphery to the centre of the tumor (Figure 10). Arterial enhancement may be inhomogeneous, because the tumor contains septa, regions of different tissue differentiation and shunting among the neoformed vessels, and sometimes necrosis[127]. Because of the high circulation velocity within HCC, there is relatively rapid nodular washout, often starting in the portal phase (Figure 11). Typically, HCC is hypovascular (hypoechoic) during the late phase of perfusion (Figure 12). At the same time, normal liver parenchyma increases the echogenicity and homogeneity because of portal venous enhancement.

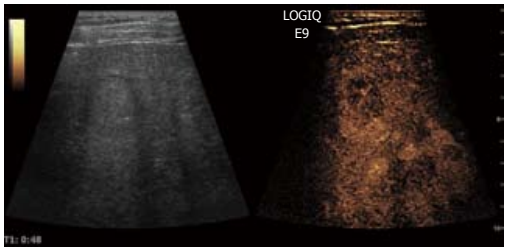

Figure 11 The portal phase of hepatocellular carcinoma. Because of high circulation velocity within hepatocellular carcinoma, there is relatively rapid washout, often starting in the portal phase.

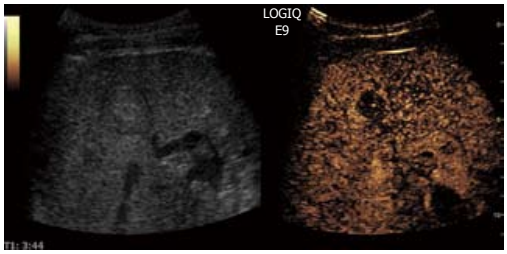

Figure 12 The sinusoidal (late) phase of hepatocellular carcinoma is shown. Typically, hepatocellular carcinoma is hypovascular (hypoechoic) during the late phase of perfusion confirming the malignant nature of the tumor.

Surveillance of patients at risk of developing HCC is based on ultrasound examinations performed at either 6 or 12 mo intervals. Early detection of HCC in patients with cirrhosis is a clinical challenge, since the different entities that are involved in the multi-step process of hepatocarcinogenesis, such as low-grade and high-grade dysplastic nodule, share common ultrasonic features. However, CEUS allows for reliable detection of arterial angiogenesis associated with a malignant transformation. When whole lesion enhancement or mosaic enhancement in the arterial phase with an enhancement defect in the portal phase was regarded as a positive finding of HCC, a sensitivity of 92% and a specificity of 87% were found[128]. It has been shown that the ability of CEUS to diagnose HCC cur-

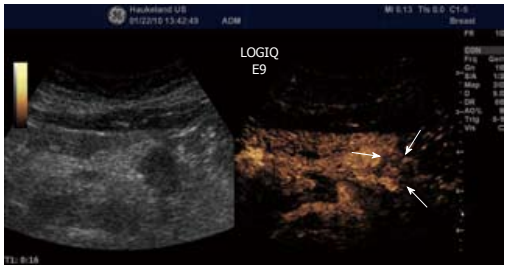

Figure 13 Ductal adenocarcinoma (between arrows) of the pancreas showing poor enhancement in the arterial phase. The same is true for the late venous phase.

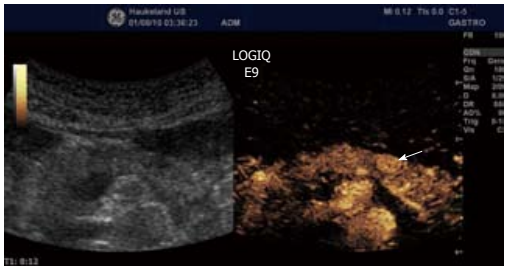

Figure 14 Neuroendocrine tumour (arrow) shows a rapid intense enhancement in the early arterial phase of contrast-enhanced ultrasound examination.

rently approaches that of optimized multi-detector CT or dynamic MR imaging protocols[129-136]. The use of CEUS to characterize nodular lesions in cirrhosis have been recommended by the clinical practice guidelines issued by the European Federation of Societies for Ultrasound in Medicine and Biology and the American Association for the Study of Liver Diseases[115].

Pancreas

The pancreas, lying deep to the stomach and duodenum, is among the most inaccessible organs in the body for visualization with ultrasonography. Hence, confirmation of pancreatic disease has remained a great challenge in clinical imaging. However, transabdominal ultrasonography has developed to be a useful tool in the differential diagnosis of pancreatic tumors because the technique is inexpensive, easy to perform, and widely available. Nevertheless, only after the introduction of second-generation contrast media[3], has transabdominal sonography yielded results comparable to those of other diagnostic modalities. CEUS can be used to improve detection of pancreatic lesions or to characterize pancreatic lesions already visible with ultrasonography. Furthermore, the staging of some pancreatic lesions can be improved by the use of contrast media. However, there is an important difference between a pancreatic CEUS study and the well-established liver CEUS study: the blood supply of the pancreas is entirely arterial and the enhancement of the gland begins almost together with the aortic enhancement. With CEUS the enhancement reaches its peak between 15 and 20 s after injection of the ultrasound contrast agent. Accordingly, pancreatic tissue enhancement is earlier and shorter than that of the liver because of the absence of a venous blood supply such as the portal vein in the liver. After a marked parenchymal enhancement in the early contrast-enhanced arterial phase, there is a progressive washout of contrast medium with gradual loss of echogenicity.

Ductal adenocarcinoma is the most frequent tumor of the pancreas, comprising between 80% and 90% of all tumors of the exocrine pancreas. Ultrasonographic findings typically are a hypoechoic lesion with ill-defined margins, often with spiculas and tending to alter the gland contour[137-139]. Characteristically, ductal adenocarcinoma shows poor enhancement in all CEUS phases (Figure 13). On the contrary, neuroendocrine tumors (NETs) appear hypervascular in CEUS imaging. Imaging is important for the differentiation between NETs and ductal adenocarcinoma in selecting the correct therapeutic strategy and determining prognosis. With color- and power-Doppler ultrasonography a spotted pattern can sometimes be observed inside endocrine tumors[140]. However, Doppler signals are not always detected because of the small size of the lesion or of the tumor vascular network. Typically, NETs show a rapid intense enhancement in the early contrast-enhanced phases (Figure 14), with the exception of possible necrotic intralesional areas.

Gastrointestinal tract

Colon cancer is one of the world's most common malignancies. The main therapy is surgical resection. To diagnose colon cancer, endoscopy is the preferred method, but in many places around the world, X-ray is still used. Using ultrasonography, the normal gastrointestinal (GI) wall is visualized as a layered structure consisting of 5 to 9 layers, depending on transmitted frequency[141-143]. When digestive cancers develop, the wall layers become blurred, wall thickness is increased, and the ultrasound appearance of the GI wall resembles a kidney, i.e. pseudo-kidney sign or target lesion. However, CEUS does not yet have a place in the work-up of patients with suspected colonic cancer.

In oncology, early evaluation of targeted treatment response with functional imaging is of major importance. Dynamic CEUS is now recognized as a functional imaging technique able to evaluate new antiangiogenic drugs targeting cancers in the abdomen. This therapy evaluation is based on analysis of the curve of signal intensity over time after injection of ultrasound contrast agents (Figure 15). Novel quantification software allows for objective quantification of tumor perfusion parameters including maximum intensity of enhancement, mean transit time, time to peak, and wash-in slope coefficient. CEUS allows for early prediction of tumor response to treatment based on changes in vascularity, before morphological changes become apparent[144]. Lassau and co-workers evaluated CEUS with perfusion software as a predictor of early tumor response to imatinib (Glivec) in c-kit-positive gas-

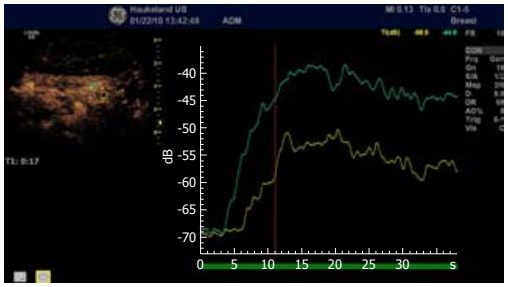

Figure 15 Analysis of time intensity curves after injection of contrast agents depicting a pancreatic carcinoma (same as Figure 13). The green curve depicts the normal pancreatic perfusion whereas the red curve illustrates the hypoenhancing malignancy.

trointestinal stromal tumors (GISTs)[145]. They studied 59 tumors with metastases or a recurrence from a GIST prospectively and found that initial contrast uptake at day 1 was predictive of the future response[145]. A strong correlation was found between the decline in tumor contrast uptake at days 7 and 14 and tumor response[145]. They concluded that CEUS is a non-invasive imaging technique that allows the early prediction of tumor response in c-kit-positive GISTs treated with Glivec[145].

Tumor growth is dependent on both endothelial and tumor cells. One question is whether changes in tumor vasculature are implicated in tumor tissue degeneration during antiangiogenic therapies. In a study using CEUS, it was shown that tumor cells abruptly became necrotic following antivascular therapy, whereas untreated tumors were protected from degeneration by a significant blood supply[146]. Because antiangiogenic therapies inhibit the growth of new tumor-associated blood vessels, as well as prune newly formed vasculature, they would be expected to reduce the supply of oxygen and thus increase tumor hypoxia. Franco and co-workers used DC101, an antivascular endothelial growth factor receptor 2 antibody to study tumor hypoxia[147]. Using ultrasonography, they observed consistent reductions in microvascular density, blood flow, and perfusion[147]. The increase in tumor hypoxia was evident within 5 d and remained so throughout the entire course of treatment[147]. These results suggest that sustained hypoxia and impairment of vascular function can be 2 consistent consequences of antiangiogenic drug treatment.

Concluding remarks

It is a challenging task to quantify and predict which bubble phenomenon occurs under which acoustic condition, and how these may be utilized in ultrasonic imaging. Aided by high-speed photography, our improved understanding of encapsulated microbubble behavior will lead to more sophisticated detection and delivery techniques.

More sophisticated methods use quantitative approaches to measure the amount and the time course of bolus or reperfusion curves and have shown great promise in revealing an effective tumor response to anti-angiogenic drugs in humans before tumor shrinkage occurs. These are beginning to be accepted into clinical practice. In the long term, targeted microbubbles for molecular imaging and eventually for directed anti-tumor therapy are expected to be developed.

In principle, in any perfused region that can be reached by ultrasound, ultrasound-directed drug delivery could be performed. However, since the ultrasonic fields used with diagnostic ultrasound scanners differ greatly per organ targeted, some regions will be far from ideal. The ultrasonic frequencies transmitted in endoscopy are much higher than the resonance frequencies of conventional ultrasound contrast agents. Therefore, for such applications, smaller carriers will have to be developed for ultrasound-directed drug delivery.

In conclusion, combining ultrasound contrast agents with therapeutic substances may lead to simple and economic methods of treatment with fewer side effects, using conventional ultrasound scanners. Ultrasound-directed drug delivery has great potential in the treatment of malignancies in the digestive system.

REFERENCES

1 **Postema M**. Bubbles and ultrasound. *Appl Acoust* 2009; **70**: 1305
2 **ter Haar G**. Safety and bio-effects of ultrasound contrast agents. *Med Biol Eng Comput* 2009; **47**: 893-900
3 **Postema M**, Schmitz G. Bubble dynamics involved in ultrasonic imaging. *Expert Rev Mol Diagn* 2006; **6**: 493-502
4 **Webb A**. Introduction to Biomedical Imaging. Hoboken: John Wiley and Sons, 2003
5 **Wells PNT**. Ultrasonic imaging of the human body. *Rep Prog Phys* 1999; **62**: 671-722
6 **British Medical Ultrasound Society**. Guidelines for the safe use of diagnostic ultrasound equipment. *Ultrasound* 2010; **18**: 52-59
7 **Postema M**, Gilja OH. Ultrasound-directed drug delivery. *Curr Pharm Biotechnol* 2007; **8**: 355-361
8 **Voigt JU**. Ultrasound molecular imaging. *Methods* 2009; **48**: 92-97
9 **Schmitz G**. Ultrasound in medical diagnosis. In: Pike R, Sabatier P, editors. Scattering: scattering and inverse scattering in pure and applied science. London: Academic Press, 2002: 162-174
10 **Macdonald CA**, Sboros V, Gomatam J, Pye SD, Moran CM, Norman McDicken W. A numerical investigation of the resonance of gas-filled microbubbles: resonance dependence on acoustic pressure amplitude. *Ultrasonics* 2004; **43**: 113-122
11 **Guan J**, Matula TJ. Using light scattering to measure the response of individual ultrasound contrast microbubbles subjected to pulsed ultrasound in vitro. *J Acoust Soc Am* 2004; **116**: 2832-2842
12 **Postema M**. Fundamentals of medical ultrasonics. London: Spon Press, 2011
13 **Postema M**, Bouakaz A, de Jong N. Noninvasive microbubble-based pressure measurements: a simulation study. *Ultrasonics* 2004; **42**: 759-762
14 **Schutt EG**, Klein DH, Mattrey RM, Riess JG. Injectable microbubbles as contrast agents for diagnostic ultrasound imaging: the key role of perfluorochemicals. *Angew Chem Int Ed Engl* 2003; **42**: 3218-3235
15 **Wrenn SP**, Mleczko M, Schmitz G. Phospholipid-stabilized microbubbles: Influence of shell chemistry on cavitation threshold and binding to giant uni-lamellar vesicles. *Appl*

Acoust 2009; **70**: 1313-1322
16 **Sboros V**. Response of contrast agents to ultrasound. *Adv Drug Deliv Rev* 2008; **60**: 1117-1136
17 **Tinkov S**, Bekeredjian R, Winter G, Coester C. Microbubbles as ultrasound triggered drug carriers. *J Pharm Sci* 2009; **98**: 1935-1961
18 **Strasberg M**. Gas bubbles as sources of sound in liquids. *J Acoust Soc Am* 1956; **28**: 20-26
19 **Plesset MS**, Prosperetti A. Bubble dynamics and cavitation. *Annu Rev Fluid Mech* 1977; **9**: 145-185
20 **Attenborough K**, Postema M. A pocket-sized introduction to dynamics. Kingston upon Hull: The University of Hull, 2008
21 **Barlow E**, Mulholland AJ, Gachagan A, Nordon A, MacPherson K. Analysis of the Rayleigh-Plesset equation with chirp excitation. *IMA J Appl Math* 2009; **74**: 20-34
22 **Church CC**. The effects of an elastic solid surface layer on the radial pulsations of gas bubbles. *J Acoust Soc Am* 1995; **97**: 1510-1521
23 **Morgan KE**, Allen JS, Dayton PA, Chomas JE, Klibaov AL, Ferrara KW. Experimental and theoretical evaluation of microbubble behavior: effect of transmitted phase and bubble size. *IEEE Trans Ultrason Ferroelectr Freq Control* 2000; **47**: 1494-1509
24 **Hoff L**, Sontum PC, Hovem JM. Oscillations of polymeric microbubbles: effect of the encapsulating shell. *J Acoust Soc Am* 2000; **107**: 2272-2280
25 **Allen JS**, May DJ, Ferrara KW. Dynamics of therapeutic ultrasound contrast agents. *Ultrasound Med Biol* 2002; **28**: 805-816
26 **Stride E**, Saffari N. On the destruction of microbubble ultrasound contrast agents. *Ultrasound Med Biol* 2003; **29**: 563-573
27 **Postema M**, Schmitz G. Ultrasonic bubbles in medicine: influence of the shell. *Ultrason Sonochem* 2007; **14**: 438-444
28 **Doinikov AA**, Dayton PA. Spatio-temporal dynamics of an encapsulated gas bubble in an ultrasound field. *J Acoust Soc Am* 2006; **120**: 661-669
29 **Zheng H**, Mukdadi O, Shandas R. Theoretical predictions of harmonic generation from submicron ultrasound contrast agents for nonlinear biomedical ultrasound imaging. *Phys Med Biol* 2006; **51**: 557-573
30 **Sarkar K**, Shi WT, Chatterjee D, Forsberg F. Characterization of ultrasound contrast microbubbles using in vitro experiments and viscous and viscoelastic interface models for encapsulation. *J Acoust Soc Am* 2005; **118**: 539-550
31 **Stride E**, Tang MX, Eckersley RJ. Physical phenomena affecting quantitative imaging of ultrasound contrast agents. *Appl Acoust* 2009; **70**: 1352-1362
32 **Mleczko M**, Postema M, Schmitz G. Discussion of the application of finite Volterra series for the modeling of the oscillation behavior of ultrasound contrast agents. *Appl Acoust* 2009; **70**: 1363-1369
33 **Stride E**, Saffari N. Theoretical and experimental investigation of the behaviour of ultrasound contrast agent particles in whole blood. *Ultrasound Med Biol* 2004; **30**: 1495-1509
34 **Qin S**, Caskey CF, Ferrara KW. Ultrasound contrast microbubbles in imaging and therapy: physical principles and engineering. *Phys Med Biol* 2009; **54**: R27-R57
35 **Dayton PA**, Rychak JJ. Molecular ultrasound imaging using microbubble contrast agents. *Front Biosci* 2007; **12**: 5124-5142
36 **Philipp A**, Lauterborn W. Cavitation erosion by single laser-produced bubbles. *J Fluid Mech* 1998; **361**: 75-116
37 **Postema M**, Bouakaz A, de Jong N. March 2002. *IEEE Trans Ultrason Ferroelectr Freq Control* 2002; **49**: c1-c2
38 **Postema M**, van Wamel A, ten Cate FJ, de Jong N. High-speed photography during ultrasound illustrates potential therapeutic applications of microbubbles. *Med Phys* 2005; **32**: 3707-3711
39 **Prentice P**, Cuschieri A, Dholakia K, Prausnitz M, Campbell P. Membrane disruption by optically controlled microbubble cavitation. *Nat Phys* 2005; **1**: 107-110
40 **Postema M**, van Wamel A, Lancée CT, de Jong N. Ultrasound-induced encapsulated microbubble phenomena. *Ultrasound Med Biol* 2004; **30**: 827-840
41 **Kodama T**, Takayama K. Dynamic behavior of bubbles during extracorporeal shock-wave lithotripsy. *Ultrasound Med Biol* 1998; **24**: 723-738
42 **Ohl CD**, Ikink R. Shock-wave-induced jetting of micron-size bubbles. *Phys Rev Lett* 2003; **90**: 214502
43 **Ohl CD**, Ory E. Aspherical bubble collapse - comparison with simulations. In: Lauterborn W, Kurz T, editors. Nonlinear acoustics at the turn of the millennium. New York: American Institute of Physics, 2000: 393-396
44 **Chomas JE**, Dayton P, May D, Ferrara K. Threshold of fragmentation for ultrasonic contrast agents. *J Biomed Opt* 2001; **6**: 141-150
45 **Brennen CE**. Fission of collapsing cavitation bubbles. *J Fluid Mech* 2002; **472**: 153-166
46 **Bloch SH**, Wan M, Dayton PA, Ferrara KW. Optical observation of lipid- and polymer-shelled ultrasound microbubble contrast agents. *Appl Phys Lett* 2004; **84**: 631-633
47 **Postema M**, Bouakaz A, Versluis M, de Jong N. Ultrasound-induced gas release from contrast agent microbubbles. *IEEE Trans Ultrason Ferroelectr Freq Control* 2005; **52**: 1035-1041
48 **Postema M**, Bouakaz A, ten Cate FJ, Schmitz G, de Jong N, van Wamel A. Nitric oxide delivery by ultrasonic cracking: some limitations. *Ultrasonics* 2006; **44** Suppl 1: e109-e113
49 **Fagan MJ**, Postema M. Introduction to stress and strain analysis. Kingston upon Hull: The University of Hull, 2007
50 **Bevan PD**, Karshafian R, Matsumura M, Tickner G, Burns PN. An acoustic study of disruption of polymer-shelled bubbles [microbubble contrast agents]. *Proc IEEE Ultrason Symp* 2004; **2**: 1391-1394
51 **Moran CM**, Anderson T, Pye SD, Sboros V, McDicken WN. Quantification of microbubble destruction of three fluorocarbon-filled ultrasonic contrast agents. *Ultrasound Med Biol* 2000; **26**: 629-639
52 **Leighton TG**. The acoustic bubble. London: Academic Press Ltd, 1994
53 **Dayton PA**, Allen JS, Ferrara KW. The magnitude of radiation force on ultrasound contrast agents. *J Acoust Soc Am* 2002; **112**: 2183-2192
54 **Dayton PA**, Morgan KE, Klibanov AL, Brandenburger G, Nightingale KR, Ferrara KW. A preliminary evaluation of the effects of primary and secondary radiation forces on acoustic contrast agents. *IEEE Trans Ultrason Ferroelectr Freq Control* 1997; **44**: 1264-1277
55 **Tortoli P**, Michelassi V, Corsi M, Righi D, Takeuchi Y. On the interaction between ultrasound and contrast agents during Doppler investigations. *Ultrasound Med Biol* 2001; **27**: 1265-1273
56 **Shortencarier MJ**, Dayton PA, Bloch SH, Schumann PA, Matsunaga TO, Ferrara KW. A method for radiation-force localized drug delivery using gas-filled lipospheres. *IEEE Trans Ultrason Ferroelectr Freq Control* 2004; **51**: 822-831
57 **Zhao S**, Borden M, Bloch SH, Kruse D, Ferrara KW, Dayton PA. Radiation-force assisted targeting facilitates ultrasonic molecular imaging. *Mol Imaging* 2004; **3**: 135-148
58 **Tortoli P**, Boni E, Corsi M, Arditi M, Frinking P. Different effects of microbubble destruction and translation in Doppler measurements. *IEEE Trans Ultrason Ferroelectr Freq Control* 2005; **52**: 1183-1188
59 **Rychak JJ**, Klibanov AL, Hossack JA. Acoustic radiation force enhances targeted delivery of ultrasound contrast microbubbles: in vitro verification. *IEEE Trans Ultrason Ferroelectr Freq Control* 2005; **52**: 421-433
60 **Lum AF**, Borden MA, Dayton PA, Kruse DE, Simon SI, Ferrara KW. Ultrasound radiation force enables targeted deposition of model drug carriers loaded on microbubbles. *J Control Release* 2006; **111**: 128-134
61 **Kotopoulis S**, Postema M. Microfoam formation in a capil-

lary. *Ultrasonics* 2010; **50**: 260-268
62 **Mettin R**, Doinikov AA. Translational instability of a spherical bubble in a standing ultrasound wave. *Appl Acoust* 2009; **70**: 1330-1339
63 **Kaul S**. Myocardial contrast echocardiography: a 25-year retrospective. *Circulation* 2008; **118**: 291-308
64 **Bao S**, Thrall BD, Miller DL. Transfection of a reporter plasmid into cultured cells by sonoporation in vitro. *Ultrasound Med Biol* 1997; **23**: 953-959
65 **Chen S**, Shohet RV, Bekeredjian R, Frenkel P, Grayburn PA. Optimization of ultrasound parameters for cardiac gene delivery of adenoviral or plasmid deoxyribonucleic acid by ultrasound-targeted microbubble destruction. *J Am Coll Cardiol* 2003; **42**: 301-308
66 **Delius M**, Hofschneider PH, Lauer U, Messmer K. Extracorporeal shock waves for gene therapy? *Lancet* 1995; **345**: 1377
67 **Frenkel PA**, Chen S, Thai T, Shohet RV, Grayburn PA. DNA-loaded albumin microbubbles enhance ultrasound-mediated transfection in vitro. *Ultrasound Med Biol* 2002; **28**: 817-822
68 **Greenleaf WJ**, Bolander ME, Sarkar G, Goldring MB, Greenleaf JF. Artificial cavitation nuclei significantly enhance acoustically induced cell transfection. *Ultrasound Med Biol* 1998; **24**: 587-595
69 **Kondo I**, Ohmori K, Oshita A, Takeuchi H, Fuke S, ShiKondo I, Ohmori K, Oshita A, Takeuchi H, Fuke S, Shinomiya K, Noma T, Namba T, Kohno M. Treatment of acute myocardial infarction by hepatocyte growth factor gene transfer: the first demonstration of myocardial transfer of a "functional" gene using ultrasonic microbubble destruction. *J Am Coll Cardiol* 2004; **44**: 644-653
70 **Lawrie A**, Brisken AF, Francis SE, Wyllie D, Kiss-Toth E, Qwarnstrom EE, Dower SK, Crossman DC, Newman CM. Ultrasound-enhanced transgene expression in vascular cells is not dependent upon cavitation-induced free radicals. *Ultrasound Med Biol* 2003; **29**: 1453-1461
71 **Lindner JR**, Kaul S. Delivery of drugs with ultrasound. *Echocardiography* 2001; **18**: 329-337
72 **Manome Y**, Nakayama N, Nakayama K, Furuhata H. Insonation facilitates plasmid DNA transfection into the central nervous system and microbubbles enhance the effect. *Ultrasound Med Biol* 2005; **31**: 693-702
73 **Miller DL**, Bao S, Gies RA, Thrall BD. Ultrasonic enhancement of gene transfection in murine melanoma tumors. *Ultrasound Med Biol* 1999; **25**: 1425-1430
74 **Miller DL**, Bao S, Morris JE. Sonoporation of cultured cells in the rotating tube exposure system. *Ultrasound Med Biol* 1999; **25**: 143-149
75 **Miller DL**, Dou C. Membrane damage thresholds for pulsed or continuous ultrasound in phagocytic cells loaded with contrast agent gas bodies. *Ultrasound Med Biol* 2004; **30**: 405-411
76 **Miller DL**, Dou C. Membrane damage thresholds for 1- to 10-MHz pulsed ultrasound exposure of phagocytic cells loaded with contrast agent gas bodies in vitro. *Ultrasound Med Biol* 2004; **30**: 973-977
77 **Mukherjee D**, Wong J, Griffin B, Ellis SG, Porter T, Sen S, Thomas JD. Ten-fold augmentation of endothelial uptake of vascular endothelial growth factor with ultrasound after systemic administration. *J Am Coll Cardiol* 2000; **35**: 1678-1686
78 **Newman CM**, Lawrie A, Brisken AF, Cumberland DC. Ultrasound gene therapy: on the road from concept to reality. *Echocardiography* 2001; **18**: 339-347
79 **Pislaru SV**, Pislaru C, Kinnick RR, Singh R, Gulati R, Greenleaf JF, Simari RD. Optimization of ultrasound-mediated gene transfer: comparison of contrast agents and ultrasound modalities. *Eur Heart J* 2003; **24**: 1690-1698
80 **Porter TR**, Xie F. Targeted drug delivery using intravenous microbubbles. In: Goldberg BB, Raichlen JS, Forsberg F, editors. Ultrasound Contrast Agents Basic principles and clinical applications. 2nd ed. London: Martin Dunitz Ltd., 2001: 347-351
81 **Porter TR**, Xie F. Therapeutic ultrasound for gene delivery. *Echocardiography* 2001; **18**: 349-353
82 **Song J**, Chappell JC, Qi M, VanGieson EJ, Kaul S, Price RJ. Influence of injection site, microvascular pressure and ultrasound variables on microbubble-mediated delivery of microspheres to muscle. *J Am Coll Cardiol* 2002; **39**: 726-731
83 **Tachibana K**, Tachibana S. The use of ultrasound for drug delivery. *Echocardiography* 2001; **18**: 323-328
84 **Tachibana K**, Uchida T, Ogawa K, Yamashita N, Tamura K. Induction of cell-membrane porosity by ultrasound. *Lancet* 1999; **353**: 1409
85 **Unger EC**, Hersh E, Vannan M, McCreery T. Gene delivery using ultrasound contrast agents. *Echocardiography* 2001; **18**: 355-361
86 **Unger EC**, Matsunaga TO, McCreery T, Schumann P, Sweitzer R, Quigley R. Therapeutic applications of microbubbles. *Eur J Radiol* 2002; **42**: 160-168
87 **Taniyama Y**, Tachibana K, Hiraoka K, Namba T, Yamasaki K, Hashiya N, Aoki M, Ogihara T, Yasufumi K, Morishita R. Local delivery of plasmid DNA into rat carotid artery using ultrasound. *Circulation* 2002; **105**: 1233-1239
88 **van Wamel A**, Bouakaz A, Bernard B, ten Cate F, de Jong N. Radionuclide tumour therapy with ultrasound contrast microbubbles. *Ultrasonics* 2004; **42**: 903-906
89 **Mehier-Humbert S**, Bettinger T, Yan F, Guy RH. Ultrasound-mediated gene delivery: kinetics of plasmid internalization and gene expression. *J Control Release* 2005; **104**: 203-211
90 **Kudo N**, Okada K, Yamamoto K. Sonoporation by single-shot pulsed ultrasound with microbubbles adjacent to cells. *Biophys J* 2009; **96**: 4866-4876
91 **Okada K**, Kudo N, Kondo T, Yamamoto K. Contributions of mechanical and sonochemical effects to cell membrane damage induced by single-shot pulsed ultrasound with adjacent microbubbles. *J Med Ultrasonics* 2008; **35**: 169-176
92 **Karshafian R**, Bevan PD, Burns PN, Samac S, Banerjee M. Ultrasound-induced uptake of different size markers in mammalian cells. *Proc IEEE Ultrason Symp* 2005; **1**:13-16
93 **Schlicher RK**, Radhakrishna H, Tolentino TP, Apkarian RP, Zarnitsyn V, Prausnitz MR. Mechanism of intracellular delivery by acoustic cavitation. *Ultrasound Med Biol* 2006; **32**: 915-924
94 **Mehier-Humbert S**, Bettinger T, Yan F, Guy RH. Plasma membrane poration induced by ultrasound exposure: implication for drug delivery. *J Control Release* 2005; **104**: 213-222
95 **Miller DL**, Nyborg WL. Theoretical investigation of the response of gas-filled micropores and cavitation nuclei to ultrasound. *J Acoust Soc Am* 1983; **73**: 1537-1544
96 **Miller DL**, Song J. Lithotripter shock waves with cavitation nucleation agents produce tumor growth reduction and gene transfer in vivo. *Ultrasound Med Biol* 2002; **28**: 1343-1348
97 **Lentacker I**, De Smedt SC, Sanders NN. Drug loaded microbubble design for ultrasound triggered delivery. *Soft Matter* 2009; **5**: 2161-2170
98 **Klibanov AL**. Targeted delivery of gas-filled microspheres, contrast agents for ultrasound imaging. *Adv Drug Deliv Rev* 1999; **37**: 139-157
99 **Christiansen JP**, French BA, Klibanov AL, Kaul S, Lindner JR. Targeted tissue transfection with ultrasound destruction of plasmid-bearing cationic microbubbles. *Ultrasound Med Biol* 2003; **29**: 1759-1767
100 **Dayton P**, Morgan K, Allietta M, Klibanov A, Brandenburger G, Ferrara K. Simultaneous optical and acoustical observations of contrast agents. *Proc IEEE Ultrason Symp* 1997; **2**: 1583-1591
101 **Takeuchi Y**. July 1999. *IEEE Trans Ultrason Ferroelectr Freq Control* 1999; **46**: c1-c2
102 **Postema M**, ten Cate FJ, Schmitz G, de Jong N, van Wamel A. Generation of a droplet inside a microbubble with the aid of

an ultrasound contrast agent: first result. *Lett Drug Des Discov* 2007; **4**: 74-77
103 **Dorbolo S**, Caps H, Vandewalle N. Fluid instabilities in the birth and death of antibubbles. *New J Phys* 2003; **5**: 161
104 **Katz JI**. Jets from collapsing bubbles. *Proc R Soc Lond A* 1999; **455**: 323-328
105 **Duchemin L**, Popinet S, Josserand C, Zaleski S. Jet formation in bubbles bursting at a free surface. *Phys Fluids* 2002; **14**: 3000-3008
106 **Bekeredjian R**, Grayburn PA, Shohet RV. Use of ultrasound contrast agents for gene or drug delivery in cardiovascular medicine. *J Am Coll Cardiol* 2005; **45**: 329-335
107 **Miller DL**, Dou C, Song J. DNA transfer and cell killing in epidermoid cells by diagnostic ultrasound activation of contrast agent gas bodies in vitro. *Ultrasound Med Biol* 2003; **29**: 601-607
108 **van Wamel A**, Bouakaz A, ten Cate F, de Jong N. Effects of diagnostic ultrasound parameters on molecular uptake and cell viability. *Proc IEEE Ultrason Symp* 2002; **2**: 1419-1422
109 **Hallow DM**, Mahajan AD, McCutchen TE, Prausnitz MR. Measurement and correlation of acoustic cavitation with cellular bioeffects. *Ultrasound Med Biol* 2006; **32**: 1111-1122
110 **Feril LB Jr**, Kondo T, Takaya K, Riesz P. Enhanced ultrasound-induced apoptosis and cell lysis by a hypotonic medium. *Int J Radiat Biol* 2004; **80**: 165-175
111 **Watanabe A**, Kawai K, Sato T, Nishimura H, Kawashima N, Takeuchi S. Apoptosis induction in cancer cells by ultrasound exposure. *Jpn J Appl Phys* 2004; **43**: 3245-3248
112 **Abdollahi A**, Domhan S, Jenne JW, Hallaj M, Dell'Aqua G, Mueckenthaler M, Richter A, Martin H, Debus J, Ansorge W, Hynynen K, Huber PE. Apoptosis signals in lymphoblasts induced by focused ultrasound. *FASEB J* 2004; **18**: 1413-1414
113 **Miller MW**, Miller DL, Brayman AA. A review of in vitro bioeffects of inertial ultrasonic cavitation from a mechanistic perspective. *Ultrasound Med Biol* 1996; **22**: 1131-1154
114 **Albrecht T**, Blomley M, Bolondi L, Claudon M, Correas JM, Cosgrove D, Greiner L, Jäger K, Jong ND, Leen E, Lencioni R, Lindsell D, Martegani A, Solbiati L, Thorelius L, Tranquart F, Weskott HP, Whittingham T. Guidelines for the use of contrast agents in ultrasound. January 2004. *Ultraschall Med* 2004; **25**: 249-256
115 **Claudon M**, Cosgrove D, Albrecht T, Bolondi L, Bosio M, Calliada F, Correas JM, Darge K, Dietrich C, D'Onofrio M, Evans DH, Filice C, Greiner L, Jäger K, Jong N, Leen E, Lencioni R, Lindsell D, Martegani A, Meairs S, Nolsøe C, Piscaglia F, Ricci P, Seidel G, Skjoldbye B, Solbiati L, Thorelius L, Tranquart F, Weskott HP, Whittingham T. Guidelines and good clinical practice recommendations for contrast enhanced ultrasound (CEUS) - update 2008. *Ultraschall Med* 2008; **29**: 28-44
116 **Bernatik T**, Becker D, Neureiter D, Hänsler J, Frieser M, Schaber S, Hahn EG, Strobel D. [Detection of liver metastases--comparison of contrast--enhanced ultrasound using first versus second generation contrast agents]. *Ultraschall Med* 2003; **24**: 175-179
117 **Strobel D**, Seitz K, Blank W, Schuler A, Dietrich C, von Herbay A, Friedrich-Rust M, Kunze G, Becker D, Will U, Kratzer W, Albert FW, Pachmann C, Dirks K, Strunk H, Greis C, Bernatik T. Contrast-enhanced ultrasound for the characterization of focal liver lesions--diagnostic accuracy in clinical practice (DEGUM multicenter trial). *Ultraschall Med* 2008; **29**: 499-505
118 **Albrecht T**, Hohmann J, Oldenburg A, Skrok J, Wolf KJ. Detection and characterisation of liver metastases. *Eur Radiol* 2004; **14** Suppl 8: P25-P33
119 **Dietrich CF**, Kratzer W, Strobe D, Danse E, Fessl R, Bunk A, Vossas U, Hauenstein K, Koch W, Blank W, Oudkerk M, Hahn D, Greis C. Assessment of metastatic liver disease in patients with primary extrahepatic tumors by contrast-enhanced sonography versus CT and MRI. *World J Gastroenterol* 2006; **12**: 1699-1705
120 **Konopke R**, Kersting S, Bergert H, Bloomenthal A, Gastmeier J, Saeger HD, Bunk A. Contrast-enhanced ultrasonography to detect liver metastases : a prospective trial to compare transcutaneous unenhanced and contrast-enhanced ultrasonography in patients undergoing laparotomy. *Int J Colorectal Dis* 2007; **22**: 201-207
121 **Torzilli G**. Contrast-enhanced intraoperative ultrasonography in surgery for liver tumors. *Eur J Radiol* 2004; **51** Suppl: S25-S29
122 **Torzilli G**, Botea F, Procopio F, Donadon M, Balzarini L, Lutman F, Calliada F, Montorsi M. Use of contrast-enhanced intraoperative ultrasonography during liver surgery for colorectal cancer liver metastases – Its impact on operative outcome. Analysis of a prospective cohort study. *Eur J Cancer Suppl* 2008; **6**: 16-23
123 **Lassau N**, Lamuraglia M, Koscielny S, Spatz A, Roche A, Leclere J, Avril MF. Prognostic value of angiogenesis evaluated with high-frequency and colour Doppler sonography for preoperative assessment of primary cutaneous melanomas: correlation with recurrence after a 5 year follow-up period. *Cancer Imaging* 2006; **6**: 24-29
124 **Cosgrove D**, Lassau N. [Assessment of tumour angiogenesis using contrast-enhanced ultrasound]. *J Radiol* 2009; **90**: 156-164
125 **Lassau N**, Koscielny S, Albiges L, Chami L, Benatsou B, Chebil M, Roche A, Escudier BJ. Metastatic renal cell carcinoma treated with sunitinib: early evaluation of treatment response using dynamic contrast-enhanced ultrasonography. *Clin Cancer Res* 2010; **16**: 1216-1225
126 **Leen E**. The role of contrast-enhanced ultrasound in the characterisation of focal liver lesions. *Eur Radiol* 2001; **11** Suppl 3: E27-E34
127 **Nicolau C**, Catalá V, Vilana R, Gilabert R, Bianchi L, Solé M, Pagés M, Brú C. Evaluation of hepatocellular carcinoma using SonoVue, a second generation ultrasound contrast agent: correlation with cellular differentiation. *Eur Radiol* 2004; **14**: 1092-1099
128 **Ding H**, Wang WP, Huang BJ, Wei RX, He NA, Qi Q, Li CL. Imaging of focal liver lesions: low-mechanical-index real-time ultrasonography with SonoVue. *J Ultrasound Med* 2005; **24**: 285-297
129 **Camaggi V**, Piscaglia F, Bolondi L. Recent advances in the imaging of hepatocellular carcinoma. From ultrasound to positron emission tomography scan. *Saudi Med J* 2007; **28**: 1007-1014
130 **Dai Y**, Chen MH, Fan ZH, Yan K, Yin SS, Zhang XP. Diagnosis of small hepatic nodules detected by surveillance ultrasound in patients with cirrhosis: Comparison between contrast-enhanced ultrasound and contrast-enhanced helical computed tomography. *Hepatol Res* 2008; **38**: 281-290
131 **Forner A**, Vilana R, Ayuso C, Bianchi L, Solé M, Ayuso JR, Boix L, Sala M, Varela M, Llovet JM, Brú C, Bruix J. Diagnosis of hepatic nodules 20 mm or smaller in cirrhosis: Prospective validation of the noninvasive diagnostic criteria for hepatocellular carcinoma. *Hepatology* 2008; **47**: 97-104
132 **Giorgio A**, De Stefano G, Coppola C, Ferraioli G, Esposito V, Di Sarno A, Giorgio V, De Stefano M, Sangiovanni V, Liorre G, Del Viscovo L. Contrast-enhanced sonography in the characterization of small hepatocellular carcinomas in cirrhotic patients: comparison with contrast-enhanced ultrafast magnetic resonance imaging. *Anticancer Res* 2007; **27**: 4263-4269
133 **Koda M**, Matsunaga Y, Ueki M, Maeda Y, Mimura K, Okamoto K, Hosho K, Murawaki Y. Qualitative assessment of tumor vascularity in hepatocellular carcinoma by contrast-enhanced coded ultrasound: comparison with arterial phase of dynamic CT and conventional color/power Doppler ultrasound. *Eur Radiol* 2004; **14**: 1100-1108
134 **Lu MD**, Yu XL, Li AH, Jiang TA, Chen MH, Zhao BZ, Zhou

XD, Wang JR. Comparison of contrast enhanced ultrasound and contrast enhanced CT or MRI in monitoring percutaneous thermal ablation procedure in patients with hepatocellular carcinoma: a multi-center study in China. *Ultrasound Med Biol* 2007; **33**: 1736-1749

135 **Suzuki S**, Iijima H, Moriyasu F, Sasaki S, Yanagisawa K, Miyahara T, Oguma K, Yoshida M, Horibe T, Ito N, Kakizaki D, Abe K, Tsuchiya K. Differential diagnosis of hepatic nodules using delayed parenchymal phase imaging of levovist contrast ultrasound: comparative study with SPIO-MRI. *Hepatol Res* 2004; **29**: 122-126

136 **Vallone P**, Gallipoli A, Izzo F, Fiore F, Delrio P. Local ablation procedures in primary liver tumors: Levovist US versus spiral CTto evaluate therapeutic results. *Anticancer Res* 2003; **23**: 5075-5079

137 **D'Onofrio M**, Zamboni G, Faccioli N, Capelli P, Pozzi Mucelli R. Ultrasonography of the pancreas. 4. Contrast-enhanced imaging. *Abdom Imaging* 2007; **32**: 171-181

138 **Faccioli N**, Crippa S, Bassi C, D'Onofrio M. Contrast-enhanced ultrasonography of the pancreas. *Pancreatology* 2009; **9**: 560-566

139 **Recaldini C**, Carrafiello G, Bertolotti E, Angeretti MG, Fugazzola C. Contrast-enhanced ultrasonograpic findings in pancreatic tumors. *Int J Med Sci* 2008; **5**: 203-208

140 **D'Onofrio M**, Mansueto G, Falconi M, Procacci C. Neuroendocrine pancreatic tumor: value of contrast enhanced ultrasonography. *Abdom Imaging* 2004; **29**: 246-258

141 **Gilja OH**, Heimdal A, Hausken T, Gregersen H, Matre K, Berstad A, Ødegaard S. Strain during gastric contractions can be measured using Doppler ultrasonography. *Ultrasound Med Biol* 2002; **28**: 1457-1465

142 **Ødegaard S**, Nesje LB, Hoff DA, Gilja OH, Gregersen H. Morphology and motor function of the gastrointestinal tract examined with endosonography. *World J Gastroenterol* 2006; **12**: 2858-2863

143 **Ødegaard S**, Nesje LB, Gilja OH. Atlas of endoscopic ultrasonography. Bergen: Fagbokforlaget, 2007

144 **Lassau N**, Brule A, Chami L, Benatsou B, Péronneau P, Roche A. [Evaluation of early response to antiangiogenic treatment with dynamic contrast enhanced ultrasound]. *J Radiol* 2008; **89**: 549-555

145 **Lassau N**, Lamuraglia M, Chami L, Leclère J, Bonvalot S, Terrier P, Roche A, Le Cesne A. Gastrointestinal stromal tumors treated with imatinib: monitoring response with contrast-enhanced sonography. *AJR Am J Roentgenol* 2006; **187**: 1267-1273

146 **Magnon C**, Galaup A, Rouffiac V, Opolon P, Connault E, Rosé M, Perricaudet M, Roche A, Germain S, Griscelli F, Lassau N. Dynamic assessment of antiangiogenic therapy by monitoring both tumoral vascularization and tissue degeneration. *Gene Ther* 2007; **14**: 108-117

147 **Franco M**, Man S, Chen L, Emmenegger U, Shaked Y, Cheung AM, Brown AS, Hicklin DJ, Foster FS, Kerbel RS. Targeted anti-vascular endothelial growth factor receptor-2 therapy leads to short-term and long-term impairment of vascular function and increase in tumor hypoxia. *Cancer Res* 2006; **66**: 3639-3648

148 **Krishna PD**, Shankar PM, Newhouse VL. Subharmonic generation from ultrasonic contrast agents. *Phys Med Biol* 1999; **44**: 681-694

149 **Guidi F**, Vos HJ, Nicchi F, Boni E, Tortoli P. Acoustical Imaging of Individual Microbubbles. In: André MP, editor. Acoustical imaging. Berlin: Springer, 2007: 257-265

150 **Postema M**, Mleczko M, Schmitz G. Mutual attraction of oscillation microbubbles. In: Buzug TM, Holz D, Weber S, Bongartz J, Kohl-Bareis M, Hartmann U, editors. Advances in medical engineering. Berlin: Springer, 2007: 75-80

151 **Postema M**, Marmottant P, Lancée CT, Versluis M, Hilgenfeldt S, de Jong N. Ultrasound-induced coalescence of free gas microbubbles. *Proc IEEE Ultrason Symp* 2004; **1**: 1-4

152 **Bevan PD**, Karshafian R, Burns PN. The influence of fragmentation on the acoustic response from shrinking bubbles. *Ultrasound Med Biol* 2008; **34**: 1152-1162

153 **Chomas JE**, Dayton PA, May D, Allen J, Klibanov A, Ferrara K. Optical observation of contrast agent destruction. *Appl Phys Lett* 2000; **77**: 1056-1058

154 **Borden MA**, Kruse DE, Caskey CF, Zhao S, Dayton PA, Ferrara KW. Influence of lipid shell physicochemical properties on ultrasound-induced microbubble destruction. *IEEE Trans Ultrason Ferroelectr Freq Control* 2005; **52**: 1992-2002

155 **Postema M**, de Jong N, Schmitz G. Shell rupture threshold, fragmentation threshold, blake threshold. *Proc IEEE Ultrason Symp* 2005; **3**: 1708-1711

156 **Postema M**, Marmottant P, Lancée CT, Hilgenfeldt S, de Jong N. Ultrasound-induced microbubble coalescence. *Ultrasound Med Biol* 2004; **30**: 1337-1344

157 **Postema M**, de Jong N, Schmitz G. Nonlinear behavior of ultrasound-insonified encapsulated microbubbles. In: Atchley AA, Sparrow VW, Keolian RM, editors. Innovations in nonlinear acoustics. Melville: American Institute of Physics, 2006: 275-278

158 **Takeuchi Y**. Industrial use thermoplastic microballoon to mimic the contrast agents and its in-vitro behavior including released gas dynamics. *Proc Proc IEEE Ultrason Symp* 1997; **2**: 1579-1582

159 **Bevan PD**, Karshafian R, Tickner EG, Burns PN. Quantitative measurement of ultrasound disruption of polymer-shelled microbubbles. *Ultrasound Med Biol* 2007; **33**: 1777-1786

S- Editor Sun H **L- Editor** Cant MR **E- Editor** Zheng XM

Available online at www.sciencedirect.com
ScienceDirect
Ultrasonics Sonochemistry 14 (2007) 438–444
Ultrasonics SONOCHEMISTRY
www.elsevier.com/locate/ultsonch

Ultrasonic bubbles in medicine: Influence of the shell

Michiel Postema *, Georg Schmitz

Institute for Medical Engineering, Department of Electrical Engineering and Information Technology, Ruhr-Universität Bochum, Building IC, 6/146, D-44780 Bochum, Germany

Received 23 July 2006; accepted 1 September 2006
Available online 10 January 2007

Abstract

Ultrasound contrast agents consist of microscopically small bubbles encapsulated by an elastic shell. These microbubbles oscillate upon ultrasound insonification, and demonstrate highly nonlinear behavior, ameliorating their detectability. (Potential) medical applications involving the ultrasonic disruption of contrast agent microbubble shells include release-burst imaging, localized drug delivery, and noninvasive blood pressure measurement. To develop and enhance these techniques, predicting the cracking behavior of ultrasound-insonified encapsulated microbubbles has been of importance. In this paper, we explore microbubble behavior in an ultrasound field, with special attention to the influence of the bubble shell.

A bubble in a sound field can be considered a forced damped harmonic oscillator. For encapsulated microbubbles, the presence of a shell has to be taken into account. In models, an extra damping parameter and a shell stiffness parameter have been included, assuming that Hooke's Law holds for the bubble shell. At high acoustic amplitudes, disruptive phenomena have been observed, such as microbubble fragmentation and ultrasonic cracking. We analyzed the occurrence of ultrasound contrast agent fragmentation, by simulating the oscillating behavior of encapsulated microbubbles with various sizes in a harmonic acoustic field. Fragmentation occurs exclusively during the collapse phase and occurs if the kinetic energy of the collapsing microbubble is greater than the instantaneous bubble surface energy, provided that surface instabilities have grown big enough to allow for break-up. From our simulations it follows that the Blake critical radius is not a good approximation for a fragmentation threshold.

We demonstrated how the phase angle differences between a damped radially oscillating bubble and an incident sound field depend on shell parameters.

Keywords: Ultrasound contrast agent; Shell disruption; Fragmentation threshold; Oscillation phase angle; Shell elasticity; Shell friction

1. Introduction

Ultrasonic imaging is an economic, reliable diagnostic technique. When taking into account the absolute hospital operating expenses [1], X-ray and ultrasound have approximately the same price per examination. Other imaging techniques are roughly three times as expensive, except for catheterization, which is 20 times as expensive [2]. However, X-ray is a less desirable imaging technique than ultrasound, due to the negative ionizing radiation effects. Therefore, novel ultrasound-based imaging techniques are being developed that may compete with other imaging techniques.

In clinical ultrasound, blood cells cannot be differentiated from surrounding tissue, due to the low acoustic impedance difference between blood cells and their surroundings. Resonant gas bubbles introduced in the blood stream are ideal markers, if rapid dissolution can be prevented. Ultrasound contrast agents consist of microscopically small bubbles encapsulated by an elastic shell. These microbubbles oscillate upon ultrasound insonification, and demonstrate highly nonlinear behavior, ameliorating their detectability. To enhance diagnostic ultrasound imaging techniques and to explore therapeutic applications, these medical microbubbles have been modeled.

* Corresponding author. Tel.: +49 234 32 27740.
E-mail address: michiel.postema@ruhr-uni-bochum.de (M. Postema).

1350-4177/$ - see front matter © 2006 Elsevier B.V. All rights reserved.
doi:10.1016/j.ultsonch.2006.09.013

For structures with radii r much less than the acoustic wavelength, such as red blood cells, the ultrasonic backscattering coefficient is [3]

$$\eta(\omega) \propto k^4 r^6 \left(\frac{\kappa_1 - \kappa_0}{\kappa_0} - \frac{\rho_1 - \rho_0}{\rho_0} \right)^2, \tag{1}$$

where k is the acoustic wave number, κ_1 is the compressibility of the scatterer, κ_0 is the compressibility of the surrounding medium, ρ_1 is the density of the scatterer, and ρ_0 is the density of the surrounding medium. Since the density and compressibility parameters of blood cells hardly differ from those of plasma, in the diagnostic ultrasonic frequency range, blood cells are poor scatterers. An ultrasound contrast agent has been added to the blood that helps to differentiate between blood and other tissue types, by providing additional and desirably characteristic backscatter [4]. Gas microbubbles are suitable contrast agents because of their high compressibility and low density compared to the surrounding medium. To prevent them from rapid dissolution, ultrasound contrast agents consist of air or slowly diffusing gas (*e.g.*, SF_6, C_3F_8) bubbles encapsulated by a stabilizing elastic (*e.g.*, albumin, lipid) shell. With mean diameters below 6 μm, these bubbles are small enough to pass through capillaries. An overview of ultrasound contrast agents currently available and their applications has been given in [2].

(Potential) medical applications involving the disruption of microbubble shells include release-burst imaging [5], localized drug delivery [6,7], and noninvasive blood pressure measurement [8]. To develop and enhance these techniques, predicting the cracking behavior of ultrasound-insonified encapsulated microbubbles has been of importance. In order to develop such predictive models, ultrasound contrast agents have been studied by measuring their acoustic response [9,10], by (high-speed) photography during insonification [11,12], and by atomic force microscopy [13].

In this paper, we explore microbubble behavior in an ultrasound field, with special attention to the influence of the bubble shell.

2. Theory

2.1. Linear, radially symmetric behavior

A bubble in a low-amplitude sound field can be considered a forced damped harmonic oscillator [14]:

$$m\ddot{x} + \beta\dot{x} + sx = F(\omega t), \tag{2}$$

where m is the mass of the bubble–liquid system [15]; x, the bubble excursion; β, the mechanical resistance; s, the stiffness of the system; and $F(\omega t)$, the driving force with an angular frequency ω. This system can be rewritten substituting the angular resonance frequency

$$\omega_0 = \sqrt{\frac{s}{m}} \tag{3}$$

and a dimensionless damping parameter

$$\delta = \frac{\beta}{m\omega}. \tag{4}$$

The damping of the pulsation is determined by the acoustic radiation, the heat conduction, and the liquid viscosity [16]. In [14], Young elegantly demonstrated that a solution of Eq. (2) has a phase angle difference $\alpha + \pi$ with the incident field, where

$$\alpha = \arctan\left(\frac{\left(\frac{\omega}{\omega_0}\right)\delta}{1 - \left(\frac{\omega}{\omega_0}\right)^2} \right). \tag{5}$$

For encapsulated microbubbles, the presence of a shell has to be taken into account, by adding an extra damping parameter:

$$\delta_s = \frac{S_f}{m\omega}, \tag{6}$$

where S_f is the shell friction [17]. Also, shell stiffness parameters χ, S_{sh} have been added, assuming that Hooke's Law holds for the bubble shell [16]:

$$\chi = \frac{S_{sh}}{8\pi} = \frac{\mathbf{E}\epsilon}{1 - \nu}, \tag{7}$$

where $\mathbf{E}$ is Young's modulus, ϵ is the shell thickness, and ν is the Poisson ratio. The shell stiffness can be assessed from atomic force microscopy [13], estimated from optical observations of radius–time curves [11,12] or derived from acoustical data using the relation [18]:

$$\omega_s^2 \approx \omega_0^2 + \frac{2\chi}{r_0^3\rho}, \tag{8}$$

where ω_s is the angular resonance frequency of the encapsulated microbubble, ω_0 is the angular resonance frequency of a free (unencapsulated) microbubble of the same size, r_0 is the equilibrium radius of the bubble, and ρ is the liquid density.

2.2. Nonlinear, radially symmetric behavior

When the ultrasonic driving pressure is sufficiently high, the nonlinear microbubble response results in harmonic dispersion, which not only produces harmonics with frequencies that are integer multiples of ω (superharmonics) but also subharmonics with frequencies less than ω of the form $m\omega/n$, where $\{m, n\} \in \mathbb{N}$ [19]. The nonlinear oscillating behavior of spherically symmetric single bubbles has been described by models based on the Rayleigh–Plesset equation [14,19]. de Jong et al. added shell stiffness and friction terms and showed that the shells surrounding the ultrasound contrast agent Albunex® could be modeled as an elastic solid [17]. This model proved to be useful for thin lipid shells, as well [20,2]. Church derived a general theoretical model for the case of a bubble whose surface is occupied by molecules which behave collectively as a

continuous, damped, elastic solid [21]. This model has been modified many times to predict the dynamic behavior of ultrasound contrast agents [11,22–27]. These models take into account the surface tension, the (in)compressibility of the liquid, the viscosity of the shell, and the fact that the gas in the bubble is compressed and expanded according to the gas law. Most of the modified models are referred to as zero-thickness encapsulation models, since these assume the bubble shell to be very thin and describe only the dynamics of the outer bubble radius. Recently, Sarkar et al. presented viscous and viscoelastic rheological models of the bubble shell [28]. Doinikov and Dayton generalized Church's theory, by allowing for the translation motion of the bubble and radiation losses due to the compressibility of the surrounding liquid. Also, models accounting for large-amplitude oscillations have become of interest [29].

At low acoustic amplitudes (mechanical index MI < 0.1), microbubbles pulsate linearly. At high-amplitudes (MI > 0.6), their elongated expansion phase is followed by a violent collapse. During the collapse phase, when the kinetic energy of the bubble surpasses its surface energy, a bubble may fragment into a number of smaller bubbles. Fragmentation has been exclusively observed with contrast agents with thin, elastic shells. Fragmentation is the dominant disruption mechanism for these bubbles [12].

During the initial part of the collapse the acceleration, $\ddot{r}$ is negative. This sign changes as the gas inside the bubble begins to be compressed, and the rebound begins [30]. Provided that surface instabilities have grown big enough to allow for break-up, microbubble fragmentation has been expected and observed close to this moment, when $\ddot{r} = 0$ [31]. This has been confirmed by means of high-speed photography [12,32]. The occurrence of fragmentation has been associated with inertial cavitation [31,10]. Thresholds have been proposed, above which a bubble behaves like an inertial cavity [14]:

$$\frac{r_B}{r_0} = c, \tag{9}$$

where $r_B = \max(r(t))|_B$ is the so-called Blake critical radius and c is the threshold constant which has been approximated by $c \approx 2$. The number of fragments N into which a microbubble breaks up, is related to the dominant spherical harmonic oscillation mode n by [30,12]:

$$N \approx n^3. \tag{10}$$

Mode 2 oscillations have been observed with lipid-encapsulated microbubbles, leading to fragmentation into eight newly formed microbubbles [12].

Let us consider a single spherically symmetric microbubble with an inner radius r_i and an outer radius r, a shell density ρ_s, negligible translation, in an infinite fluid with density ρ. The kinetic energy of such a microbubble can be approximated by [27]:

$$E_k \approx 2\pi\rho r^3\dot{r}^2 + 2\pi\rho_s r_i^3\dot{r}_i^2\left(1 - \frac{r_i}{r}\right). \tag{11}$$

Knowing that, for microbubbles with monolayer lipid shells, $\frac{r_i}{r} < 0.01$ and $\rho_s = 1.15 \times 10^3\ \mathrm{kg\,m^{-3}}$, and for blood, $\rho = 1.05 \times 10^3\ \mathrm{kg\,m^{-3}}$ [26], Eq. (11) can be simplified to [30]:

$$E_k \approx 2\pi\rho r^3\dot{r}^2. \tag{12}$$

The surface free energy E_s of a single encapsulated bubble is given by [27]:

$$E_s = 4\pi r_i^2\mu_1 + 4\pi r^2\mu_2, \tag{13}$$

where μ_1 and μ_2 denote the surface tension coefficients for the inner and outer interface, respectively. For our microbubbles with monolayer lipid shells, we consider a single interface model, using the effective surface tension μ [27]:

$$\mu = \mu_1 + \mu_2. \tag{14}$$

After fragmentation, the resulting microbubble fragments contain more surface free energy $\sum_i E_{f,i}$ than the single bubble prior to fragmentation:

$$\sum_{i=1}^{N} E_{f,i} \approx \frac{4}{3}\pi r_f^2\mu\ N \approx \frac{4}{3}\pi r^2\mu\ N^{\frac{1}{3}} = N^{\frac{1}{3}}E_s, \tag{15}$$

where r_f is the mean fragment radius. Neglecting the elastic energy of the shell and the internal energy of the gas core, it can be assumed that fragmentation will only occur if [32]:

$$E_k > \left(\sum_{i=1}^{N} E_{f,i} - E_s\right). \tag{16}$$

2.3. Nonlinear, radially asymmetric behavior

Although asymmetric shape bubble oscillations have been observed [12,33], within our size range, spherical harmonic modes higher than two can be neglected [12]. For asymmetric shape oscillations, more complicated models are being developed.

At high acoustic amplitudes (MI > 0.6), disruptive phenomena have been observed, such as microbubble fragmentation and ultrasonic cracking [12]. Again, assuming that Hooke's Law holds for the bubble shell, the critical stress at which a shell ruptures is

$$\sigma_c = \mathbf{E}\epsilon_c, \tag{17}$$

where $\mathbf{E}$ is Young's modulus and ϵ_c is the critical lateral shell deformation. For example, the critical stress of the thick-shelled contrast agent Quantison™ is $\sigma_c \geqslant 80$ kPa [34], and thus $\epsilon_c \geqslant 0.4$. Generally, for biomaterials, $\epsilon_c < 0.5$ [35].

For microbubbles with a thick, stiff shell, such as Quantison™, $\max(r(t)) \ll r_0$. The stability of such a shell under low-amplitude insonification has been modeled in [36]. Thick-shelled bubbles have demonstrated gas release during a high-amplitude ultrasonic cycle [37,12]. The increased pressure difference between inside and outside of the bubble during the expansion phase of the wave causes the shell to be stretched across the critical deformation, resulting

into its mechanical cracking. The released bubble has an oscillation amplitude much higher than an encapsulated bubble of the same size [12]. Quantitative studies on this so-called sonic cracking have been presented in [37,12].

On the contrary, microbubbles with a thin, highly elastic monolayer lipid shell, like SonoVue™ and other Bracco agents, have been observed to expand to more than 10-fold their initial surface areas during rarefaction. The shell behaves like an elastic membrane that ruptures under relatively small strain [38,39]. By the time of maximal expansion, therefore, the shell has ruptured, leaving newly formed clean free interfaces.

3. Methods

We simulated the oscillating behavior of encapsulated microbubbles with various sizes in a harmonic acoustic field:

$$p_a(t) = p^- \sin \omega t, \tag{18}$$

where p^- denotes the peak negative acoustic pressure. The modified Rayleigh–Plesset equation as stated in [20] was solved using MATLAB® (The MathWorks, Inc., Natick, MA) programs. We used the same parameters as in [20], noting that the vapor pressure should be $p_v = 2.33$ kPa. Shell parameters $\chi = 1.1$ kg s^{-2} and $S_f = 0.27 \times 10^{-6}$ kg s^{-1} were included [40]. We did not approximate $\delta(r(t))$ by a time-averaged damping coefficient. Thermal damping was neglected [16]. The acoustic amplitudes modeled correspond to MI $\ll 2$ (well within the clinical diagnostic range). We focused on simulated driving frequencies ranging from 0.5 to 5.0 MHz.

For microbubbles with radii $0.2 < r_0 < 12.0$ μm, the critical acoustic pressures p_c were computed, above which Eq. (16) holds. For comparison with the Blake critical radius, the maximal microbubble radii $\max(r(r_0, p_c))$ were computed using the modified Rayleigh–Plesset equation, and divided by the initial radii r_0.

The phase angle differences $\phi = \alpha + \pi$ between p_a and r were computed for free and encapsulated microbubbles under low-amplitude insonification. Radii were chosen $0.1 < r_0 < 8.0$ μm. Known shell stiffness and friction parameters of two ultrasound contrast agents were included. For the resonance frequencies of free gas microbubbles, we included a surface tension term [14]. Again, thermal damping was neglected [16]. Since $|x(t)| \ll r_0$, here, we approximated $\delta(r(t))$ by a time-averaged damping coefficient $\delta(r_0)$.

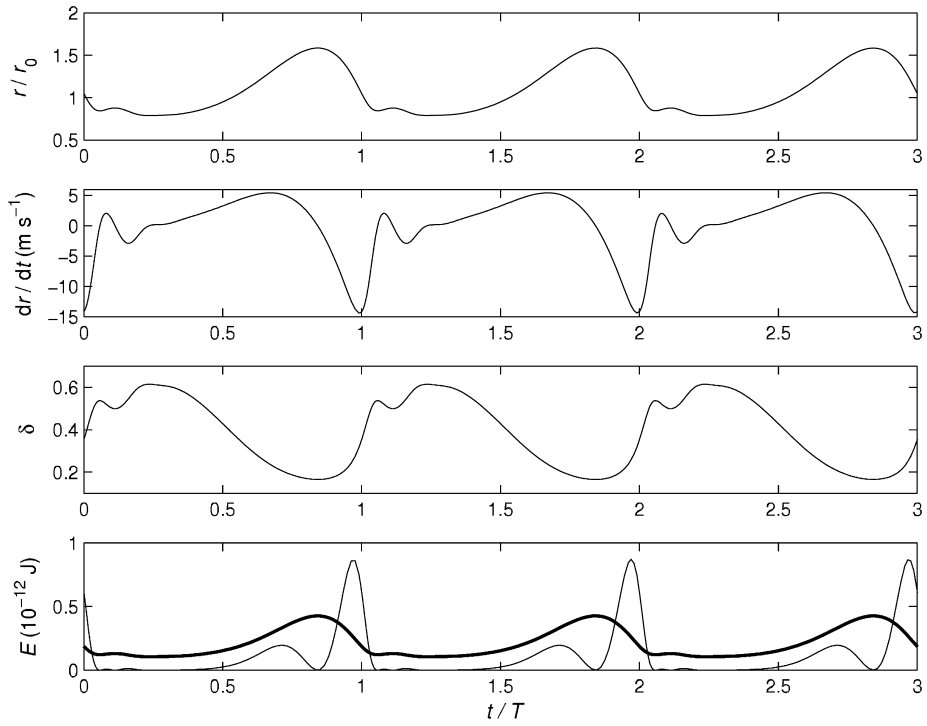

Fig. 1. Simulation of the oscillation behavior of an encapsulated microbubble with an equilibrium radius $r_0 = 0.75$ μm and shell properties $\chi = 1.1$ kg s^{-2} and $S_f = 0.27 \times 10^{-6}$ kg s^{-1} [40], during insonification at $f = 3.0$ MHz and $p^- = 1.2$ MPa, as a function of time t normalized by period T. The thin line in the lower frame is the kinetic energy of the bubble, whereas the bold line represents the right-hand side of Eq. (16).

4. Results and discussion

It has been previously demonstrated, with the aid of high-speed photography, that the oscillation, translation, coalescence, and jetting behavior of a microbubble with a thin, lipid shell is comparable to that of a free microbubble, as opposed to the behavior of thick-shelled bubbles [12].

Fig. 1 demonstrates the simulated oscillation behavior of a lipid-encapsulated microbubble, insonified at 3 MHz ultrasound with $p^- = 1.2$ MPa. The relatively slow expansion is followed by a rapid collapse. Close to the collapse, the kinetic energy of the microbubble becomes higher than the surface energy. This is the oscillation phase where microbubble break-up has been expected and observed.

Fig. 2, left column, shows the critical pressures above which Eq. (16) holds, for free gas microbubbles (frame a) and for a lipid-shelled microbubbles (frame c). In frame a, the critical pressure is minimal around resonance size ($r_0 \approx 6.5$ μm). Since the resonance frequency of the contrast microbubbles is increased, owing to stiffness of the shell, the minimum in frame c has been shifted to a radius greater than 8 μm. Furthermore, local minima can be appreciated at harmonic resonance sizes. At relatively low acoustic pressures, only microbubbles with sizes close to resonance will fragment. The corresponding maximal expansion radii at the critical pressures normalized by the initial radii are demonstrated in frames b and d, respectively. In contradiction to the assumption that the Blake critical radius is a good approximation for a fragmentation threshold, our simulations show $r_B/r_0 \ll 2$ for most microbubbles.

Fig. 3 shows three curves of the phase angle differences ϕ between a damped radially oscillating bubble and an incident 4 MHz sound field, as a function of r_0. The curves have been computed for a free microbubble, a SonoVue™ contrast microbubble, and an Albunex® contrast microbubble. With increasing shell stiffness, the bubble resonance size increases. At resonance, the bubble oscillates $\phi = \frac{3}{2}\pi$ rad out of phase with the sound field. For bubble greater than resonance, the phase angle difference approaches 2π rad, so that the bubble oscillates in phase with the sound field. Below resonance size, ϕ has a mini-

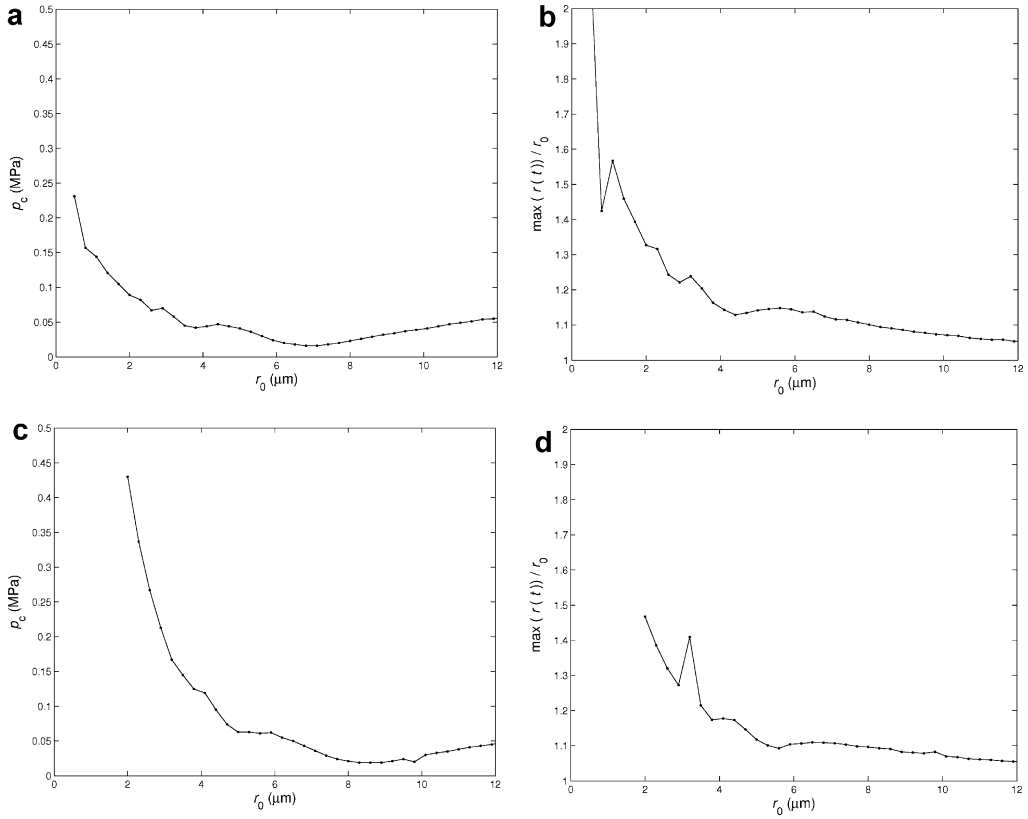

Fig. 2. Critical pressure of 0.5 MHz ultrasound as a function of initial radius (a, c). Relative critical microbubble excursion at the critical pressure as a function of initial radius (b, d). The upper frames were computed for free gas microbubbles, the lower for lipid-shelled microbubbles.

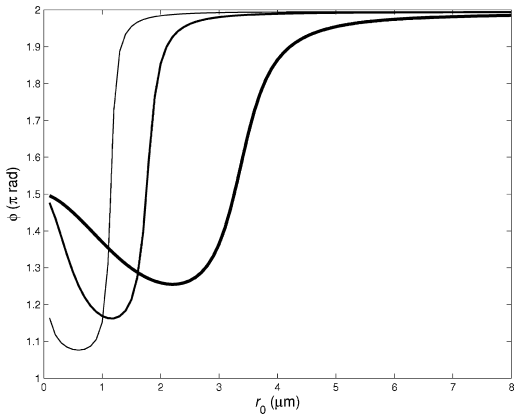

Fig. 3. Phase angle difference ϕ between a damped radially oscillating bubble and an incident 4 MHz sound field, as a function of equilibrium radius r_0. The thin line represents a free bubble: $\chi = 0\ \mathrm{kg\,s^{-2}}$, $S_f = 0\ \mathrm{kg\,s^{-1}}$; the bold line a SonoVue™ microbubble: $\chi = 1.1\ \mathrm{kg\,s^{-2}}$, $S_f = 0.27 \times 10^{-6}\ \mathrm{kg\,s^{-1}}$ [40]; the fat line an Albunex® microbubble: $\chi = 10\ \mathrm{kg\,s^{-2}}$, $S_f = 4 \times 10^{-6}\ \mathrm{kg\,s^{-1}}$ [17].

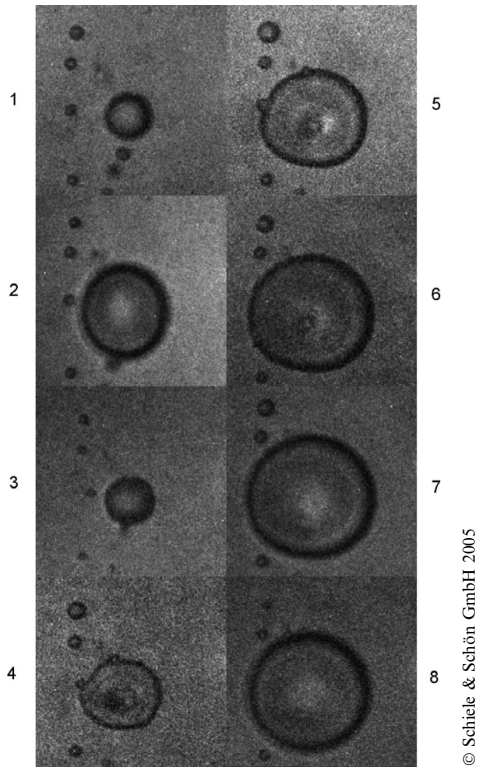

Fig. 4. Sequence of high-speed photographs of BR14 contrast microbubbles (Bracco Research SA, Genève, Switzerland) insonified at 0.5 MHz. Frame 1 has been captured prior to ultrasound arrival. The other seven frames cover one full ultrasonic cycle, *i.e.* 2 μs. Each frame corresponds to a $40 \times 40\ \mu\mathrm{m}^2$ area. Reprinted with permission from [20].

mum value still greater than π, and approaches $\frac{3}{2}\pi$ for r_0 much smaller than resonance size. Since the damping due to the liquid viscosity $\delta_v \propto r^{-2}$, ϕ approaches $\frac{3}{2}\pi$ for a free bubble radius $r_0 < 1$ μm. The approach to $\frac{3}{2}\pi$ below the minimum of ϕ is stronger with the contrast bubbles, because $\delta_s \propto r^{-3}$. As the damping becomes greater, the phase transition around resonance becomes less abrupt, as Fig. 3 demonstrates.

The high-speed photographs in Fig. 4 illustrate the shift in ϕ. The central bubble (bubble 1) has an equilibrium radius of 4.3 μm, whereas the upper left bubble (bubble 2) has an equilibrium radius of 1.7 μm. Maximal expansion of bubble 2 can be seen in frame 5, where $\max(r_2(t)) = 2.1$ μm. Maximal expansion of bubble 1, however, is seen in frame 7, where $\max(r_1(t)) = 13$ μm. Hence, bubble 1 oscillates $\frac{2}{3}\pi$ rad out of phase with respect to bubble 2.

5. Conclusions

Microbubble fragmentation occurs exclusively during the collapse phase and will only occur if the kinetic energy of the collapsing microbubble is greater than the instantaneous bubble surface energy. Our simulations demonstrate fragmentation thresholds for bubbles of different sizes. It follows that the Blake critical radius is not a good approximation for a fragmentation threshold.

We demonstrated how the phase angle differences between a damped radially oscillating bubble and an incident sound field depend on shell parameters.

References

[1] Canadian Institute for Health Information, Medical imaging in Canada, 2004.
[2] M. Postema, G. Schmitz, Bubble dynamics involved in ultrasonic imaging, Expert Rev. Mol. Diagn. 6 (3) (2006) 493–502.
[3] G. Schmitz, Ultrasound in medical diagnosis, in: R. Pike, P. Sabatier (Eds.), Scattering: Scattering and Inverse Scattering in Pure and Applied Science, Academic Press, London, 2002, pp. 162–174.
[4] E.G. Schutt, D.H. Klein, R.M. Mattrey, J.G. Riess, Injectable microbubbles as contrast agents for diagnostic ultrasound imaging: the key role of perfluorochemicals, Angew. Chem., Int. Ed. 42 (2003) 3218–3235.
[5] P.J.A. Frinking, E.I. Céspedes, J. Kirkhorn, H.G. Torp, N. de Jong, A new ultrasound contrast imaging approach based on the combination of multiple imaging pulses and a separate release burst, IEEE Trans. Ultrason. Ferroelect. Freq. Contr. 48 (3) (2001) 643–651.
[6] R. Bekeredjian, P.A. Grayburn, R.V. Shohet, Use of ultrasound contrast agents for gene or drug delivery in cardiovascular medicine, J. Am. Coll. Cardiol. 45 (3) (2005) 329–335.
[7] R. Bekeredjian, H.A. Katus, H.F. Kuecherer, Therapeutic use of ultrasound targeted microbubble destruction: a review of non-cardiac applications, Ultraschall Med. 27 (2) (2006) 134–140.
[8] A. Bouakaz, P.J.A. Frinking, N. de Jong, N. Bom, Noninvasive measurement of the hydrostatic pressure in a fluid-filled cavity based on the disappearance time of micrometer-sized free gas bubbles, Ultrasound Med. Biol. 25 (9) (1999) 1407–1415.
[9] J. Guan, T.J. Matula, M. Averkiou, Imaging the destruction of individual ultrasound contrast microbubbles with diagnostic ultrasound, Acoust. Res. Lett. 5 (4) (2004) 165–169, Online.
[10] A.Y. Ammi, R.O. Cleveland, J. Mamou, G.I. Wang, S.L. Bridal, W.D. O'Brien Jr., Ultrasonic contrast agent shell rupture detected by

inertial cavitation and rebound signals, IEEE Trans. Ultrason. Ferroelect. Freq. Contr. 53 (1) (2006) 126–136.
[11] K.E. Morgan, J.S. Allen, P.A. Dayton, J.E. Chomas, A.L. Klibanov, K.W. Ferrara, Experimental and theoretical evaluation of microbubble behavior: effect of transmitted phase and bubble size, IEEE Trans. Ultrason. Ferroelect. Freq. Contr. 47 (6) (2000) 1494–1509.
[12] M.A.B. Postema, Medical Bubbles, Universal Press, Veenendaal, 2004.
[13] V. Sboros, E. Glynos, S.D. Pye, C.M. Moran, M. Butler, J. Ross, R. Short, W.N. McDicken, V. Koutsos, Nanointerrogation of ultrasonic contrast agent microbubbles using atomic force microscopy, Ultrasound Med. Biol. 32 (4) (2006) 579–585.
[14] F.R. Young, Cavitation, McGraw-Hill, Maidenhead, 1989.
[15] H. Medwin, Counting bubbles acoustically: a review, Ultrasonics 15 (1977) 7–13.
[16] N. de Jong, L. Hoff, T. Skotland, N. Bom, Absorption and scatter of encapsulated gas filled microspheres: theoretical considerations and some measurements, Ultrasonics 30 (2) (1992) 95–103.
[17] N. de Jong, R. Cornet, C.T. Lancée, Higher harmonics of vibrating gas-filled microspheres. Part one: simulations, Ultrasonics 32 (6) (1994) 447–453.
[18] N. de Jong, A. Bouakaz, P. Frinking, Basic acoustic properties of microbubbles, Echocardiography 19 (3) (2002) 229–240.
[19] C.E. Brennen, Cavitation and Bubble Dynamics, Oxford University Press Inc., New York, 1995.
[20] M. Postema, N. de Jong, G. Schmitz, The physics of nanoshelled microbubbles, Biomed. Tech. 50 (S1) (2005) 748–749.
[21] C.C. Church, The effects of an elastic solid surface layer on the radial pulsations of gas bubbles, J. Acoust. Soc. Am. 97 (3) (1995) 1510–1521.
[22] J.S. Allen, D.J. May, K.W. Ferrara, Dynamics of therapeutic ultrasound contrast agents, Ultrasound Med. Biol. 28 (6) (2002) 805–816.
[23] E. Stride, N. Saffari, Theoretical and experimental investigation of the behaviour of ultrasound contrast agent particles in whole blood, Ultrasound Med. Biol. 30 (11) (2004) 1495–1509.
[24] E. Stride, N. Saffari, Investigating the significance of multiple scattering in ultrasound contrast agent particle populations, IEEE Trans. Ultrason. Ferroelect. Freq. Contr. 52 (12) (2005) 2332–2345.
[25] H. Zheng, A. Barker, R. Shandas, Predicting backscatter characteristics from micron- and submicron-scale ultrasound contrast agents using a size-integration technique, IEEE Trans. Ultrason. Ferroelect. Freq. Contr. 53 (3) (2006) 639–644.
[26] H. Zheng, O. Mukdadi, R. Shandas, Theoretical predicitions of harmonic generation from submicron ultrasound contrast agents for nonlinear biomedical ultrasound imaging, Phys. Med. Biol. 51 (2006) 557–573.
[27] A.A. Doinikov, P.A. Dayton, Spatio-temporal dynamics of an encapsulated gas bubble in an ultrasound field, J. Acoust. Soc. Am. 120 (2) (2006) 661–669.
[28] K. Sarkar, W.T. Shi, D. Chatterjee, F. Forsberg, Characterization of ultrasound contrast microbubbles using in vitro experiments and viscous and viscoelastic interface models for encapsulation, J. Acoust. Soc. Am. 118 (1) (2005) 539–550.
[29] P. Marmottant, S. van der Meer, M. Emmer, M. Versluis, N. de Jong, S. Hilgenfeldt, D. Lohse, A model for large amplitude oscillations of coated bubbles accounting for buckling and rupture, J. Acoust. Soc. Am. 118 (6) (2005) 3499–3505.
[30] C.E. Brennen, Fission of collapsing cavitation bubbles, J. Fluid Mech. 472 (2002) 153–166.
[31] J.E. Chomas, P. Dayton, D. May, K. Ferrara, Threshold of fragmentation for ultrasonic contrast, J. Biomed. Opt. 6 (2) (2001) 141–150.
[32] M. Postema, G. Schmitz, Ultrasonic fragmentation of microbubbles: a theoretical approach of the flash in flash-echo, Proc. IEEE Eng. Med. Biol. Soc. (2005) 4023–4026.
[33] M. Versluis, S.M. van der Meer, D. Lohse, P. Palanchon, D. Goertz, C.T. Chin, N. de Jong, Microbubble surface modes, Proc. IEEE Ultrason. Symp. 1 (2004) 207–209.
[34] P.J.A. Frinking, N. de Jong, Acoustic modeling of shell-encapsulated gas bubbles, Ultrasound Med. Biol. 24 (4) (1998) 523–533.
[35] H. Abé, K. Hayashi, M. Sato, Data Book on Mechanical Properties of Living Cells, Tissues, and Organs, Springer-Verlag, Tokyo, 1996.
[36] B. Krasovitski, E. Kimmel, Stability of an encapsulated bubbles shell, Ultrasonics 44 (2006) 216–220.
[37] S.H. Bloch, M. Wan, P.A. Dayton, K.W. Ferrara, Optical observation of lipid- and polymer-shelled ultrasound microbubble contrast agents, Appl. Phys. Lett. 84 (4) (2004) 631–633.
[38] Z. Zhou, B. Joós, Mechanisms of membrane rupture: from cracks to pores, Phys. Rev. B 56 (6) (1997) 2997–3009.
[39] M.A. Borden, D.E. Kruse, C.F. Caskey, S. Zhao, P.A. Dayton, K.W. Ferrara, Influence of lipid shell physicochemical properties on ultrasound-induced microbubble destruction, IEEE Trans. Ultrason. Ferroelect. Freq. Contr. 52 (11) (2005) 1992–2002.
[40] J.M. Gorce, M. Arditi, M. Schneider, Influence of bubble size distribution on the echogenicity of ultrasound contrast agents: a study of SonoVue™, Invest. Radiol. 35 (11) (2000) 661–671.

Ultrasonics 50 (2010) 260–268

Contents lists available at ScienceDirect

Ultrasonics

journal homepage: www.elsevier.com/locate/ultras

Microfoam formation in a capillary

Spiros Kotopoulis, Michiel Postema *

Emmy-Noether Group, Institute of Medical Engineering, Department of Electrical Engineering and Information Technology, Ruhr-Universität Bochum, D-44780 Bochum, Germany
Department of Engineering, The University of Hull, Kingston upon Hull, HU6 7RX, United Kingdom

ARTICLE INFO

Article history:
Received 6 June 2009
Received in revised form 25 September 2009
Accepted 28 September 2009
Available online 2 October 2009

PACS:
43.25.Yw
47.55.df
87.50.yt

Keywords:
Capillary blocking
Embolisation
Microfoam
Radiation forces
Ultrasound contrast agent

ABSTRACT

The ultrasound-induced formation of bubble clusters may be of interest as a therapeutic means. If the clusters behave as one entity, *i.e.*, one mega-bubble, its ultrasonic manipulation towards a boundary is straightforward and quick. If the clusters can be forced to accumulate to a microfoam, entire vessels might be blocked on purpose using an ultrasound contrast agent and a sound source.

In this paper, we analyse how ultrasound contrast agent clusters are formed in a capillary and what happens to the clusters if sonication is continued, using continuous driving frequencies in the range 1–10 MHz. Furthermore, we show high-speed camera footage of microbubble clustering phenomena.

We observed the following stages of microfoam formation within a dense population of microbubbles before ultrasound arrival. After the sonication started, contrast microbubbles collided, forming small clusters, owing to secondary radiation forces. These clusters coalesced within the space of a quarter of the ultrasonic wavelength, owing to primary radiation forces. The resulting microfoams translated in the direction of the ultrasound field, hitting the capillary wall, also owing to primary radiation forces.

We have demonstrated that as soon as the bubble clusters are formed and as long as they are in the sound field, they behave as one entity. At our acoustic settings, it takes seconds to force the bubble clusters to positions approximately a quarter wavelength apart. It also just takes seconds to drive the clusters towards the capillary wall.

Subjecting an ultrasound contrast agent of given concentration to a continuous low-amplitude signal makes it cluster to a microfoam of known position and known size, allowing for sonic manipulation.

1. Introduction

Ultrasound contrast agents are used in diagnostic imaging. They consist of microscopically small bubbles containing slowly diffusing gas encapsulated by biodegradable shells. When inserted in the blood stream, these bubbles oscillate upon ultrasonic sonication, thereby creating detectable ultrasound themselves. A brief overview of the most common ultrasound contrast agents has been presented in [1]. It follows that albumin and lipids are currently the most common bubble encapsulation materials. Because of the proven feasibility to attach therapeutic compounds to albumin and lipids, therapeutic applications of contrast agents have become of interest [2–5]. It is desirable that the therapeutic load of any such contrast agent is released close to the vessel wall. Therefore, pushing bubbles towards boundaries by means of primary radiation forces has been studied [6]. Both primary and secondary radiation forces resulting from oscillating bubbles, may cause the repulsion or mutual attraction, and eventual collision and coalescence, of contrast agent bubbles. This phenomenon has been less studied.

From the therapeutic point of view, the formation of bubble clusters may be of interest. If the clusters behave as one entity, *i.e.*, one mega-bubble, its ultrasonic manipulation towards a boundary is fairly straightforward and quick. If the clusters can be forced to accumulate to a microfoam, entire vessels might be blocked on purpose using an ultrasound contrast agent and a sound source.

In this paper, we analyse how ultrasound contrast agent clusters are formed and what happens to the clusters if sonication is continued. Furthermore, we show high-speed camera footage of microbubble clustering phenomena and discuss the therapeutic consequences of our findings.

2. Theory

A brief overview of theory on radiation forces and ultrasound contrast agent has been given in [7]. Bubble translation in the direction of the sound field is caused by a primary radiation force resulting from a pressure gradient across the bubble surface. The

* Corresponding author. Tel.: +49 234 3226504.
E-mail address: michiel.postema@rub.de (M. Postema).

0041-624X/$ - see front matter © 2009 Elsevier B.V. All rights reserved.
doi:10.1016/j.ultras.2009.09.028

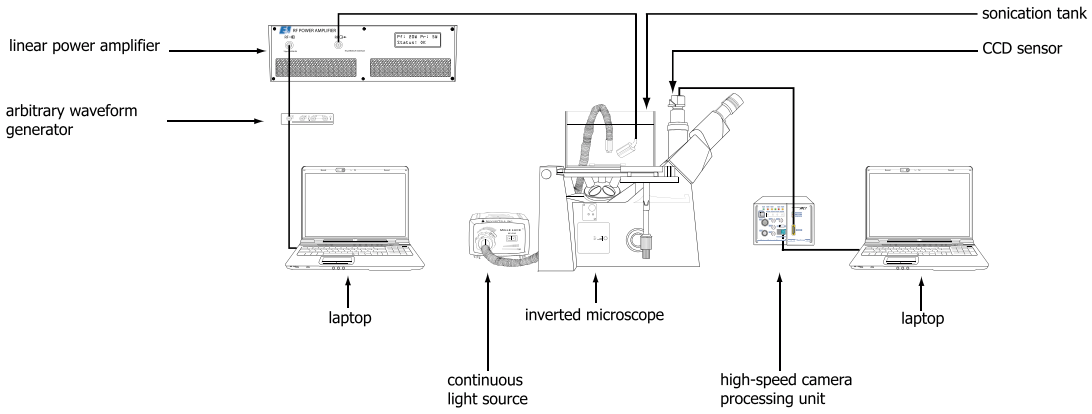

Fig. 1. Schematic overview of the experimental setup.

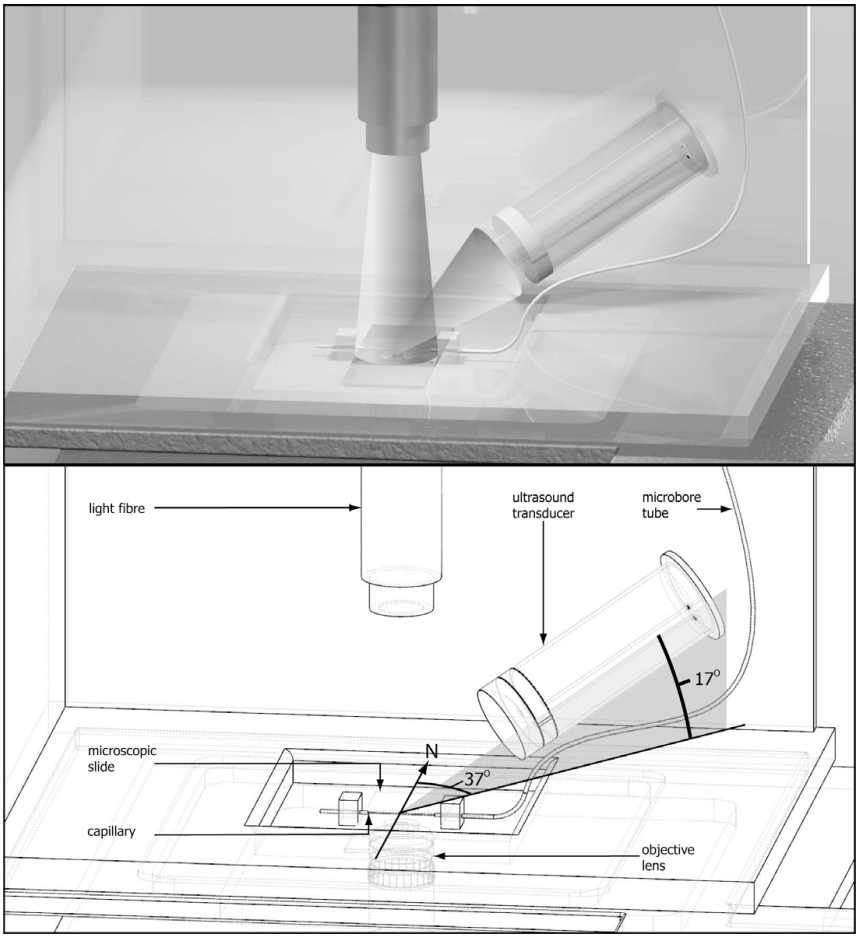

Fig. 2. Close-up of the sonication tank with coinciding sound, light beam, and objective focus (top) and definitions of the azimuth and elevation of the transducer relative to the North of the container (bottom).

translation is maximal in contraction phase. The velocity v of a bubble in a steady fluid subjected to an ultrasound field can be calculated using [8]:

$$F_r + F_d - \frac{d(mv)}{dt} \approx 0, \quad (1)$$

where F_r is the primary radiation force, F_d is the drag force, $m = \frac{2}{3}\pi\rho R_0^3$ is the added mass of the translating bubble, equivalent to half the mass of the displaced surrounding fluid, in which R_0 is the equilibrium bubble radius and ρ is the density of the surrounding fluid. Averaging over one acoustic cycle, the primary radiation force is given by [8,9]:

$$F_r = \frac{p_a^2 R_0}{\rho c f} \frac{\delta\left(\frac{f_0}{f}\right)}{\left[\left(\frac{f_0}{f}\right)^2 - 1\right]^2 + \left[\delta\left(\frac{f_0}{f}\right)\right]^2}, \quad (2)$$

where c is the speed of sound, p_a is the peak rarefactional acoustic pressure, δ is the dimensionless total damping coefficient [10], f is the driving frequency, and f_0 is the bubble resonance frequency [10]. The drag force is given by [9,11]:

$$F_d = -\frac{\pi\eta}{4} C_d \ \mathrm{Re}\ R_0\ v(t), \quad (3)$$

where η is the shear (dynamic) viscosity of the fluid, $\mathrm{Re} = \frac{2\rho R_0}{\eta}|v(t)|$ is the Reynolds number, and

$$C_d = \frac{24}{\mathrm{Re}}(1 + 0.15\ \mathrm{Re}^{0.687}) \quad (4)$$

is the drag coefficient of a contaminated system [12], such as a contrast agent.

Combining Eqs. (1)–(3) and integrating over dt gives the following expression for the average velocity of a bubble:

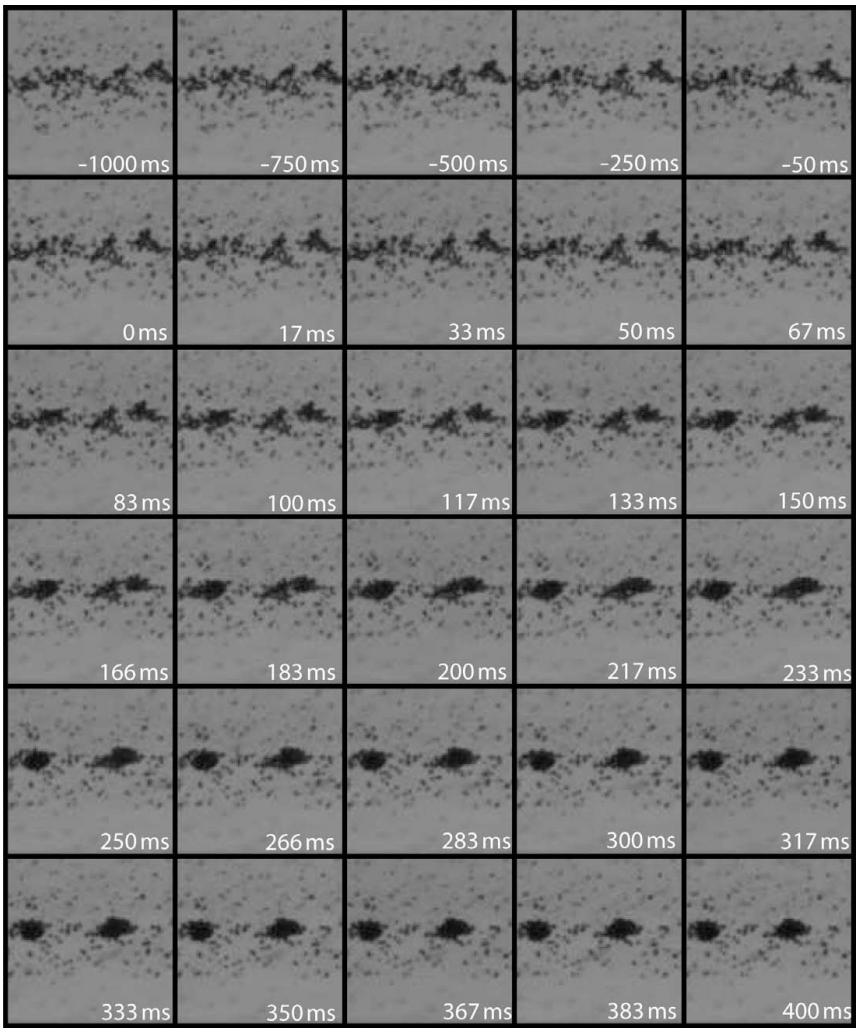

Fig. 3. Microfoam formation during continuous sonication at 2 MHz and 20 kPa peak-negative acoustic pressure. Each frame corresponds to a 120 × 120 $(\mu m)^2$ area. Time $t = 0$ was defined by the start of the sonication.

$$v = \frac{4p_a^2}{\rho c f \eta C_d \mathrm{Re}} \frac{\delta\left(\frac{f_0}{f}\right)}{\left[\left(\frac{f_0}{f}\right)^2 - 1\right]^2 + \left[\delta\left(\frac{f_0}{f}\right)\right]^2} \left[1 - e^{\left(-\frac{3\eta C_d \mathrm{Re}}{8\rho R_0^2} t\right)}\right]. \quad (5)$$

Secondary radiation forces, resulting from oscillating bubbles under sonication, may cause the mutual attraction and subsequent coalescence of contrast microbubbles. Two bubbles that oscillate in phase approach each other, whereas two bubbles that oscillate out of phase recede from each other [13,14]. At low acoustic amplitudes, the phase angle difference ϕ between excursion of the oscillating bubble and the incident sound field is given by [13,14]:

$$\phi = \pi + \arctan\left(\frac{\delta\left(\frac{f}{f_0}\right)}{1 - \left(\frac{f}{f_0}\right)^2}\right). \quad (6)$$

The presence of an encapsulating shell increases the damping coefficient by a term δ_s [15]

$$\delta_s = \frac{S_f}{2\pi\, m\, f_0}, \quad (7)$$

and increases the squared resonance frequency f_0^2 by a term f_s^2 [15]

$$f_s^2 = \frac{\chi}{2\pi R_0^3 \rho}, \quad (8)$$

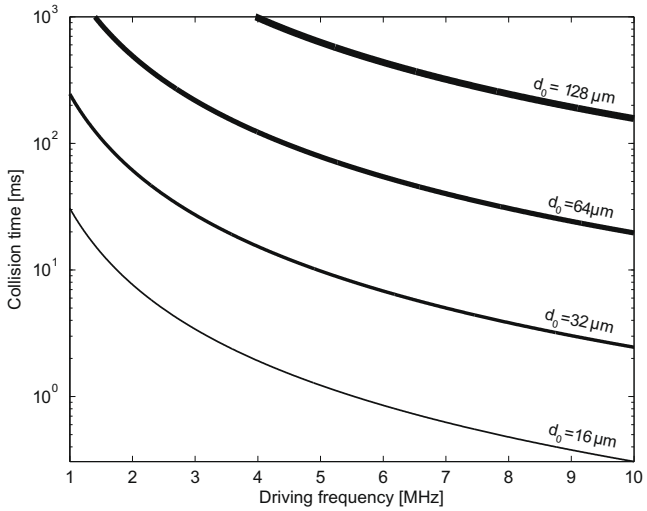

Fig. 4. Collision times of individual encapsulated microbubbles as a function of driving frequency at given distances d_0, using $p_a = 20$ kPa, $R_0 = 1.25$ μm, $\kappa = 5 \times 10^{-6}$ m^2 N^{-1}, and $\rho = 998$ kg m^{-3}.

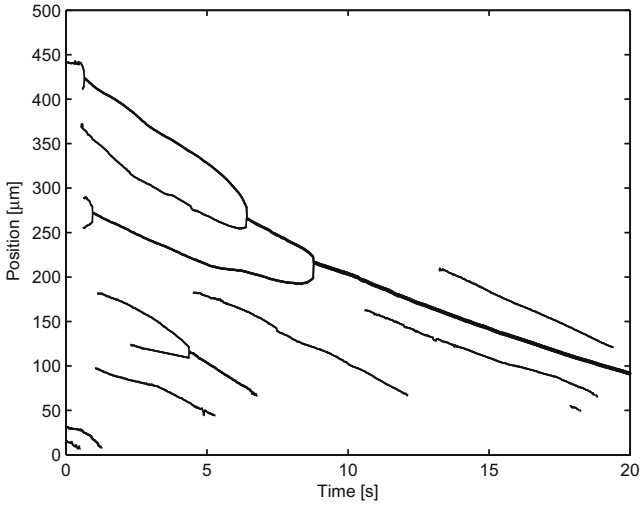

Fig. 5. Cluster positions as a function of time, during continuous sonication at 2 MHz and 20 kPa peak-negative acoustic pressure. Position in the capillary is defined from East (0 μm) to West (500 μm). Bold lines indicate merged clusters. The beginning (left) of a line indicates the formation of a cluster of diameter > 6.8 μm. The end (right) of a line indicates the disintegration or contraction of a cluster to a diameter <6.8 μm.

where S_f is the shell friction [15] and χ is the shell stiffness parameter [14,15]

$$\chi = \frac{E\epsilon}{1-\upsilon}, \tag{9}$$

in which E is Young's modulus, ϵ is the shell thickness, and υ is the Poisson ratio.

The mean approach velocity u of two identical bubbles is given by [8]:

$$u = \frac{\mathrm{d}d}{\mathrm{d}t} = -\frac{(2\pi f p_a)^2}{27\eta}\rho\kappa^2\frac{R_0^5}{d^2}, \tag{10}$$

where d is the distance between the centres of the two bubbles and κ is the compressibility of the bubble. Integrating from the initial distance between the bubbles d_0 to 0 yields the collision time

$$t_c = -\int_{d_0}^{0}\frac{27\eta}{(2\pi f p_a)^2\rho\kappa^2 R_0^5}d^2\,\mathrm{d}d = \frac{9\eta}{(2\pi f p_a)^2\rho\kappa^2}\frac{d_0^3}{R_0^5}. \tag{11}$$

In a standing wave field, bubbles with resonance frequencies higher than the transmitted sound field aggregate at the pressure antinodes, whereas bubbles with resonance frequencies lower than the transmitted sound field aggregate at the pressure nodes [13]. Hence, the ultimate distance d_∞ between clusters must be a quarter of the wavelength, *i.e.*,

$$d_\infty = \frac{\lambda}{4} = \frac{c}{4f}. \tag{12}$$

Both processes of bubble clusters aggregating and the movement of clusters in the direction of the sound field can be described by a simplified version of (5):

$$v = \frac{\mathrm{d}h}{\mathrm{d}t} \approx \frac{p_a^2}{6\rho c f\eta}\frac{\delta\left(\frac{f_c}{f}\right)}{\left[\left(\frac{f_c}{f}\right)^2-1\right]^2+\left[\delta\left(\frac{f_c}{f}\right)\right]^2}, \tag{13}$$

where h is the distance travelled by the cluster and f_c is the cluster resonance frequency, for which $f_c < f_0$ must hold, since the bubble cluster radius $R_c > R_0$. For the bubble cluster compressibility κ_c, $\kappa \leqslant \kappa_c < \kappa_f$ must hold, in which κ_f is the compressibility of a free (unencapsulated) gas bubble.

Bubble coalescence is the fusion of two or more bubbles. As adjacent bubbles collide or expand, the pressure in the film between them increases, resulting in a deformation (flattening) of the bubble surfaces. The continuing bubble expansion causes drainage of the interposed film. This thinning continues until a critical thickness around 0.1 μm is reached, at which the Van der Waals attractive forces result in film rupture and the coalescence of the bubbles [16]. Film drainage is generally much faster for free (unencapsulated) bubbles than for encapsulated bubbles, as a result of the flow pattern in the draining film [17].

The coalescence mechanism of lipid-encapsulated microbubbles was investigated, based on high-speed optical observations of sonicated lipid-encapsulated ultrasound contrast agent microbubbles [17]. It was found that, when sonicated at high acoustic amplitudes, lipid-encapsulated microbubbles expose free surfaces during the expansion phase, speeding up the coalescence process dramatically. Hence, for the formation of bubble clouds or microfoams, the use of low acoustic amplitudes is desirable.

3. Materials and methods

A schematic overview of our experimental setup for simultaneous optical observations during sonication is shown in Fig. 1. A polycarbonate container was built with internal dimensions: $24 \times 18 \times 15$ (cm)^3. To give access to a microscope objective lens, a hole with an 11-mm diameter had been drilled in the base, covered with a 2-mm thick test slide (Jencons (Scientific) Ltd., Leighton Buzzard, Bedfordshire, UK). The container was filled with 2.6 L tap water. The container was placed on an x—y-table on top of a DM IRM inverted microscope (Leica Microsystems Wetzlar GmbH, Wetzlar, Germany) with two objective lenses: a 506075 C-Plan 10× objective lens (Leica Microsystems Wetzlar GmbH) with a 0.22 numerical aperture and a 506236 N-Plan 50× objective lens (Leica Microsystems Wetzlar GmbH) with a 0.50 numerical aperture. A Mille Luce™ Fiber Optic Illuminator Model M1000 (StockerYale, Inc., Salem, NH, USA) was connected to an optic fibre

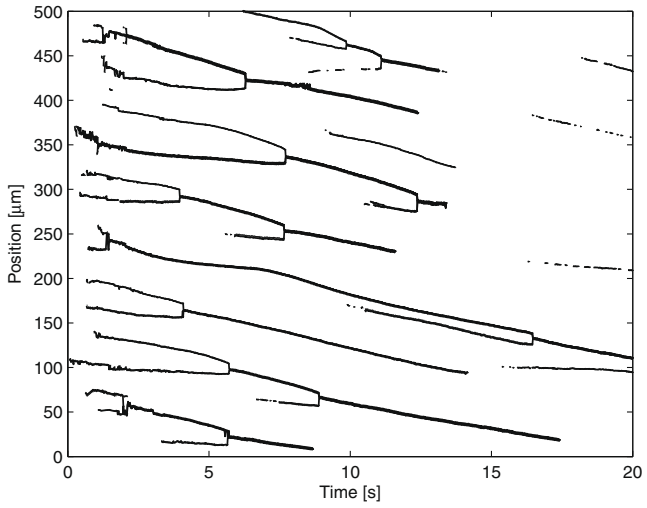

Fig. 6. Cluster positions as a function of time, during continuous sonication at 7 MHz and 22 kPa peak-negative acoustic pressure. Position in the capillary is defined from East (0 μm) to West (500 μm). Bold lines indicate merged clusters. The beginning (left) of a line indicates the formation of a cluster of diameter >6.8 μm. The end (right) of a line indicates the disintegration or contraction of a cluster to a diameter <6.8 μm.

with a 7-mm diameter leading into the water of the container. It was placed in line with the objective lens, as shown in Fig. 2.

The charge couple device (CCD) of a FASTCAM MC1 high-speed camera (Photron (Europe) Limited, West Wycombe, Bucks, United Kingdom) was mounted to the microscope and connected to its processing unit, which was capable of recording images at 10,000 frames per second. The camera was controlled by a laptop computer.

3.1. Ultrasound

A laptop computer triggered a DATAMAN-530 arbitrary waveform generator (Dataman Programmers Ltd., Maiden Newton, Dorset, UK), which was connected to a 2100L 50-dB RF power amplifier (Electronics & Innovation Ltd., Rochester, NY, USA). The power amplifier was connected to an undamped broadband single element transducer containing a Pz37 Piezo crystal (Ferroperm Piez-

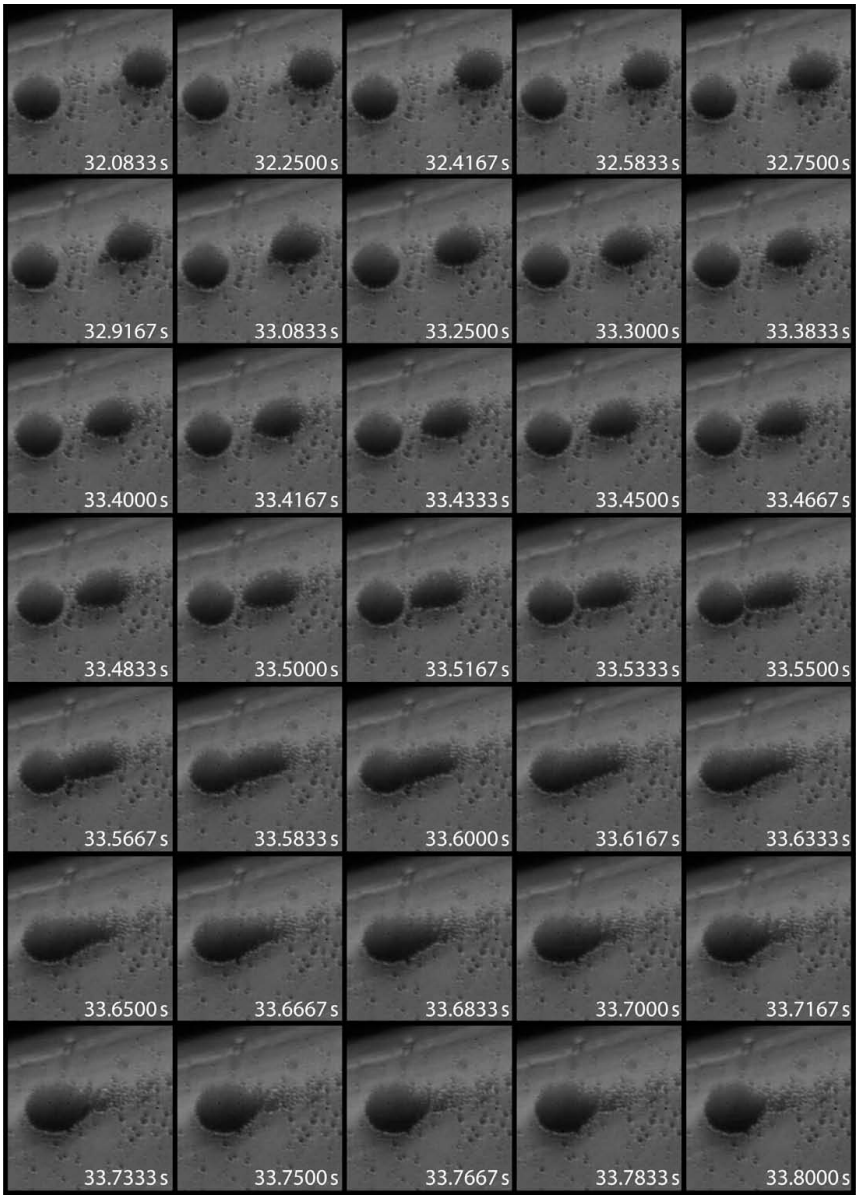

Fig. 7. Two clusters, with 22-μm diameters and an initial distance of 55 μm, colliding and coalescing during continuous sonication at a 2-MHz driving frequency and a 20-kPa peak-negative pressure. The frame size corresponds to 81×81 $(\mu m)^2$. Times were relative to the start of the sonication ($t = 0$).

oceramics A/S, Kvistgård, Denmark) with a centre frequency of 2.2 MHz. The design of the transducer has been described in [18]. Transmitted signals were typically continuous with frequencies in the range 1–10 MHz. The peak-negative acoustic pressures were determined using a PVdF needle hydrophone system with a 0.2-mm probe (Precision Acoustics Ltd., Dorchester, Dorset, UK) connected to a TDS 420A oscilloscope (Tektronix, Inc., Beaverton, OR, USA).

The ultrasound transducer was positioned in the container using a clamp stand, at a focal distance of 38 mm from the region of interest to be studied. The azimuth of the length axis of the transducer relative to the North of the container was 37° and the elevation of the length axis of the transducer relative to the base of the container was 17°, as shown in Fig. 2.

3.2. Ultrasound contrast agent

DEFINITY® (Lantheus Medical Imaging, North Billerica, MA, USA) consists of C_3F_8 gas microbubbles with mean diameters between 1.1 and 3.3 μm, encapsulated by lipid/surfactant shells. Its resonance frequency had been measured to be 2.7 MHz [19]. The 1.5-ml vials used in our experiments had been stored at 9 °C. Each vial was shaken for 45 s using a Vialmix® device (Lantheus Medical Imaging). Before introducing the ultrasound contrast agent in our setup, it was further diluted using a 0.9% saline solution.

The diluted ultrasound contrast agent was inserted using a syringe into a microbore tube with a 0.51-mm inner diameter. The tube led to a CUPROPHAN® RC55 cellulose capillary (Membrana GmbH, Wuppertal, Germany) with a 200-μm inner diameter and an 8-μm wall thickness. The middle of the capillary coincided with the optical focus of the objective lens and with the acoustic focus of the ultrasound transducer, as shown in Fig. 2. The typical field of view using the 10× objective lens was $500 \times 200\ (\mu m)^2$, whereas the diameter of the acoustic focus was greater than 5 mm. Hence, the whole field of view could be considered in acoustic focus. The capillary was positioned 2 mm from the base of the container. The flow speed of the ultrasound contrast agent through the capillary was manually controlled.

In total, 48 experiments were performed. Bubble and cluster sizes were measured and tracked using Image-Pro Plus (Media Cybernetics, Inc., Bethesda, MD, USA). Further analysis was done using MATLAB® (The MathWorks, Inc., Natick, MA, USA).

4. Results and discussion

At the high concentrations we used, clustering started instantaneously after the ultrasound generator was switched on. Fig. 3 illustrates the speed of cluster formation of DEFINITY® ultrasound contrast agent that had been further diluted to 1:20. With distances between the microbubbles of only few micrometres, collision times from (11) should be within a second, indeed, as shown in Fig. 4. Also, from (11) and Fig. 4 it is explained why cluster formation must be faster at higher frequencies, if the other acoustic parameters and the concentration are not changed. Or, after a fixed duration, larger clusters must have formed using higher frequencies, since bubble can approach from larger d_0 at higher f. These deductions are confirmed by our experimental observations: In Fig. 3, after 233 ms two clusters had been formed of approximately 15 μm each. These started to approach in the subsequent frames. Overall, newly-formed clusters collided to form larger clusters. This is illustrated by Figs. 5 and 6. Each branch represents a cluster. The branches coming together represent the collision of clusters into larger clusters. The velocities of the clusters are on the order of tens of micrometres per second. Although increasing the acoustic pressure would increase the cluster velocities dramatically, as is evident from (13), they would also lead to microbubble disruption [14]. We did not observe phenomena associated with microbubble disruption.

The larger a cluster grows, the lower its resonance frequency becomes. Hence, the velocity of a cluster in the direction of the sound field, defined by (13), should decrease in time. If two identical clusters with resonance frequency f_0 merge, the resulting resonance frequency $f_c' \approx \left(2^{-\frac{1}{3}}\right) f_0 = 0.79\, f_0$ [1]. Assuming that the compressibility and damping coefficient do not substantially change, a similar decrease in cluster velocity is expected. However, the decrease in slope magnitude of the main branch in Fig. 5 is negligible. This might be explained if the resulting cluster is much stiffer than the original clusters, increasing the damping coefficient.

Also, 7 MHz must be further off the cluster resonance frequency than 2 MHz. Hence, the magnitudes of the slopes in Fig. 6 are lower than those than in Fig. 5. Secondary radiation forces of clusters onto each other do not explain the cluster colliding times observed.

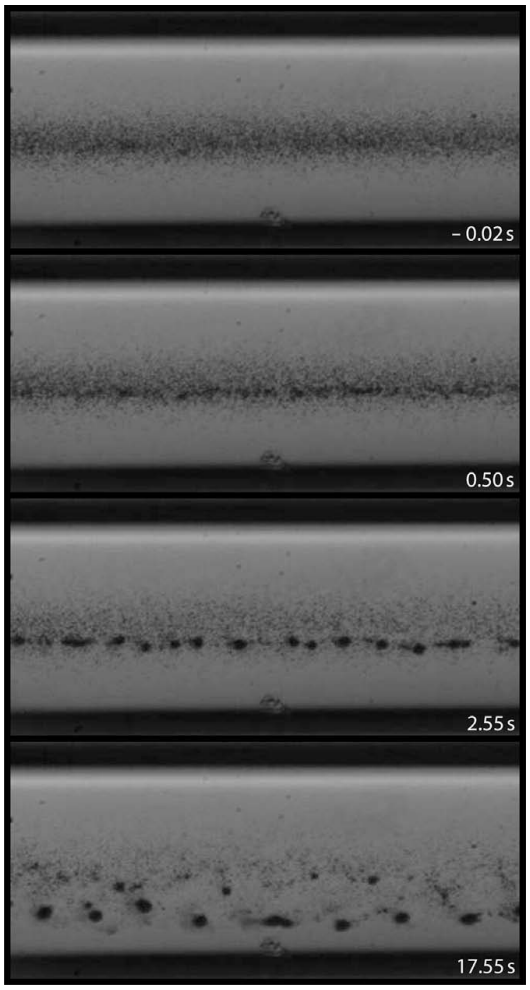

Fig. 8. Clusters forming during sonication at 7 MHz and 22 kPa peak-negative pressure. The frame size corresponds to $560 \times 264\ (\mu m)^2$. Time $t = 0$ was defined by the start of the sonication.

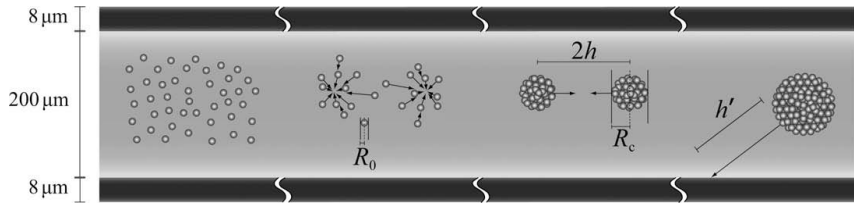

Fig. 9. Schematic representation of the four stages of microfoam formation in a capillary: (left–right) random bubble distribution before ultrasound arrival, bubbles colliding during sonication, cluster coalescing within the space of a quarter of the wavelength, microfoam translation.

Even if the compressibility of the clusters would be equal to that of a single ultrasound contrast agent microbubble, under the acoustic conditions we used, the collision times from (11) would be just milliseconds. Hence, the bubble clusters cannot be regarded as identical monopoles in our setting. A close-up of two colliding clusters with 22-µm diameters forming a 25-µm cluster is shown in Fig. 7. The total time spanning this process is slightly less than 1.8 s.

The clusters were initially formed in the middle of the capillary. These clusters were located at distances $d_0 < \frac{1}{4}\lambda$, as demonstrated in Fig. 8. However, following further cluster coalescence during 17.55 s of sonication, the final distance between the larger clusters corresponded to $\frac{1}{4}\lambda = 54$ µm. These had been pushed towards the lower capillary wall, owing to primary radiation forces.

The cluster velocities towards the capillary wall were between 5 µm s^{-1} at 7 MHz and 22 kPa peak-negative pressure and 15 µm s^{-1} at 2 MHz and 20 kPa peak-negative pressure sonication. These are of the same order as the left-hand side term in (13). The magnitudes of the slopes in Fig. 6 did not change close to the capillary wall. Hence, in our experimental setup, we neglected any effect of the capillary wall on cluster translation. With cluster diameters less than 30 µm, buoyancy effects may neglected on our timescales as well.

In summary, we observed the following stages of microfoam formation, illustrated in Fig. 9. Our initial situation was a dense, random bubble distribution before ultrasound arrival. After the sonication started, contrast microbubbles collided, owing to secondary radiation forces. Subsequently, these clusters coalesced within the space of a quarter of the wavelength, owing to primary radiation forces. The resulting microfoams translated in the direction of the ultrasound field, owing to primary radiation forces.

Small deviations in microbubble sizes or shell properties lead to deviations in individual bubbles's resonance frequencies, as expressed in (8). These in turn cause oscillation phase differences, as expressed in (6), big enough to be optically observed [7]. Therefore, predicting and manipulating individual microbubbles is technically challenging. We have demonstrated that as soon as the bubble clusters were formed and as long as they were in the sound field, they behaved as one entity. At our acoustic settings, it took seconds to force the bubble clusters to positions approximately $\frac{1}{4}\lambda$ apart. It also just took seconds to drive the clusters towards a boundary.

We may assume that vessel blocking can only be successful if a microfoam is created with a diameter equal to or greater than the vessel diameter d_v. From this study it follows that in order to create such a foam, $\frac{1}{4}\lambda > d_v$, or, $f < \frac{c}{4\,d_v}$.

For therapeutic purposes, it would be of great interest to induce microjetting on entire clusters towards a vessel wall, presumably causing sonoporation or sonolysis. Although ultrasound-induced microjetting has been observed with ultrasound contrast agents, its occurrence in *in vivo* situations is hard to control [20,21]. Predictable sonic manipulation would be better feasible if the microbubbles would be forced to clusters of known size and position first.

5. Conclusions

We observed the following stages of microfoam formation within a densely populated concentration of microbubbles. After the sonication started, contrast microbubbles collided, forming small clusters, owing to secondary radiation forces. These clusters coalesced within the space of a quarter of the ultrasonic wavelength, owing to primary radiation forces. The resulting microfoams translated in the direction of the ultrasound field, hitting the capillary wall, also owing to primary radiation forces.

We have demonstrated that as soon as the bubble clusters were formed and as long as they were in the sound field, they behaved as one entity. At our acoustic settings, it took seconds to force the bubble clusters to positions approximately a quarter wavelength apart. It also just took seconds to drive the clusters towards the capillary wall.

Subjecting ultrasound contrast agent microbubbles to a continuous low-amplitude signal makes them cluster to know positions and known microfoam sizes, allowing for straightforward sonic manipulation.

Acknowledgements

The authors are grateful to Lantheus Medical Imaging, North Billerica, MA, USA, for supplying the ultrasound contrast agent DEFINITY®. This work has been supported by DFG Emmy-Noether Programme Grant 38355133, EPSRC Grant EP/F037025/1 and the HERI Research Pump Priming Fund.

References

[1] M. Postema, G. Schmitz, Bubble dynamics involved in ultrasonic imaging, Expert Rev. Mol. Diagn. 6 (3) (2006) 493–502.
[2] J.R. Lindner, S. Kaul, Delivery of drugs with ultrasound, Echocardiography 18 (4) (2001) 329–337.
[3] E.C. Unger, T.O. Matsunaga, T. McCreery, P. Schumann, R. Sweitzer, R. Quigley, Therapeutic applications of microbubbles, Eur. J. Radiol. 42 (2002) 160–168.
[4] N. Kudo, T. Miyaoka, K. Okada, K. Yamamoto, K. Niwa, Study on mechanism of cell damage caused by microbubbles exposed to ultrasound, Proc. IEEE Ultrason. Symp. (2002) 1351–1354.
[5] M. Postema, O.H. Gilja, Ultrasound-directed drug delivery, Curr. Pharm. Biotechnol. 8 (6) (2007) 355–361.
[6] P.A. Dayton, J.S. Allen, K.W. Ferrara, The magnitude of radiation force on ultrasound contrast agents, J. Acoust. Soc. Am. 112 (5) (2002) 2183–2192.
[7] M. Postema, M. Mleczko, G. Schmitz, Mutual attraction of oscillating microbubbles, in: T.M. Buzug, D. Holz, S. Weber, J. Bongartz, M. Kohl-Bareis, U. Hartmann (Eds.), Advances in Medical Engineering, Methods of Experimental Physics, vol. 19, Springer, Berlin, 2007, pp. 75–80.
[8] P.A. Dayton, K.E. Morgan, A.L. Klibanov, G. Brandenburger, K.R. Nightingale, K.W. Ferrara, A preliminary evaluation of the effects of primary and secondary radiation forces on acoustic contrast agents, IEEE Trans. Ultrason. Ferroelect. Freq. Contr. 44 (6) (1997) 1264–1277.

[9] P. Tortoli, V. Michelassi, M. Corsi, D. Righi, Y. Takeuchi, On the interaction between ultrasound and contrast agents during Doppler investigations, Ultrasound Med. Biol. 27 (9) (2001) 1265–1273.
[10] H. Medwin, Counting bubbles acoustically: a review, Ultrasonics 15 (1977) 7–13.
[11] J. Magnaudet, I. Eames, The motion of high-Reynolds-number bubbles in inhomogeneous flows, Annu. Rev. Fluid Mech. 32 (2000) 659–708.
[12] P. Di Marco, W. Grassi, G. Memoli, Experimental study on rising velocity of nitrogen bubbles in FC-72, Int. J. Therm. Sci. 42 (2003) 435–446.
[13] T.G. Leighton, The Acoustic Bubble, Academic Press Ltd., London, 1994.
[14] M. Postema, G. Schmitz, Ultrasonic bubbles in medicine: influence of the shell, Ultrason. Sonochem. 14 (4) (2007) 438–444.
[15] N. de Jong, R. Cornet, C.T. Lancée, Higher harmonics of vibrating gas-filled microspheres. Part one: simulations, Ultrasonics 32 (6) (1994) 447–453.
[16] P.C. Duiveveld, Bouncing and coalescence of two bubbles in water, PhD Thesis, University of Twente, 1994.
[17] M. Postema, P. Marmottant, C.T. Lancée, S. Hilgenfeldt, N. de Jong, Ultrasound-induced microbubble coalescence, Ultrasound Med. Biol. 30 (10) (2004) 1337–1344.
[18] S. Kotopoulis, A. Schommartz, M. Postema, Sonic cracking of blue–green algae, Appl. Acoust. 70 (10) (2009) 1306–1312.
[19] E. Kimmel, B. Krasovitski, A. Hoogi, D. Razansky, D. Adam, Subharmonic response of encapsulated microbubbles: condition for existence and amplification, Ultrasound Med. Biol. 33 (11) (2007) 1767–1776.
[20] M. Postema, A. van Wamel, F.J. ten Cate, N. de Jong, High-speed photography during ultrasound illustrates potential therapeutic applications of microbubbles, Med. Phys. 32 (12) (2005) 3707–3711.
[21] P. Prentice, A. Cuschieri, K. Dholakia, M. Prausnitz, P. Campbell, Membrane disruption by optically controlled microbubble cavitation, Nat. Phys. 1 (2005) 107–110.

II.2 Manipulation cellulaire

L'interaction entre les microbulles ultrasonores et les cellules biologiques est interessante pour explorer des applications d'ultrasons en médecine du futur.

L'article « Sonic cracking of blue-green algae » décrit la rupture de cyanobactéries avec l'aide des ultrasons diagnostiques (p. 78). [4]

Utilisant des ultrasons de faible amplitude, des algues bleues-vertes ont été forcées de libérer du gaz aux fréquences acoustiques de 200 kHz, 1,0 MHz et 2,2 MHz. En conséquence, ces algues coulent et restent immobiles bien que vivantes.

La création expérimentale d'une mousse de globules est présentée dans « Bubble-like response of living blood cells and microparticles in an ultrasound field » (p. 85). [5] Utilisant des transducteurs cylindriques et des impulsions longues, les globules rouges s'ordonnaient en formant des cercles chacun séparé d'une demie longueur d'onde.

La réponse acoustique des globules rouges est attribuée à la compressibilité des membranes cellulaires.

En utilisant ce constat, dans l'article « Theory of red blood cell oscillations in an ultrasound field », les oscillations théoriques dans un champ ultrasonore sont dérivées pour les globules rouges (p. 89). [6]

Les equations dérivées pour les globules rouges sont similaires à celles des antibulles. Elles doivent être valides pour les liposomes aussi.

4. Kotopoulis S, Schommartz A, Postema M. Sonic cracking of blue-green algae. Applied Acoustics 2009 ; 70(10) : 1306–1312.

5. Mazzawi N, Postema M, Kimmel E. Bubble-like response of living blood cells and microparticles in an ultrasound field. Acta Physica Polonica A 2015 ; 127(1) : 103–105.

6. Johansen K, Kimmel E, Postema M. Theory of red blood cell oscillations in an ultrasound field. Archives of Acoustics 2017 ; 42(1) : 121–126.

Applied Acoustics 70 (2009) 1306–1312

Contents lists available at ScienceDirect

Applied Acoustics

journal homepage: www.elsevier.com/locate/apacoust

Sonic cracking of blue-green algae

Spiros Kotopoulis, Antje Schommartz, Michiel Postema *

Department of Engineering, The University of Hull, Cottingham Road, Kingston Upon Hull HU6 7RX, United Kingdom

ARTICLE INFO

Article history:
Available online 20 March 2009

Keywords:
Ultrasonic algae eradication
Blue-green algae
Sonic cracking

ABSTRACT

Algae are aquatic organisms classified separately from plants. They are known to cause many hazards to humans and the environment. Algae strands contain nitrogen-producing cells that help them float (heterocysts). It is hypothesized that if the membranes of these cells are disrupted by means of ultrasound, the gas may be released analogous to sonic cracking, causing the strands to sink. This is a desirable ecological effect, because of the resulting suppressed release of toxins into the water.

We subjected small quantities of blue-green algae of the *Anabaena sphaerica* species to ultrasound of frequencies and pressures in the clinical diagnostic range, and observed the changes in brightness of these solutions over time. Blue-green algae were forced to sink at any ultrasonic frequency we studied, supporting our hypothesis that heterocysts release nitrogen under ultrasound insonification in the clinical diagnostic range.

Although the acoustic fields we used to eradicate blue-green algae are perfectly safe in terms of mechanical index, the acoustic pressures surpass the NURC Rules and Procedures by over 35 dB. Therefore, caution should be taken when using these techniques in a surrounding where aquatic or semi-aquatic animals are present.

1. Introduction

Algae are aquatic, eukaryotic, photosynthetic organisms, ranging in size from single-celled forms to large kelps. Algae are classified separately from plants since they lack true roots, stems, leaves and embryos. Algae are known to cause many health hazards to humans including skin rashes, gastrointestinal, respiratory [1], allergic reactions [2], and liver cancer [3]. In addition, blue-green algae may have implications on aquatic and semi-aquatic animals [4]. Eutrophication is the increase in chemical nutrients within the ecosystem, causing blooms of algae and plant life and the subsequent decomposition of blue-green algae by bacteria, an oxygen-consuming process [5]. When billions of such bacterial cells die during a bloom, the water becomes oxygen-depleted, killing off oxygen-dependent organisms [6].

The main factors that influence algae growth are temperature and light [7,8]. At low temperatures and low light conditions, the algae do not photosynthesise and therefore do not bloom. Algae strands contain nitrogen-producing cells that help them float (heterocysts), as demonstrated in Fig. 1. The heterocysts have a diameter between 5 and 7 μm [9]. It is hypothesized that if the membranes of these cells are disrupted by means of ultrasound, the gas may be released analogous to sonic cracking [10], causing the strands to sink. At the lake bed, illumination is lower, thus reducing algae multiplication. This is a desirable ecological effect, because of resulting suppressed release of toxins into the water.

There are chemical methods to control certain species of algae, but these have side-effects such as promotion and growth of other species of algae [11] whilst also affecting aquatic life in fresh water ponds and lakes. Therefore, ultrasonic algae control has been under investigation [12–17]. In [12–17], ultrasonic insonification of different species of algae led to a decrease in algae concentrations in the frequency range 20 kHz–1.7 MHz, which is in contrast with [18], where ultrasound was observed to strengthen the cell membranes of red algae. In these studies, the exact acoustic conditions have not been specified other than the frequency and power input. Hence, from the acoustics point of view, they are not repeatable. More importantly, the mechanism causing algae eradication or membrane disruption had not been investigated.

Most commercially available equipment works in the lower ultrasonic range [19]. There have been speculations about the physical mechanism behind the algae eradication, specifically about the role of cavitation. In this study, we investigate the effectiveness of ultrasonic insonification in the clinical diagnostic range on *Anabaena* blue-green algae.

A measure for the safe use of clinical diagnostic ultrasound is the mechanical index (MI) defined by

$$\mathrm{MI} = \frac{p^-}{\sqrt{f}}, \tag{1}$$

* Corresponding author. Tel.: +44 1482 465670.
E-mail address: m.postema@hull.ac.uk (M. Postema).

0003-682X/$ - see front matter © 2009 Elsevier Ltd. All rights reserved.
doi:10.1016/j.apacoust.2009.02.003

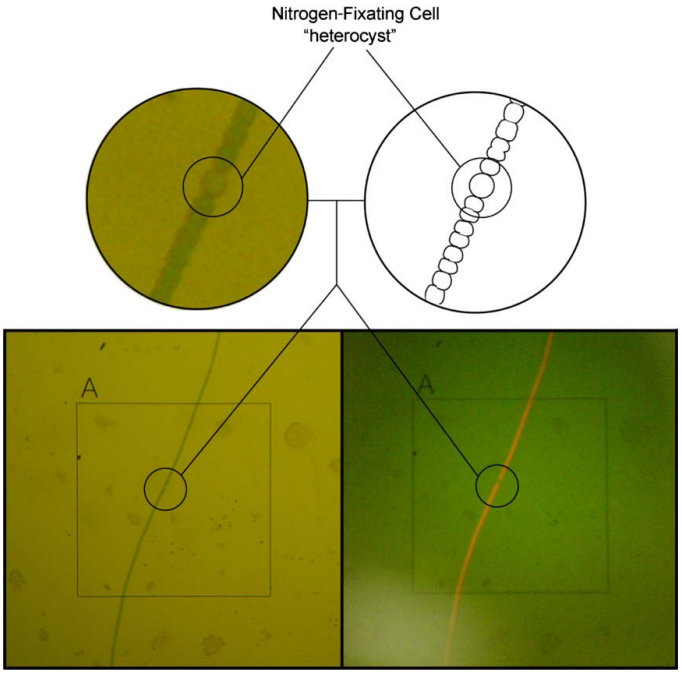

Fig. 1. Nitrogen-fixating body in *Anabaena sphaerica* algae. Under fluorescent light the body does not illuminate red, proving there is no chlorophyll in the body. Each frame corresponds to 565 × 565 μm^2.

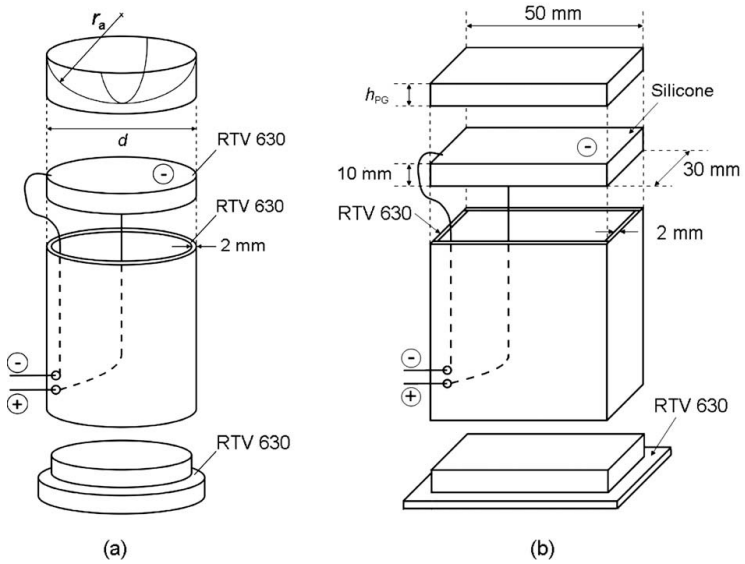

Fig. 2. (a) Undamped 2.2-MHz ultrasound transducer with $d = 1''$ diameter and $r_a = 35$ mm acoustic lens. (b) Undamped 200-kHz ultrasound transducer with modification layer $h_{PG} = 10$ mm.

where p^- is the maximum value of peak-negative pressure anywhere in the ultrasound field, measured in water but reduced by an attenuation factor equal to that which would be produced by a medium having an attenuation coefficient of 0.3 dB cm^{-1} MHz^{-1}, normalised by 1 MPa, and f is the centre frequency of the ultrasound normalised by 1 MHz [20]. For MI < 0.3, the ultrasonic amplitude is

considered low. In clinical diagnostics there is a possibility of minor damage to neonatal lung or intestine [20] for 0.3 < MI < 0.7. These are considered moderate acoustic amplitudes. For MI > 0.7, there is a risk of cavitation if gas cavitation nuclei are present, and there is a theoretical risk of cavitation without the presence of cavitation nuclei [20]. The risk increases with MI values above this threshold [20]. These are considered high acoustic amplitudes. According to the NATO Undersea Research Centre (NURC) Human Diver and Marine Mammal Risk Mitigation Rules and Procedures [21], the maximum acoustic pressure to which mammals can be exposed is 708 Pa at frequencies up to 250 kHz. This corresponds to a mechanical index MI < 0.01 ≪ 0.3. In this paper, we have chosen to work in the lower clinical diagnostic range, taking into account both guidelines.

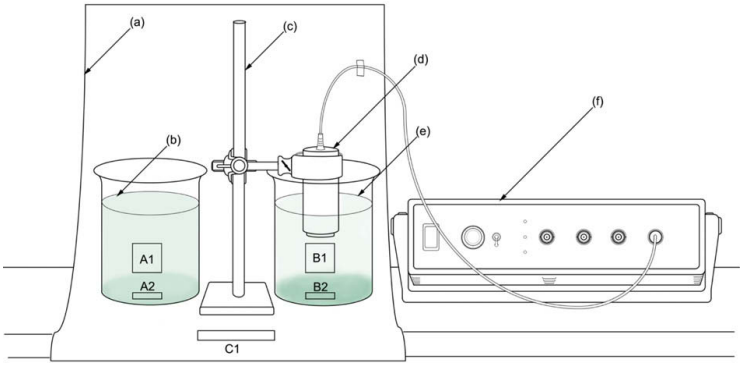

Fig. 3. Experimental setup: (a) white paper sheet; (b) control sample; (c) clamp stand; (d) transducer; (e) insonified sample; (f) pulser–receiver. Areas A1–B2 represent brightness measurement areas, C1 represents the calibration area.

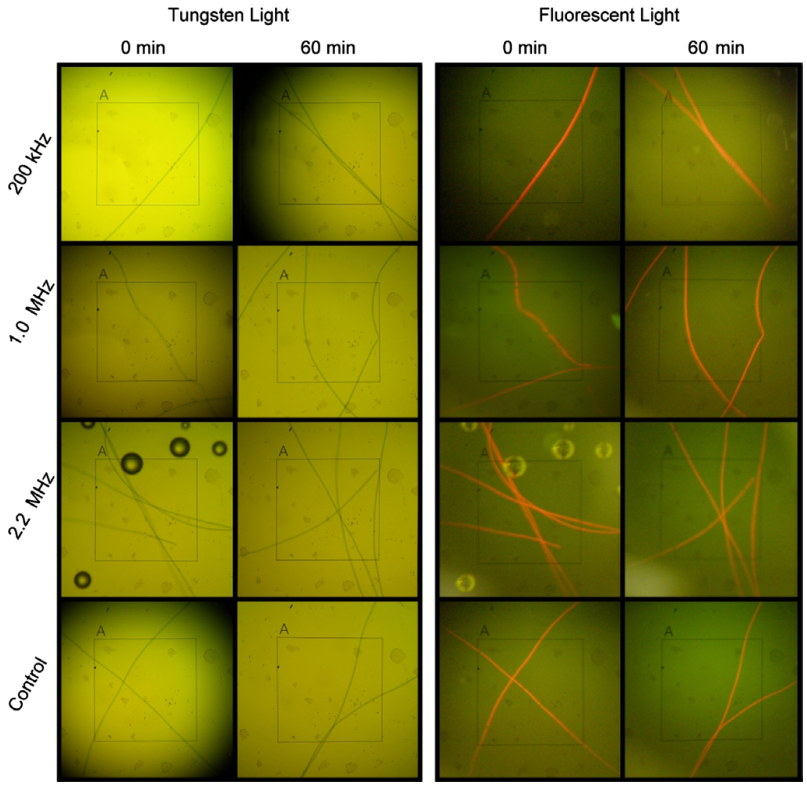

Fig. 4. Microscopic image sequence showing the effect of 200 kHz–2.5 MHz ultrasound on the floating bodies of algae. Each frame corresponds to 565 × 565 μm².

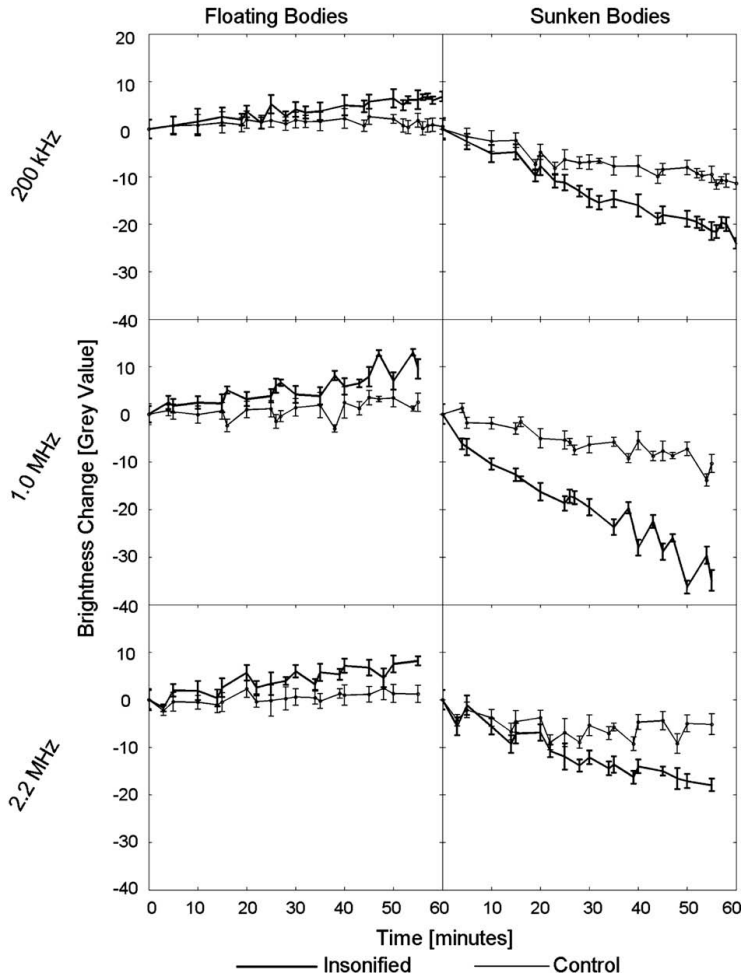

Fig. 5. Water brightness as a function of ultrasonic exposure time for samples containing floating algae or sunken algae.

2. Materials and methods

To investigate the effect of diagnostic ultrasound on algae eradication, three ultrasound transducers were used. A 200-kHz undamped single element transducer containing a PIC155 Piezo crystal (PI Ceramics, Lederhose, Germany), a PA 188 (Precision Acoustics Ltd., Dorchester, UK) 1-MHz undamped single element transducer, and a 2.2-MHz undamped single element transducer containing a Pz37 Piezo crystal (Ferroperm Piezoceramics A/S, Kvistgård, Denmark). The focal distance of the 2.2-MHz transducer was 73 mm. The design of two transducers is shown in Fig. 2. The transducers were subjected to 16-Vpp square pulses at a 11.8-kHz pulse repetition rate transmitted by a V1.0 pulser–receiver (Sonemat, Coventry, UK). Low acoustic amplitudes were used in order to comply with MI < 0.3 [20]. The acoustic amplitudes were measured in a separate water tank in the acoustic foci of the transducers with a 0.2-mm needle hydrophone (Precision Acoustics Ltd., Dorchester, UK) connected to a TDS 420A four channel digital oscilloscope (Tektronix Inc., Beaverton, USA). The peak-negative acoustic pressures were 40 kPa for the 1-MHz transducer and 68 kPa for the 2.2-MHz transducer, respectively, i.e., MI $\ll$ 0.1.

The algae used were of the *Anabaena sphaerica* species. The *Anabaena* were obtained from an outside lake and cultured in 2 L of Jaworski's medium [22] at room temperature near a South-facing window in an Erlenmeyer flask for 11 days. The solution was put in a Swirtlock2000 autoclave (Astell Scientific, Kent, UK) at 15-lb pressure for 15 min.

2.1. Brightness measurements

To measure the time-dependent change in brightness of water containing blue-green algae, the culture was split equally into four 250-mL Perspex beakers: one beaker for each transducer and one control beaker. The transducers were inserted separately in each beaker with the acoustic focus within the sample. Each transducer was turned on for 1 h. The experimental setup is shown in Fig. 3. A digital photograph of the solution was taken every 5 min using an EOS 350D digital photo camera (Canon Inc., Tokyo, Japan). The

lighting and exposure settings were controlled and maintained throughout the insonification. Full manual settings were used: ISO 100, exposure time 1/50 s, F number 3.50, focal length 18 mm, no flash, centre weighted metering mode, custom white balance, B4,0 shift. The digital photographs were converted to 8-bit grey scale. On the photographs of the insonified solution and control solution, a square area of 160 × 160 pixels was selected, whose average grey scale depth was calculated using MATLAB® (The Mathworks™, Natick, MA). The change in shade between the first image taken just before insonification and each sequential image after insonification was calculated and graphed for all 18 insonified and control samples. A white sheet was placed behind the beakers to maintain a constant background. The grey scale of the sheet was also measured and used to calibrate the results. In total, 575 measurements were analysed from 122 photographs.

2.2. Viability measurements

Every 10 min, a 20-μL sample was taken from the insonified solution. Samples were put on a test slide and observed through a CHA microscope (Olympus Corporation, Tokyo, Japan) with a 10× objective lens (Olympus Corporation, Tokyo, Japan). Digital photographs were captured from the microscope's eye piece using an FE-230 digital camera (Olympus Corporation, Tokyo, Japan). Automatic settings were used with Super Macro mode and a −1.0 exposure adjustment. From these digital images, cell deterioration and chlorophyll damage were determined. To investigate the effect of ultrasound on the viability of the cells, fluorescent light was used. When fluorescent light is projected onto chlorophyll, it is absorbed and re-emitted as a red glow. The red glow denotes that the chlorophyll is still active and can photosynthesise,

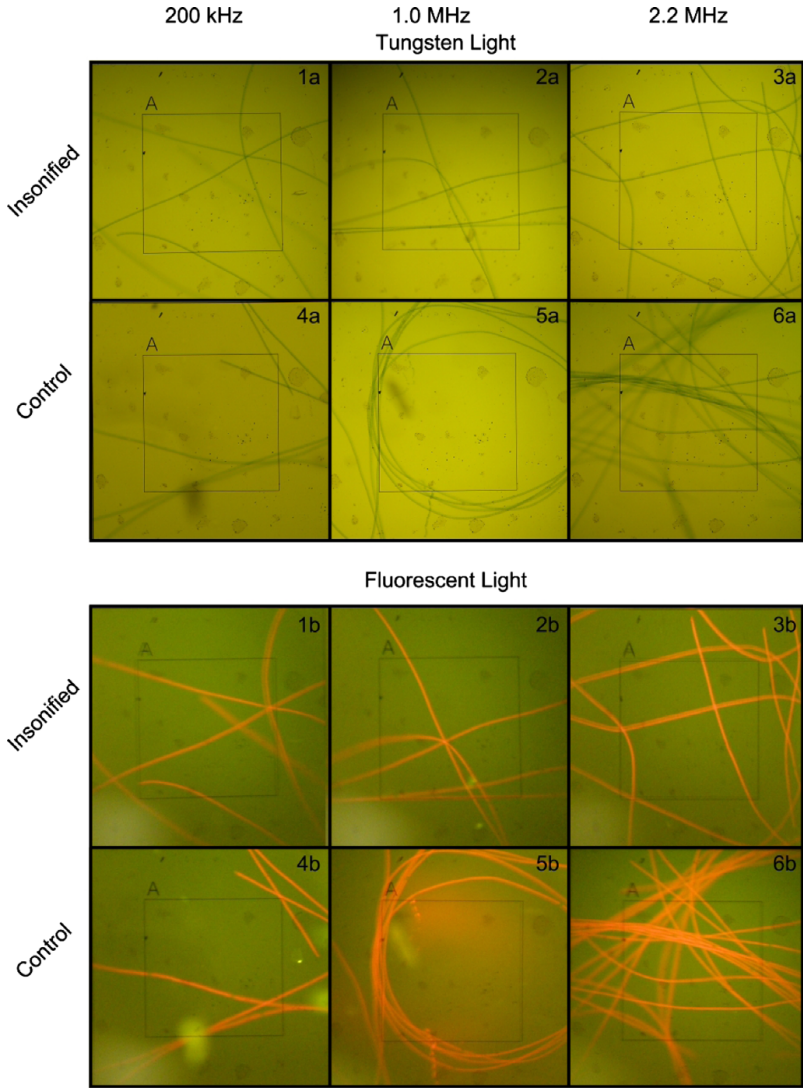

Fig. 6. Microscopic image sequence of sunken algae Each frame corresponds to 565 × 565 μm².

thus the algae strands are still alive. Fluorescent light was used as the method to check the viability of the chlorophyll, since it is a standardized and accepted method in detecting chlorophyll activity in plants [23,24]. Fluorescent light was projected onto these samples for no more than 10 s in order to capture the digital image. We may assume that there are no disadvantageous effects of the fluorescent light on the algae [25,26]. The samples were discarded after being exposed to fluorescent light. Three trials of each frequency were performed. One hundred and 31 photographs were taken of the microscopic cell structure.

2.3. Post-insonification growth measurements

To measure the effect of ultrasound on post-insonification blue-green algae growth, 24 1-mL samples were removed from three solutions that had been subjected to 1 h of insonification with 200-kHz, 1.0-MHz and 2.2-MHz ultrasound, respectively, and put into a culture tray with 96 compartments. Twenty-four control samples were taken. The culture tray was left in sunlight for 30 days. The grey scale depth was measured for each compartment.

3. Results and discussion

Fig. 4 shows the microscopic effect of ultrasound on floating bodies in the algae solution. From 0 min to 60 min of insonification, no change was seen in the physical structure of the algae for the whole frequency range. Illuminating the algae with fluorescent light showed that the ultrasound had no effect on the chlorophyll activity for the whole frequency range. The active chlorophyll shows that the algae strands are still alive and able to photosynthesise after 60 min insonification. This indicates that the ultrasound transmitted does not affect the chlorophyll-containing cells themselves, which is desirable since no toxins are released this way.

However, Fig. 5 shows that at all frequencies, for the floating bodies, the insonified samples showed greater brightness than the control samples. For the sunken bodies, all insonified samples showed reduced clarity as compared to the control samples. Thus, the ultrasound has caused the algae to sink. For example, after 60 min, the beakers subjected to 200-kHz insonification were $92 \pm 12\%$ brighter than the control samples, contrasted by the beaker bottoms, which were $53 \pm 27\%$ darker than the control samples.

Clearly, the algae that were floating in the beaker dropped to the bottom at a faster rate than the control sample. This has been attributed to the disruption of the floating bodies by the ultrasound. This is supported by Fig. 6, which shows that the sunken bodies still have active chlorophyll but contain very few heterocysts.

Fig. 7 shows the viability of the culture 30 days after insonification in terms of sample brightness. At 200 kHz, 1.0 MHz, and 2.2 MHz, the samples were $39 \pm 14\%$, $45 \pm 17\%$, and $46 \pm 17\%$ brighter than the control samples, respectively. All samples were significantly brighter than the control samples, even at the lower boundaries of the standard deviation. Thus, these results support the hypothesis that the algae that have sunk are less capable of multiplying. Hence, insonification may prevent algae bloom.

Our results can be interpreted as follows. When a heterocyst is subjected to an ultrasound pulse, the bubble encapsulated by it expands, in our frequency range [27] during the rarefaction phase of the ultrasound. If the acoustic amplitude is sufficiently high, the encapsulating membrane cannot withhold the bubble from further expanding, resulting in its rupture. This phenomenon is similar to the sonic cracking of micrometer-sized membrane-encapsulated bubbles observed in [10]. Sonic cracking exclusively occurs during the expansion phase of a bubble [28].

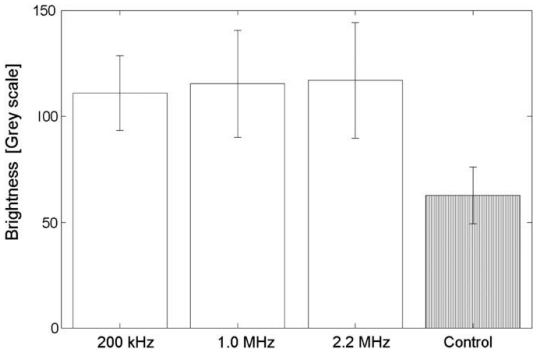

Fig. 7. Water clarity 30 days after insonification.

The resonance frequency f_0 of a an encapsulated microbubble is given by [29]

$$f_0 = \frac{1}{2\pi}\sqrt{\left(\frac{3\Gamma}{R_0^2\rho}\right)\left(p_0 + \frac{2\sigma}{R_0} + \frac{2\chi}{R_0}\right) - \left(\frac{2\sigma + 6\chi}{R_0^3\rho}\right)}, \tag{2}$$

where p_0 is the ambient pressure, R_0 is the bubble radius, Γ is the polytropic exponent of the gas, ρ is the liquid density, σ is the surface tension, and χ is the elasticity of the encapsulation [29]. Using $p_0 = 1.013 \times 10^5$ Pa, $R_0 = 3$ μm, $\Gamma = 1.4$, ρ is 998 kg m^{-3}, $\sigma = 0.072$ Nm^{-1}, and assuming that the membrane elasticity is similar to that of a lipid encapsulation, $\chi = 0.044$ Nm^{-1} [30], we can estimate $f_0 \approx 1$ MHz for *Anabaena* heterocysts used in our experiments. Since the greatest change in clarity was seen at this particular frequency, we can safely state that ultrasound insonification close to heterocyst resonance frequency leads to a more effective eradication.

The quick decrease in live algae is similar to that in previous studies [12–17]. We assume that the correlation between (high) frequency and algae eradication in these studies is related to the ultrasound proximity to heterocyst resonance as well.

According to the NURC Rules and Procedures [21], the maximum acoustic pressure to which mammals can be exposed is 708 Pa at frequencies up to 250 kHz. The transducers used had acoustic pressures of 40 kPa and 68 kPa at driving frequencies 1.0 MHz and 2.2 MHz, respectively. These pressures surpass the NURC Rules and Procedures by over 35 dB.

4. Conclusion

At any ultrasonic frequency we studied, blue-green algae were forced to sink. This supports our hypothesis that heterocysts release nitrogen under ultrasound insonification in the clinical diagnostic range. As supported by previous studies, under identical pulse length and pulse repetition, eradication is most effective close to heterocyst resonance, at a driving frequency of roughly 1 MHz.

Although the acoustic fields we used to eradicate blue-green algae are safe in terms of mechanical index, the acoustic pressures surpass the NURC Rules and Procedures by over 35 dB. Therefore, caution should be taken when using these techniques in a surrounding where aquatic or semi-aquatic animals are present.

Acknowledgements

This work has been supported by EPSRC Grant EP/F037025/1 and the HERI Research Pump Priming Fund. We would like to thank

John Adams, The University of Hull, for support with the experimental setup.

References

[1] Turner PC, Gammie AJ, Hollinrake K, Codd GA. Pneumonia associated with contact with cyanobacteria. Brit Med J 1990;300(6737):1440–1.
[2] Stewart I, Schluter PJ, Shaw GR. Cyanobacterial lipopolysaccharides and human health: a review. Environ Health 2006;5(7):1–23.
[3] Fleming LE, Rivero C, Burns J, Williams C, Bean JA, Shea KA, et al. Blue green algal (cyanobacterial) toxins, surface drinking water, and liver cancer in Florida. Harmful Algae 2002;1(2):157–68.
[4] Bury N. The toxicity of cyanobacteria (blue-green algae) to freshwater fish. Comp Biochem Physiol A 2007;146(4):S92–3.
[5] San Diego-McGlone ML, Azanza RV, Villanoy CL, Jacinto GS. Eutrophic waters, algal bloom and fish kill in fish farming areas in Bolinao, Pangasinan, Philippines. Mar Pollut Bull 2008;57(6–12):295–301.
[6] Hylland K, Sköld M, Gunnarsson JS, Skei J. Interactions between eutrophication and contaminants. IV. Effects on sediment-dwelling organisms. Mar Pollut Bull 1996;33(1–6):90–9.
[7] Dauta A, Devaux J, Piquemal F, Bouminch L. Growth rate of four freshwater algae in relation to light and temperature. Hydrobiologia 1990;207(1):221–6.
[8] Allen MB, Arnon DI. Studies on nitrogen-fixing blue-green algae. I. Growth and nitrogen fixation by *Anabaena cylindrica* lemm. Plant Physiol 1955;30(4):366–72.
[9] Lang N, Krupp J, Koller A. Morphological and ultrastructural changes in vegetative cells and heterocysts of *Anabaena variabilis* grown with fructose. J Bacteriol 1987;169(2):920–3.
[10] Postema M, Bouakaz A, Versluis M, de Jong N. Ultrasound-induced gas release from contrast agent microbubbles. IEEE Trans Ultrason Ferroelect Freq Contr 2005;52(6):1035–41.
[11] Ferrier MD, Butler Sr BR, Terlizzi DE, Lacouture RV. The effects of barley straw (*hordeum vulgare*) on the growth of freshwater algae. Bioresource Technol 2005;96(16):1788–95.
[12] Zhang G, Zhang P, Wang B, Liu H. Ultrasonic frequency effects on the removal of *Microcystis aeruginosa*. Ultrason Sonochem 2006;13(5):446–50.
[13] Ma B, Chen Y, Hao H, Wu M, Wang B, Lv H, et al. Influence of ultrasonic field on microcystins produced by bloom-forming algae. Colloid Surf B 2005;41(2–3):197–201.
[14] Zhang G, Zhang P, Liu H, Wang B. Ultrasonic damages on cyanobacterial photosynthesis. Ultrason Sonochem 2006;13(6):501–5.
[15] Hao H, Wu M, Chen Y, Tang J, Wu Q. Cavitation mechanism in cyanobacterial growth inhibition by ultrasonic irradiation. Colloid Surf B 2004;33(3–4):151–6.
[16] Tang J, Wu Q, Hao H, Chen Y, Wu M. Growth inhibition of the cyanobacterium spirulina (arthrospira) platensis by 1.7 MHz ultrasonic irradiation. J Appl Phycol 2003;15(1):37–43.
[17] Zhang G, Zhang P, Fan M. Ultrasound-enhanced coagulation for *Microcystis aeruginosa* removal. Ultrason Sonochem 2009;16(3):334–8.
[18] Chen B, Huang J, Wang J, Huang L. Ultrasound effects on the antioxidative defense systems of *Porphyridium cruentum*. Colloid Surf B 2008;61(1):88–92.
[19] Postema M. Onderzoek naar de veilige toepassing van ultrageluid gebruikt om blauwalg te bestrijden. Memo. The University of Hull; 2007.
[20] British Medical Ultrasound Society. Guidelines for the safe use of diagnostic ultrasound equipment; 2000.
[21] NATO Undersea Research Centre. Human diver and marine mammal risk mitigation rules and procedures. Technical report, NURC-SP-2006-008; 2006.
[22] Culture Collection of Algae and Protozoa. Media Recipes, vol. EG;JM; 2007.
[23] Ventrella A, Catucci L, Agostiano A. Effect of aggregation state, temperature and phospholipids on photobleaching of photosynthetic pigments in spinach photosystem II core complexes. Bioelectrochemistry 2008;73(1):43–8.
[24] Mateos-Naranjo E, Redondo-Gómez S, Cambrollé J, Enrique Figueroa M. Growth and photosynthetic responses to copper stress of an invasive cordgrass, *Spartina densiflora*. Mar Environ Res 2008;66(4):459–65.
[25] Ohl C, Wolfrum B. Detachment and sonoporation of adherent hela-cells by shock wave-induced cavitation. BBA-Gen Subjects 2003;1624(1–3):131–8.
[26] Kooiman K, Böhmer M, Emmer M, Vos H, Chlon C, Foppen-Harteveld M, et al. Ultrasound-triggered local release of lipophilic drugs from a novel polymeric ultrasound contrast agent. J Control Release 2008;132(3):e41–2.
[27] Postema M, Schmitz G. Ultrasonic bubbles in medicine: influence of the shell. Ultrason Sonochem 2007;14(4):438–44.
[28] Postema M, van Wamel A, Lancée CT, deJong N. Ultrasound-induced encapsulated microbubble phenomena. Ultrasound Med Biol 2004;30(6):827–40.
[29] Postema M, Schmitz G. Bubble dynamics involved in ultrasonic imaging. Expert Rev Mol Diagn 2006;6(3):493–502.
[30] Gorce JM, Arditi M, Schneider M. Influence of bubble size distribution on the echogenicity of ultrasound contrast agents: a study of SonoVue™. Invest Radiol 2000;35(11):661–71.

Vol. **127** (2015) *ACTA PHYSICA POLONICA A* No. 1

Acousto-Optics and Applications

Bubble-Like Response of Living Blood Cells and Microparticles in an Ultrasound Field

N. Mazzawi[a], M. Postema[b,c,*] and E. Kimmel[a]

[a]Department of Biomedical Engineering, Technion, Haifa, Israel

[b]Department of Physics and Technology, University of Bergen, Bergen, Norway

[c]The Michelsen Centre for Industrial Measurement Science and Technology, Bergen, Norway

The bilayer sonophore model suggests that ultrasound induces a pulsating structure in the intra-membrane hydrophobic space between the two lipid monolayer leaflets of the cell membrane, assembled by dissolved gas of the surrounding area, which absorbs acoustic energy and transforms it by creating intra-cellular structural changes. This void has been referred to as a bilayer sonophore. The bilayer sonophore inflates and deflates periodically when exposed to ultrasound and may itself radiate acoustic pressure pulses in the surrounding medium in the same way a gas bubble does: once exposed to ultrasound the bilayer sonophore becomes a mechanical oscillator and a source of intracellular cavitation activity. In this paper, we describe observations of the clustering behaviour of living cells and several other particles in a standing sound field generated inside a ring transducer. Upon sonication, blood cells and monodisperse polystyrene particles were observed to have been trapped in the same locations, corresponding to nodes of the ultrasound field. Because polystyrene is hydrophobic, it behaves like a particle trapped inside a thin gas shell. In fact, the sonophore model treats biological cells in a similar way. Microbubbles that form the ultrasound contrast agent Quantison™ behave differently, however. These microbubbles accumulated in circles faster than blood cells and polystyrene particles. In addition, they form tightly packed clusters at the nodes, indicating very strong secondary Bjerknes forces. Cluster formation is not to be expected in cells with predicted sonophore sizes on the order of 10–100 nm.

DOI: 10.12693/APhysPolA.127.103

PACS: 43.80.Cs, 47.55.df, 87.80.Fe

1. Introduction

The bilayer sonophore model suggests that ultrasound induces a pulsating structure in the intra-membrane hydrophobic space between the two lipid monolayer leaflets of the cell membrane, assembled by dissolved gas of the surrounding area, which absorbs acoustic energy and transforms it by creating intra-cellular structural changes [1]. The two leaflets are pulled apart when the acoustic rarefaction pressure overcomes the molecular attractive forces between them and are pushed back together by the compressive pressure. This void has been referred to as a bilayer sonophore (cf. Fig. 1). The bilayer sonophore inflates and deflates periodically when exposed to ultrasound and may itself radiate acoustic pressure pulses in the surrounding medium in the same way a gas bubble does: once exposed to ultrasound the bilayer sonophore becomes a mechanical oscillator and a source of intracellular cavitation activity.

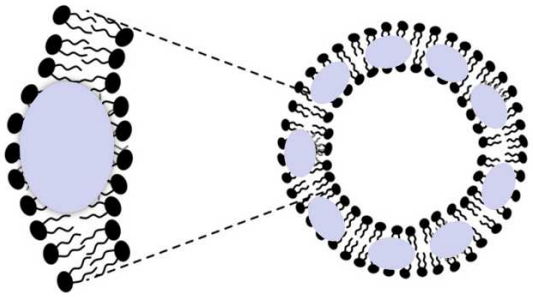

Fig. 1. Bilayer sonophore formation within the intra-membrane space of a cell.

In this paper, we describe observations of the clustering behaviour of living cells and several other particles in a standing sound field.

2. Methods

Figure 2 shows a schematic overview of the experimental setup used in this study. The main element of the setup is a ring transducer consisting of a Pz26 (OD32 ID28 L14) piezoceramic tube of lead zirconate titanate (PZT) (Ferroperm Piezoceramics, Kvistgård, Denmark) with an inner diameter of 28 mm, a height of 10 mm, and an element thickness of 2.1 mm. The ring transducer was fixed to the centre of a Petri dish with a 100 mm diameter and a 15 mm height. The Petri dish was filled with a 2% Agar solution. The transducer was connected to an AR75 power amplifier (AR Company, Souderton, PA, USA), which was connected to either a 8024 arbitrary waveform generator (Tabor Electronics, Irvine, CA, USA) or a 33120A arbitrary waveform generator (Hewlett-Packard

*corresponding author; e-mail: michiel.postema@ift.uib.no

Company, Palo Alto, CA, USA). The signal generated consisted of a continuous 1 MHz or 3 MHz sine wave with peak-to-peak amplitudes between 1 V and 10 V.

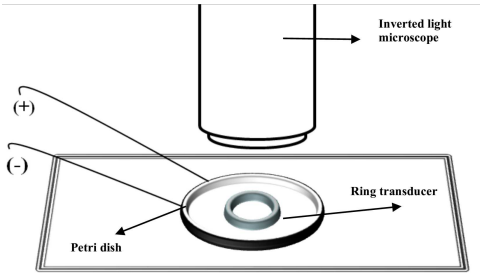

Fig. 2. Schematic of experimental setup.

The centre of the Petri dish was mounted under an Eclipse TE2000 inverted microscope (Nikon Instruments Inc., Melville, NY, USA) with 2× , 10× , and 20× magnification, to which an Infinity 3-1M camera (Lumenera Corp., Ottawa, Ontario, Canada) was connected.

Among the objects studied were (a) 0.1 ml of rat blood mixed with 0.02 g of heparin dissolved in a 2 ml PBS solution added to 2 ml of DMEM and 0.1 ml of trypsin, (b) Duke Standards 4210A, 4220A polystyrene microspheres (Thermo Fisher Scientific Inc, Waltham, MA, USA), (c) Quantison™ ultrasound contrast agent (Upperton Limited, Nottingham, UK).

3. Results and discussion

Upon sonication, particles and cells translated towards nodes of the sound field. As sonication stopped, all trapped objects maintained at these positions, whilst other free (non-trapped) objects have gradually stopped moving and circulating inside the ring. The location of the nodes and antinodes of the sound field was dependent upon the transmit frequency used.

Blood cells that had been trapped at the nodes were arranged in circles inside the ring, as shown in Fig. 3. The average radial distance measured between these circle-shaped strips was half a wavelength. This finding indicated that the resonance frequency of all cells is below the transmit frequency. In a previous study with an ultrasound contrast agent with a wide size distribution, the space between microbubble clusters was deducted and found to be a quarter wavelength [2], because the greater microbubbles would be trapped in the nodes and the smaller microbubbles would be trapped in the antinodes of the sound field.

Upon sonication, the monodisperse polystyrene particles were observed to have been trapped in the same locations as the blood cells. Because polystyrene is hydrophobic, it behaves like a particle trapped inside a thin gas shell. In fact, the sonophore model relates to biological cells in a similar way, except for the difference that sonophores develop only in a sound field.

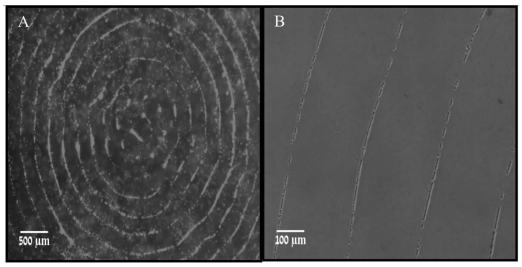

Fig. 3. Blood cells arranged in concentric circles inside the ring transducer after 3 MHz sonication, observed at A) 2× magnification, and B) 10× magnification.

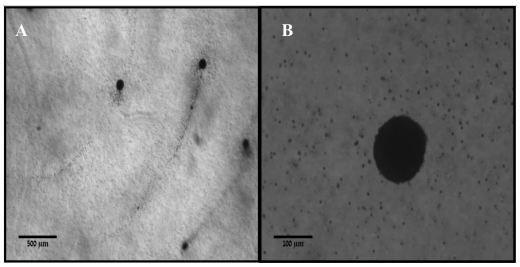

Fig. 4. Quantison™ microbubbles not only accumulate in circles, corresponding to the nodes of the 1 MHz ultrasound sound field, but also form tightly packed clusters at the nodes, when observed at A) 2× magnification and B) 10× magnification.

The microbubbles of which the ultrasound contrast agent Quantison™ consists behave differently, however, as demonstrated in Fig. 4. These microbubbles with mean diameters of 5 μm accumulated in circles faster than blood cells and polystyrene particles. Again, these circles correspond to the nodes of the ultrasound field. In addition, they form tightly packed clusters at the nodes, indicating very strong secondary Bjerknes forces [2].

Cluster formation is not to be expected in cells, because the sonophore sizes predicted from [1] are on the order of 10–100 nm. Given the fact that secondary Bjerknes forces of gas bubbles are proportional to the bubbles radius to the power of five [3], these forces must be too weak if created by sonophores. Moreover, cells in the nodes are subjected to zero acoustic pressure and therefore no sonophore formation is to be expected in standing waves [1].

In order to compare any bubble-like behaviour of cells with actual bubble-like systems, a comparison with antibubbles would be interesting, especially in a running sound field. Recently, it has been disclosed how to manufacture stable antibubbles, consisting of a liquid core,

of the same dimensions as a blood cell, and a gaseous shell [4]. If the sonophore hypothesis is correct, blood cells must demonstrate the same acoustic properties as antibubbles.

4. Conclusions

Although blood cells and polystyrene particles accumulate slower than ultrasound contrast agent microbubbles, their acoustic behaviour has similarities. The absence of tightly packed cluster formation in cells indicates that the secondary Bjerknes forces are too low for this to happen, which corresponds to sonophore theory.

More studies, e.g., by comparing the acoustic behaviour of blood cells with that of antibubbles, will bring us closer to finding whether cells form sonophores upon sonication.

Acknowledgments

The scholarship of Nasma Mazzawi has been financed by the Technion. The ring transducer was kindly given to us by Dr. Graham Brodie from the University of Dundee.

References

[1] B. Krasovitski, V. Frenkel, S. Shoham, E. Kimmel, *Proc. Natl. Acad. Sci.* **108**, 3258 (2011).

[2] S. Kotopoulis, M. Postema, *Ultrasonics* **50**, 260 (2010).

[3] M. Postema, *Fundamentals of Medical Ultrasonics*, Spon Press, New York 2011.

[4] A.T. Poortinga, *Langmuir* **27**, 2138 (2011).

PAN ARCHIVES OF ACOUSTICS
Vol. **42**, No. 1, pp. 121–126 (2017)

DOI: 10.1515/aoa-2017-0013

Theory of Red Blood Cell Oscillations in an Ultrasound Field

Kristoffer JOHANSEN[(1)], Eitan KIMMEL[(2)], Michiel POSTEMA[(3),(4)]

[(1)] *School of Engineering, James Watt Building*
University of Glasgow
Glasgow, G12 8QQ, Scotland; e-mail: k.johansen.1@research.gla.ac.uk

[(2)] *Faculty of Biomedical Engineering, Technion – Israel Institute of Technology*
Haifa 32000, Israel; e-mail: eitan@bm.technion.ac.il

[(3)] *Institute of Fundamental Technological Research*
Polish Academy of Sciences
Pawińskiego 5B, 02-106 Warsaw, Poland; e-mail: mpostema@ippt.pan.pl

[(4)] *School of Electrical and Information Engineering, Chamber of Mines Building*
University of the Witwatersrand
1 Jan Smuts Avenue, Braamfontein, Johannesburg 2050, South Africa

(*received June 3, 2016; accepted November 30, 2016*)

Manipulating particles in the blood pool with noninvasive methods has been of great interest in therapeutic delivery. Recently, it was demonstrated experimentally that red blood cells can be forced to translate and accumulate in an ultrasound field. This acoustic response of the red blood cells has been attributed to sonophores, gas pockets that are formed under the influence of a sound field in the inner-membrane leaflets of biological cells. In this paper, we propose a simpler model: that of the compressible membrane. We derive the spatio-temporal cell dynamics for a spherically symmetric single cell, whilst regarding the cell bilayer membrane as two monolayer Newtonian viscous liquids, separated by a thin gas void.

When applying the newly-derived equations to a red blood cell, it is observed that the void inside the bilayer expands to multiples of its original thickness, even at clinically safe acoustic pressure amplitudes. For causing permanent cell rupture during expansion, however, the acoustic pressure amplitudes needed would have to surpass the inertial cavitation threshold by a factor 10.

Given the incompressibility of the inner monolayer, the radial oscillations of a cell are governed by the same set of equations as those of a forced antibubble. Evidently, these equations must hold for liposomes under sonication, as well.

Keywords: spatio-temporal cell dynamics; Rayleigh-Plesset equation; spherical cell; red blood cell; erythrocyte; sonophore.

1. Introduction

Manipulating particles in the blood pool with noninvasive methods has been of great interest in therapeutic delivery, about which a review has been published by Delalande *et al.* (2012). Ultrasonic equipment is commonly used for noninvasive manipulation, owing to its reliability, safety, availability, and low operating cost. Following numerous nondestructive and destructive experimental studies on microbubbles under sonication near biological cells, *e.g.*, Prentice *et al.* (2005), Van Wamel *et al.* (2006), Kudo *et al.* (2009), and Delalande *et al.* (2011), it was speculated that cells themselves respond to sound by oscillating (Krasovitski *et al.*, 2011), which might lead to novel ways of noninvasive cell manipulation, filtration, and even eradication (Walther, Postema, 2016).

Recently, Mazzawi *et al.* (2015) demonstrated experimentally that red blood cells can be forced to translate and accumulate in an ultrasound field. This acoustic response of the red blood cells has been attributed to sonophores, gas pockets that are formed under the influence of a sound field in the inner-membrane leaflets of biological cells (Krasovitski

et al., 2011). Under sonication, such trapped gas pockets must oscillate in a similar way as encapsulated gas microbubbles do.

Although the existence of sonophores would explain experimentally observed phenomena, such as the attraction of oscillating microbubbles to fixated cells (Delalande *et al.*, 2011) and the occurrence of the transient formation of pores in cell membranes in the absence of microbubbles (Bao *et al.*, 1997), there might be a more straightforward explanation for the behaviour observed.

In this paper, we propose a simpler model: that of the compressible membrane. Initially, we follow the derivation for antibubble dynamics of Kotopoulis *et al.* (2015) step by step whilst replacing only few parameters, but from Subsec. 2.4 we deviate by including an outer cell membrane, following the derivation of encapsulated bubbles dynamics by Church (1995).

2. Theory

Let us consider a spherical cell, as schematically represented in Fig. 1. We regard the inner cell structure as an incompressible liquid of radius R_1. Instead of regarding the surrounding bilayer membrane as one layer, we split it up into three components (Boal, 2012): an inner monolayer Newtonian viscous liquid membrane of inner radius R_1 and outer radius R_2, an outer monolayer Newtonian viscous liquid membrane of inner radius R_3 and outer radius R_4, and a gas void separating both monolayers of inner radius R_2 and outer radius R_3. Even though actual cells are rarely spherical, we may disregard this fact, as the radial dynamics are predominantly determined by the surface pressure of the surface with the greatest curvature (Isenberg, 1992).

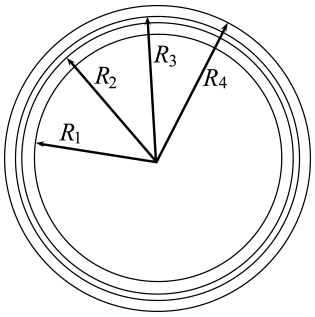

Fig. 1. Schematic representation of a spherical cell consisting of a liquid core of radius R_1, surrounded by a monolayer Newtonian viscous liquid membrane of outer radius R_2, a compressible gas void of outer radius R_3, and a monolayer Newtonian viscous liquid membrane of outer radius R_4.

Because the monolayer membranes are considered Newtonian viscous liquids, they are incompressible, as is the intracellular liquid. Consequently, the inner membrane radii do not respond to pressure changes. However, the gas void separating the inside and outside membranes must abide by the same thermodynamics that cavitation bubbles do when subjected to a sound field.

2.1. Fundamental equation of cell dynamics

Let us consider a polytropic gas void, surrounding the spherical incompressible liquid core of radius R_2 as presented in Fig. 1. For now, we ignore the outer monolayer membrane.

We are assuming adiabatic conditions. Furthermore, no mass exchange between the respective interfaces is assumed.

Following the derivation for antibubble dynamics of Kotopoulis *et al.* (2015) and introducing a driving function $P(t)$, the fundamental equation of cell dynamics becomes:

$$R_3\ddot{R}_3 + \frac{3}{2}\dot{R}_3{}^2 = \frac{1}{\rho_{\mathrm{L}}}\left[\left(p_0+\frac{2\sigma}{R_{30}}\right)\left(\frac{R_{30}^3-R_2{}^3}{R_3{}^3-R_2{}^3}\right)^{\gamma}-\frac{2\sigma}{R_3}-p_0-P(t)\right], \quad (1)$$

where p_0 is the ambient pressure, R_{30} is the initial outer radius of the gas void, γ is the polytropic exponent of the gas inside the void, ρ_{L} is the density of the liquid surrounding the cell, and σ is the surface tension.

2.2. Cell dynamics in a Newtonian viscous fluid

The viscosity η_{L} of a Newtonian viscous fluid is by definition equal to the rate of strain $\Delta\varepsilon/\Delta t$.

Again, following the derivation for antibubble dynamics of Kotopoulis *et al.* (2015) and introducing a driving function $P(t)$, the fundamental equation of cell dynamics in a Newtonian viscous fluid becomes:

$$R_3\ddot{R}_3 + \frac{3}{2}\dot{R}_3{}^2 = \frac{1}{\rho_{\mathrm{L}}}\left[\left(p_0+\frac{2\sigma}{R_{30}}\right)\left(\frac{R_{30}^3-R_2{}^3}{R_3{}^3-R_2{}^3}\right)^{\gamma} - \frac{2\sigma}{R_3}-\frac{4\eta_{\mathrm{L}}}{R_3}\dot{R}_3-p_0-P(t)\right]. \quad (2)$$

This is the Rayleigh-Plesset-like equation for a cell in a Newtonian viscous fluid, which can only be applied if the surrounding fluid is incompressible and the gas is polytropic. The equation is a second-order nonlinear ordinary differential equation.

2.3. Linear analysis for an unrestrained cell

Let us assume that (2) has a solution of the form

$$R_3(t) = R_{30}[1+\xi(t)] \quad (3)$$

for small excursions ξ of the outer surface of the void, *i.e.*, $\xi \ll R_{30}$. Then, (2) can be linearised and represented by a mass-spring-dashpot system (Postema, 2011).

The linear natural angular resonance frequency ω_0 of an unrestrained cell is given by:

$$\omega_0{}^2 = \frac{1}{{R_{30}}^2 \rho_\mathrm{L}} \left[\frac{3\gamma p_{\mathrm{g}0}}{1 - \left(\frac{R_2}{R_{30}}\right)^3} - \frac{2\sigma}{R_{30}} \right], \tag{4}$$

where $p_{\mathrm{g}0}$ is the initial gas pressure inside the void.

It can be observed that the linear damped resonance frequency of a gas void is increased by the cubic ratio of the inner cell liquid radius and the initial radius compared to that of a regular gas bubble.

If a cell is suspended in a Newtonian viscous fluid, it resonates with a linear damped natural angular resonance frequency ω_d, given by (2.2.7) in Kotopoulis *et al.* (2015):

$$\omega_\mathrm{d}{}^2 = \frac{1}{{R_{30}}^2 \rho_\mathrm{L}} \left[\frac{3\gamma p_{\mathrm{g}0}}{1 - \left(\frac{R_2}{R_{30}}\right)^3} - \frac{2\sigma}{R_{30}} - \frac{4{\eta_\mathrm{L}}^2}{{R_{30}}^2 \rho_\mathrm{L}} \right]. \tag{5}$$

It can be observed from (5) that the linear damped resonance frequency decreases when the viscosity of the surrounding fluid increases.

2.4. Presence of the outer cell membrane

Now let us take into account that the gas void is surrounded by a restraining layer. Both the liquid composing the membrane and the outer surrounding liquid are assumed to be viscous and incompressible. Assuming no mass exchange between the respective interfaces, the radial velocity $v(r,t)$ in the membrane and in the surrounding fluid at a distance r from the centre of the cell can be expressed as (Leighton, 1994):

$$v(r,t) = \frac{{R_3}^2}{r^2} \dot{R}_3, \tag{6}$$

If $R_3 < r < R_4$, $v(r,t)$ denotes the velocity inside the membrane. If $r > R_4$, $v(r,t)$ denotes the radial velocity of the surrounding liquid. From the assumption of an incompressible membrane it can be shown that

$${R_4}^3 - {R_3}^3 = {R_{40}}^3 - {R_{30}}^3 \tag{7}$$

and

$${R_3}^2 \dot{R}_3 = {R_4}^2 \dot{R}_4, \tag{8}$$

where R_{40} is the initial cell radius.

From conservation of radial momentum (Landau, Lifshitz, 1986), it follows that

$$\rho_\mathrm{M} \left(\frac{\partial v}{\partial t} + v \frac{\partial v}{\partial r} \right) = -\frac{\partial p}{\partial r} + \frac{\partial \tau_{rr}^\mathrm{M}}{\partial r} + \frac{3\tau_{rr}^\mathrm{M}}{r} \tag{9}$$

and

$$\rho_\mathrm{L} \left(\frac{\partial v}{\partial t} + v \frac{\partial v}{\partial r} \right) = -\frac{\partial p}{\partial r} + \frac{\partial \tau_{rr}^\mathrm{L}}{\partial r} + \frac{3\tau_{rr}^\mathrm{L}}{r}, \tag{10}$$

where ρ_M is the the density of the membrane, ρ_L is the density of the surrounding liquid, p is the pressure in the membrane or the liquid, τ_{rr}^M is the viscous stress tensor in the membrane, and τ_{rr}^L is the viscous stress in the liquid. Equation (9) is integrated from R_3 to R_4, and (10) is integrated from R_4 to infinity, substituting (6) for v. It is here assumed that the contribution to the radial momentum from the gas inside the void can be neglected. Combining these two integrals, the result can be expressed as

$$\begin{aligned} &\rho_\mathrm{L} R_3 \ddot{R}_3 \left[1 + \left(\frac{\rho_\mathrm{L} - \rho_\mathrm{M}}{\rho_\mathrm{M}} \right) \frac{R_3}{R_4} \right] \\ &\quad + \rho_\mathrm{L} \dot{R}_3^2 \left[\frac{3}{2} + \left(\frac{\rho_\mathrm{L} - \rho_\mathrm{M}}{\rho_\mathrm{M}} \right) \left(\frac{4{R_4}^3 - {R_3}^3}{{R_4}^3} \right) \right] \\ &= P_\mathrm{M}(R_3,t) - P_\mathrm{M}(R_4,t) + P_\mathrm{L}(R_4,r) \\ &\quad + \tau_{rr}^\mathrm{M}(R_4,t) - \tau_{rr}^\mathrm{M}(R_3,t) - \tau_{rr}^\mathrm{L}(R_4,t) \\ &\quad + 3 \int_{R_3}^{R_4} \frac{\tau_{rr}^\mathrm{M}}{r} \,\mathrm{d}r + 3 \int_{R_4}^{\infty} \frac{\tau_{rr}^\mathrm{L}}{r} \,\mathrm{d}r, \end{aligned} \tag{11}$$

where $P_\mathrm{M}(R_1,t)$ and $P_\mathrm{M}(R_2,t)$ are the pressures in the membrane at the inner and outer interfaces, respectively, $P_\mathrm{L}(R_2,t)$ is the pressure in the liquid at the outer interface, $\tau_{rr}^\mathrm{M}(R_1,t)$ and $\tau_{rr}^\mathrm{M}(R_2,t)$ are the stresses at the inner and outer interfaces, respectively, and $\tau_{rr}^\mathrm{L}(R_2,t)$ is the stress in the liquid at the outer interface (Church, 1995).

The boundary conditions from conservation of radial momentum can be stated as

$$p_\mathrm{g}(R_3,t) + \tau_{rr}^\mathrm{M}(R_3,t) = P_\mathrm{M}(R_3,t) + \frac{2\sigma_3}{R_3} \tag{12}$$

and

$$\begin{aligned} P_\mathrm{M}(R_4,t) - \tau_{rr}^\mathrm{M}(R_4,t) &= P_\mathrm{L}(R_4,t) - \tau_{rr}^\mathrm{L}(R_4,t) \\ &\quad + \frac{2\sigma_4}{R_4} + P(t), \end{aligned} \tag{13}$$

where $P_\mathrm{g}(R_1,t)$ is the instantaneous pressure inside the void, and σ_3 and σ_4 are the surface tensions at the two respective interfaces of the outer membrane. Combining (11) with the boundary conditions in (12) and (13) yields

$$\begin{aligned} &\rho_\mathrm{L} R_3 \ddot{R}_3 \left[1 + \left(\frac{\rho_\mathrm{L} - \rho_\mathrm{M}}{\rho_\mathrm{M}} \right) \frac{R_3}{R_4} \right] \\ &\quad + \rho_\mathrm{L} \dot{R}_3^2 \left[\frac{3}{2} + \left(\frac{\rho_\mathrm{L} - \rho_\mathrm{M}}{\rho_\mathrm{M}} \right) \left(\frac{4{R_4}^3 - {R_3}^3}{{R_4}^3} \right) \right] \\ &= p_\mathrm{g}(R_3,t) - \frac{2\sigma_3}{R_3} - \frac{2\sigma_4}{R_4} - p_0 - P(t) \\ &\quad + 3 \int_{R_3}^{R_4} \frac{\tau_{rr}^\mathrm{M}}{r} \,\mathrm{d}r + 3 \int_{R_4}^{\infty} \frac{\tau_{rr}^\mathrm{L}}{r} \,\mathrm{d}r, \end{aligned} \tag{14}$$

It now remains to determine the two integrals in (14). Where the first integral describes the rheological properties of the membrane, and the latter integral describes the damping from the surrounding fluid.

Assuming the void is surrounded by a Newtonian viscous liquid, the shear viscous stress can be expressed as

$$\tau_{rr}^{\mathrm{L}} = 2\eta_{\mathrm{L}} \frac{\partial v}{\partial r}, \tag{15}$$

The last integral in (14) can now be determined using (6), yielding an expression for the effect of a viscous surrounding liquid:

$$3 \int_{R_2}^{\infty} \frac{\tau_{rr}^{\mathrm{L}}}{r} \,\mathrm{d}r = -4\eta_{\mathrm{L}} \frac{{R_3}^2}{{R_4}^3} \dot{R}_3. \tag{16}$$

The general Rayleigh-Plesset-like equation for a cell with a finite membrane and surrounded by a Newtonian viscous liquid is obtained by substituting

$$p_{\mathrm{g}} = p_{\mathrm{g0}} \left(\frac{{R_{30}}^3 - {R_2}^2}{{R_3}^3 - {R_2}^3} \right)^{\gamma} \tag{17}$$

for $p_{\mathrm{g}}(R_1, t)$ and (16) for the last integral in (14):

$$\begin{aligned} &\rho_{\mathrm{L}} R_3 \ddot{R}_3 \left[1 + \left(\frac{\rho_{\mathrm{L}} - \rho_{\mathrm{M}}}{\rho_{\mathrm{M}}} \right) \frac{R_3}{R_4} \right] \\ &\quad + \rho_{\mathrm{L}} \dot{R}_3^2 \left[\frac{3}{2} + \left(\frac{\rho_{\mathrm{L}} - \rho_{\mathrm{M}}}{\rho_{\mathrm{M}}} \right) \left(\frac{4{R_4}^3 - {R_3}^3}{{R_4}^3} \right) \right] \\ &= p_{\mathrm{g0}} \left(\frac{{R_{30}}^3 - {R_2}^2}{{R_3}^3 - {R_2}^3} \right)^{\gamma} - \frac{2\sigma_3}{R_3} - \frac{2\sigma_4}{R_4} - p_0 - P(t) \\ &\quad - 4\eta_{\mathrm{L}} \frac{{R_3}^2}{{R_4}^3} \dot{R}_3 + 3 \int_{R_3}^{R_4} \frac{\tau_{rr}^{\mathrm{M}}}{r} \,\mathrm{d}r. \end{aligned} \tag{18}$$

2.5. Newtonian viscous liquid outer cell membrane

Now let us assume that the outer monolayer membrane of a cell can be regarded as a Newtonian viscous liquid, where the viscous stress in the membrane τ_{rr}^{M} is related to the membrane viscosity η_{M} by (Doinikov, Dayton, 2007):

$$\tau_{rr}^{\mathrm{M}} = 2\eta_{\mathrm{M}} \frac{\partial v}{\partial r}. \tag{19}$$

The remaining integral in (18) describes the shear viscosity in the Newtonian liquid membrane, which dampens the radial response from the void as it is excited by an acoustic pulse. Substituting (19) and using both (7) and (8), the integral can be written in terms of radial displacement:

$$3 \int_{R_3}^{R_4} \frac{\tau_{rr}^{\mathrm{M}}}{r} \,\mathrm{d}r = -4\eta_{\mathrm{M}} \frac{{R_4}^3 - {R_3}^3}{R_3 {R_4}^3} \dot{R}_3. \tag{20}$$

Substituting (20) into (18) gives a Rayleigh-Plesset-like equation for a cell with a Newtonian membrane of finite thickness surrounded by a Newtonian viscous liquid:

$$\begin{aligned} &\rho_{\mathrm{L}} R_3 \ddot{R}_3 \left[1 + \left(\frac{\rho_{\mathrm{L}} - \rho_{\mathrm{M}}}{\rho_{\mathrm{M}}} \right) \frac{R_3}{R_4} \right] \\ &\quad + \rho_{\mathrm{L}} \dot{R}_3^2 \left[\frac{3}{2} + \left(\frac{\rho_{\mathrm{L}} - \rho_{\mathrm{M}}}{\rho_{\mathrm{M}}} \right) \left(\frac{4{R_4}^3 - {R_3}^3}{{R_4}^3} \right) \right] \\ &= p_{\mathrm{g0}} \left(\frac{{R_{30}}^3 - {R_2}^2}{{R_3}^3 - {R_2}^3} \right)^{\gamma} - \frac{2\sigma_3}{R_3} - \frac{2\sigma_4}{R_4} - p_0 - P(t) \\ &\quad - 4\eta_{\mathrm{L}} \frac{{R_3}^2}{{R_4}^3} \dot{R}_3 - 4\eta_{\mathrm{M}} \frac{{R_4}^3 - {R_3}^3}{R_3 {R_4}^3} \dot{R}_3. \end{aligned} \tag{21}$$

3. Solution

To simulate a spherically oscillating cell, parameters measured on living blood cells were used. Bilayer cell membranes are 20 nm in thickness, whereas the void separating the individual monolayers is only 2 nm in thickness (Boal, 2012). The shear viscosity of red blood cell membranes is in the order of 10^3 Pa·s (Tran-Son-Tay *et al.*, 1984). The sizes of cells greatly vary. Red blood cells have in axial view an outer radius of 3 µm.

Equation (21) was solved numerically using the ode45 algorithm of Matlab® (The MathWorks, Inc., Natick, MA, USA). The parameters chosen were: $\rho_{\mathrm{M}} \approx \rho_{\mathrm{L}} = 10^3\ \mathrm{kg \cdot m^{-3}}$, $R_{40} = 3$ µm, $(R_{40} - R_{30}) = 9$ nm, $(R_{30} - R_2) = 2$ nm, $\rho_{\mathrm{g0}} = 1\ \mathrm{kg \cdot m^{-3}}$, $\gamma = 1.4$, $\sigma_3 = \sigma_4 = 0.025\ \mathrm{N \cdot m^{-1}}$, $p_0 = 10^5$ Pa, $\eta_{\mathrm{L}} = 10^{-3}$ Pa·s, and $\eta_{\mathrm{M}} = 10^3$ Pa·s.

The driving pulse consisted of a 10-cycles sinusoid wave, with a centre frequency of 1 MHz or 3 MHz. The number of cycles chosen is typical for the upper pulse duration in commercial ultrasound equipment, whereas the centre frequencies are typical for those used in clinical cardiac and gastroenterologic ultrasonic imaging. Acoustic amplitudes ranged from 300 kPa to 20 MPa. The low acoustic pressures were chosen to simulate clinically safe ultrasound, the higher pressures to investigate under what conditions ultrasound-induced cell damage should be permanent.

4. Results and discussion

Figures 2–4 show expansion-time curves of red blood cells under sonication. In all these figures, it can be observed, that all oscillations of the void are highly asymmetric, *i.e.*, greater expansive excursions than contractive excursions. This is a direct result of the incompressibility of the cellular content and of the nonlinearity of (21). It may be interesting to mention, that if the density of the outer membrane were different from the density of the surrounding fluid, more asymmetry should have occurred: According to (18),

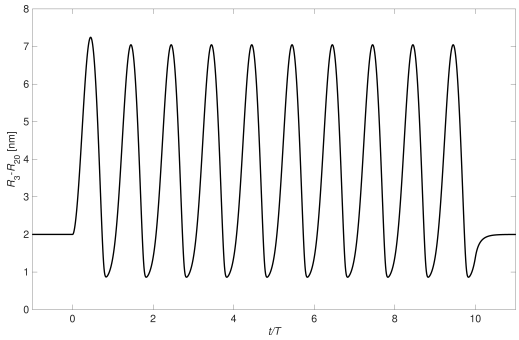

Fig. 2. Expansion-time curve of a red blood cell under 1-MHz sonication. The acoustic amplitude is 300 kPa. Time t has been normalised by period T.

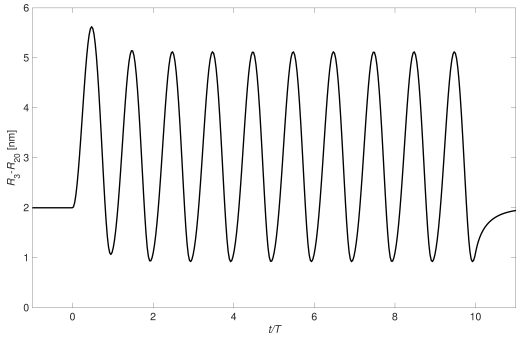

Fig. 3. Expansion-time curve of a red blood cell under 3-MHz sonication. The acoustic amplitude is 500 kPa. Time t has been normalised by period T.

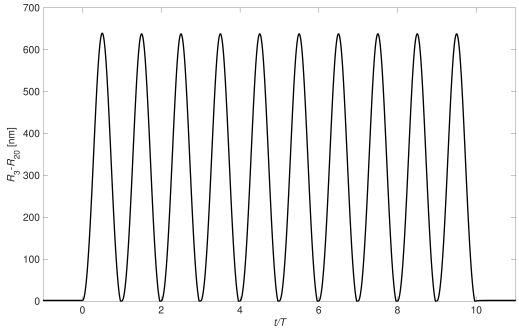

Fig. 4. Expansion-time curve of a red blood cell under 1-MHz sonication. The acoustic amplitude is 20 MPa. Time t has been normalised by period T.

it follows from the first term on the left-hand side that the acceleration increases if $\rho_{\mathrm{L}} > \rho_{\mathrm{M}}$, and the acceleration decreases if $\rho_{\mathrm{L}} < \rho_{\mathrm{M}}$. The ratios of the densities effects the second term on the left-hand side in a similar way, decreasing and increasing the degree of nonlinearity. The first term on the right-hand side is a different form of a Rayleigh-Plesset-like equation, describing the radial pulsation of a gas bubble. The pressure inside a cell is larger than in a gas bubble under the same conditions.

Figures 2 and 3 both demonstrate a maximum void expansion of more than 5 nm, *i.e.*, more than 2.5× the initial void thickness, despite the high viscosity ($\eta_{\mathrm{M}} = 10^3$ Pa·s) of the outer monolayer membrane. The acoustic amplitudes in both computations were chosen to correspond to a mechanical index of 0.3 (Apfel, Holland, 1991): At a transmit frequency of 1 MHz, acoustic amplitudes of pulsed ultrasound below 300 kPa are considered safe in neonatal scans, whereas at a transmit frequency of 3 MHz, acoustic amplitudes of pulsed ultrasound below 500 kPa are considered safe in neonatal scans (Postema, 2011).

Hence, even at low acoustics amplitudes, the void inside the bilayer membrane oscillates to multiple times its initial thickness. These excursions are not enough to permanently damage a red blood cell.

Recently, Li *et al.* (2013) measured that red blood cells need to be stretched to an area corresponding to 20% increase of their resting radius. Figure 4 shows that such excursions can be achieved during sonication at 1 MHz with an acoustic pressure amplitude of 20 MPa. This pressure amplitude corresponds to 10× the threshold of inertial cavitation (Apfel, Holland, 1991). Hence, permanent cell damage caused by the oscillating bilayer void can be neglected in clinical situations. However, diffusive processes into the void have not been accounted for in our model. Such processes might inflate the void over multiple cycles.

The purpose of this paper was to propose a model with less unknown parameters than the sonophore. Introducing compressible membranes, bulk viscosity and thermal conductivity would, albeit representing a more realistic situation, complicate the model with unknown material properties. However, real excursion amplitudes should be even lower due to these additional damping terms.

It can be noted that, given the incompressibility of the inner monolayer, the radial oscillations of a cell are governed by the same set of equations as those of a forced antibubble (Kotopoulis *et al.*, 2015).

5. Conclusions

We derived the spatio-temporal cell dynamics for a spherically symmetric single cell, whilst regarding the cell bilayer membrane as two monolayer Newtonian viscous liquids, separated by a thin gas void.

Given the incompressibility of the inner monolayer, the radial oscillations of a cell are governed by the same set of equations as those of a forced antibubble. Evidently, these equations must hold for liposomes under sonication, as well.

References

1. Apfel R.E., Holland C.K. (1991), *Gauging the likelihood of cavitation from short-pulse, low-duty cycle diagnostic ultrasound*, Ultrasound in Medicine & Biology, **17**, 2, 179–185.
2. Bao S., Thrall B.D., Miller D.L. (1997), *Transfection of a reporter plasmid into cultured cells by sonoporation in vitro*, Ultrasound in Medicine & Biology, **23**, 6, 953–959.
3. Boal D. (2012), *Mechanics of the Cell*, University Press, Cambridge.
4. Church C.C. (1995), *The effects of an elastic solid surface layer on the radial pulsations of gas bubbles*, Journal of the Acoustical Society of America, **97**, 3, 1510–1521.
5. Delalande A., Kotopoulis S., Rovers T., Pichon C., Postema M. (2011), *Sonoporation at a low mechanical index*, Bubble Science, Engineering and Technology, **3**, 1, 3–11.
6. Delalande A., Postema M., Mignet N., Midoux P., Pichon C. (2012), *Ultrasound and microbubble-assisted gene delivery: recent advances and ongoing challenges*, Therapeutic Delivery, **3**, 10, 1199–1215.
7. Doinikov A.A., Dayton P.A. (2007), *Maxwell rheological model for lipid-shelled ultrasound microbubble contrast agents*, Journal of the Acoustical Society of America, **121**, 6, 3331–3340.
8. Isenberg C. (1992), *The science of soap films and soap bubbles*, Dover edition, General Publishing Company, Don Mills.
9. Kotopoulis S., Johansen K., Gilja O.H., Poortinga A.T., Postema M. (2015), *Acoustically active antibubbles*, Acta Physica Polonica A, **127**, 1, 99–102.
10. Krasovitski B., Frenkel V. Shoham S., Kimmel E. (2011), *Intramembrane cavitation as a unifying mechanism for ultrasound-induced bioeffects*, Proceedings of the National Academy of Sciences, **108**, 8, 3258–3263.
11. Kudo N., Okada K., Yamamoto K. (2009), *Sonoporation by single-shot pulsed ultrasound with microbubbles adjacent to cells*, Biophysical Journal, **96**, 12, 4866–4876.
12. Landau L., Lifshitz E. (1986), *Theory of Elasticity*, Butterworth-Heinemann, Oxford.
13. Leighton T.G. (1994), *The Acoustic Bubble*, Academic Press, London.
14. Li F., Chan C.U., Ohl C.D. (2013), *Yield strength of human erythrocyte membranes to impulsive stretching*, Biophysical Journal, **105**, 4, 872–879.
15. Mazzawi N., Postema M., Kimmel E. (2015), *Bubble-like response of living blood cells and microparticles in an ultrasound field*, Acta Physica Polonica A, **127**, 1, 103–105.
16. Postema M. (2011), *Fundamentals of Medical Ultrasonics*, Spon Press, London.
17. Prentice P., Cuschieri A., Dholakia K., Praus-nitz M., Campbell P. (2005), *Membrane disruption by optically controlled microbubble cavitation*, Nature Physics, **1**, 107–110.
18. Tran-Son-Tay R., Sutera S.P., Rao P.R. (1984), *Determination of red blood cell membrane viscosity from rheoscopic observations of tank-treading motion*, Biophysical Journal, **46**, 1, 65–72.
19. van Wamel A., Kooiman K., Harteveld M., Emmer M., ten Cate F.J., Versluis M., de Jong N. (2006), *Vibrating microbubbles poking individual cells: drug transfer into cells via sonoporation*, Journal of Controlled Release, **112**, 2, 149–155.
20. Walther T., Postema M. (2016), *Device for the identification, separation and/or cell type-specific manipulation of at least one cell of a cellular system*, United States Patent Application US 2016/0060615 A1.

II.3 Sonoporation

La sonoporation est définie comme la perméabilité temporaire d'une membrane cellulaire soumise à une onde ultrasonore. Pour la délivrance des agents thérapeutiques, les mécanismes de la sonoporation ont été étudiés.

L'article « Sonoporation at a low mechanical index » présente des expériences in vitro, faisant preuve de l'entrée des microbulles dans les cellules cancéreuses, assistées par des ultrasons à basses pressions (p. 97). [7]

Les microbulles d'un agent de contraste ultrasonore ont été observées entrer dans les cellules HeLa pendant la sonification a la fréquence de 6,6 MHz et à basses pressions.

Les microbulles avaient des coques fluorescentes. Après l'entrée dans les cellules, le gaz des microbulles s'est dissout dans le liquide cellulaire, s'échappant de la coque.

Ces résultats prouvent que l'agent de contraste ultrasonore peut être utilisé pour la délivrance ciblée dans les cellules de substances couplées à la coque des microbulles.

En associant l'agent de contraste ultrasonore aux agents thérapeutiques, l'absorption des médicaments peut être augmentée aussi dans les cellules insonifiées.

Un régime acoustique similaire, combiné avec un agent chimiothérapeutique, a été utilisé pour le traitement du cancer de pancreas. Les premiers résultats du traitement avec cette nouvelle méthode ont été publiés dans « Treatment of human pancreatic cancer using combined ultrasound, microbubbles, and gemcitabine : a clinical case study » (p. 107). [8]

Cinq patients ont été injectés avec gemcitabine et un agent de contraste ultrasonore, SonoVue™. Un champ ultrasonore de faible pression a été utilisé pour la sonoporation. Les résultats ont montré que la croissance tumorale a été réduite chez tous les patients et a été inversée chez deux patients.

Par rapport à l'utilisation de la chimiothérapie seule, cette approche a prouvé de prolonger la vie et la qualité de la vie des patients avec ce type de tumeur.

7. Delalande A, Kotopoulis S, Rovers T, Pichon C, Postema M. Sonoporation at a low mechanical index. Bubble Science, Engineering and Technology 2011 ; 3(1) : 3–11.

8. Kotopoulis S, Dimcevski G, Gilja OH, Hoem D, Postema M. Treatment of human pancreatic cancer using combined ultrasound, microbubbles, and gemcitabine : a clinical case study. Medical Physics 2013 ; 40(7) : 072902(1–9).

Sonoporation at a low mechanical index

A. Delalande[1], S. Kotopoulis[2], T. Rovers[3], C. Pichon[1] and M. Postema*[1,2,3,4]

The purpose of this study was to investigate the physical mechanisms of sonoporation, in order to understand and improve ultrasound-assisted drug and gene delivery. Sonoporation is the transient permeabilisation and resealing of a cell membrane with the help of ultrasound and/or an ultrasound contrast agent, allowing for the trans-membrane delivery and cellular uptake of macromolecules between 10 kDa and 3 MDa. The authors studied the behaviour of ultrasound contrast agent microbubbles near cancer cells at low acoustic amplitudes. After administering an ultrasound contrast agent, HeLa cells were subjected to 6·6 MHz ultrasound with a mechanical index of 0·2 and observed with a high-speed camera. Microbubbles were seen to enter cells and rapidly dissolve. The quick dissolution after entering suggests that the microbubbles lose (part of) their shell while entering. The authors have demonstrated that lipid-shelled microbubbles can be forced to enter cells at a low mechanical index. Hence, if a therapeutic agent is added to the shell of the bubble or inside the bubble, ultrasound-guided delivery could be facilitated at diagnostic settings. In addition, these results may have implications for the safety regulations on the use of ultrasound contrast agents for diagnostic imaging.

Keywords: Sonoporation, Low mechanical index, Microbubbles, Ultrasound contrast agent, HeLa cells, Cell penetration

Introduction

Sonoporation is the transient permeabilisation and resealing of a cell membrane with the help of ultrasound and/or an ultrasound contrast agent, allowing for the trans-membrane delivery and cellular uptake of macromolecules between 10 kDa and 3 MDa.[1] Many studies have demonstrated increased drug and gene uptake of sites under sonication.[2–9] These studies presumed that a physical membrane disruption mechanism, i.e. sonoporation, caused the increased uptake, as opposed to naturally occurring active uptake processes, such as endocytosis, which are controlled by the system biology.[2–9] Although mechanical disruption with the aid of ultrasound has been attributed to violent side effects of inertial cavitation and microbubble fragmentation, most notably, the increased uptake has also been observed at low acoustic amplitudes, i.e. in acoustic regimes where inertial cavitation and microbubble fragmentation are not to be expected. An ultrasound contrast agent microbubble might act as a vehicle to carry a drug or gene load to a perfused region of interest. If the same ultrasound field that has been implicated in the sonoporation process can cause release of the therapeutic load, this load could be delivered into cells. Apart from plainly mixing ultrasound contrast agents with therapeutic agents, several schemes have been proposed to incorporate therapeutic loads to microbubbles. These include loads to the microbubble shell,[10] therapeutic gases inside the microbubble,[11] gas-filled lipospheres containing drugs,[12] and drug-filled antibubbles.[13] To understand and ameliorate ultrasound-assisted drug and gene delivery, the physics of controlled release

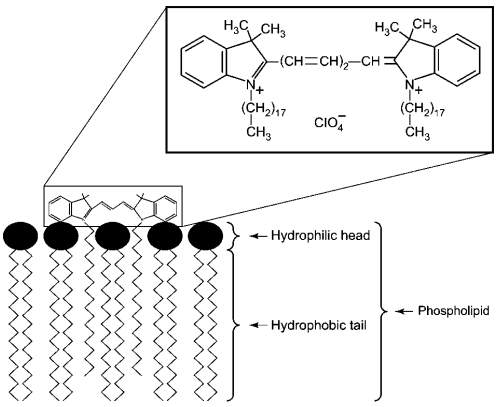

1 Schematic representation of DiD [DiIC$_{18}$(5)] lipophilic fluorescent probe bonding to phospholipid[32]

[1]Centre de Biophysique Moléculaire, UPR 4301 CNRS affiliated to the University of Orléans, rue Charles Sadron, 45071 Orléans Cedex 2, France
[2]Department of Engineering, The University of Hull, Cottingham Road, Kingston upon Hull HU6 7RX, UK
[3]Emmy Noether Research Group, Institute of Medical Engineering, Department of Electrical Engineering and Information Sciences, Ruhr-Universität Bochum, ID 04/24, 44780 Bochum, Germany
[4]Department of Physics and Technology, University of Bergen, Allégaten 55, 5007 Bergen, Norway

*Corresponding author, email michiel.postema@ift.uib.no

Received 13 December 2010; accepted 17 February 2011
DOI 10.1179/1758897911Y.0000000001

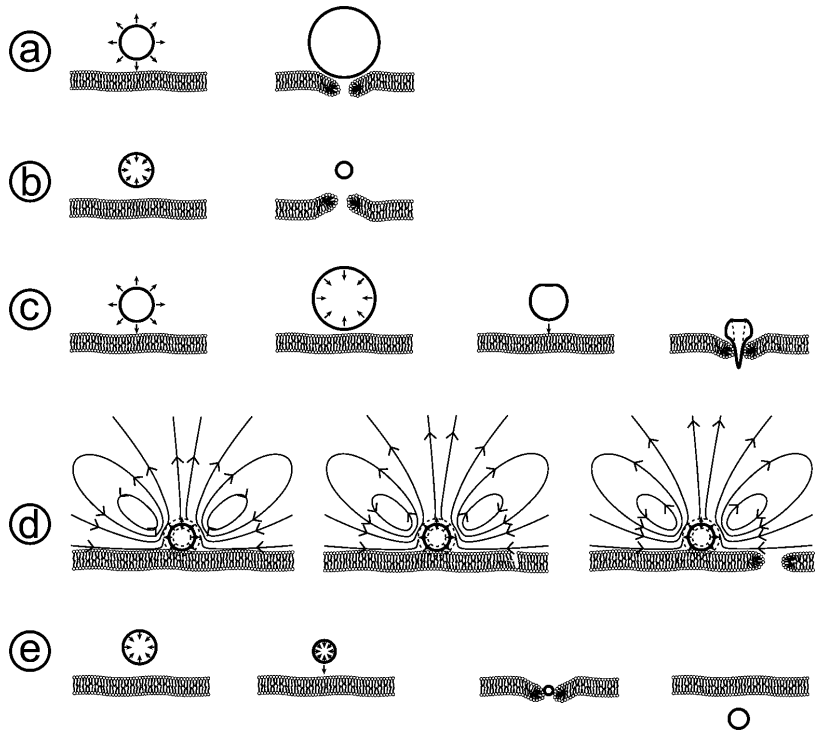

a push; *b* pull; *c* jetting; *d* shear; *e* translation

2 Possible mechanisms of sonoporation based on Fig. 9.2 in Postema *et al.*[24]

and of sonoporation have been under investigation. That objective also forms the focus for this paper. Moreover, the authors studied the behaviour of ultrasound contrast agent microbubbles near cancer cells deliberately at low acoustic amplitudes in order to probe whether sonoporation in this regime was possible; and if so, to ascertain what the microscopic mechanism might entail; and finally, to assess and scrutinise the safety aspects of ultrasound exposure in this regime.

Mechanical index

The mechanical index (MI) gives an indication of mechanical damage of tissue due to inertial cavitation. It is defined by

$$\mathrm{MI} = \frac{p^-}{\sqrt{f_c}} \tag{1}$$

where p^- is the maximum value of peak negative pressure anywhere in the ultrasound field, measured in water but reduced by an attenuation factor equal to that which would be produced by a medium having an attenuation coefficient of 0·3 dB cm^{-1} MHz^{-1}, normalised by 1 MPa, and f_c is the centre frequency of the ultrasound normalised by 1 MHz. For MI<0·3, the acoustic amplitude is considered low. For 0·3>MI<0·7, there is a possibility of minor damage to neonatal lung or intestine.[14] These are considered moderate acoustic amplitudes. For MI>0·7, there is a risk of cavitation if an ultrasound contrast agent containing gas microspheres is being used, and there is a theoretical risk of cavitation without the presence of ultrasound contrast agents.[15] The risk increases with MI values above this threshold. These are considered high acoustic amplitudes. On commercial scanners, the MI has been limited to 1·9 for medical imaging.[16] At low MI, microbubbles pulsate linearly, whereas at high MI, their greater expansion phase is followed by a violent collapse. During the collapse phase, when the kinetic energy of the bubble surpasses its surface energy, a bubble may fragment into a number of smaller bubbles. Fragmentation has been exclusively observed with contrast agents with thin, elastic shells. Fragmentation is the dominant disruption mechanism for these bubbles.[17] Although the fragmentation of therapeutic load-bearing microbubbles must release their loads, the actual drug or gene delivery is in this case a passive process, dependent on diffusion rate and proximity to the target cells. Fragmenting microbubbles may not create pores in cells, since fragmentation costs energy. However, if a microbubble collapses near a free or a solid boundary, the retardation of the liquid near the boundary may cause an asymmetry. This asymmetry causes differences in acceleration on the bubble surface. During further collapse, a funnel-shaped jet may protrude through the microbubble, shooting liquid to the boundary.[18] The pore size created by a jet has been empirically related to the microbubble expansion.[19] If jets could be directed to cell layers, in the case of a microbubble carrying a therapeutic load, the load could be delivered into cells. The jet formation is affected by the cavitation topology, synergistically interacting with local fluid

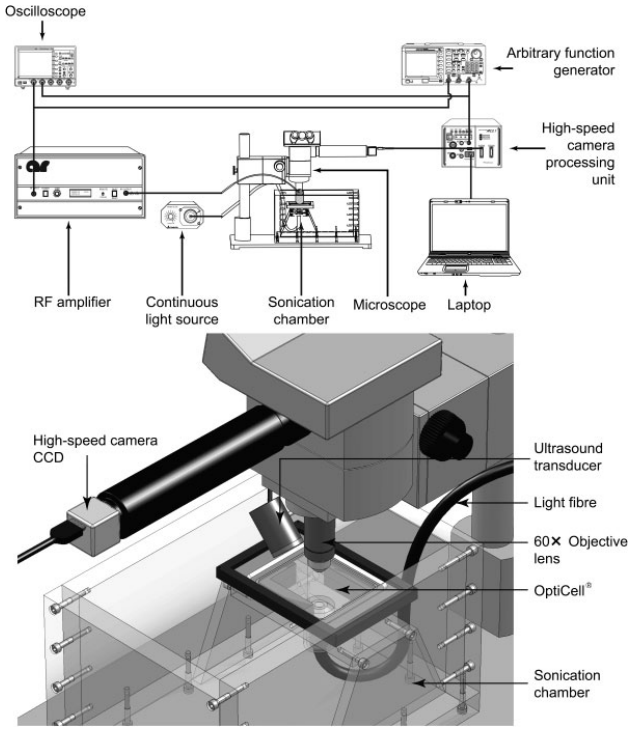

3 Experimental set-up (top) and close-up of the sonoporation configuration (bottom)

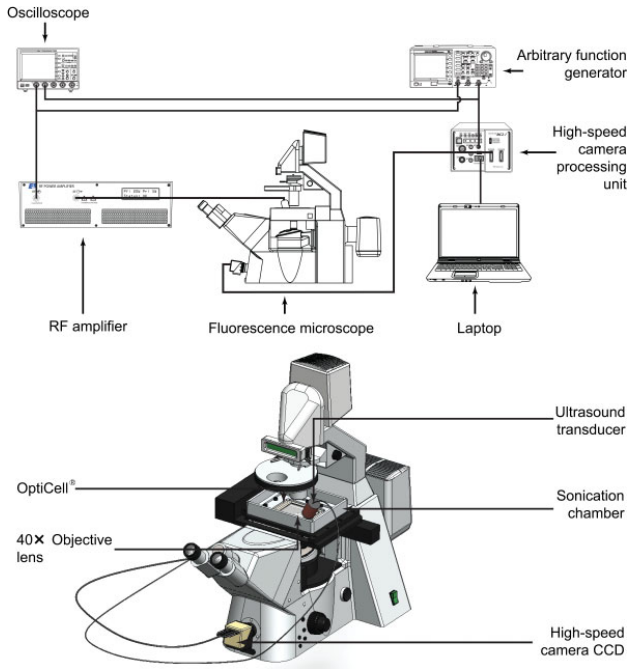

4 Experimental set-up (top) and a close-up of fluorescence configuration (bottom)

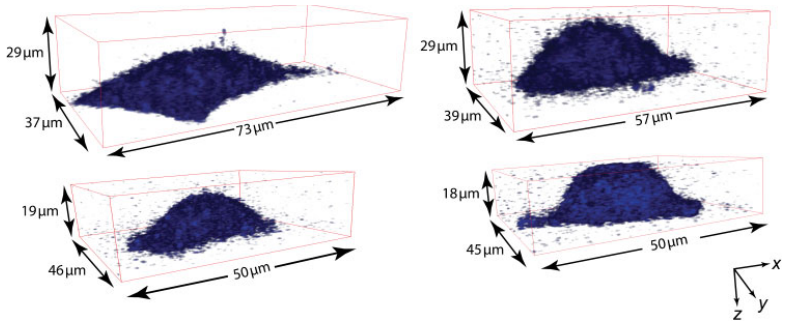

5 *z*-stacks of fluorescence emitted by DiD dye attached to membranes of four typical HeLa cells representing the cell geometry

dynamics arising through the bubble's expansion and contraction due to the ultrasound field. However, as the fluid forming the microjet is just the bulk fluid which carries no therapeutic agent, then there is no guarantee that even with the formation of a sonopore due to jet impact with the cell membrane, therapeutic agent will enter the cell. It needs to be dislodged and mobilised from the bubble first. Furthermore, jetting has not been observed at a low or moderate MI,[20] so that fragmentation is likely to occur before any delivery takes place. By pushing the loaded microbubbles towards the vessel wall using primary radiation forces,[21] release can take place closer to target vessels. In a recent study, Caskey *et al.*[22] pushed bubbles into tissue-mimicking gels at MI=1·5. The authors previously studied how microclusters consisting of lipid-encapsulated microbubbles can be formed using primary and secondary radiation forces, and how these clusters can be pushed towards vessel walls.[23] It was found that even at MI<0·15, microbubble clusters can be formed and pushed within seconds.

Sonoporation

There are five non-exclusive hypotheses for explaining the sonoporation phenomenon. These have been summarised in Fig. 2: push, pull, jetting, shear and translation.[24] It has been hypothesised that expanding microbubbles might push the cell membrane inward, and that collapsing bubbles might pull cell membranes outward.[25] These mechanisms require microbubbles to be present in the close vicinity of cells. A separate release mechanism should then ensure localised delivery. Although jetting only occurs in a high-MI regime, it is very effective in puncturing cell membranes. Jetting has been observed through cells using ultrasound contrast agent microbubbles. However, the acoustic impedance of the solid cell substratum formed the boundary to which the jetting took place, not the cell itself.[26] Also, there has not been any proof yet of cell survival after jetting. In a separate study, the authors excluded the role of jetting as a dominant mechanism in sonoporation.[27] If a microbubble is fixed to a membrane, the fluid streaming around the oscillating bubbles creates enough shear to rupture the membrane.[28] Here again, separate release mechanism should then ensure localised delivery. Finally, it has been speculated that lipid-encapsulated microbubbles, in compressed phase, translate through cell membranes or channels in the cell membrane. In the case of therapeutic loading, the load would be delivered directly into the target cell. The main advantage of the latter mechanism is that microbubble translation by means of ultrasonic radiation forces requires very low acoustic pressures. Hence, potentially damaging bioeffects due to inertial cavitation can be ruled out.

Materials and methods

Sonoporation configuration

In previous studies, increased gene uptake was demonstrated at MI<0·3.[29,30] The authors used a similar sonoporation configuration for the experiments. An overview of the experimental set-up is shown in Fig. 3. A signal consisting of 50 cycles with a centre frequency of 6·6 MHz and a pulse repetition frequency of 10 kHz, i.e. a duty cycle of 7·5%, was generated by an AFG 3102, dual channel arbitrary function generator (Tektronix, Inc., Beaverton, OR, USA), amplified by a 150A250 radio-frequency (RF) amplifier (Amplifier Research, Souderton, PA, USA) set to maximum gain, and fed to a custom built 6·6 MHz ultrasound transducer with a hexagonal lithium niobate *y*–36° cut

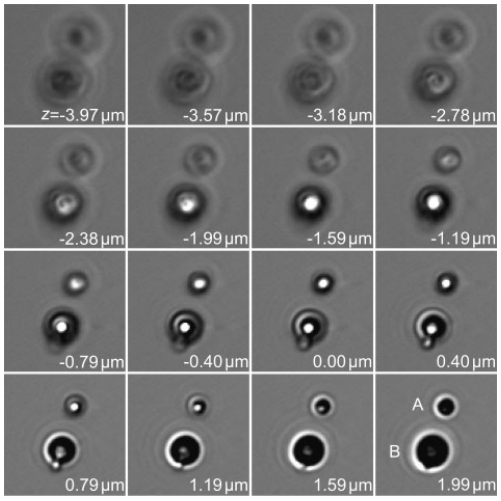

6 *z*-stack of two ultrasound contrast agent microbubbles: Proximal-to-focus Airy discs can be seen around bubbles, whereas distal-to-focus the bubble boundaries are blurred; microbubble A has a diameter of 2 μm, whereas microbubble B has a diameter of 3 μm; each frame corresponds to 11 × 11 (μm)^2 area

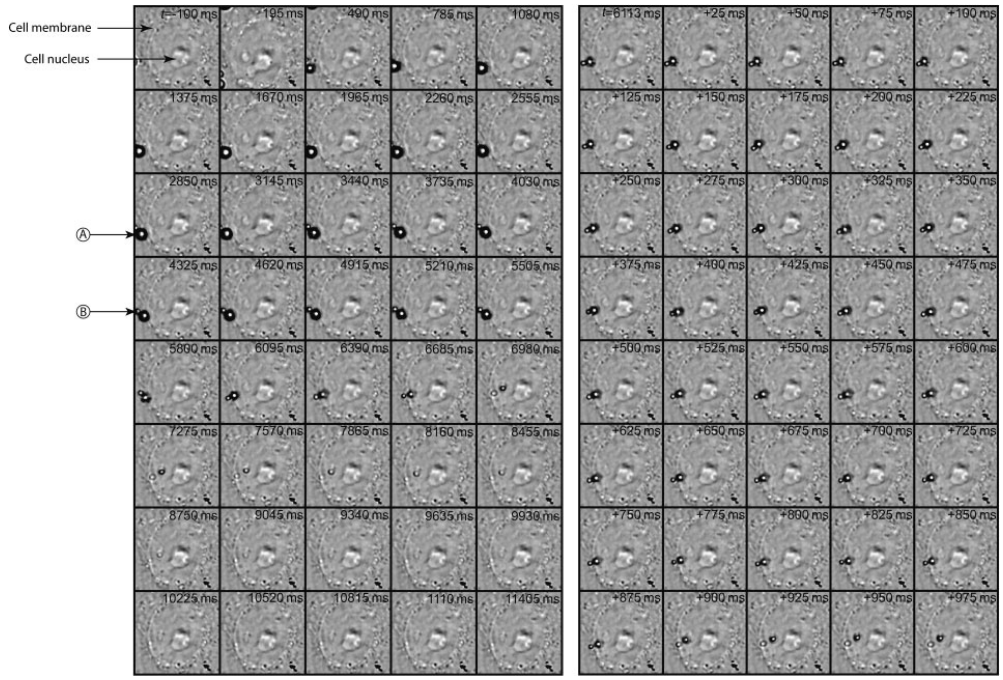

7 Sonoporation event including microbubble dissolution during 11 s of sonication (left) and selected frames of microbubble entering a cell (right): microbubble 'A' entered the cell and dissolved, whereas microbubble 'B' stuck to cell membrane; each frame corresponds to 23 × 23 (μm)^2 area

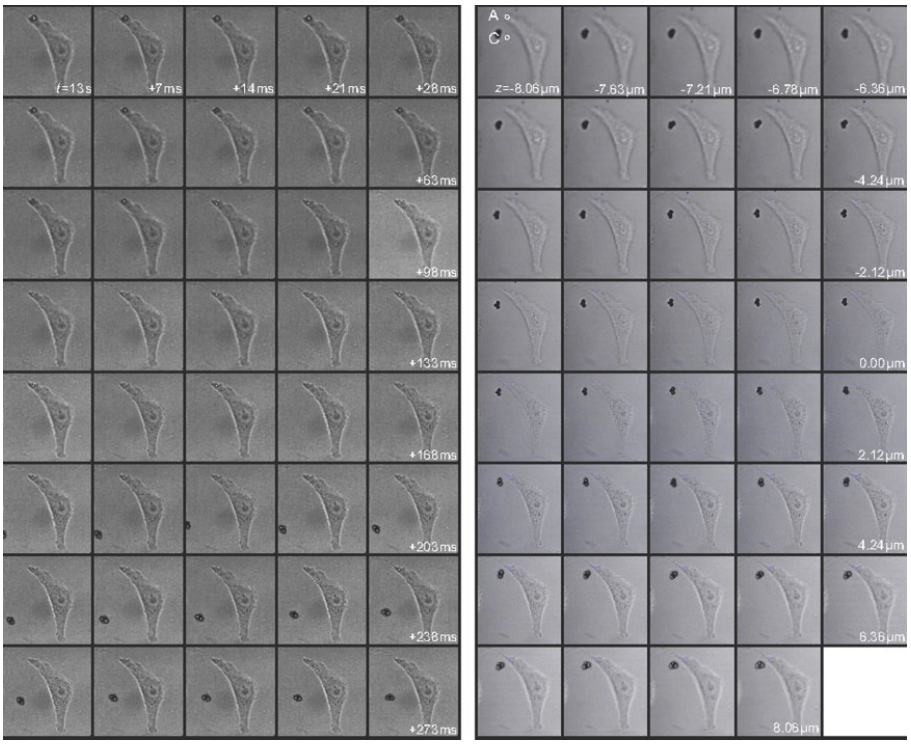

8 Microbubble of 5 μm diameter apparently penetrating through the cell membrane in optical focus (left); *z*-stack through entire cell to record whether the apparent microbubble entry is actually into the cell (right): areas A and C are regions of interest inside and outside the cell, respectively; each frame corresponds to 76 × 76 (μm)^2 area

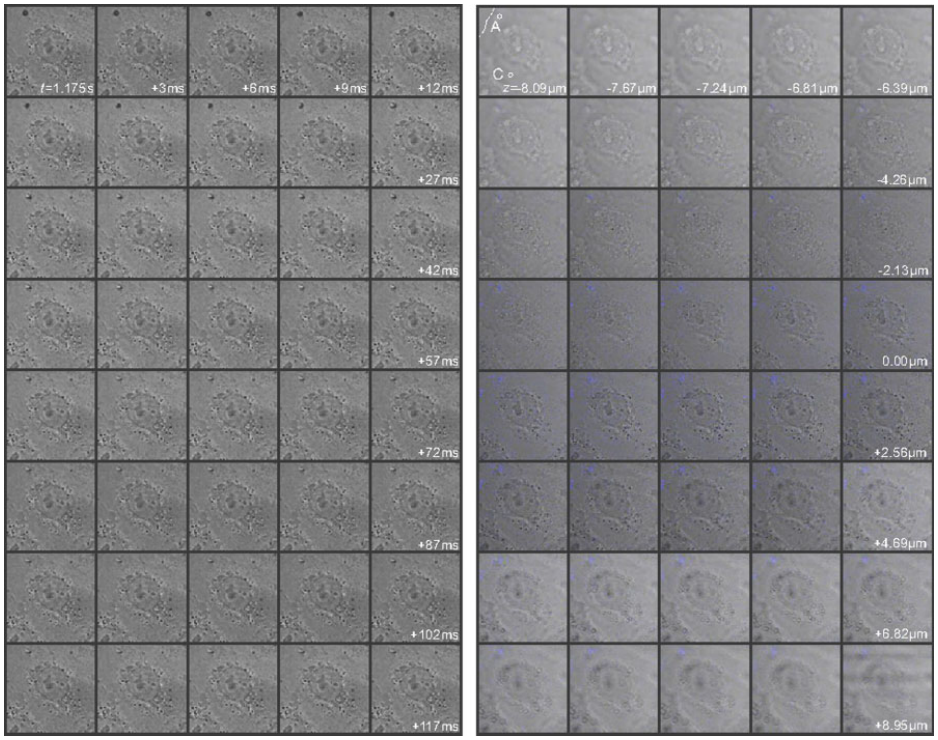

9 Microbubble of 4 µm diameter apparently penetrating through the cell membrane in optical focus (left); *z*-stack through entire cell to record whether the apparent microbubble entry is actually into the cell (right): areas A and C are regions of interest of high and low fluorescence respectively inside cell; white dotted lines in the upper left frame of the right panel indicates cell membrane; each frame corresponds to 52×52 $(\mu m)^2$ area

active element with a maximum width of 25 mm.[31] The peak-negative acoustic pressure was measured to be 0·5 MPa in a separate tank and in the sonication chamber itself. This corresponds to an MI of 0·2. The transducer was placed in a custom-built, $260 \times 160 \times 150$ $(mm)^3$ Perspex sonication chamber, in which an OptiCell® cell culture chamber (Nunc GmbH & Co. KG, Langenselbold, Germany) was placed. One side of the cell culture chamber contained a monolayer of $1{\cdot}6 \times 10^6$ HeLa cells that had been cultured in MEM with Earl's salts medium (PAA Laboratories GmbH, Pasching, Austria) supplemented with 10% *v*/*v* heat-inactivated fetal calf serum, GlutaMAX™ (Life Technologies Gibco, Paisley, Renfrewshire, UK), 1% *v*/*v* of non-essential aminoacids (PAA), penicillin (100 units mL^{-1}) and streptomycin (100 µg mL^{-1}) (PAA), at 37°C in a humidified atmosphere containing 5% CO_2. The cells were used when there was 60–80% confluency. Ultrasound contrast agent was injected into the cell culturing chamber before each experiment. Several lipid-shelled ultrasound contrast agents were tested in this study. In this paper, the authors present results of a 3·33% dilution of MicroMarker™ (VisualSonics B.V., Amsterdam, The Netherlands), a lipid-shelled agent with a mean diameter of 2·5 µm. A customised BXFM-F microscope unit with an LCAch N $20 \times$/0·40 PhC (Olympus Deutschland GmbH, Hamburg, Germany) and a LUMPlanFL $60 \times$/0·90 water-immersion objective (Olympus) was placed on top of the sonication chamber. The colour charge coupled device (CCD) of a Photron FastCam MC-2·1 high-speed camera (VKT Video Kommunikation GmbH, Pfullingen, Germany) was connected to the microscope. The sensor was rotated to make sure that in all recorded movies, the ultrasound is directed from the left to the right of the frame.

Fluorescence configuration

An overview of the set-up used for the fluorescence experiments is shown in Fig. 4. It is almost identical to the set-up described in the previous section. However, here, the signal consisting of 40 cycles with a centre frequency of 6·6 MHz and a pulse repetition frequency of 10 kHz, i.e. a duty cycle of 6·1%, was amplified using a 2100 L, +50 dB RF amplifier (Electronics & Innovation, Rochester, NY, USA) and fed to the custom-built 6·6 MHz ultrasound transducer.[31] Before injection in the OptiCell®, the MicroMarker® contrast agent was labelled using a DiD [$DilC_{18}(5)$] lipophilic fluorescent probe (Vybrant™ Molecular Probes, Invitrogen, San Diego, CA, USA). A ratio of 1 µl of DiD to 40 µl MicroMarker® was homogenised by pipetting and incubating for 5 min at room temperature. Figure 1 shows how the DiD fluorescent probe bonded to the phospholipid.[32] Emitted λ=649–703 nm fluorescence was localised on the microbubble shell when exciting at λ=633 nm. A custom-made aluminium sonication chamber with internal dimensions of $130 \times 170 \times 35$ $(mm)^3$ was locked into to the *xy* stage

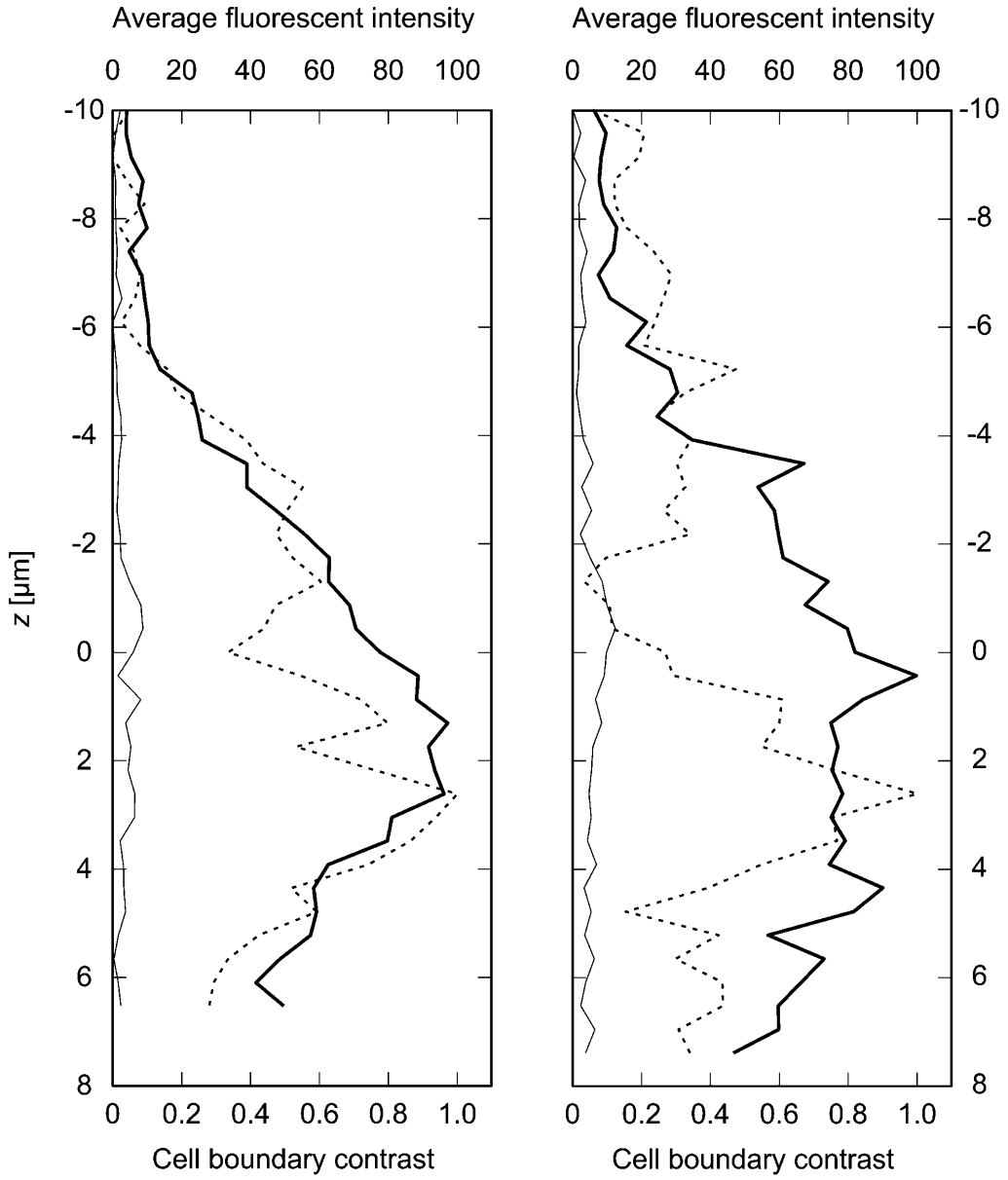

10 Average fluorescent intensities in the regions of interest (ROI) of Figs. 8 (left) and 9 (right): bold lines represent ROI (A) inside cells, whereas hairlines represent ROI (C) control regions; dotted line represents the cell boundary contrast; note that the cell boundary contrast is maximal just proximal-to-focus

of a 200 M inverted confocal microscope (Carl Zeiss AG, Oberkochen, Germany) coupled with a LSM Axiovert 510 scanning device (Carl Zeiss AG), using an EC Plan-Neofluar 40 × /1·30 Oil DIC M27 objective (Carl Zeiss AG), with automated *z*-stack functionality.

The peak-negative acoustic pressure was measured at the objective's field of view and corresponded to MI=0·2.

To evaluate the possible electrostatic attraction between microbubbles and cells, 30 µl of MicroMarker® was diluted into 700 µl of distilled water and tested for electrophoretic mobility (ζ potential) using a Zetasizer 3000 (Malvern Instruments, Malvern, Worcestershire, UK).

To measure the thickness of the cultured cells, 1×10^5 HeLa cells were seeded into an OptiCell®. The cell plasma membrane was labelled with a DiD lipophilic fluorescent probe (Vybrant™ Molecular Probes) according to the manufacturer's protocol. The membrane fluorescence was measured using a 200 M

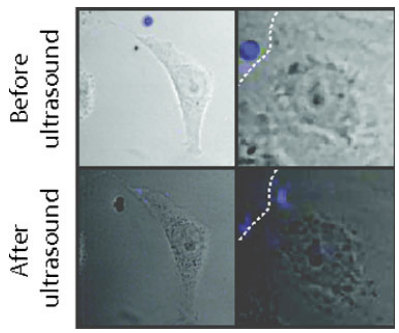

11 Columns *a* and *b* represent frames in optical focus from the events in Figs. 8 and 9 respectively before sonication and ~8 min after sonication: white dotted lines in the right frames indicate cell membrane boundary; left frames correspond to 76×76 $(\mu m)^2$ areas, whereas right frames correspond to 45×45 $(\mu m)^2$ areas

confocal microscope. Cell thickness was calculated from the difference between the upper and lower slices where fluorescence was seen.

The authors recorded 23 movies under 6·6 MHz sonication at frame rates between 500 and 2000 frames per second, representing 15 min of real-time exposure. Of these, 11 movies were recorded using fluorescence. In addition the authors recorded 10 control movies, with a total duration of 22 min.

Results and discussion

Throughout this section, the optical z-axis is defined from distal-to-focus (negative) to proximal-to-focus (positive), with $z=0$ as the focal plane.

Figure 5 shows z-stacks of fluorescence emitted by the DiD dye attached to the membranes of four typical HeLa cells, representing the cell geometry. In total, the thicknesses of 42 cells were measured. The cultured cells were found to be 13 ± 2 μm thick. Clearly, these cells had thicknesses much greater than ultrasound contrast agent microbubble oscillation amplitudes at MI=0·2.

The authors analysed the optical system and compared the results to bubbles and cells that were slightly out of focus, to rule out that the movement of the bubble takes place in a plane different from that of the cell. Figure 6 shows a z-stack of two ultrasound contrast agent microbubbles, similar to Fig. 10 of Postema *et al.*[33] Proximal-to-focus Airy discs can be seen around the bubbles, whereas distal-to-focus bubble boundaries are blurred. Note that the boundary contrast is maximal just proximal-to-focus.[33]

At a centre frequency of 6·6 MHz, the authors recorded 17 events of microbubbles entering HeLa cells. After entering, the microbubbles were observed to quickly dissolve. As an example, Fig. 7 shows an event resampled at 3·4 and 40 Hz respectively, where two bubbles were pushed to a cell during 11 s of sonication. A microbubble 'A' of 4 μm diameter entered the cell and dissolved, whereas a microbubble 'B' of 2 μm diameter stuck to the cell membrane.

Figures 8 and 9 show two similar events, where fluorescence-coated microbubbles were used. The left panels show a microbubble apparently penetrating through the cell membrane in optical focus. Approximately 70 ms after the ultrasound has been switched on a microbubble is seen to penetrate through the cell membrane in Fig. 8. In Fig. 9 the microbubble is seen to penetrate through the cell membrane approximately 24 ms after the ultrasound has been switched on. The right panels show a z-stack through the entire cell to record whether the apparent microbubble entry is actually into the cell.

For both events, Fig. 10 shows average fluorescent intensities in two regions of interest, one inside the cell, and one in the control region. In both events, most fluorescence from apparent microbubble entry can be observed within 5 μm proximal to optical focus, thus well within the cells themselves.

Figure 11 shows frames in optical focus from the events in Figs. 8 and 9, before sonication and ~8 min after sonication. Clearly, fluorescence has transferred into the cells and remained inside the cells long after sonication.

At these low acoustic amplitudes, inertial cavitation, fragmentation, and jetting should not occur. Hence, as a mechanism in sonoporation at low MI, these phenomena might justifiably be neglected.

The authors' observations do not explain why some microbubbles enter a cell and others do not. The quick dissolution after entering suggests that the microbubble loses (part of) its shell while entering.

The ζ-potential measurements showed that the microbubble shells had a charge of $-43{\cdot}9 \pm 2{\cdot}4$ mV. As cells have a natural negative charge,[34,35] the ultrasound contrast agent should be repelled by the cells, in the recordings it is seen that once the ultrasound was turned on, the microbubbles would be attracted to the closest cell, independent of the direction of the sound field. This supports the recent finding that cell membranes can be acoustically active,[36] and therefore interact with microbubbles.

Other cell types than HeLa cells must be used in follow-up studies to investigate differences in bubble–cell interaction.

Conclusions

It has been demonstrated that lipid-shelled microbubbles can be forced to enter cells at a low MI. Hence, if a therapeutic load is added to the bubble, ultrasound-guided delivery could be facilitated at diagnostic settings.

In addition, these results may have implications for the safety regulations on the use of ultrasound contrast agents for diagnostic imaging.

Acknowledgements

This work has been supported by DFG Emmy Noether Programme (grant no. 38355133) and Engineering and Physical Sciences Research Council (EPSRC) (grant no. EP/F037025/1). The authors are grateful to Conseil Regional for A. Delalande's fellowship.

References

1. M. Postema and O. H. Gilja: 'Ultrasound-directed drug delivery', *Curr. Pharm. Biotechnol.*, 2007, **8**, (6), 355–361.
2. S. Bao, B. D. Thrall and D. L. Miller: 'Transfection of a reporter plasmid into cultured cells by sonoporation in vitro', *Ultrasound Med. Biol.*, 1997, **23**, 953–959.

3. S. Chen, R. V. Shohet, R. Bekeredjian, P. Frenkel and P. A. Grayburn: 'Optimization of ultrasound parameters for cardiac gene delivery of adenoviral or plasmid deoxyribonucleic acid by ultrasound-targeted microbubble destruction', *J. Am. Coll. Cardiol.*, 2003, **42**, (2), 301–308.
4. W. J. Greenleaf, M. E. Bolander, G. Sarkar, M. B. Goldring and J. F. Greenleaf: 'Artificial cavitation nuclei significantly enhance acoustically induced cell transfection', *Ultrasound Med. Biol.*, 1998, **24**, (4), 587–595.
5. I. Kondo, K. Ohmori, A. Oshita, H. Takeuchi, S. Fuke, K. Shinomiya, T. Noma, T. Namba and M. Kohno: 'Treatment of acute myocardial infarction by hepatocyte growth factor gene transfer: the first demonstration of myocardial transfer of a ''functional'' gene using ultrasonic microbubble destruction', *J. Am. Coll. Cardiol.*, 2004, **44**, (3), 644–653.
6. N. Kudo, K. Okada and K. Yamamoto: 'Sonoporation by single-shot pulsed ultrasound with microbubbles adjacent to cells', *Biophys. J.*, 2009, **96**, (12), 4866–4876.
7. J. R. Lindner and S. Kaul: 'Delivery of drugs with ultrasound', *Echocardiography*, 2001, **18**, (4), 329–337.
8. K. Tachibana, T. Uchida, K. Ogawa, N. Yamashita and K. Tamura: 'Induction of cell-membrane porosity by ultrasound', *Lancet*, 1999, **353**, 1409.
9. S. Tinkov, R. Bekeredjian, G. Winter and C. Coester: 'Microbubbles as ultrasound triggered drug carriers', *J. Pharm. Sci.*, 2009, **98**, (6), 1935–1961.
10. A. L. Klibanov: 'Targeted delivery of gas-filled microspheres, contrast agents for ultrasound imaging', *Adv. Drug Deliv. Rev.*, 1999, **37**, 139–157.
11. M. Postema, A. Bouakaz, F. J. ten Cate, G. Schmitz, N. de Jong and A. van Wamel: 'Nitric oxide delivery by ultrasonic cracking: some limitations', *Ultrasonics*, 2006, **44**, (Suppl. 1), e109–e113.
12. M. J. Shortencarier, P. A. Dayton, S. H. Bloch, P. A. Schumann, T. O. Matsunaga, and K. W. Ferrara: 'A method for radiation-force localized drug delivery using gas-filled lipospheres', *IEEE Trans. Ultrason. Ferroelect. Freq. Contr.*, 2004, **51**, (7), 822–831.
13. M. Postema, F. J. ten Cate, G. Schmitz, N. de Jong and A. van Wamel: 'Generation of a droplet inside a microbubble with the aid of an ultrasound contrast agent: first result', *Lett. Drug Des. Discov.*, 2007, **4**, (1), 74–77.
14. 'Guidelines for the safe use of diagnostic ultrasound equipment', British Medical Ultrasound Society, London, UK, 2000.
15. G. ter Haar: 'Safety and bio-effects of ultrasound contrast agents', *Med. Biol. Eng. Comput.*, 2009, **47**, 893–900.
16. J.-U. Voigt: 'Ultrasound molecular imaging', *Methods*, 2009, **48**, 92–97.
17. M. Postema and G. Schmitz: 'Ultrasonic bubbles in medicine: influence of the shell', *Ultrason. Sonochem.*, 2007, **14**, (4), 438–444.
18. A. Philipp and W. Lauterborn: 'Cavitation erosion by single laser-produced bubbles', *J. Fluid Mech.*, 1998, **361**, 75–116.
19. T. Kodama and K. Takayama: 'Dynamic behavior of bubbles during extracorporeal shock-wave lithotripsy', *Ultrasound Med. Biol.*, 1998, **24**, (5), 723–738.
20. M. Postema, A. van Wamel, F. J. ten Cate and N. de Jong: 'High-speed photography during ultrasound illustrates potential therapeutic applications of microbubbles', *Med. Phys.*, 2005, **32**, (12), 3707–3711.
21. P. A. Dayton, J. S. Allen and K. W. Ferrara: 'The magnitude of radiation force on ultrasound contrast agents', *J. Acoust. Soc. Am.*, 2002, **112**, (5), 2183–2192.
22. C. F. Caskey, S. Qin, P. A. Dayton and K. W. Ferrara: 'Microbubble tunneling in gel phantoms', *J. Acoust. Soc. Am.*, 2009, **125**, (5), EL183–EL189.
23. S. Kotopoulis and M. Postema: 'Microfoam formation in a capillary', *Ultrasonics*, 2010, **50**, 260–268.
24. M. Postema, O. H. Gilja and A. van Wamel: 'CEUS and sonoporation', in 'Fundamentals of medical ultrasonics', (ed. M. Postema), 205–217; 2011, London, Spon Press.
25. A. van Wamel, K. Kooiman, M. Harteveld, M. Emmer, F. J. ten Cate, M. Versluis and N. de Jong: 'Vibrating microbubbles poking individual cells: drug transfer into cells via sonoporation', *J. Control. Release*, 2006, **112**, (2), 149–155.
26. P. Prentice, A. Cuschieri, K. Dholakia, M. Prausnitz and P. Campbell: 'Membrane disruption by optically controlled microbubble cavitation', *Nature Phys.*, 2005, **1**, 107–110.
27. M. Postema and O. H. Gilja: 'Jetting does not cause sonoporation', *Biomed. Eng.*, 2010, **55**, S19–S20.
28. P. Marmottant and S. Hilgenfeldt: 'Controlled vesicle deformation and lysis by single oscillating bubbles', *Nature*, 2003, **423**, 153–156.
29. A. Delalande, M.-F. Bureau, P. Midoux, A. Bouakaz and C. Pichon: 'Ultrasound-assisted microbubbles gene transfer in tendons for gene therapy', *Ultrasonics*, 2009, **50**, 269–272.
30. K. Kaddur, L. Lebegue, F. Tranquart, P. Midoux, C. Pichon and A. Bouakaz: 'Transient transmembrane release of green fluorescent proteins with sonoporation', *IEEE Trans. Ultrason. Ferroelectr. Freq. Control*, 2010, **57**, (7), 1558–1567.
31. S. Kotopoulis, H. Wang, S. Cochran and M. Postema: 'Lithium niobate ultrasound transducers for high-resolution focused ultrasound surgery', *Proc. IEEE Ultrason. Symp.*, 2010, In Press.
32. P. W. Livanec and R. C. Dunn: 'Single-molecule probes of lipid membrane structure', *Langmuir*, 2008, **24**, (24), 14066–14073.
33. M. Postema, A. Bouakaz, C. T. Chin and N. de Jong: 'Simulations and measurements of optical images of insonified ultrasound contrast microbubbles', *IEEE Trans. Ultrason. Ferroelectr. Freq. Control*, 2003, **50**, (5), 523–536.
34. B. Ehrenberg, V. Montana, M.-D. Wei, J. P. Wuskell and L. M. Loew: 'Membrane potential can be determined in individual cells from the nernstain distribution of cationic dyes', *Biophys. J.*, 1988, **53**, 785–794.
35. A. Takahashi, H. Yamaguchi and H. Miyamoto: 'Change in K+current of HeLa cells with progression of the cell cycle studied by patch-clamp technique', *Am. J. Physiol.*, 1993, **265**, (2), C328–C336.
36. B. Krasovitski, V. Frenkel, S. Shoham and E. Kimmel: 'Subcellular sonophores: ultrasound induced intramembrane cavitation', *Proc. Natl Acad. Sci.*, 2011, **108**, (8), 3258–3263.

Treatment of human pancreatic cancer using combined ultrasound, microbubbles, and gemcitabine: A clinical case study

Spiros Kotopoulis[a)]
National Centre for Ultrasound in Gastroenterology, Haukeland University Hospital, Bergen 5021, Norway and Department of Physics and Technology, University of Bergen, Bergen 5007, Norway

Georg Dimcevski and Odd Helge Gilja
National Centre for Ultrasound in Gastroenterology, Haukeland University Hospital, Bergen 5021, Norway and Department of Clinical Medicine, University of Bergen, Bergen 5021, Norway

Dag Hoem
Department of Surgery, Haukeland University Hospital, Bergen 5021, Norway

Michiel Postema
Department of Physics and Technology, University of Bergen, Bergen 5007, Norway and The Michelsen Centre for Industrial Measurement Science and Technology, Bergen 5892, Norway

(Received 28 November 2012; revised 10 May 2013; accepted for publication 13 May 2013; published 6 June 2013)

Purpose: The purpose of this study was to investigate the ability and efficacy of inducing sonoporation in a clinical setting, using commercially available technology, to increase the patients' quality of life and extend the low Eastern Cooperative Oncology Group performance grade; as a result increasing the overall survival in patients with pancreatic adenocarcinoma.
Methods: Patients were treated using a customized configuration of a commercial clinical ultrasound scanner over a time period of 31.5 min following standard chemotherapy treatment with gemcitabine. SonoVue® ultrasound contrast agent was injected intravascularly during the treatment with the aim to induce sonoporation.
Results: Using the authors' custom acoustic settings, the authors' patients were able to undergo an increased number of treatment cycles; from an average of 9 cycles, to an average of 16 cycles when comparing to a historical control group of 80 patients. In two out of five patients treated, the maximum tumor diameter was temporally decreased to 80 ± 5% and permanently to 70 ± 5% of their original size, while the other patients showed reduced growth. The authors also explain and characterize the settings and acoustic output obtained from a commercial clinical scanner used for combined ultrasound microbubble and chemotherapy treatment.
Conclusions: It is possible to combine ultrasound, microbubbles, and chemotherapy in a clinical setting using commercially available clinical ultrasound scanners to increase the number of treatment cycles, prolonging the quality of life in patients with pancreatic adenocarcinoma compared to chemotherapy alone. [http://dx.doi.org/10.1118/1.4808149]

Key words: ultrasound, microbubbles, sonoporation, chemotherapy

I. PURPOSE

Cancer is the world's second largest cause of death with over 7.6×10^6 deaths a year (21% of NCD deaths).[1] There are over 217 000 new cases of pancreatic cancer worldwide every year.[2] Pancreatic cancer is very difficult to treat due to its aggressive biology, late diagnosis, the encasement of large blood vessels, and the presence of metastasis. Hence, surgery is rarely an option. Chemotherapy produces modest responses but is not curative in this setting, mainly because its use is severely hampered by toxic effects to vital organs. As a result, the survival is very low. The mortality of the inoperable patients is 50% within 3 months and 90% within 12 months.[3,4]

Sonoporation is a novel method for noninvasive targeted drug and gene delivery.[5–8] Sonoporation is defined as the transient formation of pores in cell membranes owing to ultrasound or a combination of ultrasound and microbubbles. These pores range in size from several nanometers to several micrometers,[9–12] allowing for increased drug uptake in highly targeted regions.[13–15]

The acoustic parameters used for sonoporation showing increased cellular uptake of chemotherapeutics and genes vary from low-intensity diagnostic ultrasound [mechanical index (MI) < 0.3] (Refs. 16–29) to high-intensity diagnostic ultrasound (MI > 1.0).[9,30–34] Throughout literature, the acoustic settings used to induce sonoporation vary drastically, with a broad range of these settings showing improved drug and gene delivery. Several studies also show the effect of clinical diagnostic ultrasound in standard color-Doppler and B-mode imaging on cellular uptake.[19,20] These studies, which made use of clinical diagnostic scanners, concluded that a larger duty cycle was necessary to increase the effect of sonoporation. It has been shown that the ideal settings to induce sonoporation are when shock-waves were not present, in

order to sustain the microbubbles, and when the duty cycle is long enough, to excite the microbubbles in the targeted area without heating the surrounding tissue.[16] Furthermore, higher intensities correlating to cavitation and jetting result in increased cell death due to mechanical damage instead of (transient) sonoporation.[33,35–37] As a result, there is no consensus on the exact ultrasound settings to be used for sonoporation.[38] For this reason, we aimed to use settings that matched our previous *in vitro* and *in vivo* work as much as possible, i.e., an *in situ* MI = 0.2, maximum duty cycle, and minimum shockwave generation in order to preserve the microbubbles.[7,8,23]

To date, all sonoporation experiments have been done either *in vitro* or in animal models, hence the effect of sonoporation in humans is not truly known yet.

Ultrasound has been used as a tool in the clinic for many years, especially in transabdominal imaging. Specifically, the pancreas can easily be imaged ultrasonically.[39] In clinical ultrasonic imaging, ultrasound is combined with so-called ultrasound contrast agents to locate tumors.[40,41] These agents consist of gas microbubbles encapsulated by elastic shells.[42] Using a clinical diagnostic scanner for combined imaging and treatment allows for precise acoustic field alignment ensuring that the correct ultrasound intensity reaches the target area.

In this study, we worked toward optimizing the ultrasonic settings for invoking sonoporation in the target region of a pancreatic tumor using a common commercial clinical ultrasound scanner without physical modifications.

II. METHODS

A clinical scanner was calibrated in a degassed water bath in order to map the beam profile and optimize the acoustic settings. After the chemotherapeutic dose was delivered, the clinical probe was positioned aiming directly at the pancreatic tumor and locked in place for 31.5 min. The probe was attached to a ball joint and was positioned near the upper abdomen. Stomach and intestine were avoided in all cases to ensure propagation only through soft tissue, to ensure delivery of the aimed ultrasound intensity at the desired area. Once the tumor was located the probe orientation was fine-tuned in order to locate the largest slice of the tumor and as much vasculature as possible, i.e., the feeding vessels. The probe was then locked in position until the completion of the treatment. The natural breathing motion aided the treatment as the ultrasound slice gently oscillated through the tumor. By visualizing the vasculature and tumor, it could be ensured that the microbubbles were being sonicated at the target. These vessels were then used as a reference point for future treatments. Nine doses of ultrasound contrast agent were intravenously injected over this time period to enhance the sonoporation effect. To evaluate the efficacy of the combined treatment, we compared the amount of chemotherapy cycles the patient was able to receive. Furthermore, the tumor size was measured over the course of the treatment cycles to monitor and compare the tumor growth.

II.A. Ultrasound scanner configuration

A GE LOGIQ 9 ultrasound scanner (GE Healthcare, Waukesha, WI) combined with a 4C curvilinear probe (GE Healthcare) was used for both diagnosis and therapy.

To calibrate and program the diagnostic scanner for the optimized therapeutic settings, the probe was locked in position in a custom-made 250-l 3D scanning tank, containing degassed water. A calibrated HGL-200 bullet-type hydrophone (Onda, Sunnyvale, CA) connected to a WaveJet 354a oscilloscope (Teledyne LeCroy SA, Geneva, Switzerland) was used to measure the acoustic signal. The scanning tank had a spatial resolution of 0.4 μm. For the calibration, a 200-μm resolution was used. AQUASONIC® ultrasound transmission gel (Parker Laboratories, Fairfield, NJ) was placed on the transducer transmission surface and the probe was subsequently covered using a latex ultrasound probe cover (Sheathing Technologies, Inc., Morgan Hill, CA) prior to submersion. The diagnostic scanner settings were modified in order to achieve a maximum duty cycle without completely degrading the image quality, in addition to having a linear acoustic signal. We aimed for minimal acoustic shockwaves and harmonics minimizing potential cavitation. The absence of nonlinear content was verified by visualizing the temporal extent of the pulses and performing a fast Fourier transform (FFT).[43] Multiple focal depths (from 2.8 to 8.4 cm) and different settings (varying gain, changing window size, etc.) were evaluated to ensure similar acoustic conditions in all cases. To calculate the *in situ* acoustic pressures and intensities, the *inwater* values were derated by 0.3 dB/MHz/cm, an approximation of soft tissue attenuation in accordance to FDA and IEC guidelines.[44,45] The attenuation factor of 0.3 dB/MHz/cm is only valid for soft tissue. Hence, this calibration was representative for our clinical positioning for targeting the pancreas.

Table I shows the ultrasound scanner settings used to perform the simultaneous observation and treatment of the pancreatic tumors. Skilled clinical sonographers were called upon to judge the image quality. As there are variations between patients, such as tumor depth and tissue attenuation, certain settings had to be adjusted to ensure the correct ultrasound intensity reached the required area while maintaining the image quality. The settings that were varied are labeled as *patient-depending*. The three settings that were adjusted prior to treatment were: the focal depth, image depth, and gain. The focal and image depths were adjusted in order to visualize and position the acoustic focus directly in the middle of the tumor. By doing so, we could ensure that the acoustic conditions the tumor received were as similar as possible in all patients. The gain is only applied after the received signal; hence, it did not affect the acoustic output. The gain simply allowed for a brighter image.

Once the probe was locked in position and the tumor was "targeted", no changes to the ultrasonic conditions were made.

The settings chosen resulted in acoustic conditions shown in Table II and beam profiles shown in Fig. 1.

The beam profile showed formation of multiple foci in close proximity along the lateral direction merging to form

TABLE I. Parameters as indicated on a GE LOGIQ 9 clinical ultrasound scanner.

Parameter	B-mode	Contrast mode	Unit	Description	Variability
	Value				
MI	0.4	0.4		Mechanical index	None
TIs	0.0	0.0		Thermal index of soft tissue	None
Freq	4.0	4.0	MHz	Center receive frequency	None
AO	1	36	%	Normalized acoustic output	None
FR	4	4	fps	Frame rate	None
Gn	30–45	30–45	dB	Gain	Patient-depending
S/A	3/3	2/0		Synthetic aperture	None
Map	F/0	2/0		Color map	None
F	5.2–6.8	5.2–6.8	cm	Focal depth	Patient-depending
D	10–15	10–15	cm	Image depth	Patient-depending
DR	66	66	dB	Dynamic range	None
SRI HD	3	3		Image smoothing	None
Gray map	F/0	H		Image color maps	None
Trig	−0.25	...	s	Trigger delay	None
Tint map	D	...		Image color maps	None
Trig	...	0–1		Image triggering	None
TAD	...	On		True agent detection	None
F. average	...	3	Frames	Frame averaging	None

a quasicontinuous focus [Fig. 1(e)]. In the elevation direction, side lobes can be clearly seen [Figs. 1(a) and 1(d)]. Using the full width half maximum (FWHM) to define the beam size, the active or treatment area can be defined as a volume of $69 \times >100 \times 1.0\ (\text{mm})^3$ (l × w × h). It is assumed that this is the region where sonoporation occurred most efficiently. Figure 2 shows the pulse repetition pattern generated by these settings. The pulse was amplitude-modulated, consisting of five cycles (2.1 μs) every 210 μs corresponding to a 1% duty cycle (repetition rate optimized). The duty cycle is defined as the percentage of time that ultrasound is being generated. This was measured during the spatial calibration process, in the acoustic focus with the hydrophone, for the duration of the inverse of the frame rate. Due to synthetic aperture and contrast enhanced imaging, the pulse pattern at the focus was amplitude-modulated.[46,47] This can be seen in the upper panel of Fig. 2. The lower panel of Fig. 2 shows the time signal of a single pulse. The pulse is still relatively sine-shaped, thus the transfer function of the propagation path is linear. Minor nonlinear effects can be seen after the fourth cycle. This indicates that shockwave occurrence and therefore microbubble destruction is negligible.

A FFT of the acoustic signal is shown in Fig. 3. The center frequency is 1.9 MHz. Using a −3-dB or FWHM cutoff, the bandwidth was measured to be 1.1 MHz; from 1.3 to 2.4 MHz. A second harmonic peak can be seen at 3.6 MHz due to the minor nonlinear effects. This peak was 11 dB lower than the primary peak.

These settings complied with current safety guidelines for clinical diagnostic imaging.[44,48,49] Figure 4 shows two images of pancreatic cancer in two separate patients captured using the sonoporation treatment settings.

II.B. Chemotherapeutic and microbubble dosage

The recommended chemotherapeutic protocol was followed.[50] This protocol dictates which patients are eligible for chemotherapy and the dosages that can be administered. It includes dosage reduction values depending on platelet

TABLE II. Acoustic conditions generated by the 4C probe for sonoporation *inwater* and derated for *in situ* values (Refs. 44 and 45).

	Center frequency (MHz)	Duty cycle (%)	Mechanical index	Acoustic power I_{SATA} (mW/cm^2)	Peak peak-negative acoustic pressure (MPa)
Inwater values at 6.7 cm depth	1.9	1 (4 cycles every 0.21 ms)	0.49	0.59	0.41
Derated *in situ* values at 6.7 cm depth	1.9	1 (4 cycles every 0.21 ms)	0.20	0.25	0.27

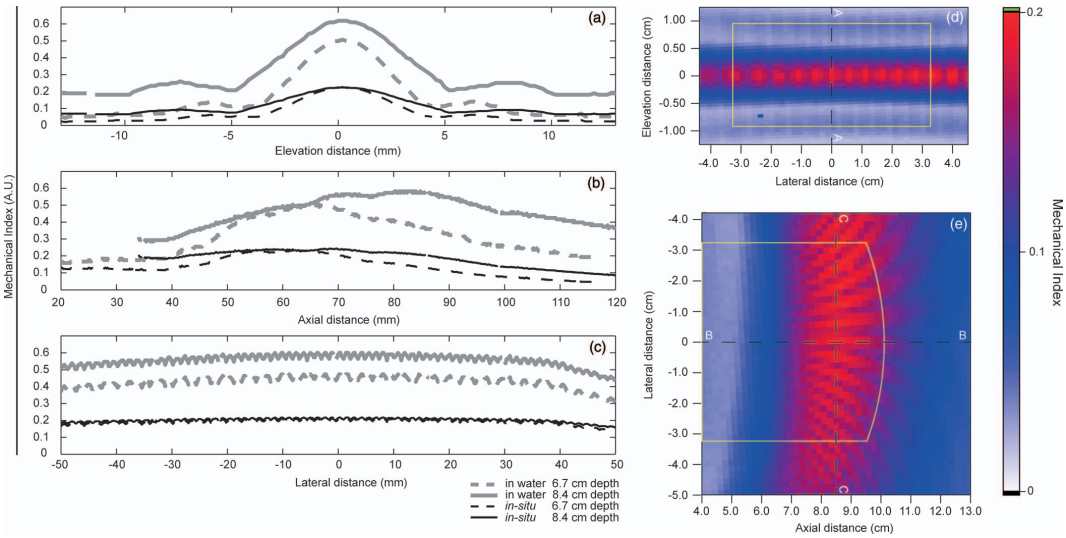

FIG. 1. 1D and 2D beam profiles at sonoporation settings using the 4C probe at two focal depths: 6.7 and 8.4 cm for the 1D plots and 8.4 cm for the 2D plots. The beam profile was characterized in water and derated for *in situ* values (Refs. 44 and 45). Lines A-A, B-B, and C-C in panels (d) and (e) represent the position of the 1D scans shown in panels (a), (b), and (c), respectively. The bounding boxes in panels (d) and (e) represent the area visible on the clinical scanner screen. In the elevation direction, the bounding box was defined by when a 0.5 mm needle could not be distinguished on screen. The tumor was positioned at the intersection of lines B-B and C-C in frame (e), and at an elevation distance of 0 mm in frame (d).

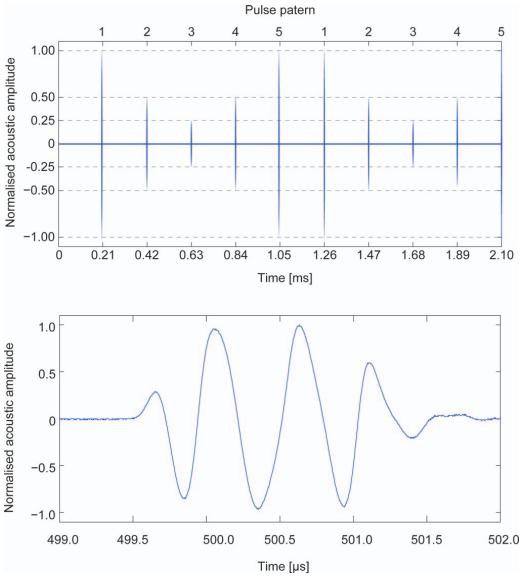

FIG. 2. Ultrasonic pulse generated by the clinical scanner. The top panel shows the pulse repetition frequency and pattern. The lower panel shows the temporal extent of the pulse with the largest amplitude. The pulses were amplitude-modulated. Each pulse consisted of four cycles (2.1 μs) every 210 μs.

and absolute granulocyte count. The chemotherapeutic used, gemcitabine (Gemzar®, Eli Lilly and Company, Indianapolis, IN) was administered once weekly for up to 7 weeks (or until toxicity necessitates reducing or holding a dose), followed by a week of rest from treatment. Subsequent cycles consisted of infusions once weekly for 3 consecutive weeks out of every 4 weeks. Our protocol used the Eastern Cooperative Oncology Group (ECOG) performance status as a measure of the clinical condition.[51] The ECOG performance status ranges from 0 to 5, where 0 denotes a "fully active patient able to carry on all predisease performance without restriction," and 5 denotes a "dead" patient. Chemotherapy was halted if the patient exceeded a grade of 2 that states the patient is "ambulatory and capable of all self-care but unable to carry out any work activities. Up and about more than 50% of waking hours." The ECOG guidelines can be considered as a measure of how "healthy" a patient is. We used the ECOG guidelines to monitor the effectiveness of the combined treatment, i.e., the longer a patient stays below an ECOG grade of 3, the more effective the treatment is considered.

A single treatment cycle is defined as a single infusion of chemotherapeutic followed by ultrasound and microbubble treatment. The week pause was not counted as a treatment cycle. Once the granulocyte or platelet count was permanently too low, or the patient surpassed an ECOG performance status grade of 2, no more treatment was administered.

Gemcitabine was administered by intravenous infusion at a dose of 1000 mg/m^2 over 30 min. The start of the

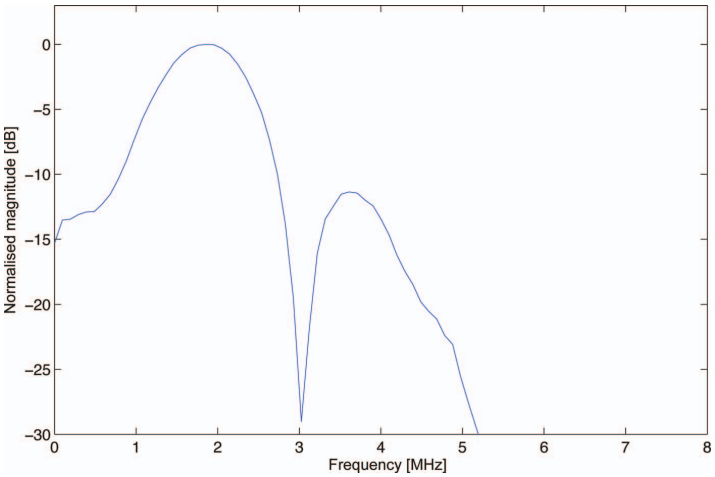

FIG. 3. Fast Fourier transform of ultrasonic signal. The center frequency of the transmitted signal is 1.9 MHz. A bandwidth of 1.1 MHz can be seen.

chemotherapeutic delivery is defined as $T = 0$ min. During the last 10 min ($T = 20$ min) of chemotherapeutic delivery, diagnostic imaging was performed in standard abdominal imaging mode and the tumor was located. Here, the tumor dimensions were measured with ultrasonography. Once the tumor was located, a custom-made clamp was used to lock the probe in position and the clinical scanner was switched to therapeutic settings (Fig. 5). As the maximum systemic concentration of the chemotherapeutic starts at the finish of delivery ($T = 30$ min), this was chosen as the initiation point for the ultrasound treatment. Clinically approved SonoVue® (Bracco Imaging Scandinavia AB, Oslo, Norway) ultrasound contrast agent was used as the microbubble for sonoporation. To ensure microbubbles were present throughout the whole treatment, 0.5 ml of contrast agent followed by 5 ml saline were injected every 3.5 min, i.e., at $T = 30.0$, 33.5, 37.0, 40.5, 44.0, 47.5, 51.0, 54.5, and 58.0 min. A single vial (4.5 ml) was used throughout each treatment. Treatment was stopped at $T = 61.5$ min. The total cumulated ultrasound treatment time was only 18.9 s. This time frame can be seen in Fig. 5(a).

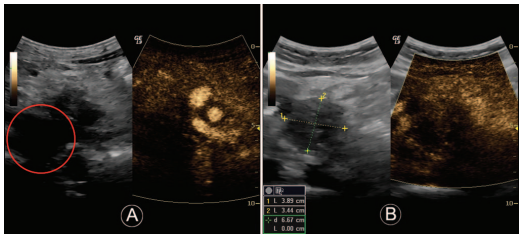

FIG. 4. Images captured using customized sonoporation settings using a clinical ultrasound scanner. The dense vasculature in early arterial phase to the right of the main tumor (circled in the B-mode frame) can be seen in panel (a). Panel (b) shows the dimensions of the main tumor, indicated by lines 1 and 2, using the sonoporation settings.

II.C. Measurement of disease and tumor progression

The primary measure for evaluating the effectiveness of the treatment was the amount of cycles the patient could undergo. The more treatment cycles the patient underwent, the longer the patient was considered healthy.[50,51] Furthermore, if

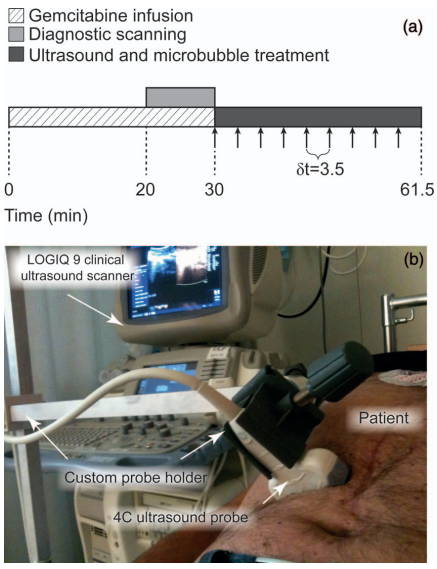

FIG. 5. Time frame of each chemotherapy cycle [panel (a)] and photograph of probe and custom-made probe holder during patient treatment using microbubble sonoporation for pancreatic cancer [panel (b)]. Panel (a) shows the time frame for each treatment cycle from the start of the gemcitabine infusion. Arrows indicate intravenous injection time of 0.5 ml SonoVue® followed by a 5-ml intravenous injection of saline. Time between each injection (δt) is 3.5 min.

the tumor size was reduced substantially in accordance to the Response Evaluation Criteria in Solid Tumors (RECIST),[52] the treatment modality was re-evaluated, e.g., transfer to radiation therapy or surgery. This was considered a successful treatment.

Diagnostic ultrasound imaging was performed weekly assessing the tumor size. As computerized tomography (CT) scans are considered the golden standard for following tumor growth,[53] every 8 weeks a CT scan was also performed to validate the tumor size. This value was used to follow the tumor progression.

Positron emission tomography (PET) imaging was also performed at the start of the treatment to assess the presence of metastasis.

Figure 6 shows the pancreatic adenocarcinoma in patient 5 prior to ultrasound and microbubble treatment as seen by CT and PET imaging modalities.

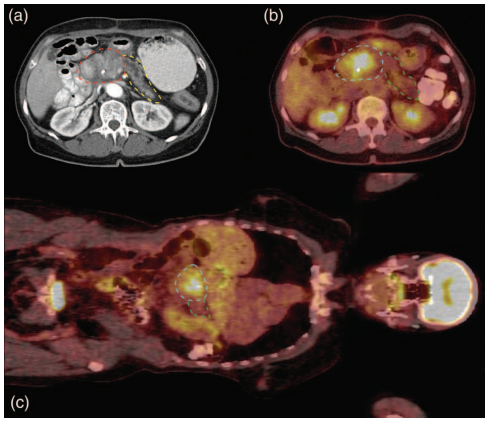

FIG. 6. CT [panel (a)] and PET [panels (b) and (c)] images of patient 5 showing pancreatic adenocarcinoma prior to treatment. Panel (a) shows a CT scan in the transverse plane with the primary tumor in the head of the pancreas, and the pancreas indicated by the dashed lines. Panels (b) and (c) show PET scans in transverse and coronal planes, respectively. The location of the tumor can be clearly identified by the brighter region in the middle of the abdomen. In panels (b) and (c), the tumor and pancreas are, respectively, indicated by the dashed lines. The pancreas tail is behind the large colon in panel (c).

II.D. Treatment group

Patients with inoperable pancreatic cancer and fulfilled the inclusion criteria at the Haukeland University Hospital, Bergen, Norway, who have volunteered to participate, were included. The inclusion criteria primarily stated that the patients must be >18 years of age, a diagnosis of inoperable pancreatic cancer, histologically verified, locally advanced (stage II/III) or metastatic (stage IV) adenocarcinoma of the pancreas, and must be ambulatory with an ECOG performance status between 0 and 2. For this case report, a total of five patients were recruited. Table III shows the characteristics of the five patients enrolled in this pilot study prior to treatment in addition to the start and end dates of the treatment for every patient.

II.E. Control group

Taking into account the guidelines for gemcitabine treatment, it can be deduced that the more treatment cycles the patient can undergo, the longer the patient can be considered healthy; hence, the more effective the treatment. Once the patient surpasses a Level 2 in the ECOG performance status guidelines, they would no longer receive treatment; this would accordingly define the end of the healthy and ambulatory period. Our control group consisted of 80 patients from 2009 to 2011 with histology showing pancreatic adenocarcinoma (matching the same criteria as our patients). These patients received the identical chemotherapy treatment (in accordance to Gemzar guidelines[50]) at Haukeland University Hospital, Bergen, Norway. The control treatments were also discontinued once they surpassed an ECOG performance grade of 2 or their blood counts dropped below the chemotherapy guidelines. Patients who received a different treatment were excluded from the control group. The data were accessed through the internal hospital medical system. The same anonymous data will be available on the Norwegian national cancer registry.

TABLE III. Patient characteristics prior to treatment. ND denotes nondiscernable values. Start and end date of treatment are also stated.

			Patient 1	Patient 2	Patient 3	Patient 4	Patient 5
Age			66	55	70	68	51
Sex			Male	Male	Female	Female	Female
Pathology findings			Pancreatic ductal adenocarcinoma				
ECOG performance			0	1	1	0	1
Biochemistry	ALAT	IU/l	20	55	138	23	66
	LD	IU/l	121	146	153	117	176
	Leuk	$\times 10^9$ U/l	6.8	3.8	6.9	6.1	11.1
	Neutr	$\times 10^9$ U/l	4.3	5.8	3.8	3.5	7.1
Tumor markers	Ca 125		ND	54.1	102	ND	136.6
	Ca 19-9		59	ND	ND	4608	ND
Treatment dates (dd/mm/yyyy)	Start date		06/01/2012	04/04/2012	07/03/2012	22/02/2012	15/02/2012
	End date		26/09/2012	01/08/2012	11/07/2012	11/05/2012	08/06/2012

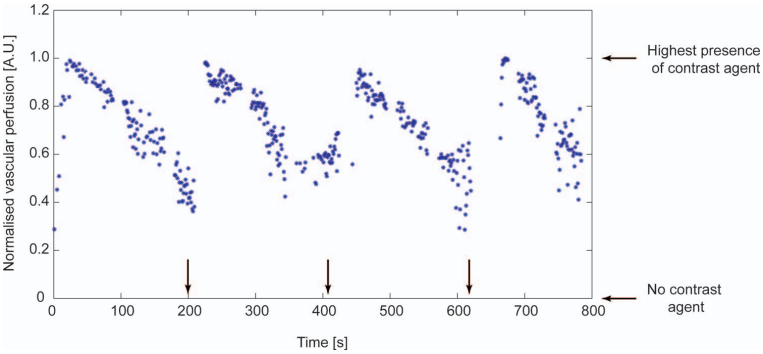

FIG. 7. Normalized microbubble presence in tumor locality during the first 800 s of treatment. Arrows indicate contrast injection time.

II.F. Ethical considerations

All experiments were performed with approval from the regional ethics committee under Reference No. 2011/1601/REK vest.

III. RESULTS AND DISCUSSION

The beam characterization showed that the clinical scanner took into account the attenuation of soft tissue when varying the focal depth. This allowed for a good prediction of the ultrasound profile *in situ* and easy manipulation of the ultrasound intensity and positioning. The "active" area that we assume enhances the chemotherapy effect was long and wide in all cases independent of depth, surpassing the tumor size, allowing a maximum flexibility on treatment area. It has to be assumed that there are some fluctuations in the sound field pressures due to tissue property variations, but this should not drastically change the sound field in our case, as acoustic propagation was only through soft tissue. Taking into account the vast range of ultrasound intensities used to induce sonoporation, as seen in literature, we assume that sonoporation may be occurring at lower or higher acoustic pressures independent of the varying attenuation of tissue. A benefit of using a clinical probe is also that due to the synthetic aperture, objects obscuring the field of view do not affect the beam formation in other areas; hence, we can predict the ultrasound dose delivered to our target area.

The image generated using our customized treatment settings allowed easy identification of both microbubbles and tumors. Figure 4(a) shows clear signs of microbubble presence in the tumor vasculature and surrounding tissue. Figure 4(b) shows the dimensions of a pancreatic tumor indicating the ease of detecting and aligning the probe to the tumor using the modified settings.

Figure 7 shows the normalized perfusion curve where the arrows indicate the contrast injection time, as measured by the clinical scanner during the first 13 min of ultrasound and microbubble treatment. A pseudosinusoidal perfusion curve can be seen. Throughout the whole treatment, we can see that there are always microbubbles present. By using this pseudocontinuous method, we can ensure that there are always microbubbles present without the added complexity of continuous infusion equipment.

Our control group, treated with the same chemotherapeutic protocol, received an average of 9 ± 6 treatment cycles. To date all patients participating in this trial have already surpassed this indicating the potential benefit of our combined treatment on a clinical scale with minimal changes to chemotherapy protocols. The patients enrolled in this clinical pilot study received an average of 16 ± 7 treatment cycles.

Figure 8 and Table IV show the effect of our combined treatment on the tumor size. After 8 weeks two patients showed a tumor diameter reduction. Patient 1 had a temporary tumor reduction from 4.0 to 3.1 cm. The next CT image was taken 24 weeks later and showed a growth to 4.6 cm; an increase of 15% from the original tumor size after 32 weeks of treatment. In patient 2, the treatment resulted in a continuous tumor reduction over 16 weeks, a very rare response from chemotherapy alone. As a result of his increased health, after ten treatment cycles, he was removed from the clinical trial to undergo radiation therapy. As this patient was removed from the trial due to the success of the treatment, a lower number of total and average treatments was seen, reducing the apparent effectiveness of the treatment as a whole. It should be noted that none of the patients in the control group stopped

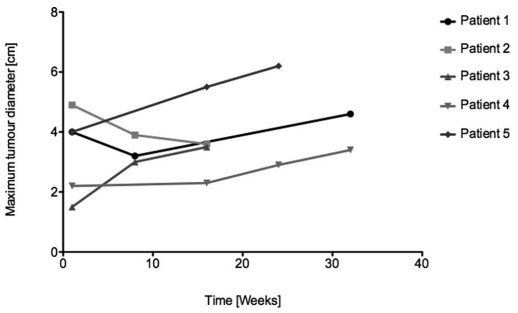

FIG. 8. Change in tumor diameter over time measured from CT images in patients with pancreatic malignancy.

TABLE IV. Maximum tumor diameter as measured from CT images. Empty values denote skipped CT scans.

	Maximum tumor diameter (cm)					
Patient	Inclusion day	Week 8	Week 16	Week 24	Week 32	Total number of cycles
1	4.0	3.1	...	...	4.6	27
2	4.9	3.9	3.6	...	...	10
3	1.5	3.0	3.5	...	...	11
4	2.2	...	2.3	2.9	3.4	16
5	4.0	...	5.5	6.2	...	16

treatment due to its success but on the contrary, due to their deterioration.

Two patients showed slow tumor growth from the eighth week onward (patient 3 and patient 4). Patient 5 also had a biopsy verified primary tumor in the pancreas. This was surgically removed but reoccurred with a small tumor in the operation sight and a large metastasis. This indicated that the tumor was at a late stage of development hence a limited response could be expected from the chemotherapeutic. Nevertheless, this patient was also able to receive 11 cycles of treatment.

As pancreatic cancer is such an aggressive form of cancer, it is very uncommon to see any decrease in tumor growth from chemotherapy. Our aim was to improve quality of life, to extend the healthy period of life, and conclusively extend the patients survival. If the patient was "healthy" enough [well-defined state in both groups, ECOG performance status 0–2 (Ref. 51)], they would be able to receive treatment for a longer period. In fact, as long as they are ambulatory and capable of all self-care, they are able to receive the treatment. Seeing a decrease in the primary tumor size was an added benefit to the increased number of treatment cycles and thereby the anticipated survival.

The addition of the sonoporation procedure following the standard chemotherapeutic protocol did not add any discomfort to the patients. All patients were very relaxed during the treatment to a state where they could comfortably sleep throughout the whole treatment.

In this study, we also aimed to show that it is possible to induce sonoporation in the clinic using existing commercial equipment, while fitting in the current safety regulations for the use of diagnostic ultrasound. In our previous work, we showed that a duty cycle of 40% was ideal for sonoporation.[7,23] Here, we are using a duty cycle of 1%; hence, expecting a small effect of sonoporation. There are many ways to improve this method of therapy such as by increasing the duty cycle from 1% to 40% and introducing targeted microbubbles that could attach to specific cancer cells.[40]

The efficacy of our combined treatment should be compared to the efficacy of the current golden standard, the chemotherapeutic gemcitabine alone, where the viability of the patient has been extended by approximately 1 month.[3,4]

IV. CONCLUSION

Using a clinical diagnostic scanner for therapeutic purposes allows accurate acoustic field alignment ensuring that the desired ultrasound dose reaches the target area. This configuration allows simultaneous visualization of the microbubbles present while treating the pancreatic tumor. In this pilot study, we saw an extended treatment period when comparing to the control group. Furthermore, we did not notice any adverse side effects. Combined ultrasound, microbubble, and chemotherapeutic treatment could pave the way for a novel enhanced drug delivery pathway.

ACKNOWLEDGMENTS

This study has been supported by funds from the Norwegian Cancer Society (NCS) and MedViz (http://medviz.uib.no/), an interdisciplinary research cluster from Haukeland University Hospital, University of Bergen and Christian Michelsen Research AS. The authors would like to thank Dr. Martin Biermann, Dr. Tormod Bjårnes, Dr. Bjørn Tore Gjertsen, Dr. Anders Molven, and Dr. Halfdan Sørbye for their support throughout this project.

[a]Author to whom correspondence should be addressed. Electronic mail: Spiros.Kotopoulis@uib.no

[1]World Health Organization, *World Health Statistics* (World Health Organization, Geneva, Switzerland, 2012) (available URL: http://www.who.int/gho/publications/world_health_statistics/2012/en/index.html).
[2]D. Hariharan, A. Saied, and H. M. Kocher, "Analysis of mortality rates for pancreatic cancer across the world," HPB (Oxford) **10**, 58–62 (2008).
[3]J. P. Neoptolemos, J. A. Dunn, D. D. Stocken, J. Almond, K. Link, H. Beger, C. Bassi, M. Falconi, P. Pederzoli, C. Dervenis, L. Fernandez-Cruz, F. Lacaine, A. Pap, D. Spooner, D. J. Kerr, H. Friess, M. W. Buchler, and European Study Group for Pancreatic Cancer, "Adjuvant chemoradiotherapy and chemotherapy in resectable pancreatic cancer: A randomised controlled trial," Lancet **358**, 1576–1585 (2001).
[4]J. P. Neoptolemos, D. D. Stocken, H. Friess, C. Bassi, J. A. Dunn, H. Hickey, H. Beger, L. Fernandez-Cruz, C. Dervenis, F. Lacaine, M. Falconi, P. Pederzoli, A. Pap, D. Spooner, D. J. Kerr, M. W. Buchler, and European Study Group for Pancreatic Cancer, "A randomized trial of chemoradiotherapy and chemotherapy after resection of pancreatic cancer," N. Engl. J. Med. **350**, 1200–1210 (2004).
[5]S. Bao, B. D. Thrall, and D. L. Miller, "Transfection of a reporter plasmid into cultured cells by sonoporation *in vitro*," Ultrasound Med. Biol. **23**, 953–959 (1997).
[6]A. van Wamel, K. Kooiman, M. Harteveld, M. Emmer, F. J. ten Cate, M. Versluis, and N. de Jong, "Vibrating microbubbles poking individual cells: Drug transfer into cells via sonoporation," J. Controlled Release **112**, 149–155 (2006).
[7]A. Delalande, S. Kotopoulis, T. Rovers, C. Pichon, and M. Postema, "Sonoporation at a low mechanical index," Bub. Sci. Eng. Tech. **3**, 3–11 (2011).
[8]M. Postema, S. Kotopoulis, A. Delalande, and O. H. Gilja, "Sonoporation: Why microbubbles create pores," Ultraschall Med. **33**, 97–98 (2012).
[9]N. G. Lee, J. L. Berry, T. C. Lee, A. T. Wang, S. Honowitz, A. L. Murphree, N. Varshney, D. R. Hinton, and A. A. Fawzi, "Sonoporation enhances chemotherapeutic efficacy in retinoblastoma cells *in vitro*," Invest. Ophthalmol. Visual Sci. **52**, 3868–3873 (2011).

[10]C. X. Deng, F. Sieling, H. Pan, and J. Cui, "Ultrasound-induced cell membrane porosity," Ultrasound Med. Biol. **30**, 519–526 (2004).

[11]R. K. Schlicher, H. Radhakrishna, T. P. Tolentino, R. P. Apkarian, V. Zarnitsyn, and M. R. Prausnitz, "Mechanism of intracellular delivery by acoustic cavitation," Ultrasound Med. Biol. **32**, 915–924 (2006).

[12]Y. Z. Zhao, Y. K. Luo, C. T. Lu, J. F. Xu, J. Tang, M. Zhang, Y. Zhang, and H. D. Liang, "Phospholipids-based microbubbles sonoporation pore size and reseal of cell membrane cultured *in vitro*," J. Drug Target. **16**, 18–25 (2008).

[13]M. Postema and O. H. Gilja, "Ultrasound-directed drug delivery," Curr. Pharm. Biotechnol. **8**, 355–361 (2007).

[14]M. Postema, O. H. Gilja, and A. van Wamel, "CEUS and sonoporation," in *Fundamentals of Medical Ultrasonics*, edited by M. Postema (Spon, London, 2011), pp. 205–217.

[15]M. Postema, S. Kotopoulis, A. Delalande, and O. H. Gilja, "Ultrasound-guided delivery and sonoporation," *Ultrasound in Gastroenterology: 10-years Anniversary of National Center for Ultrasound in Gastroenterology* (National Center for Ultrasound in Gastroenterology, Bergen, Norway, 2011), pp. 57–59.

[16]J. M. Escoffre, A. Novell, J. Piron, A. Zeghimi, A. Doinikov, and A. Bouakaz, "Microbubble attenuation and destruction: Are they involved in sonoporation efficiency?," IEEE Trans. Ultrason. Ferroelectr. Freq. Control **60**, 46–52 (2013).

[17]D. L. Miller and C. Dou, "Membrane damage thresholds for 1- to 10-MHz pulsed ultrasound exposure of phagocytic cells loaded with contrast agent gas bodies *in vitro*," Ultrasound Med. Biol. **30**, 973–977 (2004).

[18]D. L. Miller and C. Dou, "Membrane damage thresholds for pulsed or continuous ultrasound in phagocytic cells loaded with contrast agent gas bodies," Ultrasound Med. Biol. **30**, 405–411 (2004).

[19]D. L. Miller, C. Dou, and J. Song, "DNA transfer and cell killing in epidermoid cells by diagnostic ultrasound activation of contrast agent gas bodies *in vitro*," Ultrasound Med. Biol. **29**, 601–607 (2003).

[20]D. L. Miller and J. Quddus, "Sonoporation of monolayer cells by diagnostic ultrasound activation of contrast-agent gas bodies," Ultrasound Med. Biol. **26**, 661–667 (2000).

[21]M. W. Miller, "Gene transfection and drug delivery," Ultrasound Med. Biol. **26**, S59–S62 (2000).

[22]K. Kooiman, M. Harteveld, A. F. W. van der Steen, and N. de Jong, "Sonoporation of endothelial cells by vibrating targeted microbubbles," J. Controlled Release **154**, 35–41 (2011).

[23]A. Delalande, A. Bouakaz, G. Renault, F. Tabareau, S. Kotopoulis, P. Midoux, B. Arbeille, R. Uzbekov, S. Chakravarti, M. Postema, and C. Pichon, "Ultrasound and microbubble-assisted gene delivery in Achilles tendons: Long lasting gene expression and restoration of fibromodulin KO phenotype," J. Controlled Release **156**, 223–230 (2011).

[24]S. M. Nejad, S. H. R. Hosseini, H. Akiyama, and K. Tachibana, "Optical observation of cell sonoporation with low intensity ultrasound," Biochem. Biophys. Res. Commun. **413**, 218–223 (2011).

[25]F. Yang, N. Gu, D. Chen, X. Xi, D. Zhang, Y. Li, and J. Wu, "Experimental study on cell self-sealing during sonoporation," J. Controlled Release **131**, 205–210 (2008).

[26]Y. Qiu, C. Zhang, J. Tu, and D. Zhang, "Microbubble-induced sonoporation involved in ultrasound-mediated DNA transfection *in vitro* at low acoustic pressures," J. Biomech. **45**, 1339–1345 (2012).

[27]M. Matsuo, K. Yamaguchi, L. B. Feril, Jr., H. Endo, K. Ogawa, K. Tachibana, and J. Nakayama, "Synergistic inhibition of malignant melanoma proliferation by melphalan combined with ultrasound and microbubbles," Ultrason. Sonochem. **18**, 1218–1224 (2011).

[28]N. Lamanauskas, A. Novell, J. M. Escoffre, M. Venslauskas, S. Satkauskas, and A. Bouakaz, "Bleomycin delivery into cancer cells *in vitro* with ultrasound and SonoVue® or BR14® microbubbles," J. Drug Target. **21**(4), 407–414 (2013).

[29]Y. Watanabe, A. Aoi, S. Horie, N. Tomita, S. Mori, H. Morikawa, Y. Matsumura, G. Vassaux, and T. Kodama, "Low-intensity ultrasound and microbubbles enhance the antitumor effect of cisplatin," Cancer Sci. **99**, 2525–2531 (2008).

[30]J. Wu, J. Pepe, and M. Rincon, "Sonoporation, anti-cancer drug and antibody delivery using ultrasound," Ultrasonics **44**, E21–E25 (2006).

[31]C. Y. Lai, C. H. Wu, C. C. Cheng, and P. C. Li, "Quantitative relations of acoustic inertial cavitation with sonoporation and cell viability," Ultrasound Med. Biol. **32**, 1931–1941 (2006).

[32]D. M. Hallow, A. D. Mahajan, T. E. McCutchen, and M. R. Prausnitz, "Measurement and correlation of acoustic cavitation with cellular bioeffects," Ultrasound Med. Biol. **32**, 1111–1122 (2006).

[33]M. M. Forbes, R. L. Steinberg, and W. D. O'Brien, "Examination of inertial cavitation of optison in producing sonoporation of Chinese hamster ovary cells," Ultrasound Med. Biol. **34**, 2009–2018 (2008).

[34]J. L. Tlaxca, C. R. Anderson, A. L. Klibanov, B. Lowrey, J. A. Hossack, J. S. Alexander, M. B. Lawrence, and J. J. Rychak, "Analysis of *in vitro* transfection by sonoporation using cationic and neutral microbubbles," Ultrasound Med. Biol. **36**, 1907–1918 (2010).

[35]C. D. Ohl and B. Wolfrum, "Detachment and sonoporation of adherent HeLa-cells by shock wave-induced cavitation," Biochim. Biophys. Acta **1624**, 131–138 (2003).

[36]D. L. Miller and C. Y. Dou, "Induction of apoptosis in sonoporation and ultrasonic gene transfer," Ultrasound Med. Biol. **35**, 144–154 (2009).

[37]M. Postema and O. H. Gilja, "Jetting does not cause sonoporation," Biomed. Eng. **55**, S19–S20 (2010).

[38]B. Geers, H. Dewitte, S. C. De Smedt, and I. Lentacker, "Crucial factors and emerging concepts in ultrasound-triggered drug delivery," J. Controlled Release **164**, 248–255 (2012).

[39]F. G. Erchinger, G. Dimcevski, T. Engjom, and O. H. Gilja, "Transabdominal ultrasonography of the pancreas: Basic and new aspects," Imaging Med. **3**, 411–422 (2011).

[40]M. Postema and O. H. Gilja, "Contrast-enhanced and targeted ultrasound," World J. Gastroenterol. **17**, 28–41 (2011).

[41]F. Piscaglia, C. Nolsoe, C. F. Dietrich, D. O. Cosgrove, O. H. Gilja, M. Bachmann Nielsen, T. Albrecht, L. Barozzi, M. Bertolotto, O. Catalano, M. Claudon, D. A. Clevert, J. M. Correas, M. D'Onofrio, F. M. Drudi, J. Eyding, M. Giovannini, M. Hocke, A. Ignee, E. M. Jung, A. S. Klauser, N. Lassau, E. Leen, G. Mathis, A. Saftoiu, G. Seidel, P. S. Sidhu, G. ter Haar, D. Timmerman, and H. P. Weskott, "The EFSUMB Guidelines and Recommendations on the Clinical Practice of Contrast Enhanced Ultrasound (CEUS): Update 2011 on non-hepatic applications," Ultraschall Med. **33**, 33–59 (2012).

[42]M. Postema, *Fundamentals of Medical Ultrasonics* (Spon, New York, 2011).

[43]B. Gerold, S. Kotopoulis, C. McDougall, D. McGloin, M. Postema, and P. Prentice, "Laser-nucleated acoustic cavitation in focused ultrasound," Rev. Sci. Instrum. **82**, 044902 (2011).

[44]U.S. Department of Health and Human Services, *Information for Manufacturers Seeking Marketing Clearance of Diagnostic Ultrasound Systems and Transducers* (Food and Drug Administration, 2008).

[45]International Electrotechnical Commission, "Ultrasonics - Hydrophones - Part 2: Calibration for ultrasonic fields up to 40 MHz," Report No. 62127-2 ed1.0 (IEC, Geneva, Switzerland, 2013).

[46]J. A. Jensen, S. I. Nikolov, K. L. Gammelmark, and M. H. Pedersen, "Synthetic aperture ultrasound imaging," Ultrasonics **44**(Suppl. 1), e5–e15 (2006).

[47]E. Quaia, "Microbubble ultrasound contrast agents: An update," Eur. Radiol. **17**, 1995–2008 (2007).

[48]*Guidelines for the Safe Use of Diagnostic Ultrasound Equipment* (British Medical Ultrasound Society, London, UK, 2000).

[49]S. B. Barnett, G. R. Ter Haar, M. C. Ziskin, H. D. Rott, F. A. Duck, and K. Maeda, "International recommendations and guidelines for the safe use of diagnostic ultrasound in medicine," Ultrasound Med. Biol. **26**, 355–366 (2000).

[50]*Highlights of Prescribing Information: Gemzar* (Eli Lilly and Company, Indianapolis, Indiana, 2010) (available URL: http://pi.lilly.com/us/gemzar.pdf).

[51]M. M. Oken, R. H. Creech, D. C. Tormey, J. Horton, T. E. Davis, E. T. Mcfadden, and P. P. Carbone, "Toxicity and response criteria of the Eastern-Cooperative-Oncology-Group," Am. J. Clin. Oncol. **5**, 649–655 (1982).

[52]E. A. Eisenhauer, P. Therasse, J. Bogaerts, L. H. Schwartz, D. Sargent, R. Ford, J. Dancey, S. Arbuck, S. Gwyther, M. Mooney, L. Rubinstein, L. Shankar, L. Dodd, R. Kaplan, D. Lacombe, and J. Verweij, "New response evaluation criteria in solid tumours: Revised RECIST guideline (version 1.1)," Eur. J. Cancer **45**, 228–247 (2009).

[53]S. A. Sohaib, B. Turner, J. A. Hanson, M. Farquharson, R. T. Oliver, and R. H. Reznek, "CT assessment of tumour response to treatment: Comparison of linear, cross-sectional and volumetric measures of tumour size," Br. J. Radiol. **73**, 1178–1184 (2000).

Partie III

Projet de recherche

Cette partie contient trois chapitres sur mes perspectives de recherche à court et plus long termes.

Le premier chapitre décrit l'analyse des antibulles thérapeutiques.

Le deuxième chapitre décrit le système expérimental pour manipuler les cellules individuelles.

Le troisième chapitre conclut ce mémoire avec ma vision sur ce champ de recherche.

III.1 Antibulles thérapeutiques

Comme décrit précédemment, les microbulles peuvent être utilisées pour augmenter l'effet local d'agents thérapeutiques. Néanmoins, pour prévenir des effets secondaires, les agents thérapeutiques doivent être couplés aux microbulles. Le couplage aux capsules change la viscosité des capsules et en conséquence limite l'amplitude des oscillations des microbulles, prévenant la libération d'agent thérapeutique de la capsule. Idéalement, l'agent thérapeutique devrait être chargé dans le noyau d'une microbulle. Une microbulle gazeuse avec un noyau liquide est appelée une antibulle.

Une photographie d'une antibulle expérimentale est présentée Figure 1. [1]

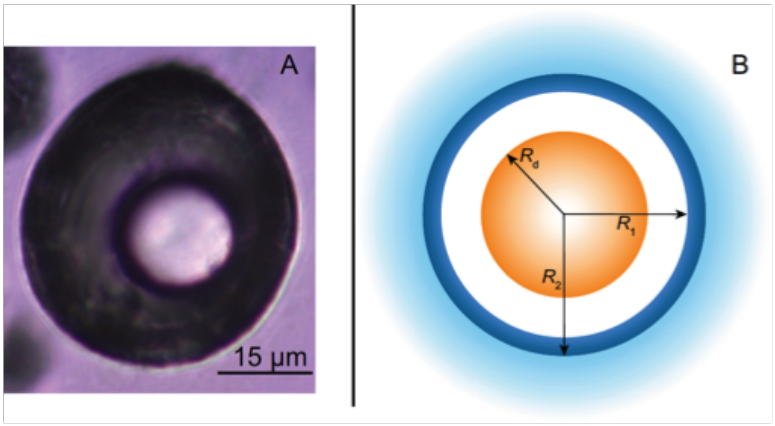

Figure 1 : Image microscopique d'une antibulle (A) et sa représentation schématique d'un fluide (bleu clair) contenant une antibulle avec un noyau de gouttelette (orange) de rayon R_d, entourée par une couche de gaz (blanc) et une coque mince (bleu foncé) de rayon instantané intérieur R_1 et rayon instantané extérieur R_2 (B).[1]

Le comportement oscillant des antibulles ultrasonores est dérivé et discuté dans « Lagrangian formalism for computing oscillations of spherically symmetric encapsulated acoustic antibubbles » (p. 121). [2]

Ensemble avec M. Kristoffer Johansen, j'analyserai les réponses des antibulles expérimentales aux champs ultrasonores, pour prédire les conditions sous lesquelles les noyaux liquides sont libérés hors des antibulles. Nous continuerons la recherche des signaux harmoniques acoustiques des antibulles, indiquant la présence et la taille des noyaux liquides.

1. Johansen K, Kotopoulis S, Poortinga AT, Postema M. Nonlinear echoes from encapsulated antibubbles. Physics Procedia 2015 ; 70 : 1079–1082.
2. Johansen K, Postema M. Lagrangian formalism for computing oscillations of spherically symmetric encapsulated acoustic antibubbles. Hydroacoustics 2016 ; 19 : 197–208.

Lagrangian formalism for computing oscillations of spherically symmetric encapsulated acoustic antibubbles

Kristoffer JOHANSEN[1], Michiel POSTEMA[2,3,4]

[1]School of Engineering, James Watt Building, University of Glasgow,
Glasgow, G12 8QQ, Scotland, email: k.johansen.1@research.gla.ac.uk
[2]Institute of Fundamental Technological Research, Polish Academy of Sciences,
ulica Adolfa Pawińskiego, 02-106 Warsaw, Poland, email: mpostema@ippt.pan.pl
[3]School of Electrical and Information Engineering, Chamber of Mines Building,
University of the Witwatersrand, 1 Jan Smuts Avenue, Braamfontein, Johannesburg 2050,
South Africa, email: michiel.postema@wits.ac.za
[4]Department of Physics and Technology, University of Bergen,
Allégaten 55, 5007 Bergen, Norway, email: michiel.postema@uib.no

Antibubbles are gas bubbles containing a liquid droplet core and, typically, a stabilising outer shell. It has been hypothesised that acoustically driven antibubbles can be used for active leakage detection from subsea production facilities. This paper treats the dynamics of spherically symmetric microscopic antibubbles, building on existing models of bubble dynamics. A more complete understanding of microbubble dynamics demands that the effects of the translational dynamics is included into the Rayleigh-Plesset equation, which has been the primary aim of this paper. Moreover, it is a goal of this paper to derive a theory that is not based on ad-hoc *parameters due to the presence of a shell, but rather on material properties. To achieve a coupled set of differential equations describing the radial and translational dynamics of an antibubble, in this paper Lagrangian formalism is used, where a Rayleigh-Plesset-like equation allows for the shell to be modelled from first principles. Two shell models are adopted; one for a Newtonian fluid shell, and the other for a Maxwell fluid shell. In addition, a zero-thickness approximation of the encapsulation is presented for both models. The Newtonian fluid shell can be considered as a special case of the Maxwell fluid shell. The equations have been linearised and the natural and damped resonance frequencies have been presented for both shell models.*

Keywords: Microbubbles, spatio–temporal bubble dynamics, Rayleigh-Plesset equation.

1. Introduction

Recently, it has been proposed to locate offshore hydrocarbon production facilities below the sea instead of at the surface [1]. The construction of subsea production facilities reduces operation costs, and thereby allows for the production of hydrocarbons at greater depths. Several of

the new production fields in the Northern Hemisphere are placed in Arctic climates. Therefore, transportation processes at low temperatures are becoming of increasing importance. However, under the extreme conditions in such regions, leakages in transportation pipelines may be hard to detect [2].

Recently, a full overview of acoustic leakage detection methods was published [3]. Because of the similarity in acoustic response from bubbles and from other subsea phenomena, it has been hypothesised that acoustically driven antibubbles can be used for active leakage detection from subsea production facilities [4]. Antibubbles are gas bubbles containing a liquid droplet core. Typically, antibubbles are encapsulated by a stabilising outer shell.

This paper treats the dynamics of spherically symmetric microscopic antibubbles, building on existing models of bubble dynamics. In recent years it has been suggested that a more complete understanding of microbubble dynamics demands that the effects of the translational dynamics is included into the Rayleigh-Plesset equation [5]. Moreover, it is a goal to derive a theory that does not include any *ad-hoc* shell parameters, but is rather based on material properties, *e.g.*, the shear viscosity and the shear modulus. This is of interest as *ad-hoc* parameters describing the shell are not general, but depend on, *inter alia*, the bubble resting radius.

To achieve a coupled set of differential equations describing the radial and translational dynamics of an antibubble, Lagrangian formalism is used, where a Rayleigh-Plesset-like equation allows for the shell to be modelled from first principles. Two shell models are adopted; one for a Newtonian fluid shell and one for a Maxwell fluid shell. In addition, a zero-thickness approximation of the encapsulation is presented for both models.

2. Theory

In Lagrangian formalism, a Lagrangian function $L = T - U$ is defined, where L is the Lagrangian function, T is the kinetic energy, and U is the potential energy. The Lagrangian equation (1) is given by

$$\frac{\mathrm{d}}{\mathrm{d}t}\frac{\partial L}{\partial \dot{q}_i} - \frac{\partial L}{\partial q_i} = -\frac{\partial F}{\partial \dot{q}_i} \,, \tag{1}$$

where F is the dissipative function which is expressed as a sum of the dissipating mechanisms such as the shear viscosity of the water and the shear viscosity of the shell, q_i is the generalised coordinate system, and the overdot indicates the first time derivative. Let us consider an antibubble as presented in Figure 1, where R_1 and R_2 are the instantaneous radii from the centre of the bubble to the two interfaces of the shell, and R_d is the radius of the droplet core inside the bubble. As the liquid droplet core can be considered incompressible, R_d is constant when the bubble undergoes oscillations and translation. The shell and the surrounding liquid are assumed incompressible, too. From these assumptions, L and F are found, and subsequently substituted into (1).

2.1. Kinetic energy

The kinetic energy T of the dynamic antibubble system is given by

$$T = \frac{1}{2} m_\mathrm{b} \dot{x}^2 + T_\mathrm{L} + T_\mathrm{S} \,, \tag{2}$$

where T_L is the kinetic energy of the liquid surrounding the antibubble and T_S is the kinetic energy of the shell, and $m_\mathrm{b} = \frac{4}{3}\pi R_\mathrm{d}^3 \rho_\mathrm{L} + \frac{4}{3}\pi \left(R_{10}^3 - R_\mathrm{d}^3\right) \rho_\mathrm{g}$ is the sum of the mass of the core

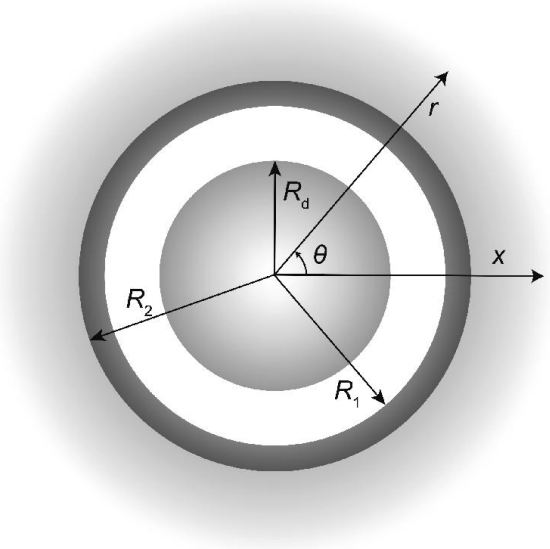

Fig. 1. Schematic of a fluid (opaque grey) containing an antibubble consisting of a droplet core (grey) of radius R_d, surrounded by a gas layer (white), and a thin shell (dark grey) of inner radius R_1 and outer radius R_2. The antibubble is initially centred in the two respective coordinate systems used in this paper.

and the mass of the gas inside the bubble, in which ρ_L is the is the density of the liquid outside and inside the antibubble, R_{10} is the initial inner radius, and ρ_g is the density of the gas layer of the antibubble. The kinetic energy of an incompressible liquid is the following integral over volume V [6]:

$$T_\mathrm{L} = \frac{\rho_\mathrm{L}}{2} \int_V |\nabla\varphi|^2 \,\mathrm{d}V \,, \tag{3}$$

where φ is the velocity potential of the liquid surrounding the bubble. We introduce a spherical coordinate system (r, θ, ϕ) that always has its origin in the centre of the antibubble. The centre of the antibubble is allowed to move exlusively in x-direction. The boundary condition at the surface $r = R_2$ is

$$\frac{\partial\varphi}{\partial r} = \dot{R}_2 + \dot{x}\cos\theta \,. \tag{4}$$

The velocity potential, which must satisfy Laplace's equation $\nabla^2\varphi = 0$, has the form

$$\varphi = \frac{a}{r} + \frac{b\cos\theta}{r^2} \,. \tag{5}$$

For the following functions a and b, (4) and (5) hold:

$$a(t) = -\dot{R}_1 R_1^2 \,, \qquad b(t) = -\frac{\dot{x} R_1^2}{2} \,. \tag{6}$$

Substituting (4) into (3), the kinetic energy of the incompressible surrounding fluid is given by

$$T_{\mathrm{L}} = 2\pi\rho_{\mathrm{L}} R_2^3 \left(\dot{R}_2^2 + \frac{\dot{x}}{6}\right) . \tag{7}$$

When assuming an incompressible fluid, the damping due to acoustic radiation from the oscillating bubble cannot be accounted for. However, this problem can be overcome if we assume a weakly compressible fluid, as elegantly demonstrated in [7]. Considering the kinetic energy of the shell, the deformation of the shell is assumed negligible while the antibubble undergoes oscillations and translation. In this case, the volume of the shell V_{S} is constant, and the velocity inside the shell $v_{\mathrm{S}} = R_1^2 \dot{R}_1 / r$. The assumption of an incompressible shell means that

$$R_2^3 - R_1^3 = {R_{20}}^3 - {R_{10}}^3 , \tag{8}$$

and

$$R_1^2 \dot{R}_1 = R_2^2 \dot{R}_2 , \tag{9}$$

where R_{20} is the initial outer resting radius. Thus, the kinetic energy of the incompressible shell can be written as

$$T_{\mathrm{S}} = \frac{1}{2} \int_{V_{\mathrm{S}}} \rho_{\mathrm{S}} \, {v_{\mathrm{S}}}^2 \, \mathrm{d}V_{\mathrm{S}} = 2\pi\rho_{\mathrm{S}} R_1^3 \dot{R}_1^2 \left(1 - \frac{R_1}{R_2}\right) , \tag{10}$$

where ρ_{S} is the density of the shell.

2.2. Potential energy

The potential energy U of the antibubble system is given by

$$U = U_{\mathrm{g}} + U_\sigma + U_{\mathrm{X}} , \tag{11}$$

where U_{g} is the potential energy of the gas inside the antibubble, U_σ is the potential energy owing to surface tensions at the gas–shell and shell–liquid interface, and U_{X} is the work done by the external pressure on the outer surface of the shell. Let us consider a pressure change in the surrounding fluid under adiabatic conditions. For an ideal gas, the potential energy of the gas inside the antibubble is

$$U_{\mathrm{g}} = \frac{p_{\mathrm{g}} V}{\gamma - 1} , \tag{12}$$

where p_{g} is the instantaneous pressure inside the antibubble, $V = \frac{4}{3}\pi \left(R_1^3 - R_{\mathrm{d}}^3\right)$ is the instantaneous gas volume inside the antibubble, and γ is the polytropic exponent of the gas. Using that $p_{\mathrm{g}}/p_{\mathrm{g0}} = (V_0/V)^\gamma$, in which p_{g0} is the initial gas pressure inside the antibubble at rest and V_0 is the initial gas volume inside the antibubble at rest, the potential energy of the gas inside the antibubble can be written as

$$U_{\mathrm{g}} = \frac{p_{\mathrm{g0}} V_{\mathrm{g0}}}{\gamma - 1} \left(\frac{{R_{10}}^3 - R_{\mathrm{d}}^3}{R_1^3 - R_{\mathrm{d}}^3}\right)^{(\gamma-1)} , \tag{13}$$

where

$$p_{\mathrm{g0}} = p_0 + \frac{2\sigma_1}{R_{10}} , \tag{14}$$

where p_0 is the ambient pressure and σ_1 is the surface tension of the gas–shell interface. The potential energy owing to surface tensions at the gas–shell and shell–liquid interface is given by

$$U_\sigma = 4\pi R_1^2 \sigma_1 + 4\pi R_2^2 \sigma_2 \ , \tag{15}$$

where σ_2 is the surface tension of the shell–liquid interface. The work done by the external pressure on the outer surface of the shell is given by

$$U_{\mathrm{X}} = \frac{4\pi}{3} R_2^3 \left(p_0 + P\right) \ , \tag{16}$$

where $P(x,t)$ is the driving pressure function.

2.3. Dissipative function

Energy is dissipated as the antibubble oscillates and translates in the surrounding fluid. The total dissipation is given by

$$F = F_{\mathrm{L}} + F_{\mathrm{S}} = \int_{V_{\mathrm{L}}} f_{\mathrm{L}} \, \mathrm{d}V + \int_{V_{\mathrm{S}}} f_{\mathrm{S}} \, \mathrm{d}V \ , \tag{17}$$

where F_{L} and F_{S} are the dissipative functions of the viscous fluid and the shell, respectively, f_{L} and f_{S} are the respective density functions of the dissipative functions, and V_{L} is the volume of the fluid outside the bubble. For the surrounding fluid, f_{L} is given by [8]

$$f_{\mathrm{L}} = \eta_{\mathrm{L}} \left(v_{ij} - \frac{1}{3} \, \delta_{ij} \, v_{kk} \right)^2 + \frac{1}{2} \, \zeta_{\mathrm{L}} \, {v_{kk}}^2 \ , \tag{18}$$

where η_{L} is the shear viscosity of the fluid, ζ_{L} is the bulk viscosity of the liquid, δ_{ij} is the Kronecker delta, and v_{ij} is the rate-of-strain tensor of the surrounding fluid, which is given by [5]

$$v_{ij} = \frac{1}{2} \left(\frac{\partial v_i}{\partial x_j} + \frac{\partial v_j}{\partial x_i} \right) \ , \tag{19}$$

where $v_{i,j,k}$ is the liquid velocity. Assuming an incompressible surrounding fluid, $v_{kk} = \vec{\nabla} \cdot \vec{v} = 0$. Hence, (18) is simplified to

$$f_{\mathrm{L}} = \eta_{\mathrm{L}} \left(v_{ij} \right)^2 \ , \tag{20}$$

where v_{ij} is given by [5]

$$\begin{aligned} \left(v_{ij} \right)^2 = & \frac{6 R_2^4 \dot{R}_2^2}{r^6} + \frac{9 R_2^6 \dot{x}^2}{8 r^8} + \frac{9 R_2^2 \dot{R}_2 \dot{x}}{r^4} \left(\frac{R_2}{r} - \frac{R_2^3}{r^3} \right) \cos\theta \\ & + \frac{\dot{x}^2}{8} \left(\frac{27 R_2^2}{r^4} - \frac{54 R_2^4}{r^6} + \frac{18 R_2^6}{r^8} \right) \cos^2\theta \ . \end{aligned} \tag{21}$$

Substitution of (25) into (20) and subsequent integration over V_{L}, yields the dissipative function for the liquid

$$F_{\mathrm{L}} = 8\pi \eta_{\mathrm{L}} R_2 \dot{R}_2^2 + 3\pi \eta_{\mathrm{L}} R_2 \dot{x}^2 \ . \tag{22}$$

Finally, the dissipation function F_{S} for the viscous shell is the missing piece of the puzzle. For f_{S} we have [5, 8]

$$f_{\mathrm{S}} = \eta_{\mathrm{S}}(v_{ij})^2 = \eta_{\mathrm{S}} \left[\left(\frac{\partial v_{\mathrm{S}}}{\partial r} \right)^2 + \frac{2v_{\mathrm{S}}^2}{r^2} \right] , \tag{23}$$

where $v_{\mathrm{S}} = R_1^2 \dot{R}_1 / r^2$ is the radial velocity in the shell. Now, integrating (23) over V_{S} results in

$$F_{\mathrm{S}} = 8\pi \eta_{\mathrm{S}} \left({R_{20}}^3 - {R_{10}}^3 \right) \frac{R_1 \dot{R}_1^2}{R_2^3} . \tag{24}$$

2.4. General Rayleigh-Plesset equation for a fluid shell

The expressions derived in the sections above for the respective kinetic energies, potential energies and the dissipative functions, or more specifically the translational kinetic energy of the antibubble (2), the kinetic energy of incompressible surrounding fluid (7), the kinetic energy of the shell (10), the potential energy of the gas (13), the potential energy of the surface-free energy (15), the potential energy from the work done on the antibubble by the external pressure on the outer surface of the bubble (16), the dissipative function for the liquid (22), and the dissipative function for the shell (24) are now combined to express L and F, respectively. Substituting the resulting expressions into (1), where R_1 and x are the generalised coordinates, whilst (8) and (9) are used to express R_2 in terms of R_1, a set of coupled second order differential equations is obtained that describe the radial and translational dynamics of an antibubble with a fluid shell of finite shell thickness.

Studying the equations above, it can be recognized that modelling the shell as a fluid is not a complex operation to achieve. For a fluid shell, the dissipative function F_{S} for the shell is left undefined. It can now be shown that a set of equations, which are general, governing the radial and translation dynamics of an antibubble with a fluid shell can be obtained, albeit with some skill and cunning, eventually resulting in an equation set consisting of a Rayleigh-Plesset-like equation, and a translational equation:

$$\begin{aligned} R_1 \ddot{R}_1 \left[1 + \left(\frac{\rho_{\mathrm{L}} - \rho_{\mathrm{S}}}{\rho_{\mathrm{S}}} \right) \frac{R_1}{R_2} \right] + \dot{R}_1^2 \left[\frac{3}{2} + \left(\frac{\rho_{\mathrm{L}} - \rho_{\mathrm{S}}}{\rho_{\mathrm{S}}} \right) \left(\frac{4R_2^3 - R_1^3}{2R_2^3} \right) \frac{R_1}{R_2} \right] \\ = \frac{\rho_{\mathrm{L}}}{\rho_{\mathrm{S}}} \frac{\dot{x}^2}{4} + \frac{1}{\rho_{\mathrm{S}}} \left[p_{\mathrm{g0}} \left(\frac{{R_{10}}^3 - R_{\mathrm{d}}^3}{R_1^3 - R_{\mathrm{d}}^3} \right)^{\gamma} - \frac{2\sigma_1}{R_1} - \frac{2\sigma_2}{R_2} - p_0 - P(x,t) \right. \\ \left. - 4\eta_{\mathrm{L}} \frac{R_1^2}{R_2^3} \dot{R}_1 + S \right] , \end{aligned} \tag{25}$$

and

$$m_{\mathrm{b}} \ddot{x} + \frac{2\pi}{3} \rho_{\mathrm{L}} \frac{\mathrm{d}}{\mathrm{d}t} \left(R_2^3 \dot{x} \right) = -\frac{4\pi}{3} R_2^3 \frac{\partial}{\partial x} P(x,t) + F_{\mathrm{d}} , \tag{26}$$

where F_{d} is the drag force, and S describes the radial stress in the shell, which can be represented by

$$S = 3 \int_{R_1}^{R_2} \frac{\tau_{rr}^{(\mathrm{S})}(r,t)}{r} \mathrm{d}r , \tag{27}$$

where $\tau_{rr}^{(\mathrm{S})}$ is the radial tension function of the shell.

The rheological law suitable for the shell of a particular antibubble can now be applied. For a Newtonian fluid shell, the radial stress in the shell is given by

$$S = -4\eta_{\mathrm{S}} \frac{\dot{R}_1 \left({R_{20}}^3 - {R_{10}}^3 \right)}{R_1 R_2^3} \,. \tag{28}$$

For a Maxwell fluid shell, the radial stress in the shell is given by

$$S = -4\eta_{\mathrm{S}} \frac{D \left({R_{20}}^3 - {R_{10}}^3 \right)}{R_1^3 R_2^3} \,, \tag{29}$$

where $D(t) = -\lambda \dot{D}(t) + R_1^2 \dot{R}_1$, in which λ is the relaxation time.

2.5. Zero-thickness approximation

For antibubbles with a thin shell, *i.e.*, $R_{\mathrm{S}} \equiv (R_2 - R_1) \ll R_1$, we can model the dynamics in first order without considering the correction for a finite shell. This can be done without a tangible loss of numerical accuracy. We may take the unrestrained radius equal to R_0, $\rho_{\mathrm{S}} \Rightarrow \rho_L$, $R_2 \Rightarrow R_1$, and $\sigma = \sigma_1 + \sigma_2$. Both the Newtonian and Maxwell shell models can now be represented with their respective zero-thickness approximation.

For a Newtonian fluid shell, the zero-thickness approximation is

$$R\ddot{R} + \frac{3}{2}\dot{R}^2 = \frac{\dot{x}}{4} + \frac{1}{\rho_{\mathrm{L}}} \left[p_{\mathrm{g}0} \left(\frac{R_0^3 - R_{\mathrm{d}}^3}{R^3 - R_{\mathrm{d}}^3} \right)^{\gamma} - \frac{2\sigma}{R} - p_0 - P(x,t) - 4\eta_{\mathrm{L}} \frac{\dot{R}}{R} \right. \\ \left. -12\eta_{\mathrm{S}} R_{\mathrm{S}} \frac{\dot{R}}{R^2} \right] \,, \tag{30}$$

whereas, for a Maxwell fluid shell, the zero-thickness approximation is

$$R\ddot{R} + \frac{3}{2}\dot{R}^2 = \frac{\dot{x}}{4} + \frac{1}{\rho_{\mathrm{L}}} \left[p_{\mathrm{g}0} \left(\frac{R_0^3 - R_{\mathrm{d}}^3}{R^3 - R_{\mathrm{d}}^3} \right)^{\gamma} - \frac{2\sigma}{R} - p_0 - P(x,t) - 4\eta_{\mathrm{L}} \frac{\dot{R}}{R} \right. \\ \left. -12\eta_{\mathrm{S}} R_{\mathrm{S}} D \frac{\dot{R}}{R^4} \right] \,. \tag{31}$$

2.6. Linear analysis for an encapsulated antibubble

By linearisation of the respective models derived in the previous sections, we seek to understand underlying the mechanisms of oscillation. In this section, we illustrate the linearised versions' explicit expressions for the individual damping mechanisms, the linear natural resonance frequency, the second-order natural resonance frequency, and the damped linear resonance frequency for a finite thickness Maxwell shell. The damped linear resonance frequency is presented both with and without damping from reradiation.

For a small excursion $|x|$ of an antibubble where $|x| \ll R_{10}$, an analytical solution exists of the Rayleigh-Plesset-like equation (25), incorporating the radial stress of a Maxwell fluid shell (29). The small amplitude solution must satisfy

$$R_1 = R_{10} + x(t) \tag{32}$$

and

$$R_2 = R_{20} + \frac{{R_{10}}^2}{{R_{20}}^2} x(t) \; . \tag{33}$$

The coupling to the translational dynamics is also disregarded.

Now, the linearised version of $D(t)$ can be expressed as

$$\dot{D} + \frac{1}{\lambda} D = \frac{{R_{10}}^2}{\lambda} \dot{x} \tag{34}$$

Taking $P(t) = P_{\mathrm{a}} \exp(i\omega t)$, in which P_{a} is the pressure amplitude, a solution of (34) has the form

$$D(t) = ax + b\dot{x} \; . \tag{35}$$

When substituting (35) into (34), the constants a and b are found:

$$a = \frac{\lambda\, \omega^2 {R_{10}}^2}{1 + (\lambda\, \omega)^2} \; , \qquad b = \frac{{R_{10}}^2}{1 + (\lambda\, \omega)^2} \; . \tag{36}$$

After substitution of (32) and (34) into (25), the resulting linearised equation can be written as:

$$\ddot{x} + \delta_{\mathrm{M}}\, \dot{x} + \left(\omega_0^{\mathrm{M}}\right)^2 x = -\frac{P(t)}{\alpha\, \rho_{\mathrm{S}}\, R_{10}} \; , \tag{37}$$

where δ_{M} is the sum of the respective damping terms $\delta_{\mathrm{M}} = \delta_{\mathrm{L}} + \delta_{\mathrm{S}}^{\mathrm{M}}$, in which δ_{L} represents the damping from the viscous surrounding fluid and $\delta_{\mathrm{S}}^{\mathrm{M}}$ represents the damping from the Maxwell fluid shell, ω_0^{M} is the linear resonance frequency, and α is a coefficient related to the density difference between the shell and the surrounding liquid

$$\alpha = 1 - \left(1 - \frac{\rho_{\mathrm{L}}}{\rho_{\mathrm{S}}}\right) \frac{R_{10}}{R_{20}} \; . \tag{38}$$

The damping from the surrounding fluid can be expressed as

$$\delta_{\mathrm{L}} = \frac{4\, \eta_{\mathrm{L}}\, R_{10}}{\alpha\, \rho_{\mathrm{S}}\, {R_{20}}^3} \; , \tag{39}$$

whereas the damping from the Maxwell fluid shell can be expressed as

$$\delta_{\mathrm{S}}^{\mathrm{M}} = \frac{4\, \eta_{\mathrm{S}}\, \left({R_{20}}^3 - {R_{10}}^3\right)}{\alpha\, \rho_{\mathrm{S}}\, {R_{10}}^2\, {R_{20}}^3\, [1 + (\lambda\, \omega)^2]} \; . \tag{40}$$

The linear resonance frequency is given by

$$\left(\omega_0^{\mathrm{M}}\right)^2 = \omega_0^2 + \lambda\, \omega^2\, \delta_{\mathrm{S}}^{\mathrm{M}} \; , \tag{41}$$

where ω_0 is the linear natural resonance frequency of an antibubble with a fluid shell:

$$\omega_0^2 = \frac{1}{\alpha\, \rho_{\mathrm{S}}\, {R_{10}}^2} \left[p_{\mathrm{g0}} \frac{3\gamma}{1 - \left(\frac{R_{\mathrm{d}}}{R_0}\right)^3} - \frac{2\sigma_1}{R_{10}} - \frac{2\sigma_2 {R_{10}}^3}{{R_{20}}^4} \right] \; . \tag{42}$$

From (41), it can be observed that the linear resonance frequency is dependent on ω, which is slightly unconventional [9]. However, it is not of major concern, because a damped system resonates with the linear damped resonance frequency when excited. To assess the linear damped, *i.e.*, the "real", resonance frequency of (37), one studies a solution of the equation given by

$$x(t) = A e^{i(\omega t + \psi)} \,, \tag{43}$$

in which the phase ψ between the radial excursion and the acoustic excitation is

$$\psi = \arctan\left[\frac{\omega\ \delta_{\mathrm{M}}}{\omega^2 - \left(\omega_0^{\mathrm{M}}\right)^2}\right] \,, \tag{44}$$

and the amplitude A is

$$A = \frac{P_{\mathrm{a}}\, Q}{\alpha\ \rho_{\mathrm{S}}\ R_{10}\ {\omega_0}^2} \,, \tag{45}$$

in which the Q-value of the antibubble $Q(\omega)$ is

$$Q(\omega) = \frac{{\omega_0}^2}{\sqrt{\left[\omega^2 - \left(\omega_0^{\mathrm{M}}\right)^2\right]^2 + \omega^2 {\delta_{\mathrm{M}}}^2}} \,. \tag{46}$$

The maximum value of (46) is the linear damped resonance frequency, which can be computed numerically.

From the linear resonance frequency for a Maxwell fluid shell, we can find the resonance frequency for a Newtonian fluid shell ω_0^{N}. Let us take $\lambda = 0$, $\delta_{\mathrm{N}} = \delta_{\mathrm{M}}$, in which δ_{N} is the total damping for an antibubble with a Newtonian fluid shell. Knowing that the linear damped resonance frequency for a Newtonian fluid shell must satisfy $\left(\omega_0^{\mathrm{N}}\right)^2 = \omega_0^2 - {\delta_{\mathrm{N}}}^2/4$, it can be rewritten as

$$\left(\omega_0^{\mathrm{N}}\right)^2 = \frac{1}{\alpha \rho_{\mathrm{S}} {R_{10}}^2}\left[\frac{3\gamma p_{\mathrm{g0}}}{1 - \left(\frac{R_{\mathrm{d}}}{R_0}\right)^3} - \frac{2\sigma_1}{R_{10}} - \frac{2\sigma_2 {R_{10}}^3}{{R_{20}}^4} - \frac{4{\eta_{\mathrm{L}}}^2 {R_{10}}^4}{\alpha \rho_{\mathrm{S}} {R_{20}}^6} - \frac{4{\eta_{\mathrm{S}}}^2\left({R_{20}}^3 - {R_{10}}^3\right)^2}{\alpha \rho_{\mathrm{S}} {R_{10}}^2 {R_{20}}^6}\right] \,. \tag{47}$$

3. Example

An example of two radius–time curves of an oscillating antibubble is shown in Figure 2. The curves are numerical solutions of (30), computed with the ode45 algorithm of MATLAB® (The MathWorks, Inc., Natick, MA, USA). Droplet core sizes were chosen 40% and 80% or the resting radius, respectively.

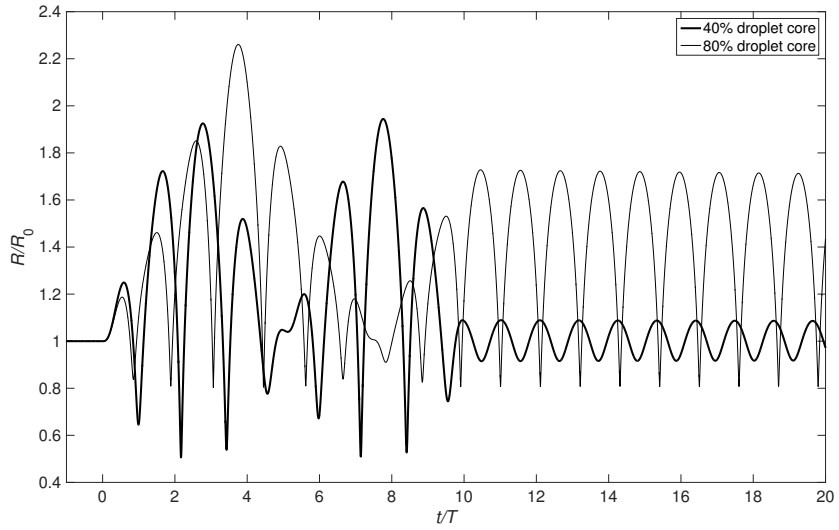

Fig. 2. Radius–time curves of an antibubble with a Newtonian shell.

The instantaneous radius has been normalised by the initial resting radius, and the time has been normalised by the period of the excitation pulse. An ambient pressure of $p_0 = 30\,\text{atm}$, representing subsea conditions, was chosen. Other relevant parameters used were $P_\text{a} = 2\,\text{MPa}$, $R_0 = 100\,\mu\text{m}$, $R_\text{S} = 2\,\text{nm}$, $\gamma = 1.4$, $\eta_\text{L} = 0.001\,\text{Pa s}$, $\eta_\text{S} = 50\,\text{Pa s}$, $\rho_\text{L} = 1054\,\text{kg m}^{-3}$, $\sigma = 0.072\,\text{N m}^{-1}$, and $\omega = 2\pi\,\text{rad}\times 200\,\text{kHz}$. Also, the coupling with (26) has been neglected here.

At the given excitation frequency, the antibubble excursions are clearly higher for the antibubble with the larger core. Especially, the asymmetric oscillation is worth noticing.

4. Conclusion

Using Lagrangian formalism, equations describing the spatio–temporal dynamics of antibubbles with a fluid shell have been derived, specifically for a Newtonian fluid shell and a Maxwell fluid shell. For both shell models, finite thickness shells and their zero-thickness approximations have been presented. The Newtonian fluid shell can be considered a special case of the Maxwell fluid shell. The equations have been linearised and the natural and damped resonance frequencies have been presented for both shell models.

References

[1] J. Moreno-Trejo, R. Kumar, T. Markeset, Mapping factors influencing the selection of subsea petroleum production systems: a case study, Int. J. Syst. Assur. Eng. Manag., vol. 3, no. 1, pp. 6–16, 2012.

[2] J. Blackford, H. Stahl, Preface to the QICS special issue, Int. J. Greenhouse Gas Control, vol. 38, p. 1, 2015.

[3] T.G. Leighton, P.R. White, Quantification of undersea gas leaks from carbon capture and storage facilities, from pipelines and from methane seeps, by their acoustic emissions, Proc. Roy. Soc. A, vol. 468, pp. 485–510, 2012.

[4] K. Johansen, S. Kotopoulis, M. Postema, Ultrasonically driven antibubbles encapsulated by Newtonian fluids for active leakage detection, Lect. Notes in Eng. Comp. Sci., vol. 2216, pp. 750–754, 2015.

[5] A. A. Doinikov, P. A. Dayton, Spatio-temporal dynamics of an encapsulated gas bubble in an ultrasound field, J. Acoust. Soc. Am., vol. 120, no. 2, pp. 661–669, 2006.

[6] A. A. Doinikov, Translational motion of a spherical bubble in an acoustic standing wave of high intensity, Phys. Fluids, vol. 14, no. 4, pp. 1420–1425, 2002.

[7] A. A. Doinikov, Equations of coupled radial and translational motions of a bubble in a weakly compressible liquid, Phys. Fluids, vol. 17, no. 12, pp. 128101-1–128101-4, 2005.

[8] L. Landau, E. Lifshitz, Theory of Elasticity, Pergamon, Oxford, 1986.

[9] A. A. Doinikov, P. A. Dayton, Maxwell rheological model for lipid-shelled ultrasound microbubble contrast agents., J. Acoust. Soc. Am., vol. 121, no. 6, pp. 3331–3340, 2007.

III.2 Système expérimental

Le traitement du cancer peut être simplifié quand les cellules malignes répondent directement aux ultrasons. Dans ce cas, on doit trouver les conditions acoustiques pour lesquelles des cellules spécifiques peuvent être lysées.

Le système expérimental pour ce but a été décrit dans la demande de brevet « Device for the identification, separation and/or cell type-specific manipulation of at least one cell of a cellular system » (p. 134). [3]

Ensemble avec M. Thomas Walther, je construirerai un système similaire, présenté dans la Figure 2, qui se dirige vers les cellules individuelles et s'attaque à celles ci. Les chaînes microfluides permettent les passages des cellules individuelles.

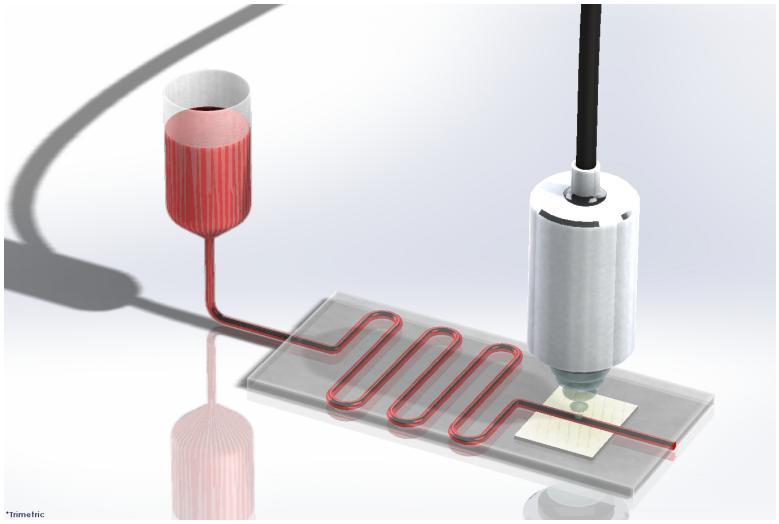

Figure 2 : Schématique d'un système expérimental pour détecter et manipuler des cellules individuelles. Le fluide (rouge) passe par une chaîne microfluide ; puis, les cellules individuelles sont sonifiées par un transducteur focalisé (métallique). Un hydrophone à large bande (jaune) détecte des signaux harmoniques des cellules.

En utilisant des transducteurs ultrasonores à bande étroite, on peut déterminer la fréquence de résonance des cellules spécifiques. Le but ultime est d'éliminer certaines cellules malignes, sans perturber les autres cellules.

3. Walther T, Postema M. Device for the identification, separation and/or cell type-specific manipulation of at least one cell of a cellular system. United States Patent Application US 2016/0060615 A1.

US 20160060615A1

(19) **United States**

(12) **Patent Application Publication**

Walther et al.

(10) **Pub. No.: US 2016/0060615 A1**

(43) **Pub. Date: Mar. 3, 2016**

(54) **DEVICE FOR THE IDENTIFICATION, SEPARATION AND / OR CELL TYPE-SPECIFIC MANIPULATION OF AT LEAST ONE CELL OF A CELLULAR SYSTEM**

(71) Applicants: **Thomas Walther**, Cork (IE); **Michiel Postema**, Bergschenhoek (NL)

(72) Inventors: **Thomas Walther**, Cork (IE); **Michiel Postema**, Bergschenhoek (NL)

(21) Appl. No.: **14/476,187**

(22) Filed: **Sep. 3, 2014**

Publication Classification

(51) **Int. Cl.**

C12N 13/00	(2006.01)
C12M 1/42	(2006.01)
C12M 1/00	(2006.01)
C12M 1/34	(2006.01)
C12N 5/073	(2006.01)
C12N 5/071	(2006.01)

(52) **U.S. Cl.**

CPC ***C12N 13/00*** (2013.01); ***C12N 5/0603*** (2013.01); ***C12N 5/0686*** (2013.01); ***C12M 47/04*** (2013.01); ***C12M 47/02*** (2013.01); ***C12M 41/46*** (2013.01); ***C12M 35/04*** (2013.01); *C12N 2521/10* (2013.01)

(57) **ABSTRACT**

The invention, in part, relates to devices for the identification, separation, and/or cell type-specific manipulation of at least one cell of a cellular system.

Figure 1

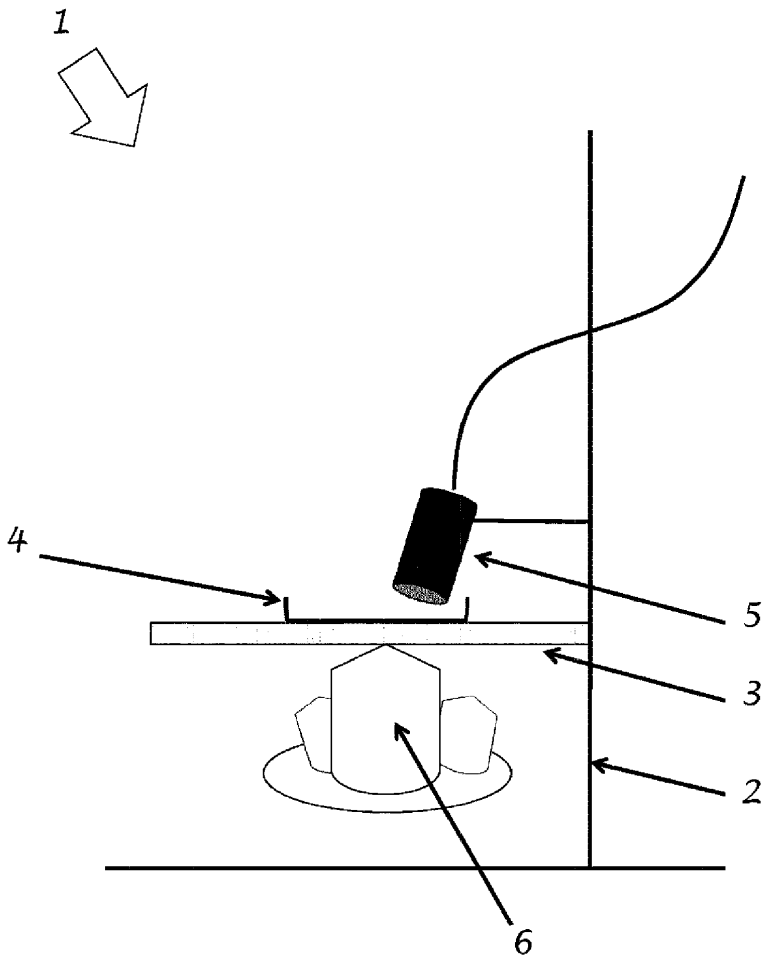

Figure 2

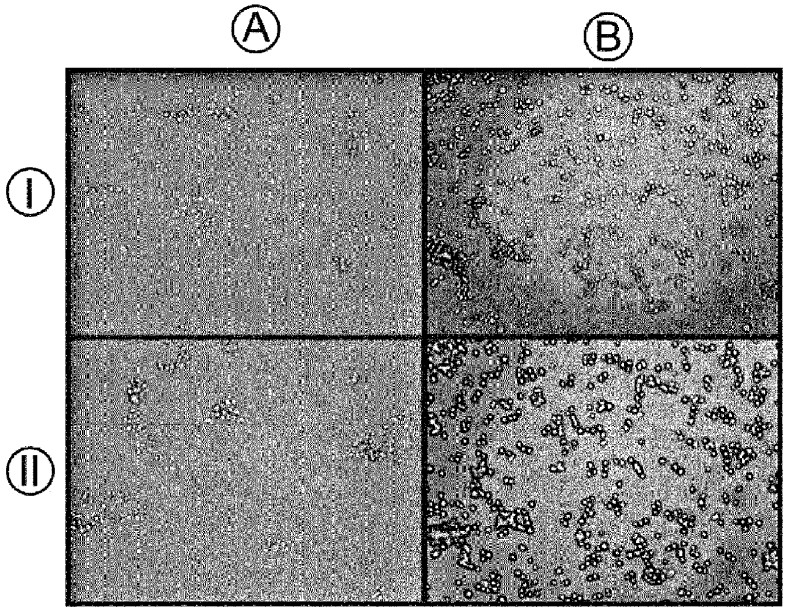

US 2016/0060615 A1 Mar. 3, 2016

DEVICE FOR THE IDENTIFICATION, SEPARATION AND / OR CELL TYPE-SPECIFIC MANIPULATION OF AT LEAST ONE CELL OF A CELLULAR SYSTEM

TECHNICAL FIELD

[0001] The invention relates to devices for the identification, separation and/or cell type-specific manipulation of at least one cell of a cellular system.

BACKGROUND OF THE INVENTION

[0002] Cell cultures play a major role in many areas of the life sciences, especially in biotechnology and biomedical research. Cell cultures are used in the diagnosis and treatment of a variety of diseases, both in humans and in animals. Due to the growing reservations about animal testing, the establishment of biologically relevant in vitro test systems, and thus cell cultures, is becoming more important. Primary cells are the basis for the development of complex in vitro models and test methods (assays) and therefore offer an excellent alternative to animal testing. The preparation of primary cultures from a tissue sample as well as their further cultivation for experimental purposes represents a major challenge.

[0003] For this purpose, the cell type-specific separation of the cells is of crucial importance in order to obtain clean primary cell cultures. In the current state of the art, the cells must be separated by flow cytometry. A disadvantage of this technique is that the specific cells must be selectively stained, for example with fluorescent dyes, which is not always possible so that the cells cannot be distinguished from each other. A further possibility consists in the selection of cells by specific and labelled antibodies. However, for many cell types, no specific antibodies are available. This method is also very time consuming and costly. Furthermore, this method cannot be employed for cells which are not free-floating in a cell culture. This is especially true for cells in a multi-cell system, as a tissue, organ, or multicell system. Different cell types can be sorted by morphological studies. However, this method depends very much on the skill and the experience of the person who performs this separation. Furthermore, this method is extremely time-consuming. The cells themselves must be removed from the multi-cell system, so that the sterile cell culture conditions are compromised. In organisms, this kind of manipulations is often not feasible without fatally damaging the organism.

[0004] It is known that particles or particles in a liquid, e.g. encapsulated microbubbles, have a different resonance frequency in sonication waves than free gas bubbles in the liquid, and can be therefore discriminated (Postema M. Fundamentals of Medical Ultrasonics. Spon Press, London, 2011). Based on their acoustic properties, microbubbles are also suitable as ultrasound contrast agent for applications such as diagnostic imaging. Here, particles with same acoustic properties attract each other, while particles with different acoustic properties repel each other. The mutual attraction of particles with same acoustic properties can lead to the fusion of such micro gas bubbles. This phenomenon can be explained by the secondary Bjerknes forces.

[0005] The publication Kotopoulis S., Postema M. Microfoam formation in a capillary. Ultrasonics 2010; 50:206-268 describes the formation of a microfoam through the manipulation of microbubbles with ultrasound. Due to the excitation of microbubbles with ultrasound, the individual micro gas bubbles begin to attract and in this way form a cluster consisting of micro gas bubbles. This happens immediately, already in the first second of the action of ultrasound. If the thus formed microbubbles clusters continue to be exposed to the ultrasound, than the resulting clusters begin to form larger clusters arranged together and thus form a micro-foam. As long as the micro-foam for annealed clusters is in the ultrasonic wave field, the clusters behave as a unit.

[0006] Furthermore, the publication Jönsson H., C. Holm, A. Nilsson, F. Petersson, P. Johnsson, Laurell T. *Ultrasound can radically reduce embolic load to brain after cardiac surgery*. Ann. Thorac. Surg. 2004; 78:1572-1578 demonstrates the separation of particles in liquids using acoustic standing waves. In a specific example it is shown how lipid particles may be separated and removed by means of ultrasound from blood and other present compartments (plasma, blood cell, sugar, etc.). This allows the prevention of microemboli caused by increased lipid content in the blood and especially those that occur after cardiac surgery (bypass surgery).

[0007] Each cell type and any microorganism should have a specific acoustic behavior, which depends on its compressibility, density, and geometry. Each cell type or microorganism thus responds most strongly to a characteristic sound frequency. This characteristic sound frequency is referred to as its specific resonance frequency. If a cell is exposed to a sound wave of its specific resonant frequency, the cell responds with a dynamic signal in the form of an oscillation. However, if a certain amplitude of this resonant frequency is exceeded, the cell or microorganism can vibrate so strongly that it is destroyed. The publication Delalande A., Kotopoulis S., Rovers T., Pichon C., Postema M. Sonoporation at low mechanical index. Bubble Science, Engineering and Technology 2011; 3:3-11 shows the acoustic activity of certain cancer cells.

[0008] WO 01/00084 A1 discloses an apparatus and method for non-invasive destruction of (tumor) tissue by treatment of the tissue with acoustic shock waves generated by predetermined frequencies. These shock waves cause only the seriously degenerated tissue to vibrate, thus protecting the surrounding tissue. The amplitude of the corresponding shock wave is so high that the mechanical friction in the tissue is high enough for the destruction of cells by cavitation and heating. The down side is that all the irradiated cells are destroyed. Furthermore, the shock waves penetrate deep into the tissue which can also be damaged.

[0009] U.S. Pat. No. 6,406,429 discloses an apparatus and a method for non-invasive detection of cystic structures and precursors of cancer cells in all tissues by ultrasonic waves. It is an imaging technique. Methods for the elimination of individual cell types are not disclosed.

[0010] The publication Kotopoulis S., A. Schommartz, Postema M. Sonic cracking of blue-green algae. Applied Acoustics 2009; 70:1306-1312 describes how ultrasonic waves of frequency, as used in the clinical diagnostic range (200 kHz to 2.2 MHz) can be used to destroy the heterocysts in blue-green algae (cyanobacteria). The irradiated algae, which now lack their buoyancy units, begin to sediment. The sedimented algae continue to have perfectly intact chloroplasts, which remain unaffected by the action of ultrasound. It is therefore possible to manipulate or destroy specific cells with ultrasound, while other cell types in the environment are not affected.

[0011] The object of the invention is therefore to provide an apparatus and a method for the identification, separation and/or cell type-specific manipulation (Sonopulation) of at least one cell of a cellular system as well as of microorganisms. Said manipulation can also comprise the selective killing of cells, at least one cell of a cellular system, as well as of microorganisms without compromising the sterile cell culture conditions or having to remove the cells from the cell system.

SUMMARY OF THE INVENTION

[0012] According to one aspect of the invention, a device (**1**) for the identification, separation and/or cell type-specific manipulation of at least one cell of a cellular system as well as of microorganisms, is provided. The device (**1**) includes an ultrasound transmitter (**5**), a control unit (**2**) and a receiving unit (**3**), wherein the ultrasound transmitter (**5**) includes a piezo-electric component, which is controlled with a frequency greater than 5 MHz, and has a narrow bandwidth. In some embodiments, the piezoelectric member is a piezoelectric crystal, a piezoelectric ceramic or a piezoelectric polymer. In some embodiments, the piezoelectric component has a resonance of 7 MHz per millimeter. In some embodiments, the piezoelectric component is a wafer which is cut in an orientation of 36° to the Y-axis of a lithium niobate ($LiNbO_3$) crystalline lattice. In some embodiments, the control unit (**2**) has a magnification lens (**6**), and comprises a binocular or an inverted microscope. In some embodiments, the receiving unit (**3**) is a cell culture dish, petri dish (**4**) or the like.

[0013] According to another aspect of the invention, methods for one or more of the identification, separation and cell type-specific manipulation of at least one cell of a cellular system as well as of microorganisms with any embodiment of an aforementioned device (**1**) are provided. The methods include steps of a) introducing the cell system into the receiving unit (**3**) of the device (**1**), and sonicating the cell system with the Ultrasound transmitter (**5**) with a cell type-specific frequency. In some embodiments, the method further comprises at least one of the following steps: c) distinguishing and sorting of cells of the multi-cell system or the cell system in primary cell cultures; d) creating a resonance profile for the sonicated cells of the multi-cell system or the cell system; e) transforming the sonicated cells of the multi-cell system or the cell system; f) transfecting the sonicated cells of the multi-cell system or the cell system; g) discriminating the cells of the multi-cell system or the cellular system based on their genotype, wherein the cells are sperm; h) isolating and destroying cells of the multi-cell system, or the cellular system, wherein the cells are viral or parasite bearing cells or tumor cells; i) acting on the cells of the multi-cell system, or the cellular system to prevent restenosis, where the cells are cells of the neointima; j) isolating and identifying different subpopulations within the multi-cell system or the cell system, the multi-cell system or the cell system comprising microorganisms in mixed populations; k) activating specific dendritic cells; and l) manipulating intracellular signalling.

[0014] According to yet another aspect of the invention, use of any embodiment of an aforementioned device (**1**) is provided for performing a method for the identification, separation and/or cell type-specific manipulation of at least one cell of a cellular system as well as of microorganisms, the method comprising the steps of: a) introducing the cell system into the receiving unit (**3**) of the device (**1**), and b) sonicating the cell system with the Ultrasound transmitter (**5**) with a cell type-specific frequency. In some embodiments, the method also includes at least one of the following steps: c) distinguishing and sorting of cells of the multi-cell system or the cell system in primary cell cultures; d) creating a resonance profile for the sonicated cells of the multi-cell system or the cell system; e) transforming the sonicated cells of the multi-cell system or the cell system; f) transfecting the sonicated cells of the multi-cell system or the cell system; g) discriminating the cells of the multi-cell system or the cellular system based on their genotype, wherein the cells are sperm; h) isolating and destroying cells of the multi-cell system, or the cellular system, wherein the cells are viral or parasite bearing cells or tumor cells; i) acting on the cells of the multi-cell system, or the cellular system to prevent restenosis, where the cells are cells of the neointima; j) isolating or identifying different sub-populations within the multi-cell system, or the cellular system, wherein the multi-cell system, or the cell system comprises microorganisms in mixed populations; k) activating specific dendritic cells; and l) manipulating intracellular signalling.

[0015] The invention provides a device for the identification, separation and/or cell type-specific manipulation of at least one cell of a cellular system as well as of microorganisms comprising a Ultrasound transmitter, a control unit and a receiving unit, wherein the Ultrasound transmitter comprises a piezo-electric component, which emits a controllable narrow-bandwidth frequency greater than 5 MHz.

[0016] With the device, a fast and convenient separation and identification of different cell types in a multi-cell system is made possible without damaging the individual cells or the sterile cell culture conditions. Removal of the individual cells of the multi-cell system is not necessarily required. This is very important especially for primary cell cultures. And manipulating (Sonopulation), such as transfection or transformation of individual cell types in a cell system or a multi-cell system can be performed in this way. With the control unit one can observe directly, when necessary, the success of this manipulation. Furthermore, this device can determine the resonant frequency of a particular cell type and precisely target this specific resonance frequency for cell type-specific manipulation. Particularly in cells that are infected with viruses or other parasites, this presents an opportunity to separate these cells from the cell culture and subsequently remove them or, if appropriate, to destroy these cells without affecting or damaging other cells.

[0017] In certain embodiments of the device according to the invention, the piezoelectric member is a piezoelectric crystal, a piezoelectric ceramic, or a piezoelectric polymer. The oldest and best known piezoelectric components for ultrasonic generation are piezoelectric crystals. This includes for example the stable a-quartz modification, lithium niobate or gallium orthophosphate. More piezo-electric crystals are berlinite, tourmalines and Seignette's salt. Piezoelectric ceramics include, for example, lead titanate (PT), lead zirconate titanate (PZT), bismuth titanate, barium titanate and lead metaniobate (PMN). The most widely used piezoelectric polymers include polyvinylidene fluoride (PVDF) or a copolymer of polyvinylidene fluoride and trifluoroethylene. Thus, the piezoelectric component can be optimally adapted to the required design or use and thus optimally adapted to the respective requirements (coupling factor, cross-coupling, acoustic impedance (acoustic impedance and bandwidth).

[0018] Furthermore, it is advantageous if the piezo-electric device has a resonance of 7 MHz per millimeter, so as to

obtain an optimum conversion of electrical signals to mechanical signals. Piezo-electric components with a specific resonance frequency show, when excited by a voltage at this resonant frequency, the highest amplitude of the generated ultrasound. Thus, the resonance frequency should be in the frequency range in which the ultrasonic frequency is needed. A large scatter of the resonance frequencies would mean a deterioration of the issued ultrasonic signal (sound pressure). However, other resonances of the piezo-electric device are also conceivable.

[0019] In a further advantageous embodiment, the piezoelectric component is a wafer which is cut into an orientation of 36° to the Y-axis of a lithium niobate ($LiNbO_3$) crystalline lattice. Lithium niobate is a piezoelectric crystal, which is not broken even at a high applied voltage, and thus is suitable for the generation of ultrasound in high frequency ranges (250 kHz to 40 MHz). Furthermore, lithium niobate has a very high resonance. In certain embodiments of the invention, the piezo-electric wafer is made of lithium niobate ($LiNbO_3$) and has a thickness of 0.5 mm and a diameter of 7.6 cm. Such wafers are provided by e.g. Boston Piezo-Optics. Inc., Boston, Mass., USA.

[0020] To study or observe the separation and/or cell type-specific manipulation of at least one cell of a cell system and micro-organisms, it is a great advantage if the control unit of the device according to the invention is a microscope with magnifying optics, which in certain embodiments of the invention may be a binocular inverted microscope. Thus, during irradiation of the sample with ultrasonics, the results can be checked immediately and the ultrasonic irradiation reduced to a minimum in order to exclude possible damage to other cells.

[0021] It is advantageous if the receiving unit is a support for a cell culture dish, petri dish, or the like. Especially then, the to be identified, separated or manipulated cells can be brought into the device, without taking them from their surrounding medium, whereby the sterile environment is maintained. Also a possibly harmful contact with air and oxygen can be excluded if the cells can remain in the nutrient medium. In particular for cell cultures, this can be beneficial as cell cultures are usually created in petri dishes. However, other sample types can also be easily and conveniently introduced into cell culture dishes or Petri dishes. Also the introduction of petri dishes into cell culture cabinets or incubators is possible.

[0022] In a method for the identification, separation and/or cell type-specific manipulation of at least one cell of a cellular system as well as of microorganisms with a device according to the invention, the invention provides that the method comprises the steps of

[0023] a) Introduction of the cell system into the receiving unit of the apparatus and

[0024] b) Sonication of the cell system with the Ultrasound transmitter with a cell type-specific frequency.

[0025] It is particularly advantageous when the method comprises at least one of the following steps

[0026] Distinguishing and sorting of cells of the multi-cell system or the cell system in primary cell cultures;

[0027] Creation of a resonance profile for the sonicated cells of the multi-cell system or the cell system;

[0028] Transformation of the sonicated cells of the multi-cell system or the cell system;

[0029] Transfection of the sonicated cells of the multi-cell system or the cell system;

[0030] Discrimination of the cells of the multi-cell system or the cellular system based on their genotype, wherein the cells are preferably sperm;

[0031] Isolation and destruction of cells of the multi-cell system, or the cellular system, wherein the cells are preferably viral or parasite bearing cells or tumor cells;

[0032] Acting on the cells of the multi-cell system, or the cellular system to prevent restenosis, where the cells are preferably cells of the neointima;

[0033] Isolation or identification of different sub-populations within the multi-cell system, or the cellular system, wherein the multi-cell system, or the cell system preferably comprises microorganisms in mixed populations;

[0034] Activation of specific dendritic cells;

[0035] Manipulation of intracellular signalling.

[0036] The inventive method is therefore suitable to separate cells of a multi-cell system according to different cell types. This is particularly important in cell cultures, and particularly in primary cell cultures. The cells in the cell culture can be sorted and separated quickly and accurately. Furthermore, a response profile can be created for the cells of the multi-cell system whereby only these specific cell types may be influenced or manipulated by the ultrasound frequency.

[0037] Furthermore, the targeted transformation or transfection of a particular cell type in a multi-cell system using ultrasound is possible with the method without having to make a manual separation of the cell types. Cells, which in some embodiments of the invention may be sperm can be discriminated against based on the genotype. Another advantage of the method is that special cell types, in particular virus or parasite-infected cells or otherwise degenerated cells, particularly tumor cells, with exposure to ultrasonic waves of a specific resonance frequency of these cells in the multi-cell system can be isolated and destroyed. The remaining cells are unaffected in the multi-cell system.

[0038] In order to avoid restenosis after a treated vasoconstriction the treatment can be performed with ultrasound. This is especially important for the cells of the neointima. The isolation or identification of subpopulations of different cell types within a multi-cell system can be performed with the inventive method. Thus, the method offers a lot of advantages and new opportunities for the identification, separation, and/or cell type-specific manipulation of different cells in a multi-cell system. Activation of dendritic cells which are cells of the immune system and one of the key cell types in inflammatory processes, is used to generate an immune response or to mobilize the immune system. The manipulation of intracellular signalling processes also allows for the stimulation of the proliferation of stem or progenitor cells with specific diseases that require regenerative processes for wound healing. By influencing the intracellular signalling processes within the cell is also possible to initiate apoptosis and initiate the targeted cell death. This is particularly important in cancer research.

[0039] With the optimal adjustment of the acoustic parameters relating to one type of cell and the subsequent irradiation of the cells with these sound frequencies, the permeability of the cell membrane can be increased, whereby an improved uptake of drugs, contrast agents, etc. is facilitated without undesirable side-effects in, for example, the intracellular signalling processes or cell physiological processes.

[0040] The invention further provides the use of the inventive device for carrying out the method according to the invention.

[0041] The use of the method comprises at least one of the steps

[0042] Distinguishing and sorting of cells of the multi-cell system or the cell system in primary cell cultures;

[0043] Creation of a resonance profile for the sonicated cells of the multi-cell system or the cell system;

[0044] Transformation of the sonicated cells of the multi-cell system or the cell system;

[0045] Transfection of cells of the multi-cell system or the cell system treated with ultrasound;

[0046] Discrimination of the cells of the multi-cell system or the cellular system based on their genotype, wherein in some embodiments of the invention the cells are sperm;

[0047] Isolation and destruction of cells of the multi-cell system, or the cellular system, wherein in some embodiments of the invention, the cells are viral or parasite bearing cells or tumor cells;

[0048] Acting on the cells of the multi-cell system, or the cellular system to prevent restenosis, wherein in some embodiments of the invention, the cells are cells of the neointima;

[0049] Isolation or identification of different sub-populations within the multi cell system or cell system, whereby in some embodiments of the invention, the multi-cell system, or the cell system comprises microorganisms in mixed populations;

[0050] Activation of specific dendritic cells;

[0051] Manipulation of intracellular signalling.

BRIEF DESCRIPTION OF THE DRAWINGS

[0052] FIG. **1** shows a diagram of an embodiment of a structure of a device for the identification, separation and/or cell type-specific manipulation of at least one cell of a cellular system, as well as microorganisms;

[0053] FIG. **2** provides photomicrographic images and cells. FIG. **2**A shows an image of CHO cells before and after treatment with ultrasound. FIG. **2**B shows an image of HEK cells before and after treatment with ultrasound.

[0054] Further features, details and advantages of the invention will become apparent from the wording of the claims and from the following description of embodiments with reference to the drawings.

DETAILED DESCRIPTION OF THE INVENTION

Definitions

[0055] Microorganism: micro-organisms, microscopic unicellular or multicellular organisms, such as bacteria, protozoa, fungi, yeasts and algae.

Cell system:

[0056] a) mono cell system: Each organic system containing only one type of cell; or

[0057] b) multi-cell system: Each organic system containing more than one type of cell, such as cell cultures or organisms.

Primary cell culture: Not immortalized (i.e., mortal) cell culture, which was obtained directly from a tissue.

Ultrasound transmitter: A component which generates acoustic signals in the ultrasonic range.

Sonopulation: alteration or manipulation of cells by sonic (acoustic waves).

Cell type: Cells which perform the same function in an organism. Therefore, they are also similar mostly in their appearance, their structure and their internal structure, and intracellular signalling. However, individual protozoa can be seen as a special type of cell.

The terms "cell" and "cellular" may be used interchangeably herein.

LIST OF REFERENCE NUMERALS

[0058] **1** Device

[0059] **2** Control unit

[0060] **3** Receiving unit

[0061] **4** Petri dish

[0062] **5** Ultrasound transmitter

[0063] **6** Magnification optics

[0064] The generally designated device according to the invention (FIG. **1**) for the identification, separation and/or cell type-specific manipulation of at least one cell of a cell system as well as of microorganisms has a control unit **2**, and a biological inverted microscope **6** (MBL 3200, A. Kruss Optronic GmbH, Hamburg, Germany). On the control unit **2**, a receiving unit **3** is installed for a Petri dish **4**. The Petri dish **4** has a diameter of 10 cm and is filled with cells detached from the bottom of the dish **4** in Dulbecco's Modified Eagle Medium (DMEM)—a standardized culture medium for cell cultures. The cells in the petri dish **4** are, for example, Chinese hamster ovary (*Cricetulus griseus*) (CHO) cells, human embryonic kidney cells (HEK cells), endothelial cells of the aorta of cattle (BAEC cells), or embryonic Mouse fibroblast cells (3T3 his/NIH cells).

[0065] The ultrasound is generated by an Ultrasound transmitter **5**, wherein the Ultrasound transmitter **5** comprises a piezo-electric component, which is controlled with a frequency greater than 5 MHz, and has a narrow bandwidth. The Ultrasound transmitter **5** consists of a 7 MHz transducer having a piezo-electric crystal as a piezoelectric component, which may also be a piezoelectric ceramic or a piezoelectric polymer. The piezoelectric crystal is made of lithium niobate ($LiNbO_3$), which is cut with an orientation of 36° to the Y axis and having a resonance of 7 MHz per millimeter. This Ultrasound transmitter **5** is arranged at an angle of 17° above the petri dish **4**.

[0066] A not shown AFG3102 frequency generator (Tektronix, Everett, Wash., USA) controls the Ultrasound transmitter **5** with a fundamental frequency of a continuous wave. The signal of the not shown frequency generator is routed through a 20 dB attenuator (not shown) before it is directed as an input signal to a also not shown power amplifier 2100L 50 dB RF (Electronics & Innovation Ltd., Rochester, N.Y., USA), and there finally comes to the Ultrasound transmitter **5**, where the ultrasound generated is conducted into the sample in the petri dish **4**.

[0067] FIG. **2**A shows Chinese hamster ovary (CHO) cells in a petri dish **4**. The top image (**2** AI) shows the cells from the bottom of the dish placed in a nutrient medium prior to sonication. The lower picture (**2** A II) shows the same sample after a treatment of 30 seconds with ultrasound at a frequency of 7 MHz. The cells have assembled into larger and more densely packed clusters. This clustering has already started after a few seconds of sonication.

[0068] FIG. **2**B shows human embryonic kidney cells (HEK cells) in a petri dish **4** which have previously been detached from the bottom of the dish **4** and are freely movable in the nutrient medium. The upper frame (**2** Bi) showing the cells in the broth before the ultrasound treatment. The image (B **2** II) shows the cells after 30 seconds ultrasound treatment

at a frequency of 7 MHz. These cells, as opposed to CHO cells, show no cluster formation. Different cell types therefore show different behavior upon ultrasonic treatment with the same frequency. Each of these images represents a sample area of 960×720 (microns).

[0069] A mixture of both cell types (CHO cells and HEK cells) in a sample dish **4** also shows a clustering, with only the same types of cells forming a cluster (not shown).

[0070] The invention is not limited to the embodiments described above, but can be modified in many ways.

[0071] All of the claims, the description and the drawing features and advantages, including construction details, spatial arrangements and process steps can be inventive per se and in various combinations.

[0072] The contents of all literature references, patents, and published patent applications cited throughout this application are incorporated herein by reference in their entirety.

We claim:

1. A device (**1**) for the identification, separation and/or cell type-specific manipulation of at least one cell of a cellular system as well as of microorganisms, wherein the device (**1**) has a Ultrasound transmitter (**5**), a control unit (**2**) and a receiving unit (**3**), wherein the Ultrasound transmitter (**5**) comprises a piezo-electric component, which is controlled with a frequency greater than 5 MHz, and has a narrow bandwidth.

2. The device of claim **1**, wherein the piezoelectric member is a piezoelectric crystal, a piezoelectric ceramic or a piezoelectric polymer.

3. The device of claim **1**, wherein the piezoelectric component has a resonance of 7 MHz per millimeter.

4. The device (**1**) of claim **1**, wherein the piezoelectric component is a wafer which is cut in an orientation of 36° to the Y-axis of a lithium niobate ($LiNbO_3$) crystalline lattice.

5. The device (**1**) of claim **1**, wherein the control unit (**2**) has a magnification lens (**6**), and comprises a binocular or an inverted microscope.

6. The device (**1**) of claim **1**, wherein the receiving unit (**3**) is a cell culture dish, petri dish (**4**) or the like.

7. A method for the identification, separation and/or cell type-specific manipulation of at least one cell of a cellular system as well as of microorganisms with a device (**1**) of claim **1**, comprising the steps of

a) introducing the cell system into the receiving unit (**3**) of the device (**1**), and

b) sonicating the cell system with the Ultrasound transmitter (**5**) with a cell type-specific frequency.

8. The method of claim **7**, wherein the method further comprises at least one of the following steps:

c) distinguishing and sorting of cells of the multi-cell system or the cell system in primary cell cultures;

d) creating a resonance profile for the sonicated cells of the multi-cell system or the cell system;

e) transforming the sonicated cells of the multi-cell system or the cell system;

f) transfecting the sonicated cells of the multi-cell system or the cell system;

g) discriminating the cells of the multi-cell system or the cellular system based on their genotype, wherein the cells are sperm;

h) isolating and destroying cells of the multi-cell system, or the cellular system, wherein the cells are viral or parasite bearing cells or tumor cells;

i) acting on the cells of the multi-cell system, or the cellular system to prevent restenosis, where the cells are cells of the neointima;

j) isolating and identifying different subpopulations within the multi-cell system or the cell system, the multi-cell system or the cell system comprising microorganisms in mixed populations;

k) activating specific dendritic cells; and

l) manipulating intracellular signalling.

9. Use of a device (**1**) of claim **1** for performing a method for the identification, separation and/or cell type-specific manipulation of at least one cell of a cellular system as well as of microorganisms, the method comprising the steps of:

a) introducing the cell system into the receiving unit (**3**) of the device (**1**), and

b) sonicating the cell system with the Ultrasound transmitter (**5**) with a cell type-specific frequency.

10. The use according to claim **9**, wherein the method further comprises at least one of the following steps:

c) distinguishing and sorting of cells of the multi-cell system or the cell system in primary cell cultures;

d) creating a resonance profile for the sonicated cells of the multi-cell system or the cell system;

e) transforming the sonicated cells of the multi-cell system or the cell system;

f) transfecting the sonicated cells of the multi-cell system or the cell system;

g) discriminating the cells of the multi-cell system or the cellular system based on their genotype, wherein the cells are sperm;

h) isolating and destroying cells of the multi-cell system, or the cellular system, wherein the cells are viral or parasite bearing cells or tumor cells;

i) acting on the cells of the multi-cell system, or the cellular system to prevent restenosis, where the cells are cells of the neointima;

j) isolating or identifying different sub-populations within the multi-cell system, or the cellular system, wherein the multi-cell system, or the cell system comprises microorganisms in mixed populations;

k) activating specific dendritic cells; and

l) manipulating intracellular signalling.

* * * * *

III.3 Vision sur le champ de recherche

A plus long terme, les ultrasons peuvent jouer un rôle dans le traitement instantané des lésions malignes immédiatement après le diagnostic. Si l'intensité acoustique pour le traitement doit être imposée inférieure au seuil de cavitation inertielle, une plateforme d'échographie unique peut être utilisée pour le diagnostic de la lésion et également adaptée pour la thérapie ultrasonore. Cette procédure clinique est plus simple et plus rapide que la norme actuelle.

A partir du moment que les ultrasons pénètrent les tissus, ceux-ci peuvent être utilisés pour la délivrance ciblée de médicaments. De plus, l'avènement des agents de contraste ultrasonore capables de passer au travers de la barrière hémato-encéphalique permettrait de déposer l'énergie des ultrasons directement au niveau des tumeurs profondes du cerveau.

L'utilisation des antibulles pour la délivrance des agents thérapeutiques assistée par des ultrasons et la manipulation des cellules malignes individuelles sur la base de leur signature acoustique sont des méthodes attrayantes pour réduire les effets secondaires pendant la traitement des maladies. Pour ces méthodes, une meilleure compréhension de l'interaction entre les ultrasons, les microbulles et les cellules est nécessaire.

S'il existe un seuil acoustique de perturbation, les globules rouges peuvent être utilisés comme véhicules de transport des agents thérapeutiques au lieu d'injecter des microbulles ou des antibulles dans le corps pour la délivrance des médicaments assistée par des ultrasons. L'analyse des réponses mécaniques des globules rouges dans les champs ultrasonores, surtout des globules d'une autre densité ou compressibilité, peut être éventuellement utilisée dans l'identification instantanée des maladies parasitaires telles que le paludisme.

Pour toutes les applications ci-dessus, nous avons besoin de comprendre et prévoir la réponse mécanique des cellules individuelles aux champs ultrasonores et la contribution à cette réponse de la membrane cellulaire et le noyau.

En présumant que les caractéristiques acoustiques des cellules individuelles ont des différences minimales entre les types de cellules, le ciblage des cellules individuelles requiert la sonification à des fréquences spécifiques. En conséquence, parallèlement à ces études, des transducteurs à bande étroite devront être développés pour la manipulation des cellules individuelles.